PETROLOGIC COMPARISON OF THE WEST BENNETT HILLS RHYOLITES TO THE CENTRAL SNAKE RIVER PLAIN RHYOLITES

By

WILLIAM AUSTIN STARKEL

A thesis submitted in partial fulfillment of the requirements for the degree of

MASTER OF SCIENCE IN GEOLOGY

WASHINGTON STATE UNIVERSITY
School of Earth and Environmental Sciences

MAY 2008

To the Faculty of Washington State University:

The members of the Committee appointed to examine the thesis of WILLIAM AUSTIN STARKEL find it satisfactory and recommend that it be accepted.

_____
Chair

_____

_____

ACKNOWLEDGEMENTS

First I would like to thank my advisor, Dr. John Wolff. He was immediately approachable as soon as I arrived in Pullman, and his enthusiasm and unwavering support throughout the project were crucial parts of my success here at WSU.

My field advisors, Bill Bonnichsen & Martha Godchaux, gave this project to me and were my field guides in the Snake River Plain. Without their expertise and generosity, this project would never have happened.

Scott Boroughs generated nearly half the data in this study and entrusted it to me without hesitation. Scott also accompanied me in the field multiple times, including the infamous “Bennett Mounain Death March”, one of the most important (and grueling) days I spent in the field.

The technical staff here at WSU’s GeoAnalytical Lab are the most generous and patient group of folks I’ve had the pleasure of working with. Many thanks to Diane Cornelius, Scotty Cornelius, Rick Conrey and Charles Knaack for all their help.

My fellow graduate students helped me through the past three years with their friendship and guidance.

Most of all, I wish to thank my family. Their love and support has given me everything I have.

PETROLOGIC COMPARISON OF THE WEST BENNETT HILLS RHYOLITES TO THE CENTRAL SNAKE RIVER PLAIN RHYOLITES

Abstract

by William Austin Starkel, M.S.
Washington State University
May 2008

Chair: John A. Wolff

The Miocene high-temperature, low-$\delta^{18}O$, A-type rhyolites of the West Bennett Hills (WBH) share similar physical and petrologic characteristics with the high-grade ash-flow tuffs of the southern central Snake River Plain (SCSRP), but no detailed comparison of the geochemistry of these rocks has been undertaken prior to this study. By comparing units across the Snake River Plain with similar stratigraphic positions, the purpose of this study is to determine if cross-plain North-South correlations can be made on the basis of chemical compositions.

If it can be demonstrated that the SCSRP ash-flow tuffs have traveled on the order of tens of km to the WBH, this would have profound implications for physical volcanology, namely that an ash-flow tuff can travel tens of km and subsequently form a strongly rheomorphic ignimbrite following emplacement. If no correlations can be made, this would have implications for petrogenesis in the central Snake River Plain (CSRP), suggesting that similar magmas were generated in discrete locations over a wide area.

Samples were collected in the field and were analyzed for oxygen isotopes, as well as whole rock major and trace elements. Microprobe and LA-ICP-MS trace element methods were used to analyze feldspars, pyroxenes and volcanic glass. The data from this study indicates that the SCSRP rhyolites did not travel as far north as the WBH, and therefore the rhyolites of the CSRP were likely generated from spatially discrete magma chambers over a large area.

TABLE OF CONTENTS

LIST OF TABLES

LIST OF FIGURES

Chapter 1: Introduction

The Snake River Plain (SRP) volcanic province consists of a topographical lowland that extends 100s of kilometers from the Yellowstone Volcanic Plateau to northern Nevada (Fig 1). Onset of SRP volcanic activity coincides geographically and temporally (~16.5 Ma) with the Columbia River Basalt flows of eastern Washington and eastern Oregon. SRP magmatism progressed to the NE in a time-transgressive manner, creating a series of massive eruptive centers (Fig 1). The most productive eruptive center, in terms of volume of material erupted, is the Bruneau – Jarbidge eruptive center (BJEC) in the central Snake River Plain (CSRP). The Bruneau - Jarbidge erupted volcanic materials from approximately 12.5 to 8 Ma, with the most prominent eruptions coming in the first two million years of activity (Bonnichsen et al., 2008). This early period in the BJEC produced several voluminous high-temperature densely welded ash-flow tuffs, known collectively as the Cougar Point Tuff (CPT, Bonnichsen and Citron, 1982). Rhyolites erupted during this time period outcrop along the margins of the CSRP in a few prominent escarpments: the Black Rock Escarpment (type section of the Cougar Point Tuffs) and Brown's Bench escarpment (BB) in the southern central Snake River Plain (SCSRP), and the West Bennett Hills (WBH) on the northern margin of the CSRP (Figs 2a-d). Though not indicated on Figure 1, the escarpments in the Jarbidge Canyon east of the Black Rock Escarpment in Bruneau Canyon are also quite prominent.

The purpose of this study is two-fold: 1) geochemical characterization of the stratigraphic sequence of rhyolite units in the West Bennett Hills and 2) to determine whether or not the widespread silicic rhyolites of the CSRP can be correlated from north to south based on detailed geochemical comparisons of the rhyolites in the northern

CSRP (WBH rhyolites) with the rhyolites in the SCSRP (CPT, BB, and several other units in the area).

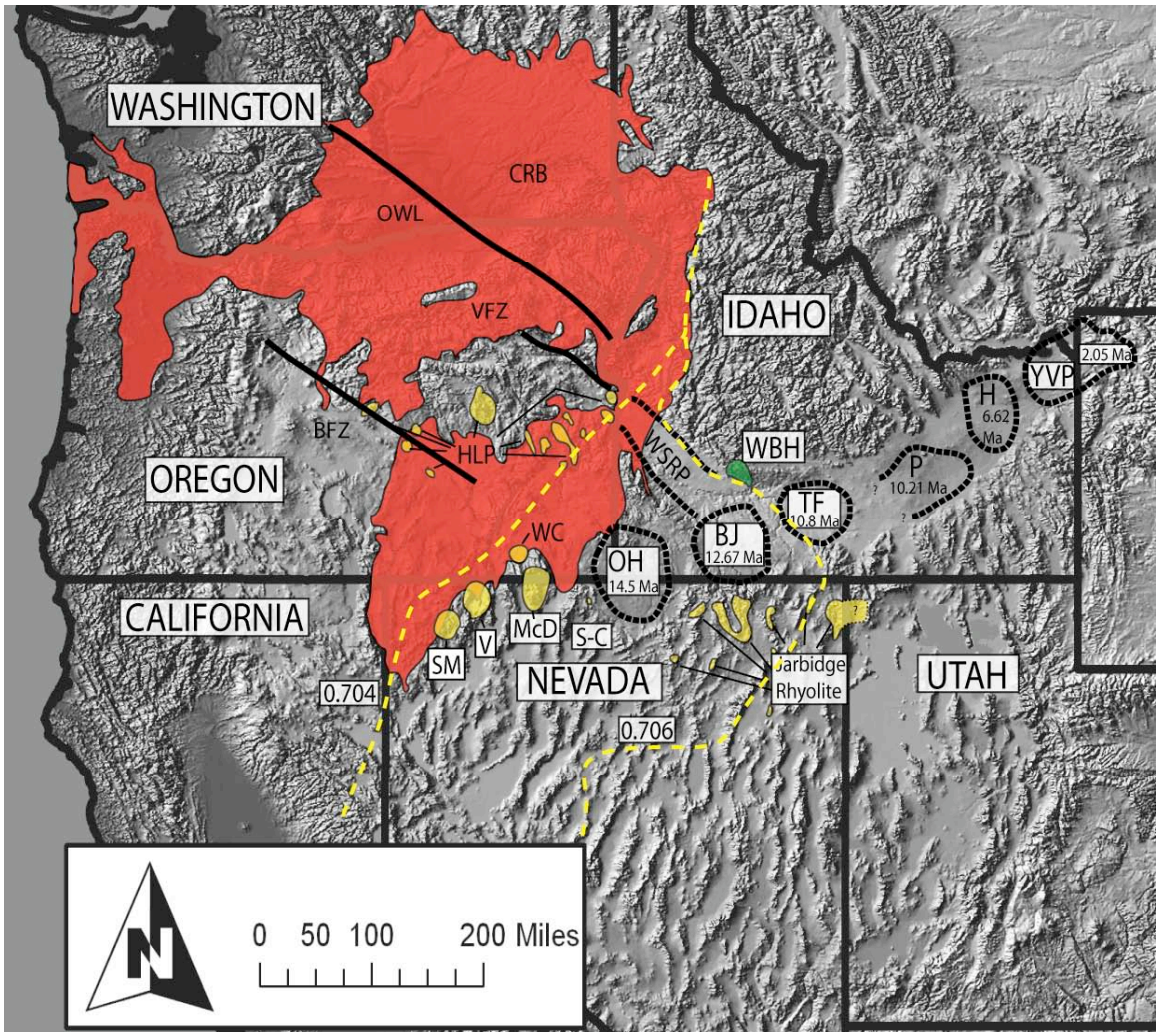

Figure 1: map of the northwest USA, showing location of volcanic units and eruptive centers pertinent to the geologic history of this study. The extent of the Columbia River Basalt (CRB) group is shown in red (Wolff et al., 2008). The silicic units erupted from 16.5 – 15 Ma are shown in yellow: HLP = High Lava Plains rhyolites (Jordan et al, 2004), McD = McDermitt caldera (Rytuba and McKee, 1984), Jarbidge rhyolite (Coats, 1987; Bill Bonnichsen, personal comm., 2008), numerous silicic centers in northern

Nevada: SM = Soldier Meadow caldera, V = Virgin Valley caldera, WC = Whitehorse Creek caldera (Chris Henry, personal comm., 2007), and S-C = Santa-Rosa Calico volcanic field (Brueseke et al., 2008). The approximate locations of the Brothers Fault Zone (BFZ), Vale fault zone (VFZ) and Olympic – Wallowa lineament (OWL) were taken from a figure in Camp et al. (2003). The Snake River Plain eruptive centers are labeled with the earliest known magmatic event associated with each respective caldera: OH = Owyhee Humboldt, BJ = Bruneau-Jarbidge, TF = Twin Falls, P = Picabo, H = Heise, YVP = Yellowstone Volcanic Plateau (Bonnichsen et al., 2008). West Bennett Hills (WBH) shown in green. Approximate locations of ^{87}Sr / ^{86}Sr isopleths shown as dashed yellow lines taken from a figure in Camp and Ross (2004) and references therein. Western Snake River Plain rift basin (WSRP) location taken from Wood and Clemens (2002).

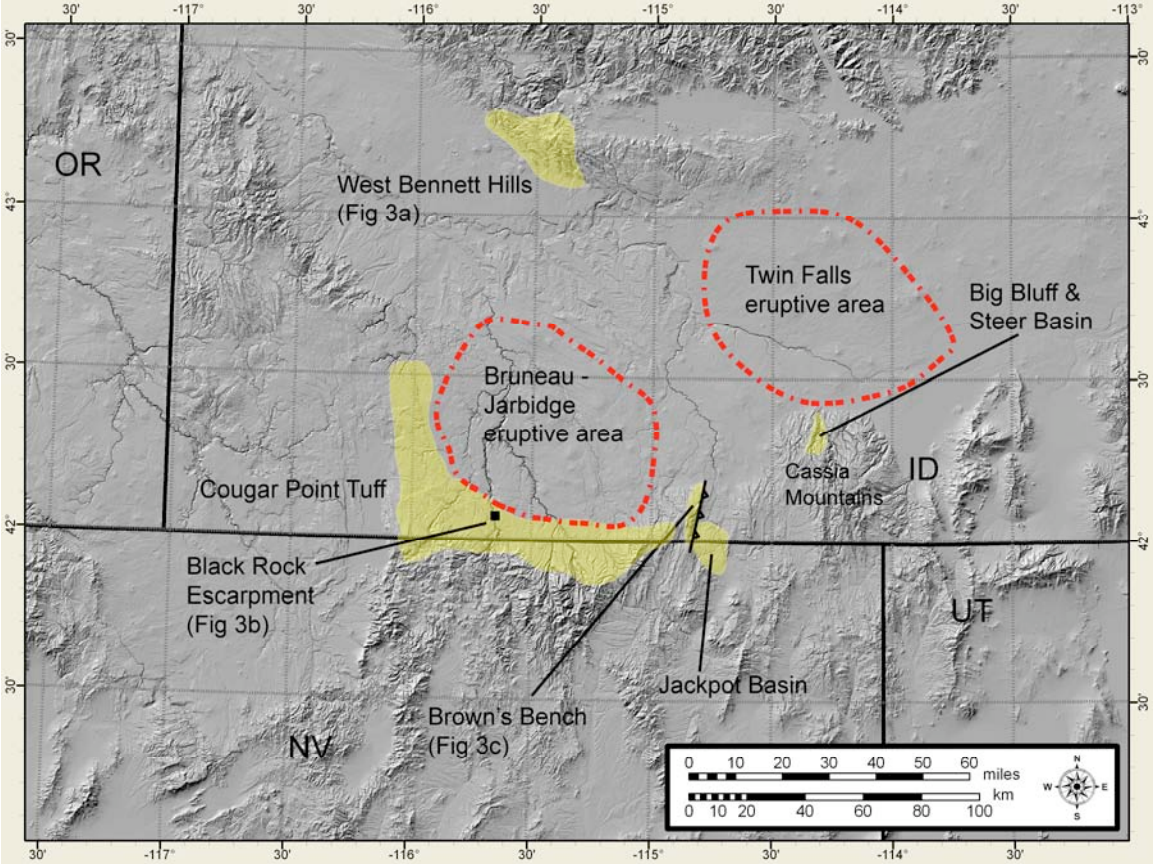

Figure 2: map of the central Snake River Plain (CSRP), showing the approximate locations for the Bruneau – Jarbidge and Twin Falls eruptive areas, the prominent escarpments in the CSRP (West Bennett Hills, Black Rock Escarpment and Brown's Bench) and approximate extents for the CSRP rhyolites discussed in this study.

Review of high-temperature rhyolites

The central Snake River Plain is one of the best examples of intracontinental bimodal volcanism on the planet. It is the type location for Branney et al.'s (2008) proposed "Snake River (SR)-type" volcanism. The West Bennett Hills rhyolites fall directly into this proposed category. The diagnostic SR-type volcanic products described by Branney et al. (2008) include:

- bimodal high-temperature volcanism consisting of tholeiitic basalts and H_2O – poor metaluminous rhyolites with anhydrous mineral assemblages and elevated high field strength elements (Zr, Hf, Ta, Nb). Volcanism in the WBH is not bimodal in the strict sense of the term, as the basalts were erupted at least a million years after the last of the rhyolites were deposited and no intercalation of the basalts and rhyolites exist in the WBH.
- voluminous high to low aspect-ratio rhyolitic ignimbrites; rhyolitic lava flows are widespread with low aspect ratios and lack features such as domes and coulees.
- ignimbrites are generally lithic-poor and lack proximal lithic breccias.
- most ignimbrites are extremely high-grade, with very few low- to medium- grade ignimbrites (no low- or medium- grade units in the WBH).
- rheomorphism is intense and widespread; lava-like facies are common and dominate many of the ignimbrite sheets.
- ignimbrites have well developed upper and lower vitrophyres with extensive spherulite zones, some with large (up to 30cm) lithophysae. Although these characteristics are by no means unique to the Snake River Plain, they are important aspects of the ignimbrites of the CSRP.

- numerous ashfall layers with parallel bedding and lamination (only locally exposed in the WBH); fused ashfall deposits are common and often associated with baked paleosols.
- scarcity of pumice lapilli (or fiamme in the case of welded ignimbrites), pumice lenses and pumice-rich zones; conventional Plinian pumice fall layers are rare.

Note that this list is not the complete set of characteristics of SR-type volcanism set forth by Branney et al. (2008); it is a summary of the most important characteristics readily seen in the WBH rhyolites, and lacks some important details regarding unwelded deposits in the CSRP that are either absent, poorly or rarely exposed in the WBH.

Geologic History

The Snake River Plain (SRP) is a topographic lowland that extends southwest from the Yellowstone Volcanic Plateau to Twin Falls, Idaho and from there runs towards the northwest to the Oregon/Idaho border (Fig 1). It is divided into two parts, the Western Snake River Plain (WSRP) and Eastern Snake River Plain (ESRP). The ESRP, the Owyhee Plateau (denoted as the Owyhee-Humboldt eruptive center in Figure 1) and Bruneau-Jarbidge (BJ) regions to the south-southwest, are believed by many to have been formed by the Yellowstone hotspot as it propagated northeast with the North American continent over the last 14 Ma. The WSRP is a large intracontinental rift basin that is oriented roughly perpendicular to the northeast - southwest trend of the hotspot track, and was active from approximately 9 – 7 Ma, with the majority of activity occurring in the first 2 million years (Hooper et al., 2002). The WSRP and ESRP converge in the central Snake River Plain (CSRP), an area that produced copious amounts of rhyolite magma in

the OH, BJ and Twin Falls eruptive centers from approximately 14 – 8 Ma (Bonnichsen et al., 2008).

The Yellowstone hotspot track is a time-transgressive series of eruptive centers stretching from northern Nevada / southeastern Oregon / western Idaho to its present location in northwestern Wyoming (Fig 1). The earliest volcanism associated with the Yellowstone hotspot track began at approximately 16.5 Ma in eastern Oregon, southeastern Washington, northern Nevada and western Idaho (Pierce and Morgan, 1992). Over the next 1.5 million years, an immense amount of magma was erupted in this region: the Columbia River basalts (CRB) consist of approximately 230,000 km^3 of mafic lava flows in the inland Northwest (Camp and Ross, 2004). Silicic volcanism was also prominent in the region during this time: McDermitt caldera (Rytuba and McKee, 1984) and the Santa Rosa – Calico volcanic field of northern Nevada (Brueseke et al., 2008), the first of the High Lava Plains volcanics in Oregon (Jordan et al., 2004) and various other silicic centers in northern Nevada / southeast Oregon (Fig 1) were all erupted between 16.7 and 15 Ma.

Volcanism progressed from SE Oregon / NE Nevada / SW Idaho to the northeast over the time period of 14 – 9 Ma, creating the three primary eruptive centers of the central Snake River Plain: the Owyhee-Humboldt (active from 14 – 12Ma), Bruneau-Jarbidge (12.5 to 8 Ma), and the Twin Falls (10 – 8 Ma) eruptive centers. Bonnichsen et al. (2008) view these CSRP volcanics as the first to be directly associated with the Yellowstone hotspot track. From approximately 8 Ma to the present time, the volcanism of the SRP has continued its NE progression, forming the ESRP (which consists of the

Picabo, and Heise volcanic centers) and Yellowstone Volcanic Plateau (Pierce and Morgan, 1992).

Origins of the Snake River Plain / Yellowstone Volcanic Province

Several models have been proposed by various researchers to explain the origin of SRP volcanics. This study does not necessarily promote one model over the other; the cause of the anomalous heat source that produced SRP magmatism is an issue that the author will leave to future researchers. The model that most researchers have adopted invokes a two-stage stationary mantle plume interacting with the overriding North American plate, creating the time-transgressive volcanism of the SRP / Yellowstone volcanic province. The first stage involved the impingement of the plume head on the lithosphere below the region of eastern Oregon, northern Nevada and southwestern Idaho around 16.5 Ma (Pierce and Morgan, 1992; Glen and Ponce, 2002; Camp and Ross, 2004). According to the mantle plume model, this initial interaction of the plume head with the accreted terrane-derived crust was the source of heat for the voluminous Columbia River Basalt group (Camp and Ross, 2004) as well as the likely heat source for the coevally emplaced silicic units of the Santa-Rosa Calico field in northern Nevada (Brueseke et al., 2008) and the High Lava Plains rhyolites (Jordan et al., 2004). At around 15 Ma, the plume head was sheared off from its tail by the deep lithospheric roots of the North American craton as the North American plate moved SW over the stationary plume (Camp and Ross, 2004).

The second stage of the plume hypothesis involves the interaction of the relatively narrow plume tail with the interior of the North American craton. From 14 – 9 Ma, the

nature of magmatism of the SRP changed dramatically as the source material went from the accreted terranes beneath the Oregon-Idaho-Nevada border region where the plume first impinged upon the lithosphere through the region between the $^{87}Sr/^{86}Sr$ isopleths (Fig 1) to the Precambrian basement east of the 0.706 $^{87}Sr/^{86}Sr$ isopleths. The stationary plume tail providing hot mantle material to upper mantle & lower crustal parts of the lithosphere coupled with the progressive west-southwest movement of the North American plate created the time-transgressive series of eruptive centers in the Snake River Plain (Fig 1). The SRP volcanism of this time period is dominated by large volume (≥ 500 km^3 for some units), high temperature (850 – 1000^{O} C) aerially extensive rhyolites with anhydrous mineral assemblages, most notably the Cougar Point Tuffs of the Bruneau-Jarbidge eruptive center, followed by relatively small volume capping basalt lava flows (Bonnichsen et al., 2008; Bonnichsen, 1982).

From approximately 6.5 Ma to the present, SRP magmatism continued its NE progression but the characteristics of the rhyolites underwent significant changes. The rhyolites of the eastern Snake River Plain (ESRP) and Yellowstone Volcanic Province have lower magmatic temperatures than the CSRP rhyolites and some units contain hydrous phenocrysts, such as biotite and hornblende in some units from the YVP (Christiansen 2001). Perkins and Nash (2002) suggest that the change in magmatic temperatures is caused by a greater degree of basaltic magma underplating the craton (as opposed to intruding into the craton) beneath the ESRP. If basaltic magma is intruded into the crust its ability to transfer heat, and therefore produce rhyolitic magma, is much more effective than if the basaltic magma is pooled underneath the crust. This process is

debatable, however, due to the fact that deeper crust is considerably hotter than shallow crust and therefore requires less thermal energy to initiate melting.

Alternative Models

Although many aspects of SRP volcanism are well explained by the anorogenic two-stage plume model, some workers disagree with the plume hypothesis. Christiansen et al.'s (2002) arguments against the plume model state that the inception of magmatism along a pre-existing structural weakness at the time of Basin and Range extension and the contemporaneous emplacement of the High Lava Plains units in central Oregon is purely coincidental. In addition, the persistence of young basaltic volcanism along the SRP track occurring millions of years after the hotspot had passed a given region is not accounted for by the simple plume model. Christiansen et al. (2002) promote a scenario where Basin and Range extension facilitated upwelling of mantle beneath northern Nevada and southern Oregon at approximately 18-17 Ma, creating the voluminous CRB group. Continuous extension allowed the magma to travel west, creating the Newberry trend of volcanism. The SRP magmatism to the east was formed by shear melting at the base of the lithosphere; newly melted materials would then rise, creating a pressure sink in the upper mantle and promote further melting, effectively making a self-sustaining melting anomaly. The eastward-propagating time-transgressive nature of the SRP eruptive centers is accounted for by invoking a pre-existing "ancient structural zone" which would provide a path of least resistance for the magma to travel through (Christiansen et al., 2002).

Christiansen et al.'s (2002) work is commendable for questioning the widely accepted deep mantle plume model, but there are several inconsistencies in their refutations. The "coincidental" nature of Basin and Range extension with CRB magmatism is, according to Hooper's 1990 study, not a coincidence at all. Hooper (1990) states that the majority of the CRB magma was erupted prior to significant extension and crustal thinning in SE Washington, and indeed the northward progression of Basin and Range extension from the Brothers and Vale fault zones to the Olympic-Wallowa lineament (Fig 1) was triggered by crustal weakening due to the voluminous outpouring of CRB magma.

Waite et al.'s (2006) thermal imaging data show that there is a low-velocity feature beneath Yellowstone that extends to 400km below the surface, indicating that the thermal anomaly does not extend down to the core-mantle boundary as some researchers have proposed (Pierce and Morgan, 1992; Camp and Ross, 2004, among others), but originated in the upper mantle instead. Another imaging study by Yuan and Duecker (2005) shows a low-velocity anomaly that extends 500km beneath Yellowstone, and although their image of the thermal anomaly is 100km deeper than Waite et al.'s, it is still consistent with an upper-mantle origin of the Yellowstone plume. Waite et al. (2006) invoke a plume-fed upper mantle small-scale convection model, with lateral movement aided by pre-existing structural weaknesses to account for the time-transgressive movement of the SRP eruptive centers.

Hamilton (1987) attributed Snake River Plain volcanism to an active continental rift basin. Although this theory can explain the time-transgressive nature of SRP magmatism, it fails to account for the lack of regional structural evidence for NW-SE

extension, while significant evidence exists for NE-SW extension to the northeast and southwest of the Snake River Plain (Pierce and Morgan, 1992). Alt et al. (1988) proposed that a meteorite impact in eastern Oregon was the trigger for magmatism in the SRP, but there is no record of any geologic features (shocked quartz, shatter cones, high-pressure minerals, etc) which would indicate a large-scale impact at Alt et al.'s proposed impact site in southeast Oregon (Pierce and Morgan, 1992).

Smith (1992) suggested that CRB magmatism is a product of back-arc convection associated with the subducting Farallon plate. According to Smith's model, the source components involve input from mantle inputs (partial melt derived from the asthenosphere, young subcontinental lithoshpere, asthenospheric material with possible subduction-derived fluids from the buried Farallon plate, and Proterozoic subcontinental lithosphere) and crustal contaminants (Paleozoic-Mesozoic accreted terranes, Proterozoic-Paleozoic crust, and Archean crust) interacting at different stages of magmatism to produce the variety of geochemical signatures of the CRBs. A recent study from Wolff et al. (2008) suggests that plume-derived magmas assimilating continental crust in a centralized magma chamber in the boundary between the Archean craton and the accreted terranes to the west can produce the range of compositions found in the CRB group.

Bruneau – Jarbidge Eruptive Center

The Bruneau – Jarbidge eruptive center (BJEC) erupted bimodal volcanic products in three overlapping episodes from 12.67 Ma to approximately 8 Ma. The first stage was dominated by explosive silicic volcanism, followed by an effusive silicic

volcanism stage, following which the final stage produced a thin veneer of basaltic lava flows over the BJEC. The Bruneau – Jarbidge area is currently an oval structural basin of approximately 95km x 55km. The basin was probably formed by subsidence due to voluminous rhyolite outpourings and caldera collapse(s) associated with the explosive volcanism stage (Bonnichsen 1982). The bulk of the magmatism occurred as rhyolitic ash-flow tuff eruptions, to form the Cougar Point Tuff units, from 12.67 to 10.2 Ma (Bonnichsen et al., 2008).

The first stage of magmatism (12.67 – 10.4 Ma) in the Bruneau – Jarbidge was dominated by explosive silicic volcanism and high temperature, widespread, voluminous ash-flow tuffs. The Cougar Point Tuffs, and indeed all CSRP tuffs, are only found as outflow material. It is inferred that the record of caldera structures and associated caldera-filling units either was erased during caldera collapse following explosive eruptions or was covered by younger basalt flows. The CPT units are single cooling units consisting of single to multiple emplacement events representing a single eruptive event. Soils are commonly developed between units, signifying that the CSRP tuffs were produced by discrete volcanic events separated by significant periods of time. The second stage of magmatism in the BJEC (~10.4 – 8 Ma) is represented by numerous large, effusive rhyolite lava flows. The transition from explosive to effusive volcanism was gradational, as some of the older lavas are intercalated with the younger ash-flow tuffs (Bonnichsen, 1982; Bonnichsen and Citron, 1982; Bonnichsen et al., 2008).

The final stage of volcanism in the Bruneau – Jarbidge consists of a thin veneer of basaltic eruptive units, most of which were extruded after the rhyolitic volcanism had subsided, although some intercalation does exist. Most of these lavas erupted as small,

low profile shield volcanoes within the Bruneau – Jarbidge eruptive center. These SRP basalts are broadly tholeiitic in composition and most likely represent the magmas that underplated the continental crust (Bonnichsen, 1982; Bonnichsen and Godchaux, 2002). Hanan et al.'s (2008) investigation of radiogenic (Sr, Pb and Nd) isotopic composition of SRP basalts indicates that the Archean craton imparted significant crustal signatures on these basalts during magma genesis.

West Bennett Hills

The Mount Bennett Hills are an elongate E-W trending horst that lies between the central Snake River Plain to the south and the Camas Prairie to the north. They consist of multiple voluminous rhyolitic volcanic units of late Miocene age with minor interbedded sediments and younger basalt flows capping the silicic sequence. The western Mount Bennett Hills, or West Bennett Hills (WBH) lie at the western end of the horst near the intersection of the western Idaho suture zone to the west and the CSRP to the south. The rhyolites of the WBH share similar ages and physical, petrographic and geochemical attributes with the units in the CSRP, while the rhyolites of the eastern MBH are more closely associated with the younger eastern SRP volcanics.

The exposed basement rocks that unconformably underlie the WBH rhyolites consists of Cretaceous granites of the Idaho batholith and Eocene volcanics from the Challis group. The West Bennett Hills rhyolites are easily distinguished from the older Challis volcanics by their lack of hydrous phases, whereas the Challis rocks have abundant biotite phenocrysts.

CAT groups and CSRP stratigraphy

The central Snake River Plain's extensive rhyolitic volcanic products have been well documented (Bonnichsen, 1982; Bonnichsen and Citron, 1982; Honjo et al., 1992; Cathey and Nash, 2004; Boroughs et al., 2005; Bonnichsen et al., 2008; among many others), including the stratigraphy of prominent escarpments (Black Rock, Brown's Bench, and Bennett Mountain; Figs 3a-3c) and inferred stratigraphic locations of dozens of other units not associated with 500m-scale escarpments in the CSRP. These units all share similar physical characteristics (Branney et al., 2008), chemical compositions, and in the case of some unit-to-unit comparisons, eruption ages (Bonnichsen et al., 2008). This begs the question whether or not individual units are correlative to each other, or if not the same eruptive unit, perhaps originated from the same (or a similar) magma chamber (Fig 4). For example, the unit at the base of Black Rock escarpment, Cougar Point Tuff III (CPT 3, 12.67 Ma, Bonnichsen et al., 2008), has a stratigraphic position similar to the unit at the base of Brown's Bench (BB 1). However, a detailed study of the chemical and mineralogical compositions as well as additional radiometric dates would have to be done in order to correlate these units into a single erupted unit or claim they were erupted from a similar source.

Bonnichsen et al.'s (2008) composition and time (CAT) groups are an initial attempt at a "coherent stratigraphic framework" for the rhyolites of the CSRP, and provide an excellent starting point for unit-to-unit comparison. The CAT groups are segregated based on ^{40}Ar / ^{39}Ar ages, whole rock compositions, paleomagnetic data and stratigraphic positions. Bonnichsen et al. (2008) emphasizes that their CAT groups are not intended to imply that units within the same CAT group are the same unit nor are

they necessarily cogenetic. The CAT groups are simply an initial attempt to empirically segregate the dozens of rhyolites in the CSRP into similar groups that provide a good starting point for detailed unit-to-unit comparison studies such as this one. Table 1 shows the CAT group designations for the rhyolites in the CSRP that are pertinent to this study.

CAT Group	Age Range (Ma)	$\%TiO_2$ Range	Magnetic Polarity	units from Bruneau - Jarbidge area	units from Twin Falls area	units from WBH
8 (a & b)	10.4 - 10.7	0.39 - 0.67	Normal	CPT XV	BBU 8 Jackpot 7 Steer Basin Beaver Meadow	Rattlesnake Springs High Springs
7	10.7 - 11.0	0.22 - 0.38	Normal	CPT XIII	BBU 7 Lower Jackpot Big Bluff	Frenchman Springs Dive Creek Henley
6	11.0 - 11.2	0.46 - 0.56	Normal & Reverse	CPT XII	------	Bennett Mountain
5	11.2 - 11.5	0.26 - 0.43	Reverse	CPT XI, X	BBU 5, 6	Windy Gap Lower Reverse
4	11.5 - 11.7	0.31 - 0.41	Normal	CPT IX	BBU 4	Lower Normal
3	11.7 - 11.9	0.38 - 0.59	Reverse	CPT VII	BBU 3	Willow Creek

Table 1: Composition and Time group designations from Bonnichsen et al., 2008.

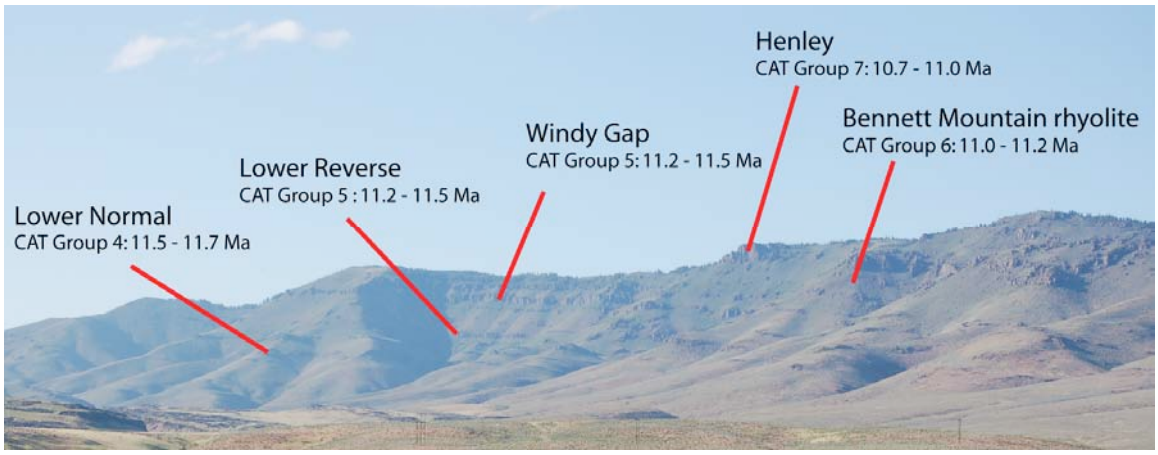

Figure 3a: NW-facing photograph of the Bennett Mountain escarpment in the West Bennett Hills (WBH) showing five of the WBH rhyolites. The stratigraphically lowest unit, Willow Creek (CAT Group 3, 11.7 – 13.0 Ma) outcrops only locally at the base of the Bennett Mountain escarpment and is not visible in this photo. The younger Danskin Group (Frenchman Springs + Dive Creek, CAT Group 7, 10.7 – 11.0 Ma; High Springs + Rattlesnake Springs, CAT Group 8a, 10.4 – 10.7 Ma) sits topographically lower than the units photographed and lie southwest of the face of the escarpment. CAT Group information taken from Bonnichsen et al., 2008.

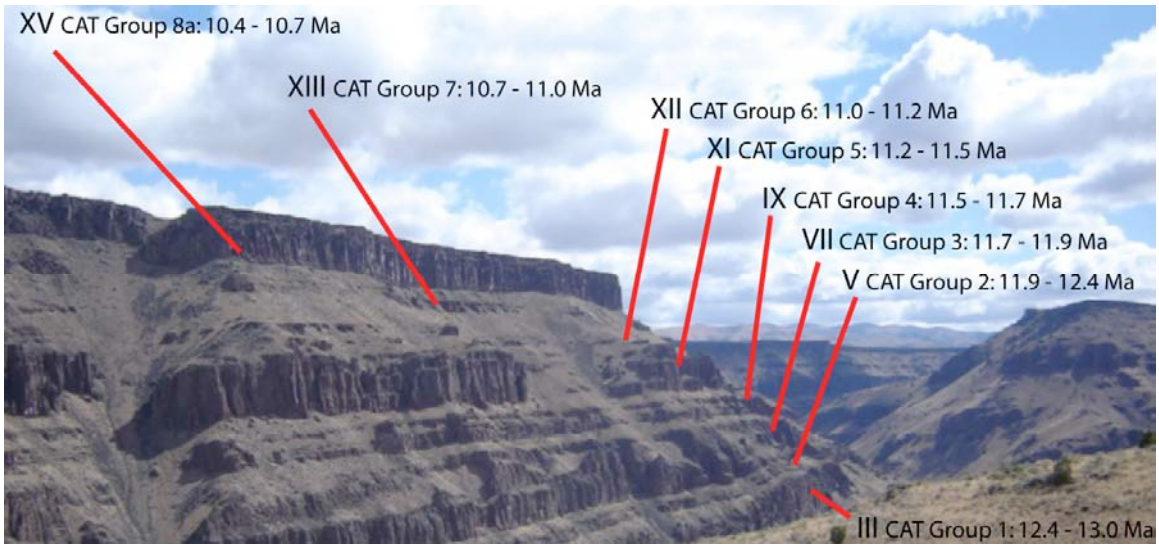

Figure 3b: South-southeast-facing photograph of the Black Rock Escarpment as seen from the western edge of Bruneau Canyon. This is the type section of the Cougar Point Tuff rhyolites (individual units labeled with roman numerals). Note that CPT X (CAT Group 5: 11.5 – 11.7 Ma) is not found at this escarpment. CAT Group information taken from Bonnichsen et al., 2008.

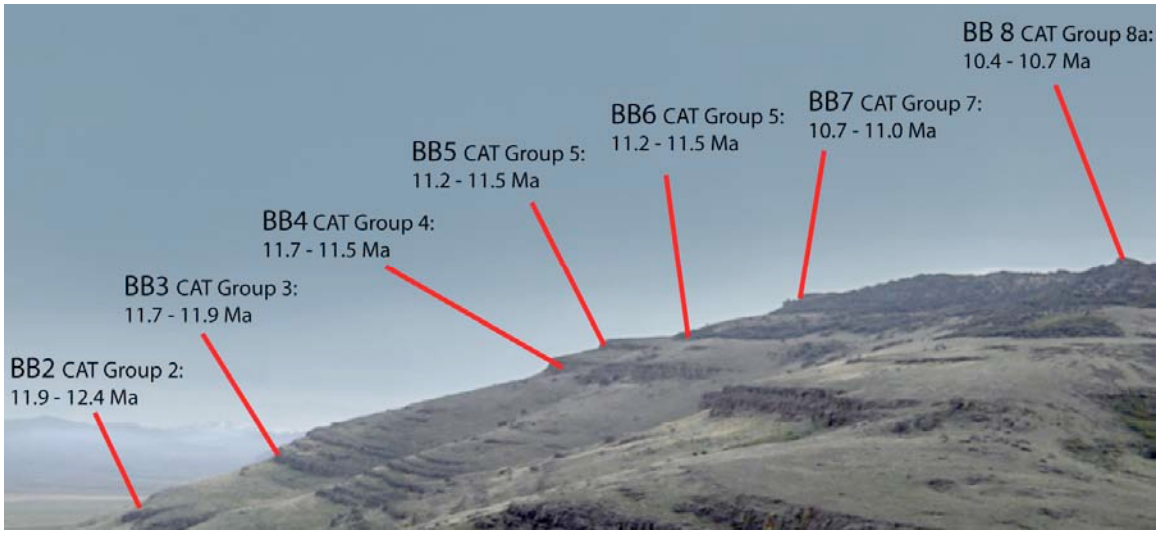

Figure 3c: photograph of Brown's Bench escarpment with the individual units labeled and pertinent CAT group information (Bonnichsen et al., 2008).

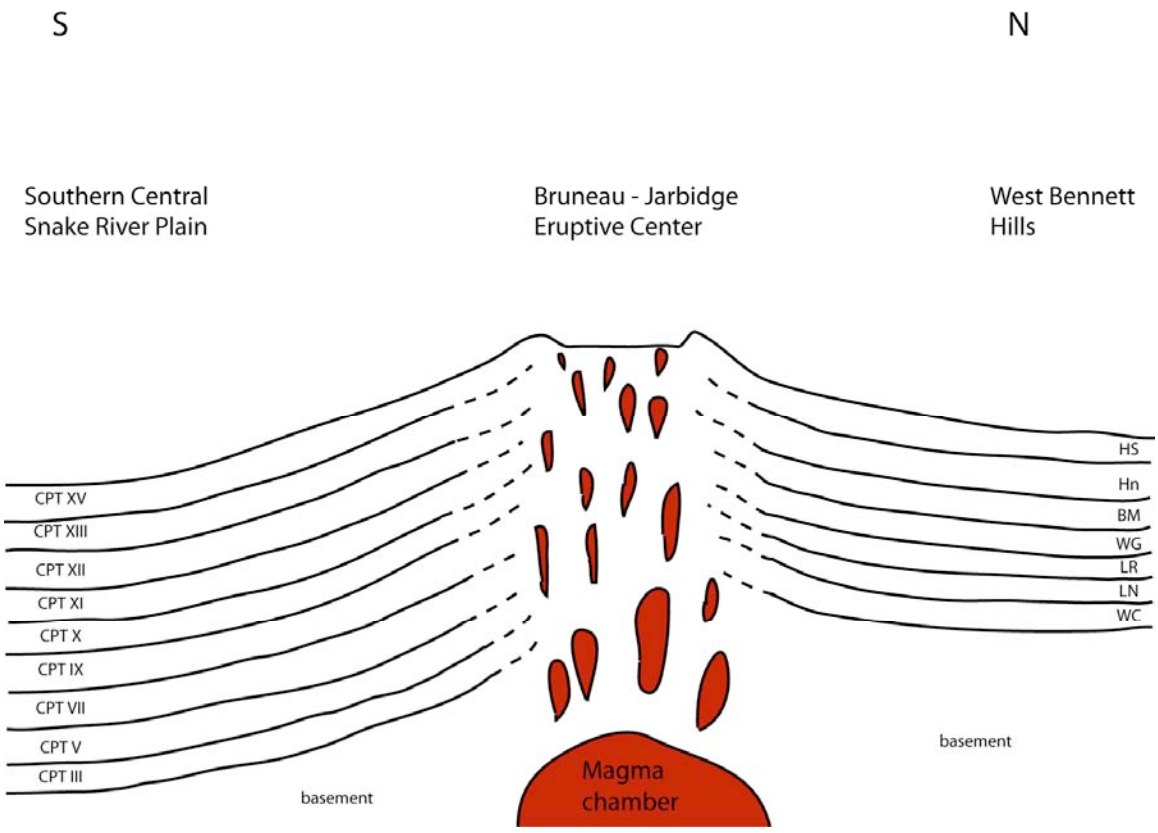

Figure 4: cartoon illustrating the basic principle behind the possibility of correlated units in the CSRP. Unit abbreviations for the West Bennett Hills: HS = High Springs, Hn = Henley, BM = rhyolite of Bennett Mountain, WG = Windy Gap, LR = Lower Reverse, LN = Lower Normal, WC = Willow Creek.

rhyolites pertinent to this study in their assigned CAT groups. This study focuses mainly on the units in the prominent escarpments of Black Rock Escarpment (which contains the Cougar Point Tuff (CPT) units), Brown's Bench (BB) and Jackpot 1-7 in the SCSRP and the West Bennett Hills rhyolites on the northern margin of the CSRP, but there are several other units included that are not associated with these escarpments. Figures 2 and 3a-c shows locations, pictures and stratigraphic relations of the previously mentioned escarpments.

Researchers have shown that several rhyolites of the Yellowstone volcanic plateau have a pronounced low-$\delta^{18}O$ magmatic signature (Hildreth et al., 1984, 1991; Bindeman and Valley, 2001; Bindeman et al., 2008; amongst several others). Boroughs et al. (2005) were the first to investigate oxygen isotope ratios in the central Snake River Plain, and made the discovery that all rhyolites in the CSRP had significant $\delta^{18}O$ depletions, but all units analyzed were from the SCSRP. The oxygen isotope data for the WBH rhyolites would add to the understanding of the extent of the low-$\delta^{18}O$ magma in the CSRP due to their location on the northern margin of the CSRP, and could serve as an additional tool for unit-to-unit comparisons in order to determine possible correlations.

It has been demonstrated that far-traveled rhyolitic ignimbrites such as the Bishop Tuff (Hildreth 1979; Michael 1983) and the Bandelier Tuff (Smith and Bailey, 1966) can be compositionally zoned. If the CSRP rhyolites are chemically zoned, this would make cross-plain correlations difficult with a relatively limited data set. However, Hooper (2000) demonstrated that individual widespread Columbia River basalt flows can be mapped across 100s of kilometers on the basis of chemical trends, due to the homogeneity of individual eruptions. Although Hooper (2000) advises caution that

chemical similarity alone does not prove that two widely separated units are from the same event, the lack of detailed geochemical comparisons for the central Snake River Plain rhyolites would make any matched compositions a significant step towards constructing a coherent stratigraphic framework for the region.

Comparing the geochemical compositions, specifically whole rock major and trace elements and phase (fresh volcanic glass, pyroxenes and feldspars) major and trace elements, of the units within Bonnichsen et al.'s (2008) CAT groups would add great depth to the understanding of a plain-wide stratigraphy. This study aims to confirm whether or not North-South cross-plain correlations can be made on the basis of geochemical comparisons. The West Bennett Hills rhyolites provide a unique opportunity to investigate N-S correlations in the central Snake River Plain due to their location on the northern margin of the CSRP and their previously mentioned temporal, stratigraphic and chemical similarities with rhyolites in the SCSRP. The outcome of this study will be significant regardless of whether or not unit-to-unit correlations can be made. If it can be demonstrated that N-S cross-plain correlations exist, it would prove that a high-temperature ash-flow tuff has the ability to travel distances on the order of 10's of km and then form a high-grade rheomorphic ignimbrite after emplacement. If, on the other hand, no definitive correlations can be made, it would have significant implications for the petrogenesis of CSRP rhyolites; mainly that similar (low-$\delta^{18}O$, high temperature, low-H_2O, metaluminous) yet discrete magmas were generated over a wide area.

Chapter 2: Geology of the West Bennett Hills

Previous work in the West Bennett Hills

Malde et al. (1963) mapped the West Bennett Hills rhyolites and noted that they shared similar physical and petrographic characteristics with the "Idavada Group" of Miocene volcanic rocks found in the southern CSRP, and mapped them as part of that group. This study was the first to outline the stratigraphy of units in the Bennett Mountain section and the topographically lower Danskin Mountain group (Fig 5). Wood and Gardner (1984) carried out more detailed mapping (specifically the structural geology of the area) and provided unit descriptions in their report of the WBH rhyolites. The main contributions in their report are the first published paleomagnetic data for the WBH rhyolites and implications for the relationships between the older Bennett Mountain group and younger, topographically lower Danskin Group. Wood and Gardner (1984) claim that the Danskin Group was emplaced following structural down-faulting along the face of the Bennett Mountain escarpment based on detailed mapping and paleomagnetic data. Honjo et al. (1992) published the first study to include geochemical data of the WBH rhyolites. Whole rock major and trace elements compositions were analyzed as well as microprobe analyses. Honjo et al. (1992) calculated eruption temperature ranges from mineral pairs of Fe-Ti oxides (880 - 919^{o} C), feldspars (879 – 1015^{o} C) and pyroxenes (890 – 1050^{o} C). The reader is referred to Honjo et al. (1992) for references to the calculation methods utilized.

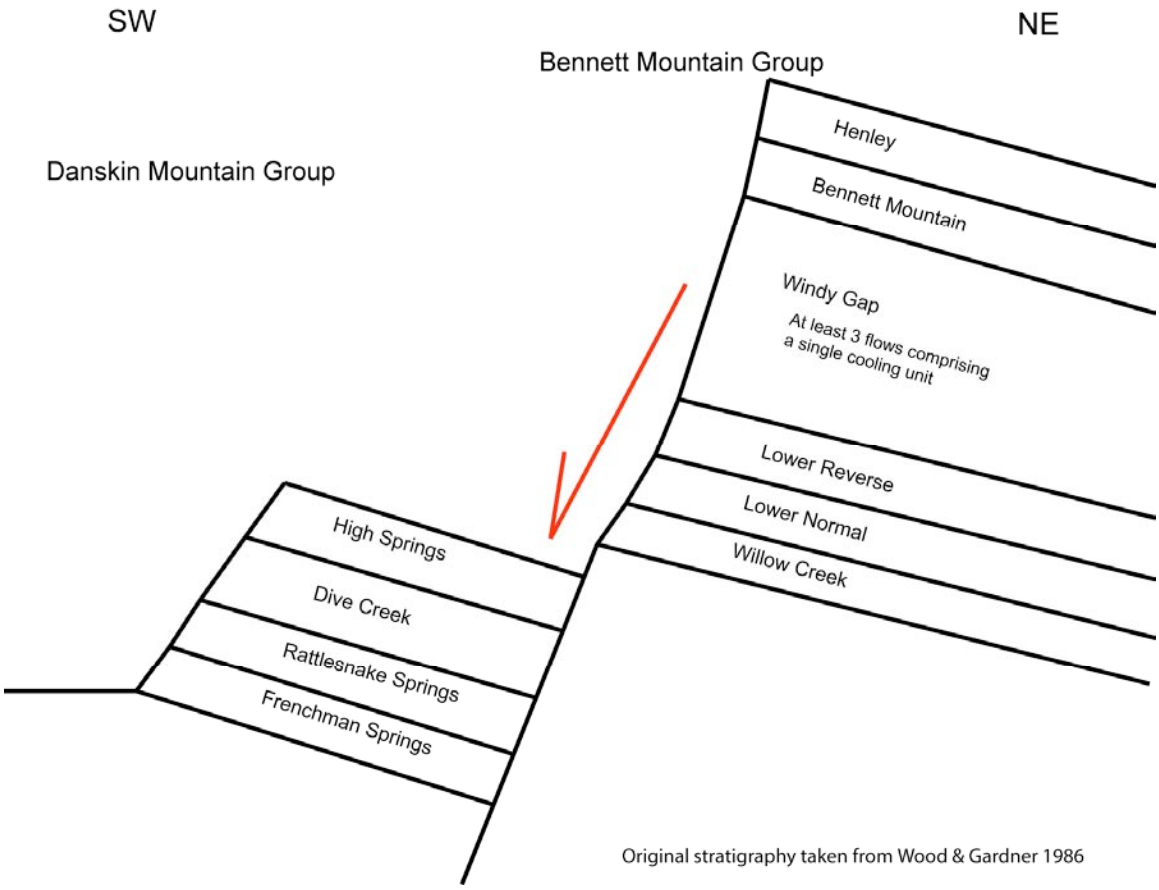

Figure 5: cartoon illustrating the original stratigraphy of the West Bennett Hills rhyolites set forth by Malde et al. (1963) and the stratigraphic relationships of the younger Danskin Group with the older, topographically higher Bennett Mountain Group set forth by Wood and Gardner (1984).

Revised stratigraphy of the West Bennett Hills

The original stratigraphy of the West Bennett Hills (Fig 6) made by Wood & Gardner (1984) requires restructuring after analysis of field relations and geochemistry done for this study. Figure 6 is a diagram of this study's proposed new stratigraphic column for the West Bennett Hills rhyolites. The Danskin Group, originally comprised of four rhyolites (from lowest stratigraphic location to highest: Frenchman Springs (FS), Rattlesnake Springs (RS), Dive Creek (DC), and High Springs (HS)), is condensed to two units, (HS + RS, FS + DC). Frenchman Springs and Dive Creek are both genetically related to the uppermost unit from the Bennett Mountain group, Henley (H). Henley was likely deposited prior to the emplacement of the Danskin group, but is chemically and petrographically identical to the Dive Creek and Frenchman Springs units (Wood and Gardner 1984, Bonnichsen et al., 2008). Because these units were erupted at different times, Henley is not grouped as a part of the Dive Creek + Frenchman Springs erupted unit, but was erupted from the same (or similar source) as the DC + FS unit. The Danskin group's units are repeated via normal down faulting and are combined based on physical and petrographic similarities and geochemical data.

High Springs' and Rattlesnake Springs' physical similarities are easily recognizable in the field: in outcrop scale, both units' stony interiors are prominent cliff formers with vitrophyre often exposed at the base. In hand sample, the best way to discriminate the rhyolites of the WBH is by plagioclase phenocryst size and abundance. For the High Springs and Rattlesnake Springs units, they share identical plagioclase distributions: most crystals are 1 – 2.5 mm in length, and constitute 10-12 percent of the rock. Frenchman Springs, Dive Creek and Henley are sparsely porphyritic (< 5 percent)

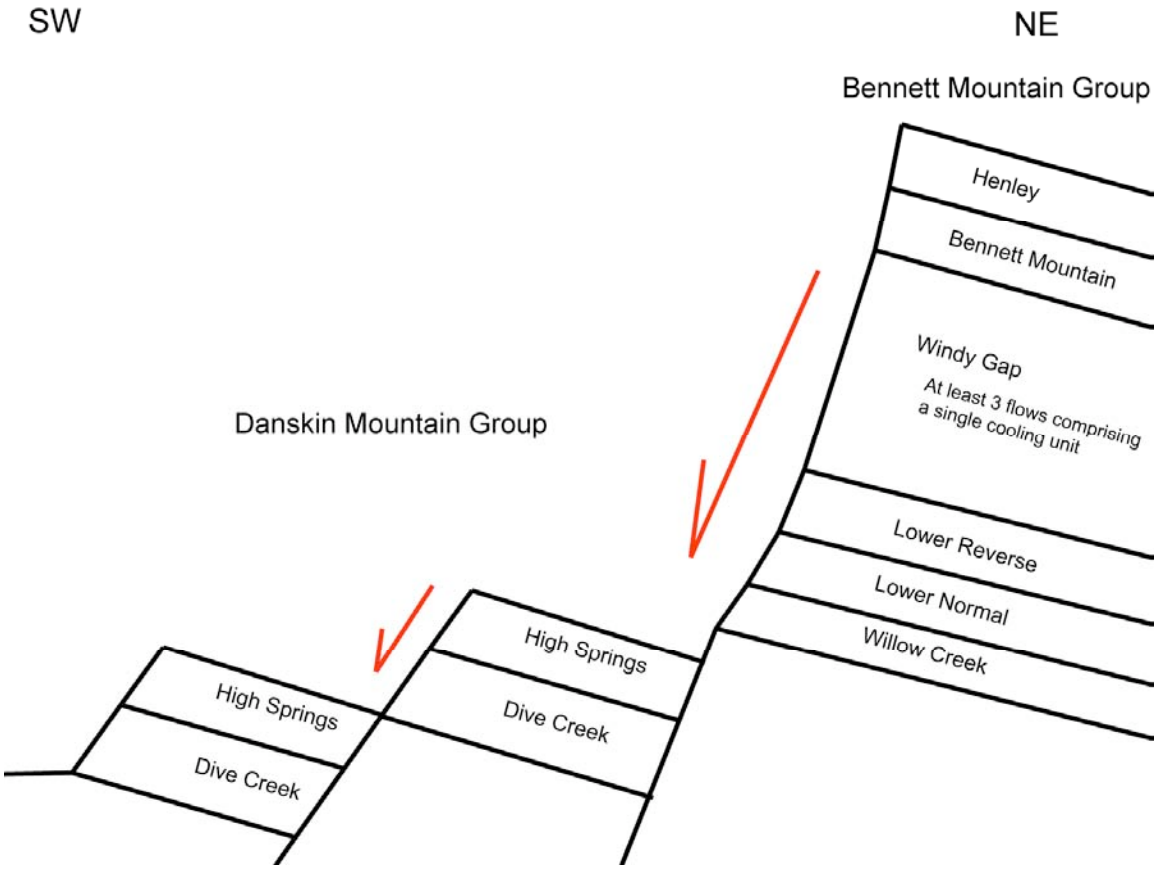

Figure 6: cartoon illustrating the proposed new stratigraphy and structural relations of the West Bennett Hills rhyolites.

and all share the same plagioclase phenocryst distributions: one population consists of crystal shards generally < 1mm across, and the second population consists of large phenocrysts from 2 – 5mm across. Although the Frenchman Springs and Dive Creek outcroppings are not prominent cliff formers like the Henley outcrops at the top of Bennett Mountain, the petrographic and geochemical evidence overwhelmingly supports a correlation for the three units. Bonnichsen et al. (2008) stated that the Henley unit was erupted prior to major faulting in the WBH and the Frenchman Springs and Dive Creek units were erupted following this structural episode, but all three were erupted the same or a similar magma chamber.

Figure 7 is a diagram of whole rock La and Nb concentrations in the previously mentioned units and illustrates the similarities for the HS + RS and FS + DC + H respective correlations, as well as the distinct composition of one group of units from the other. The data chapter of this study has several compositional diagrams that show these units grouped together and compared to units in the southern CSRP. These plots illustrate the distinct compositional trends of these combined units and with very few outliers, and reinforce the physical and whole rock La / Nb concentration evidence presented in this section.

For the reasons explained above, the four units of the Danskin Group will be condensed into two units: High Springs and Rattlesnake Springs will hereafter be referred to as High Springs. Dive Creek and Frenchman Springs will hereafter be referred to as Dive Creek. Although Dive Creek and Henley are separate erupted units, for the purposes of comparison with rhyolites in the southern central Snake River Plain they will be considered as parts of the same genetic unit due to their geochemical similarities.

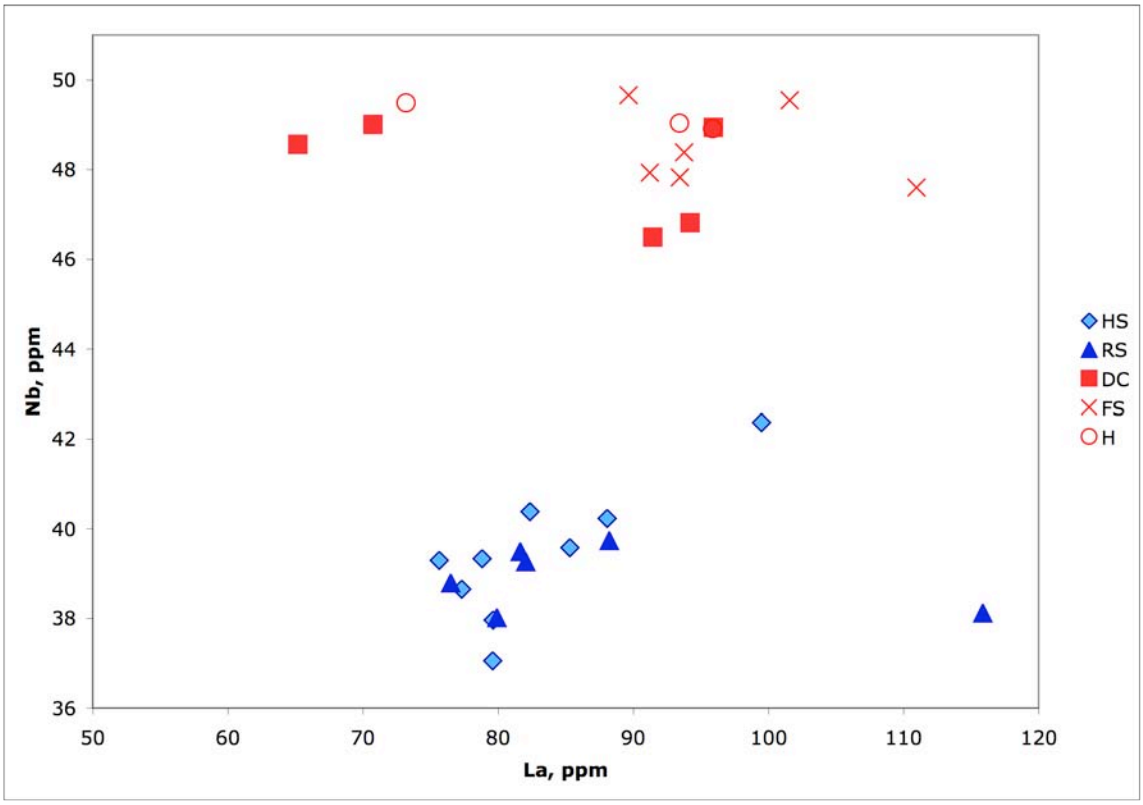

Figure 7: whole rock trace element diagram showing the respective similar compositions for WBH rhyolites High Springs (HS) and Rattlesnake Springs (RS) and Dive Creek (DC), Frenchman Springs (FS) and Henley (H). The size of the individual data points approximate the analytical error.

Lithologic descriptions of the West Bennett Hills rhyolites

The rheomorphic features found in the stony interiors of the WBH rhyolites are fairly uniform throughout all units, and will therefore be described in a general sense. The following facies descriptions are primarily taken from written and spoken communication from Martha Godchaux (2006). These features are widespread throughout the CSRP rhyolites.

The unwelded bases of the CSRP rhyolites usually sit on a reddish-orange baked paleosol layer (thicknesses of paleosols are generally on the scale of 10s of cm) that is rich in glass shards 1 to 3mm across. The paleosol is often overlain by numerous ash layers (thicknesses are generally in the cm's to 10s of cm) sintered to varying degrees from unit to unit.

The base of the rhyolites is a glassy vitrophyre, often showing cm-scale flow folds in the lower portions and weathered to a perlitic texture. Spherulites form close to the boundary with the stony interior varying in size from a few cm to 10's of cm (Fig 8). The boundary between the basal vitrophyre and the stony interior is often gradational with lenses of devitrified rhyolite within the upper portions of the basal vitrophyre increasing in size and abundance as the boundary is approached.

The stony interior is segregated into four separate facies based upon the style of rheomorphic folding found in the vertical location of the unit. The base of the stony interiors is considered the "flat facies" and is characterized by elongate recumbent isoclinal mm- to cm-scale folds that may elongate into sheath folds. This portion of the stony interior often weathers into elongate slabs of flaggy rhyolite which subsequently form prominent talus slopes in many units.

The flat facies lies beneath the “sheath-folded facies”, which is characterized by simple (i.e. formed from a single deformation event) sheath folds. Figure 9 shows an excellent example of a sheath fold from the High Springs rhyolite.

Figure 8: large spherulite contained in the lower vitrophyre of High Springs. Hammer for scale.

Figure 9: example of a sheath fold found in the stony interior of the High Springs rhyolite. Approximate dip of rock surface from this view is 75^{o}. Hammer for scale.

The “chaotic facies” typically lies stratigraphically above the sheath-folded facies and is formed by sheath folds undergoing continuous deformation. Figure 10 shows the typical mm-scale bands forming cm- to 10’s of cm-scale folds in a highly chaotic fashion.

The stratigraphically highest facies within the stony interiors of CSRP rhyolites is the “ramped-up facies”, which is characterized by meter-scale folds which can exhibit chevron-folding in the direction of motion. Figure 11 is a photo of the ramped-up facies within the High Springs rhyolite.

The top of the rhyolites in the CSRP is typically a glassy dense vitrophyre, but the upper vitrophyre can also be pumiceous. Locally, upper vitrophyres of a rheomorphic ignimbrite can exhibit brecciated textures with red colors (caused by oxidized Fe-oxide microlites) swirled in with the black glass. In lava flows, upper breccias are commonplace.

The nature of emplacement (ash-flow tuff or effusive lava flow) of the West Bennett Hills rhyolites could not be determined during field studies, mainly due to limited exposure of the bases of the units. As researchers have noted (Bonnichsen and Kaufman, 1988; Henry and Wolff, 1992), the base of a rhyolite is a crucial portion of the unit that must be well exposed in order to determine whether or not that unit is a high-grade rheomorphic tuff or a lava. Possible mechanisms for empacement of high-T rhyolites include spatter-fed lava flows and syn-depositional agglutination from pyroclastic flows.

Figure 10: example of the “chaotic facies” in the stony interior of the Gray’s Landing ignimbrite. Although this unit is not in the West Bennett Hills, this facies is often found in the WBH rhyolites, though not as spectacularly preserved and exposed. Pencil for scale.

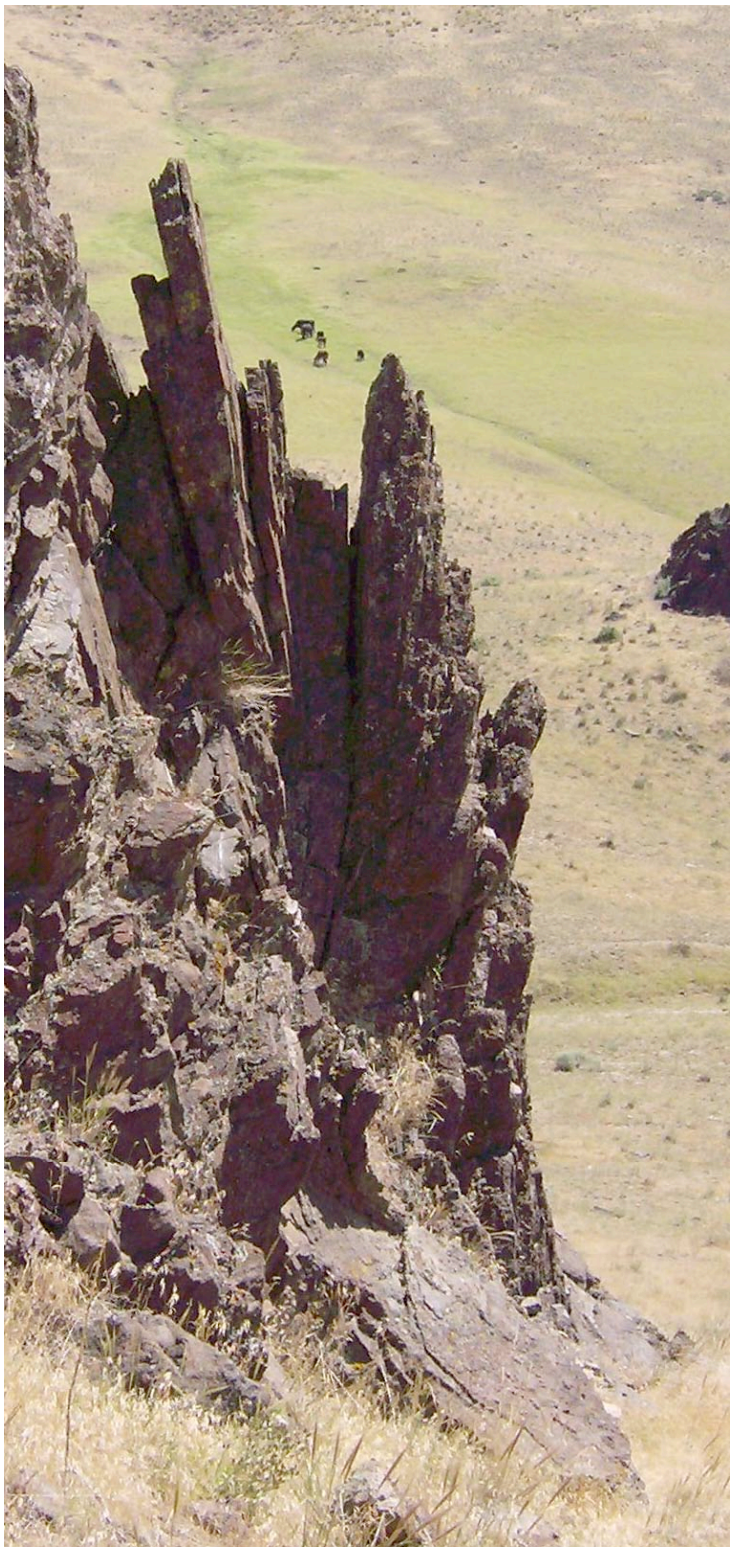

Figure 11: Photograph of a “ramped up” fold in the stony interior of the High Springs rhyolite. Total height of outcrop pictured is ~ 2m.

Individual unit descriptions of the WBH rhyolites

Lithologic and petrographic descriptions and thicknesses of individual units are taken from Wood & Gardner (1984), modified by the author as appropriate.

The Willow Creek rhyolite is a brown moderately porphyritic stony rhyolite with 6-8 percent subhedral to anhedral plagioclase phenocrysts 1.5 – 3 mm in length. Phenocryst assemblage is (in order of relative abundance) plagioclase, < 1 mm long pigeonites, magnetite, ilmenite and accessory apatite and zircon. Willow Creek is only locally exposed in the topographically lowest portions of the Bennett Mountain escarpment, with no basal vitrophyre exposed but a prominent dense black upper vitrophyre. Total exposed thickness is approximately 60m.

The Lower Normal rhyolite is a gray to purplish-gray porphyritic rhyolite containing 8-10 percent euhedral to subhedral plagioclase crystals with two populations: the majority (~75 percent) of plagioclase phenocrysts are 1-3mm in length, and the second population contains large crystals (up to 5mm in length) with glass inclusions in the cores. The phenocryst assemblage is listed in order of decreasing abundance: plagioclase, < 1 mm long pigeonites, magnetite and ilmenite with apatite and zircon as accessory phases. Dense, glassy black vitrophyre can be found at the top and bottom of the Lower Normal rhyolite. Stony interior forms prominent cliffs. Total thickness ranges from 60 to 120m.

The Lower Reverse rhyolite is a gray devitrified moderately porphyritic (5-7 percent) rhyolite with dense, black glassy basal vitrophyre and locally exposed upper vitrophyre. Phenocryst assemblage is, in order of decreasing abundance, subhedral to anhedral plagioclase crystals 1-3mm in length, < 1 mm long pyroxenes, magnetite,

ilmenite and apatite and zircon accessory phases. The stony interior portions form prominent cliffs. Total thickness is up to 100m.

The Windy Gap rhyolite is a series of at least three separate flows, all included as a single cooling unit. The rhyolite is light grayish-purple in the interior devitrified portions, and is sparsely porphyritic (<5 percent) with plagioclase phenocrysts ranging from 1.5 to 5mm across, pigeonite and augite <1mm across, sanidine, magnetite and ilmenite, rare quartz, apatite and zircon as accessory phases. The flows are separated by prominent vitrophyre layers 5 to 10m high. Stony portions are prominent cliff formers. Total thickness of the Windy Gap is as much as 360m.

The Bennett Mountain rhyolite is a gray-brown moderately porphyritic devitrified rhyolite with variable exposure of vitrophyre. Wood and Gardner (1984) stated that the unit always has a basal vitrophyre associated with the stony interior, but field investigations showed that a basal vitrophyre is only locally exposed, as is the upper vitrophyre. The phenocryst assemblage has small subhedral to anhedral plagioclase crystals generally <2mm across, <1mm long pigeonite, magnetite and ilmenite and apatite and zircon as accessory phases. Wood and Gardner (1984) mapped the Bennett Mountain rhyolite as a continuous unit that always separates the Windy Gap unit from the uppermost unit on the Bennett Mounain escarpment, the Henley rhyolite. The rhyolite of Bennett Mountain outcrops in the northern, topographically higher portion of the Bennett Mountain escarpment, and underlies the Henley rhyolite. Field work in the lower portion of the Bennett Mountain escarpment 5.5 km to the southwest of the location where samples 06WS-063 and 065 were obtained (Appendix J) reveals that the Bennett Mounain rhyolite must thin and eventually pinch out at some point along the escarpment,

as no outcropping of the Bennett Mountain rhyolite was found between Windy Gap and Henley. Total thickness of this unit never exceeds 17m.

Henley, Frenchman Springs and Dive Creek all share similar hand sample petrography: purplish-gray devitrified rhyolite with sparse phenocrysts (<5 percent). Phenocryst assemblage is as follows: subhedral to euhedral plagioclase phenocrysts that range from 1mm to 5mm across; many of the larger plagioclase crystals exhibit mottled cores with glass inclusions. Augites <1mm long, sanidine, rare quartz, magnetite and ilmenite and apatite and zircon accessory phases constitute the rest of the phenocryst assemblage. Upper and lower vitrophyres are only locally exposed; no continuous outcroppings were found.

The base of the Frenchman Springs unit is locally exposed as a breccia. Angular brecciated fragments range in size from 1mm to >30cm (Fig 12) and are darker in color than the surrounding red-gray host groundmass. Some brecciated fragments have prominent mm- to cm-scale vesicles. Phenocryst assemblage appears to be the same for both fragments and host groundmass, indicating that this is an auto-breccia.

There are significant differences between the Henley unit and Frenchman Springs and Dive Creek units with regard to their physical weathering characteristics. Henley forms prominent cliffs up to 15m high on the top of the Bennett Mountain escarpment, whereas the topographically lower Frenchman Springs and Dive Creek only locally form small cliffs that do not exceed 3m in height. Thickness of Henley never exceeds 65m, and the thickness of Frenchman Springs + Dive Creek is as much as 260m.

The High Springs and Rattlesnake Springs rhyolites share identical petrographic characteristics. They are brown to gray stony rhyolites with abundant phenocrysts (10-15

percent) of subhedral to euhedral plagioclase crystals 1-2.5 mm in length, sanidines 1- 2.5 mm in length, <1mm long pyroxenes (both augite and pigeonite composition), uncommon quartz, magnetite and ilmentite and apatite and zircon accessory phases. These units both form prominent cliffs 10-15m high and commonly preserve fresh basal vitrophyre below the cliffs. Local upper vitrophyres can also be found, but are not as common as basal vitrophyres. Upper vitrophyres often show red and black colored slightly vesicular textures. The base, where exposed, is a non-welded deposit of black vitrophyre blocks in an ash matrix overlying a series of layered ash beds, which in turn lies over a reddish-orange baked paleosol (Fig 13a - c).

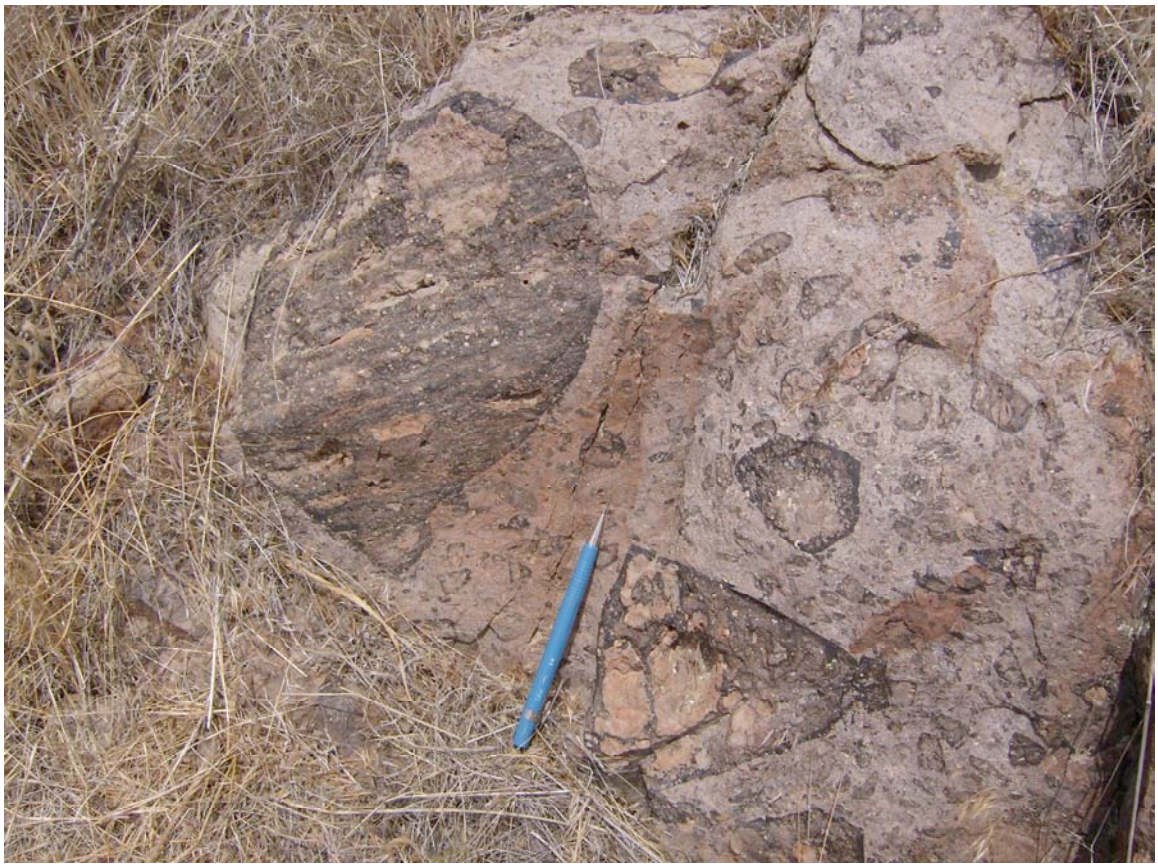

Figure 12: photo of the basal breccia of the Dive Creek rhyolite, showing the range of clast size (mm- to 10's of cm-scale), variations in roundness from angular to sub-rounded and presence of vesicles in many clasts. Pencil for scale.

Figure 13a: unwelded base of High Springs, showing black vitrophyre blocks in an unwelded ash matrix. Hammer for scale.

Figure 13b: unwelded base of High Springs. A lens of the red-colored baked paleosol is present in the bottom central portion of the photo. Layered ash beds overly this paleosol (gray and beige layers). The upper portion of the base is an unwelded breccia of black vitrophyre clasts in an unwelded ash matrix. Hammer for scale.

Figure 13c: photo showing 10s of cm-scale deformation of the layered ash beds in the unwelded base of the High Springs rhyolite. Hammer for scale.

Relationship of the WBH rhyolites with the CAT groups

The CAT groups of Bonnichsen et al. (2008) are the result of an initial attempt at a coherent stratigraphy for the CSRP rhyolites. The West Bennett Hills rhyolites occupy a unique position in these CAT groups because they are the only manifestation of exposed northern CSRP rhyolites that were emplaced during the eruptive center's most active phase. As stated in the geologic background portion of this study, there are three main phases of volcanism in the CSRP, but the designation of the CSRP rhyolites into CAT groups allowed Bonnichsen et al. (2008) to further subdivide the evolution of rhyolitic magmatism in the CSRP into stages A thru F. To avoid confusion with terminology used in the geologic background section, these evolutionary stages will be referred to as "sub-stages" in this study. The CAT groups are discussed below in order from oldest to youngest. The specific characteristics of each CAT group (age ranges, TiO_2 compositions and magnetic polarities) can be found in Table 1.

The units from CAT group 3 that are included in this study are the CSRP units CPT VII, BBU 3, and the WBH rhyolite Willow Creek. CAT group 3 signifies the end of sub-stage A (13.0 – 11.7 Ma) in the evolution of rhyolitic volcanism in the CSRP and is characterized by eruption centers located in the western portion of the CSRP. Sub-stage A culminated in the large explosive eruptions that formed the voluminous CPT VII unit and its possible correlatives to the east (BBU 3), west (Buckhorn ignimbrite) and north (Willow Creek). The volumes erupted suggest that significant crustal subsidence occurred following the eruptions, likely resulting in formation of now buried calderas (Bonnichsen et al., 2008).

The units in CAT group 4 are CPT IX, BBU 4 (both in the CSRP) and Lower Normal (in the WBH). CAT group 4 is the beginning of sub-stage B (11.7 to 11.0 Ma), which saw the progression of eruptive centers begin to move east into the middle of the CSRP as well as the coeval eruption of (chemically non-related) rhyolites along the Owyhee Front and in the southern margin of the WSRP graben (Bonnichsen et al., 2008).

CAT group 5 contains the units CPT X, CPT XI, and the WBH rhyolites Windy Gap and Lower Reverse. CAT group 5 is in the middle of sub-stage B, during which the voluminous units erupted (specifically CPT XI) undoubtedly caused crustal subsidence and caldera formation(s) in the western and middle portions of the CSRP (Bonnichsen et al., 2008).

CAT group 6 includes the CSRP unit CPT XII and the WBH unit Bennett Mounain. CAT group 6 signifies the end of sub-stage B. The units of this CAT group are generally more mafic in composition than the previous CAT groups covered, which could be a product of basaltic magma recharging the earlier magma system. CAT 6 also has the first rhyolite lava flows in the CSRP, the Black Rock Escarpment and Marys Creek flows (Bonnichsen et al., 2008).

CAT group 7 contains the CSRP units CPT XIII, BBU 7, lower Jackpot (referred to as Jackpot 1-6 in Bonnichsen et al., 2008), the tuff of Big Bluff and the WBH unit FS + DC + H. CAT group 7 signifies the beginning of sub-stage C, where volcanic centers continued their eastward progression in the CSRP (Bonnichsen et al., 2008).

CAT group 8 is split into two sub-groups, 8a and 8b. The distinction lies in compositional differences between the more mafic units in 8a and CPT XV's slightly more silicic composition. The units in 8a are the SCSRP rhyolites Steer Basin, Jackpot 7,

BBU 8 and the WBH unit HS + RS. The only unit in 8b is CPT XV. CAT group 8 signifies the end of sub-stage C. The timing of eruptions during this sub-stage implies that the source calderas were formed in piecemeal fashion (Bonnichsen et al., 2008).

Chapter 3: Data

Methods and Sampling

Samples were collected from the ten rhyolite units of the West Bennett Hills (WBH) and fifteen rhyolite units of the southern Central Snake River Plain (SCSRP). SCSRP units were selected for analysis and comparison based on their assignments in the "composition and time" (CAT) groups of Bonnichsen et al. (2008). The CAT Groups are an initial attempt to provide a coherent stratigraphic framework for the rhyolites of the CSRP and are based on radiometric ages, whole rock major element compositions, magnetic polarity, and stratigraphic sequences. See Table 1 for CAT Group designations for the WBH and SCSRP rhyolites in this study.

Whole rock major and trace element abundances were determined by x-ray fluorescence (XRF) and inductively coupled plasma source mass spectrometry (ICPMS) using the respective methods of Johnson et al. (1999) and Knaack et al. (1994). Hand sample selection in the field was based on the freshest (i.e. unweathered) rocks available. Further removal of weathered material was done during the crushing stage of sample preparation for XRF and ICPMS.

Only fresh vitrophyre samples were used to collect microanalytical data (microprobe and LA-ICP-MS) because the devitrified portions of the rhyolites had weathered pyroxenes.

Microprobe data was collected from a single thin section from each unit sampled, with the exception of the following units in the SCSRP: CPT XV (3 samples), CPT XIII (2 samples), and CPT XII (3 samples). All microprobe analyses were performed on a Cameca Camebax at Washington State University. Pyroxenes and feldspars were

analyzed using the following parameters: beam energy = 15 keV, beam current = 15 nA and beam diameter = 4μm. Fresh glass was analyzed using the following parameters: beam energy = 15keV, beam current = 15 nA, and beam diameter = 10μm. Fe-Ti oxide pairs were analyzed for thermometry calculations using the following parameters: beam energy = 20 keV, beam current = 16.22 nA, and beam diameter = 2μm. All microprobe analyses operated with a 40^{o} takeoff angle. Detection limits for the Cameca Camebax are generally 300ppm, or 0.03 weight percent. Analytical errors on all analyses are +/- 2 percent relative.

Trace element abundances in pyroxenes and glasses were obtained via the laser ablation ICPMS (LA ICPMS) method described by Olin (2007). The WSU GeoAnalytical Lab uses a ThermoFinnigan Element2 ® high resolution ICP-MS coupled to a New Wave UP213 Nd:YAG laser to perform LA-ICP-MS analyses. The sample is ablated and delivered to the mass spectrometer by a constant flow of He gas, merging with an Ar gas stream and ionized in the plasma once the sample is inside the mass spectrometer. Internal normalization is necessary to account for matrix, drift and sample volume problems. This is achieved by having prior knowledge of the concentration of at least one element naturally occurring in both sample and standard. For this study, SiO_2 abundance for every sample was collected by microprobe analysis prior to LA-ICP-MS analysis. This known concentration is then used to normalize the raw data in counts per second (cps) and to calculate elemental concentrations. Background levels are established by scanning with the laser running and the shutter closed for 20 seconds prior to sample ablation. Ablation analyses last for approximately 2 minutes apiece, yielding ~25 scans of 32 selected elements for each analysis.

The following parameters were used for both glass and pyroxene analyses: beam width = 16 μm, scan speed = 6 μm/s, trough length = 600 μm (approximate). The following parameters were used for feldspar analyses: beam width = 30 μm, scan speed = 12 μm/s with trough length = 1100 μm (approximate). Parameters used for analyzing BCR-2g standards are: beam width = 20 μm, scan speed = 11 μm /s and trough length = 1100 μm. Universal parameters for LA-ICP-MS analyses in this study are as follows: laser warm up time = 20s, on delay = 0s, laser frequency = 20 Hz, and laser output = 70-75 percent. All LA analyses were performed by ablating a trough rather than a pit to avoid inclusions unseen below the surface. Trace element-rich accessory phases such as zircon, apatite, allanite and chevkinite are often found as inclusions in phases, and would impart a signature that is not representative of the phase being analyzed. It is therefore crucial to avoid these different phases when performing LA-ICP-MS analyses. Another important reason for ablating a trough as opposed to a pit in trace element analyses is the issue of inter-element fractionation, which becomes problematic as the depth of sample ablated becomes greater than the width of the ablated sample.

Offline data reduction is performed in Microsoft Excel. The user selects suitable background and sample scans and spurious data is removed from each scan. An analysis with <15 quality scans is used with caution and an analysis with <8 scans is discarded. Background counts are then subtracted from sample counts, and the resulting data is internally normalized using predetermined Si abundance from microprobe analyses and compared to ^{29}Si cps from the laser data. A basaltic whole rock glass standard, BCR-2g, is used to calibrate elemental abundances. This method is generally accurate to ~10ppm and maximum errors are 5 percent relative to elemental abundance.

Oxygen isotope ratios were collected on several WBH units, analyzing handpicked feldspar phenocrysts from fresh vitrophyres at the Washington State University stable isotope lab. Feldspar crystals were selected based on physical integrity; crystals displaying extensive fracturing, weathering, and/or iron oxide staining were avoided. Oxygen isotopes were extracted using 2-4 mg of sample using laser fluorination and analyzed on a Finnigan Delta S mass spectrometer using the method of Sharp (1990). Oxygen isotope data was normalized to a value of $\delta^{18}O = 5.8‰$ versus Vienna Standard Mean Ocean Water (VSMOW) from the UWG-2 standard (Valley et al., 1995). Standards were generally analyzed every third sample for the units analyzed. Please see Appendix I for details on the order of analyses. Feldspar values are assumed to represent magmatic values (Taylor, 1979) and are reported as per mil (‰) $\delta^{18}O_{VSMOW}$.

Petrogenesis

The whole rock data for the WBH rhyolites reveals a petrogenesis that is essentially similar to the CSRP rhyolites as described by Cathey and Nash (2003) and Boroughs et al. (2005). The rhyolites' chemistry is typical of A-type continental rhyolites (SiO_2 values of 70 to 76 weight percent) with the exception of high large ion lithophile elements (LILE) abundances (Figures 14 a and c), specifically Rb, Th and U (Whalen et al., 1987; Patino Douce, 1997). Typical A-type rhyolites are regarded as being products of deep crustal melting of granulitic meta-igneous source rocks that were previously depleted in hydrous felsic melt, and should exhibit significant depletions in LILE (Whalen et al., 1987; Eby, 1990). Patino Douce (1997) proposed an alternative mechanism for A-type magma generation invoking melting of calc-alkaline granitoid

source material over a range of pressures (8 kbar to 4 kbar; consistent with the mid-crust) with plagioclase and orthopyroxene as residual phases. The CSRP rhyolites show depressed Al, Ca, Eu and Sr contents (Figs 14 a and b), as well as high K/Na, TiO_2/MgO and Ga/Al ratios (Figs 15a – d), all of which are consistent with the residue described by Patino Douce (1997). Low Eu and Sr abundances relative to other incompatible trace elements and a negative SiO_2 / Sr correlation indicates plagioclase fractionation during magma genesis (Figs 14 a, b, d).

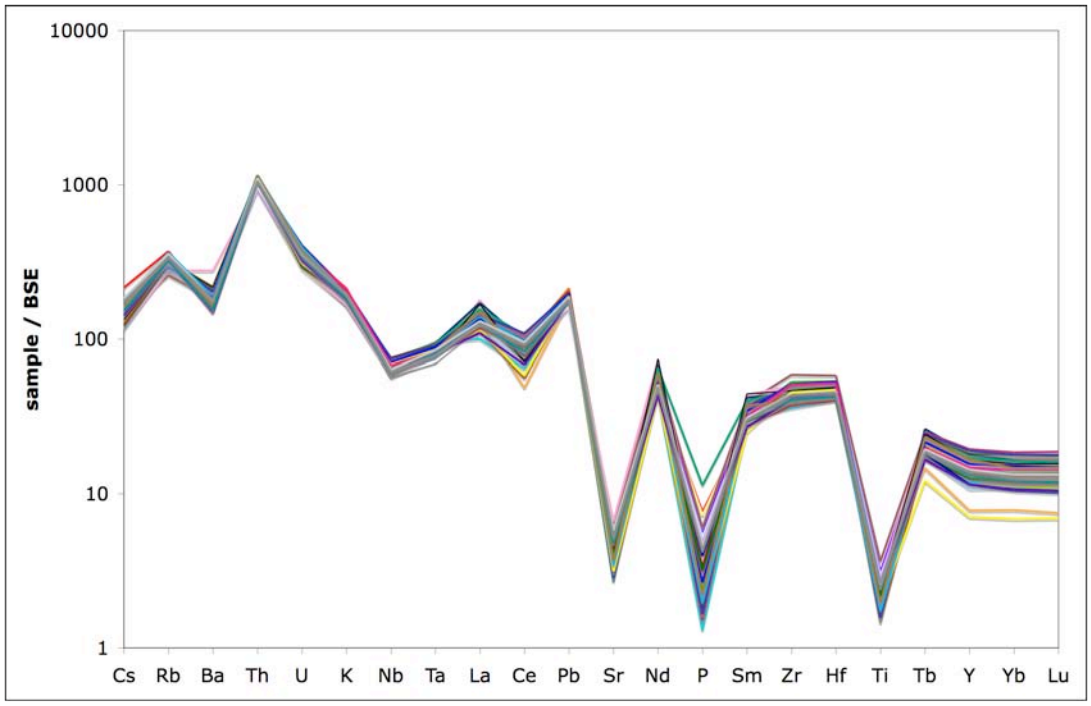

Figure 14a: trace element diagram showing depleted Sr and enriched Rb and Th concentrations for all WBH samples in this study. All samples normalized to bulk silicate earth values (BSE) from McDonough and Sun, 1995.

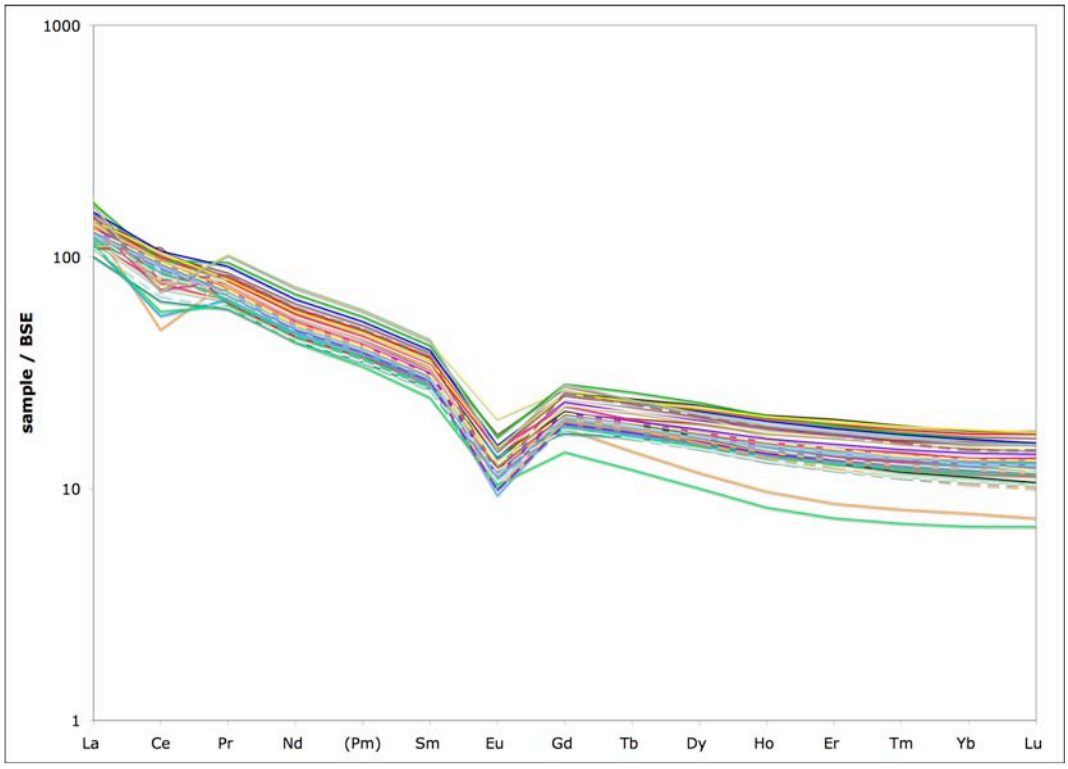

Figure 14b: REE diagram showing a negative Eu anomaly for all samples and a negative Ce anomaly for some samples. All samples normalized to BSE (McDonough and Sun, 1995).

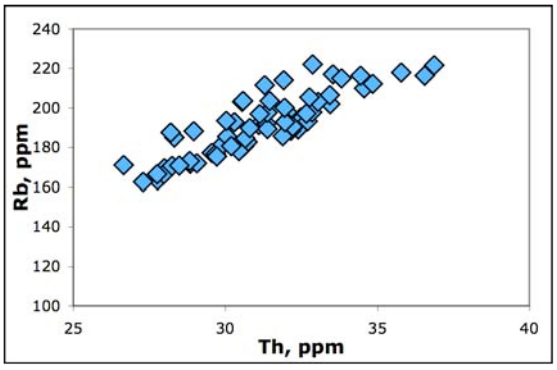

Figure 14c

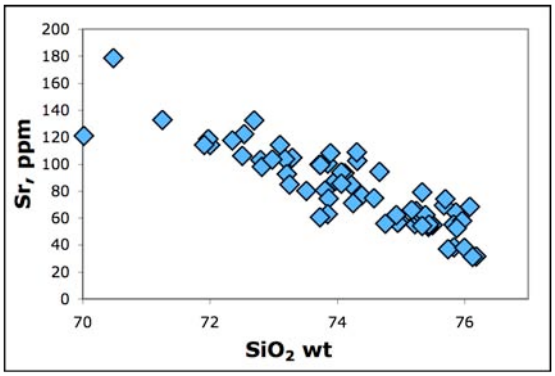

14d

Figure 14 c: Th vs Rb displaying elevated LILE abundances indicative of shallow melting of source material (Chapter 3, this study). 14 d: SiO_2 vs Sr showing a strong negative trend indicating plagioclase fractionation during magma genesis.

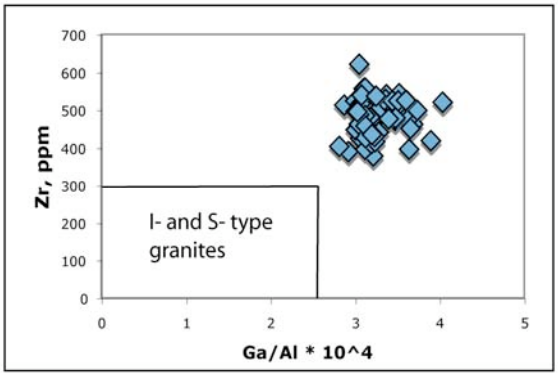

Figure 15 a

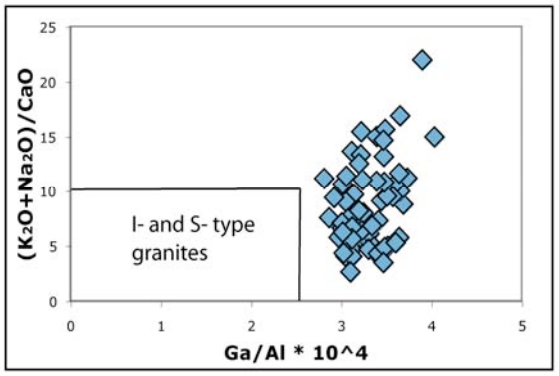

15 b

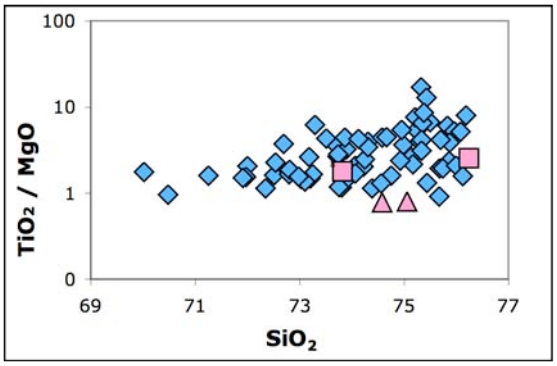

15 c

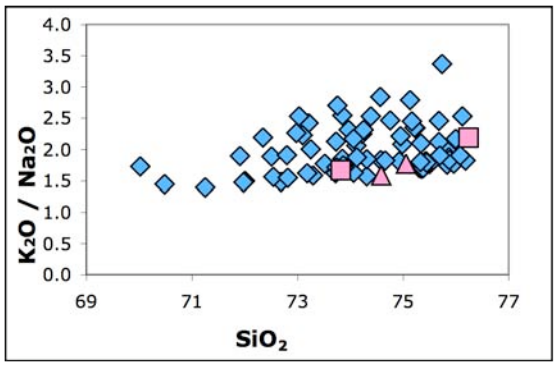

15 d

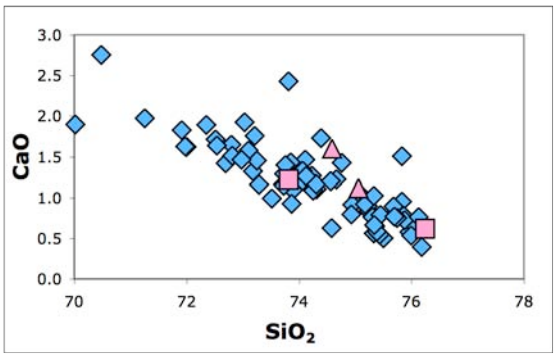

15 e

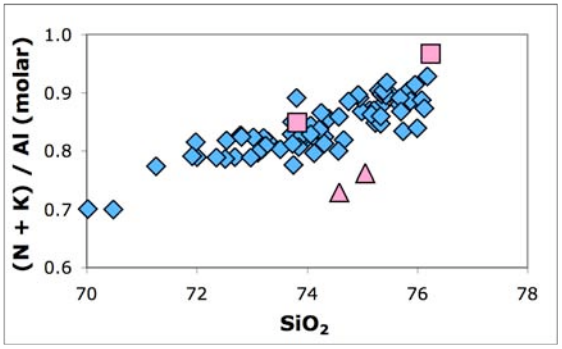

15 f

Figure 15: Major and trace element abundances displaying shallow melting characteristics:

A and B) West Bennett Hills rhyolites plotted on A-type magma discrimination diagrams from Whalen et al, 1987. C thru F) West Bennett Hills rhyolites plotted with experimental data from Patino Douce, 1997. Pink boxes represent experimental results at 4 kbar, pink triangles represent experimental results at 8 kbar.

Ce anomaly

While the bulk of the WBH rhyolite samples analyzed display rare earth element (REE) patterns that are similar to the majority of continental rhyolites (Fig 14 b), at least one sample of every unit (except Willow Creek) displays a noticeable negative cerium anomaly (Fig 16), and one sample from the Dive Creek unit with a strong positive Ce anomaly (Ce/Ce* = 1.28). For the purposes of this study, we define a cerium anomaly as Ce/Ce* is less than 0.8 or greater than 1.2, where $Ce^* = (La_N + Pr_N)/2$. An important feature of these samples with significant Ce/Ce* values is that they are all samples of stony rhyolite flow interiors. Fractionation of Ce from neighboring rare earth elements implies that some of the Ce is present as the +4 ion, which requires oxygen fugacities higher than magmatic values (Bilal and Mueller, 1992).

Although the Ce anomaly is present in most of the units of the WBH, there are two strong lines of evidence against this signature having a magmatic origin. The first of which is that there is no evidence of zircon fractionation affecting Ce when Ce/Ce* is plotted against Zr and Zr/Hf (Fig 17 a and b). Zr and Hf are tetravalent cations, and as discussed previously, Ce can also be tetravalent. Even though Ce^{4+}'s ionic radius (0.87Å for CN = VI, 1.00 Å for CN = VIII) is noticeably larger than both Zr^{4+} (0.72 Å for CN = VI, 0.84 Å for CN = VIII) and Hf^{4+} (0.71 Å for CN = VI, 0.83 Å for CN = VIII), it is still compatible in zircon. The second is a lack of consistent Ce anomalies in all samples from the units analyzed. This indicates that the Ce anomaly is caused by a post-magmatic process, but could still involve the crystallization of an accessory phase (or phases) during devitrification. This scenario of an accessory phase controlling Ce values is somewhat encouraged by Figures 17 c and d, which show a weak correlation with Th and

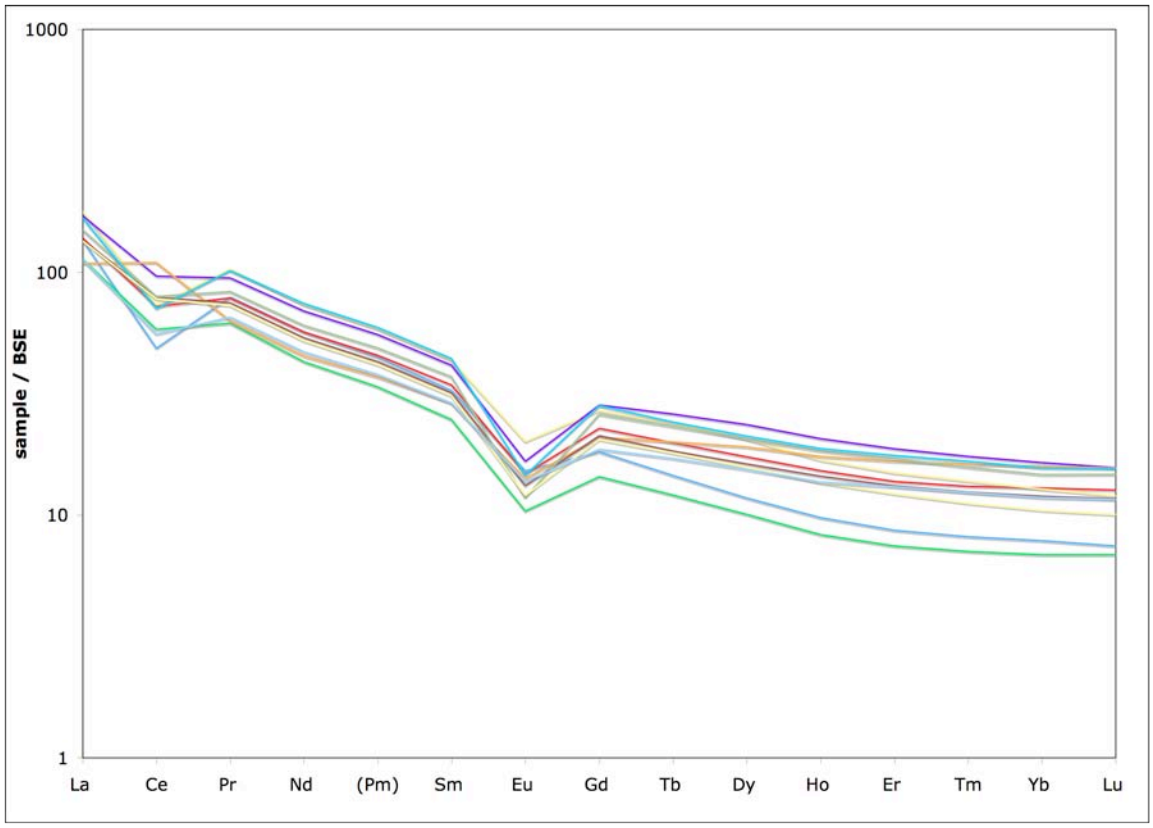

Figure 16: REE diagram of West Bennett Hills (and two SCSRP) samples with prominent Ce anomalies. Note the sample with a positive Ce anomaly. All samples normalized to BSE (McDonough and Sun, 1995).

U values. Ionic radii for the three cations are nearly identical (Ce^{4+} = 0.87Å for CN = VI, 1.00 Å for CN = VIII; Th^{4+} = 0.94 Å for CN = VI, 1.05 Å for CN = VIII; U^{4+} = 0.89 Å for CN = VI, 1.05 Å for CN = VIII), so an accessory phase rich in U and Th would be likely to accept Ce^{4+} and therefore impart a noticeable signature on the whole rock composition.

Patino et al. (2003) describe variable REE values, including prominent Ce/Ce* anomalies in basaltic rocks from tropical climates where the heavily weathered rind is preferentially stripped of REE^{3+} elements by fluids. As previously stated, Ce is known to change to a 4+ valence state in oxidizing environments and in its quadrivalent state is not as soluble as the REE^{3+} elements. When the relatively REE^{3+}- rich fluids travel to the less altered interior corestones, the concentration of Ca^{2+} and Na^{+} ions increase in the solution after leaching them from the fresher rock materials. This causes the pH of the weathering solution to increase, facilitating precipitation of the REE^{3+} elements out of the fluid (Patino et al., 2003, and references therein). The result of this process leaves the corestones with an enriched REE^{3+} signature and a relatively low Ce abundance, while the exterior rocks display a depleted REE^{3+} signature and a strong positive Ce anomaly (Patino et al. 2003).

Apart from the presence of the Ce anomaly, there are few similarities between Patino et al.'s data and the WBH rhyolites. Patino et al.'s (2003) study involves basaltic rocks weathering in wet, tropical climates immediately adjacent to oceans (Hawaii and Guatemala), whereas the rocks of this study are rhyolites that are in a semi-arid, temperate environment located in the interior of a continent. Another concern is the REE^{3+} signature of the WBH samples with low Ce anomalies: according to Patino et al.'s

(2003) study, trivalent REEs should be enriched in the samples with low Ce anomalies. Although some samples show this relationship quite well, most only show a depletion in Ce abundance without any addition of trivalent REEs (Fig 16). Furthermore, there is only one sample out of 47 whole rock analyses that displays a prominent positive Ce anomaly (WS 007 of the Dive Creek unit). If the process that Patino et al. (2003) described is occurring in the WBH rhyolites, there should be multiple samples with positive Ce anomalies in addition to the samples with negative Ce anomalies. However, it is possible that samples with positive Ce anomalies were rejected due to their high degree of visible weathering. The subjectively-assessed degree of weathering of the samples showing Ce anomalies is variable, and no trends can be found relating the extent of weathering to the extent of the Ce anomaly both in terms of physical appearance and in quantitative data such as a plot of Na_20 / K_20 vs Ce/Ce* (Fig 17 e). Na_20 / K_20 values are a good indicator of chemical weathering because Na^+ and K^+ are both highly soluble, and if the anomalous Ce values were caused by weathering, there would likely be a strong correlation between the two values. A weak correlation has been found between low Ce abundance and negative Ce anomaly (Fig 17 f), which indicates Ce mobility is involved in the anomalous Ce values. Ce oxidation is likely in the stony rhyolite interior of densely welded ignimbrites.

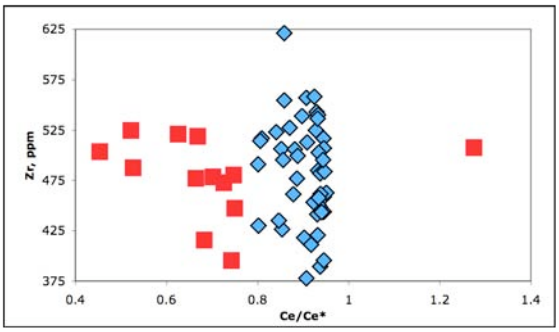

Figure 17 a

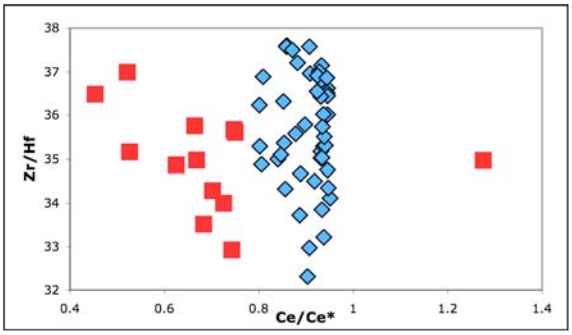

17 b

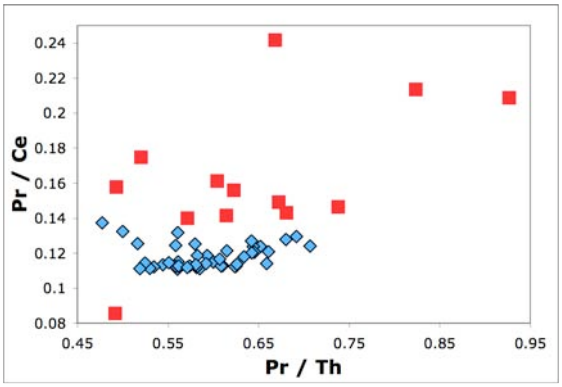

17 c

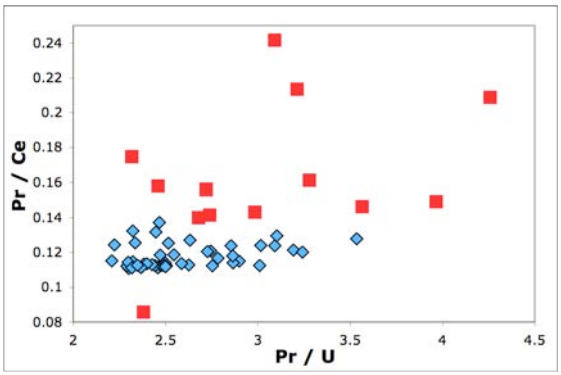

17 d

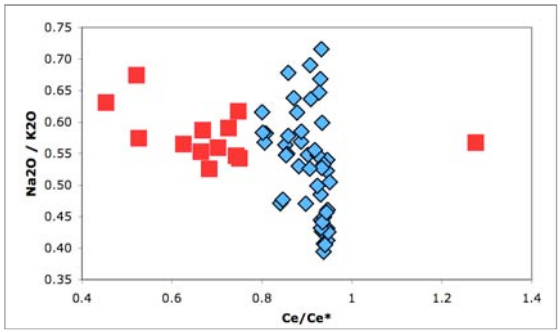

17 e

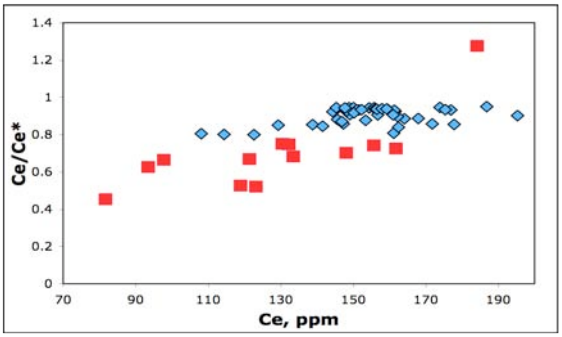

17 f

Figure 17: blue diamonds are WBH + SCSRP samples with normal Ce/Ce* values (1.0 +/- 0.2), red boxes are samples with anomalous Ce/Ce* values. Ce/Ce* vs Zr (a), Ce/Ce* vs Zr/Hf (b) plots showing no relationship between Ce/Ce* and zircon fractionation. Pr / Th vs Pr / Ce (c) and Pr / U vs Pr / Ce (d) showing faint relationship with U and Th abundances. Ce/Ce* vs Na_2O / K_2O (e) showing no relationship between Ce/Ce* and weathering. Ce, ppm vs Ce/Ce* (f) shows a weak correlation between low Ce abundances and Ce/Ce* values.

Stable Oxygen Isotope Ratios

Boroughs et al. (2005) established the central Snake River Plain as one of the world's largest centers of low-$\delta^{18}O$ magma, and coupled with the studies of the low-$\delta^{18}O$ magmatic signature for some units in the Yellowstone Volcanic Plateau (Hildreth et al, 1984, 1991; Bindeman and Valley, 2001; Bindeman et al, 2001), the Yellowstone hotspot track constitutes an impressive collection of low-$\delta^{18}O$ magma. One of the most significant findings in a study by Boroughs et al. (2005) was that all units analyzed in the CSRP were severely depleted in $\delta^{18}O$ as opposed to the low-$\delta^{18}O$ rhyolites of Yellowstone, which are intercalated with normal-$\delta^{18}O$ signature rhyolites (Hildreth et al, 1984). This oxygen isotope signature of the CSRP, assuming it extends to all rhyolites in the area, coupled with a minimum estimate for silicic volcanism in the CSRP from Boroughs et al. (2007) yields at least 20,000 km^3 of erupted low-$\delta^{18}O$ magma.

The rhyolites of the West Bennett Hills were analyzed for oxygen isotopes in order to better constrain the volume of low-$\delta^{18}O$ magma erupted in the CSRP by determining the northern extent of the low-$\delta^{18}O$ signature. Table 2 shows all analyses of $\delta^{18}O$ values from WBH feldspars. The data conforms well with Boroughs et al's (2005) findings: all units analyzed are severely depleted ($\delta^{18}O < 3$ ‰ vs VSMOW) and fall within the range of -1 to 3 ‰.

Oxygen isotope data is a key requirement for a correlation study of the CSRP rhyolites; unless all units in the West Bennett Hills have a significant depletion in $\delta^{18}O$ values, there is no possibility of correlation to units in the SCSRP. On a basis of unit-to-unit correlation, it is not certain whether or not oxygen isotopes may be a useful tool.

There are very few units with negative $\delta^{18}O$ values (Boroughs et al., 2005), and as such any units in the same CAT group that have a negative $\delta^{18}O$ value could indicate a possible correlation. Use of oxygen isotope data as a correlation tool in the CSRP should remain a limited one until a study of oxygen isotope data can be completed that tracks the $\delta^{18}O$ values of a widespread rhyolite over a large area. This is due to the fact that the possibility of zoning of $\delta^{18}O$ values in a widespread rhyolite of the CSRP has not been investigated. The oxygen isotope data collected for this study indicates variations in excess of 0.5‰ occur in a single hand sample (Table 2), so variations across 10s of kilometers should be investigated before oxygen isotopes are used as a correlation tool in the CSRP.

Unit	$\delta^{18}O$ feldspar, VSMOW
High Springs	1.93
High Springs	1.77
Rattlesnake Springs	1.76
Rattlesnake Springs	2.08
Dive Creek	1.78 *
Dive Creek	2.56 *
Frenchman Springs	1.23
Frenchman Springs	2.35
Windy Gap (upper flow)	0.83 *
Windy Gap (upper flow)	1.52 *
Windy Gap (middle flow)	2.34 *
Windy Gap (middle flow)	1.79 *
Lower Normal	-0.42 *
Willow Creek	0.82
Willow Creek	0.77

Table 2: oxygen isotope data for the WBH rholites. All values are reported as per mil versus VSMOW. Errors for all samples are +/- 0.2 per mil except for samples marked with *, which have errors of +/- 0.5 per mil.

Microprobe data

Microprobe analyses were done on one vitrophyre sample from each rhyolite in the WBH with the exception of Lower Reverse and Dive Creek due to a lack of fresh material in the field. The lack of samples from these units is remediated by the fact that Dive Creek is correlative to Frenchman Springs and Henley, and that Lower Reverse is in the same CAT group as the Windy Gap rhyolite. Pyroxenes, feldspars and fresh glasses were the phases analyzed.

Pyroxenes

Two pyroxene compositions are present in the WBH rhyolites (Fig 18a): augite (found in Rattlesnake Springs, High Springs, Frenchman Springs, Henley and Windy Gap) and pigeonite (found in all units except Frenchman Springs and Henley). All pyroxene crystals were analyzed at both the core and rim of the grain, with no evidence of major-element zoning in any crystal from any sample analyzed. Similar to the pyroxene compositions for the Cougar Point Tuff (CPT) rhyolites described in Cathey and Nash (2003), the FeO, CaO, and MgO contents of WBH pyroxenes define a trend of distinct compositional modes in a linear array (Figs 18b and 18c). Most of the WBH rhyolites analyzed displayed the multi-modal pyroxene trend found in many of the CPT units to varying extents; some units, most notably Rattlesnake Springs + High Springs, show variations in pigeonite of up to 3 weight percent FeO. Lower Normal and Willow Creek both contain unimodal pigeonite compositions.

Cathey and Nash (2003) reported up to three pyroxene compositional modes within a single eruptive unit, and units often shared groups of modes in the CPT

pyroxenes. This is not found in the WBH pyroxenes, but it is not uncommon for two units to share a single compositional mode (e.g., Lower Normal and Willow Creek pigeonite compositions). This lack of pyroxene mode diversity could be attributed to a more limited sampling regimen in this study; Cathey and Nash (2003) analyzed pyroxenes in both the upper and lower vitrophyre portions of each CPT unit, whereas this study used a single hand sample from each WBH unit (with the exception of High Springs + Rattlesnake Springs, which is discussed later in this paragraph). Cathey and Nash (2003) found that the upper vitrophyre contained the bulk of MgO-rich pyroxenes in units with multiple modes while the majority of FeO-rich pyroxenes are in the lower vitrophyre. The only unit that has both upper and lower vitrophyre pyroxene data is the High Springs + Rattlesnake Springs, and this relationship between composition and stratigraphic location of pyroxenes is not present. If this relationship holds true for the other WBH rhyolites, the complete range of pyroxene compositions may not have been analyzed for those units. Table 3 shows average pyroxene compositions for every WBH unit analyzed.

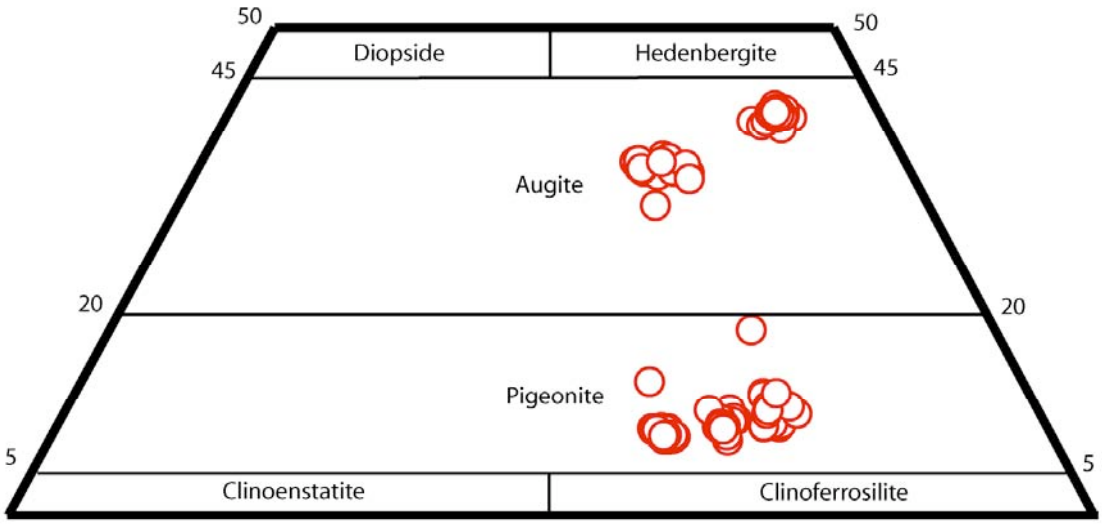

Figure 18 a: pyroxene compositions for West Bennett Hills rhyolites (in mol percent).

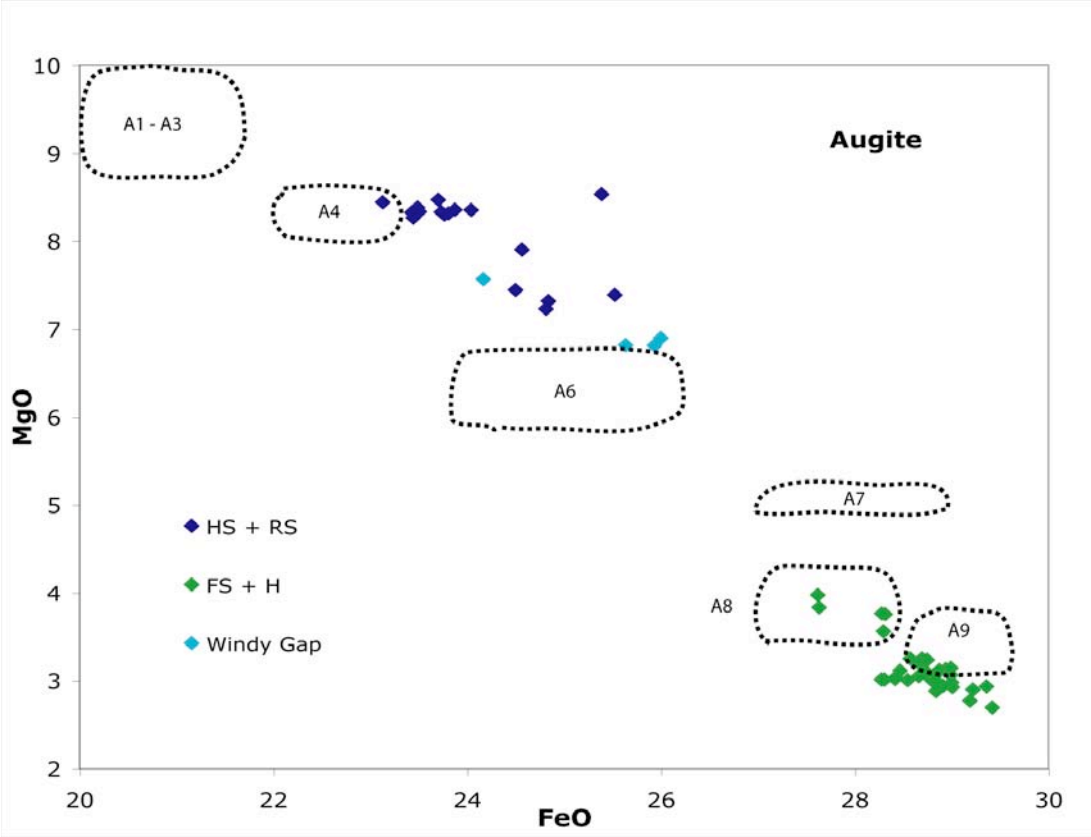

Figure 18 b: FeO vs MgO (weight percent) compositions of augites for West Bennett Hills rhyolites High Springs + Rattlesnake Springs (HS + RS), Frenchman Springs + Henley (FS + H), and Windy Gap. Data fields A1 through A9 are approximate pyroxene composition modes in CPT from Cathey and Nash, 2003.

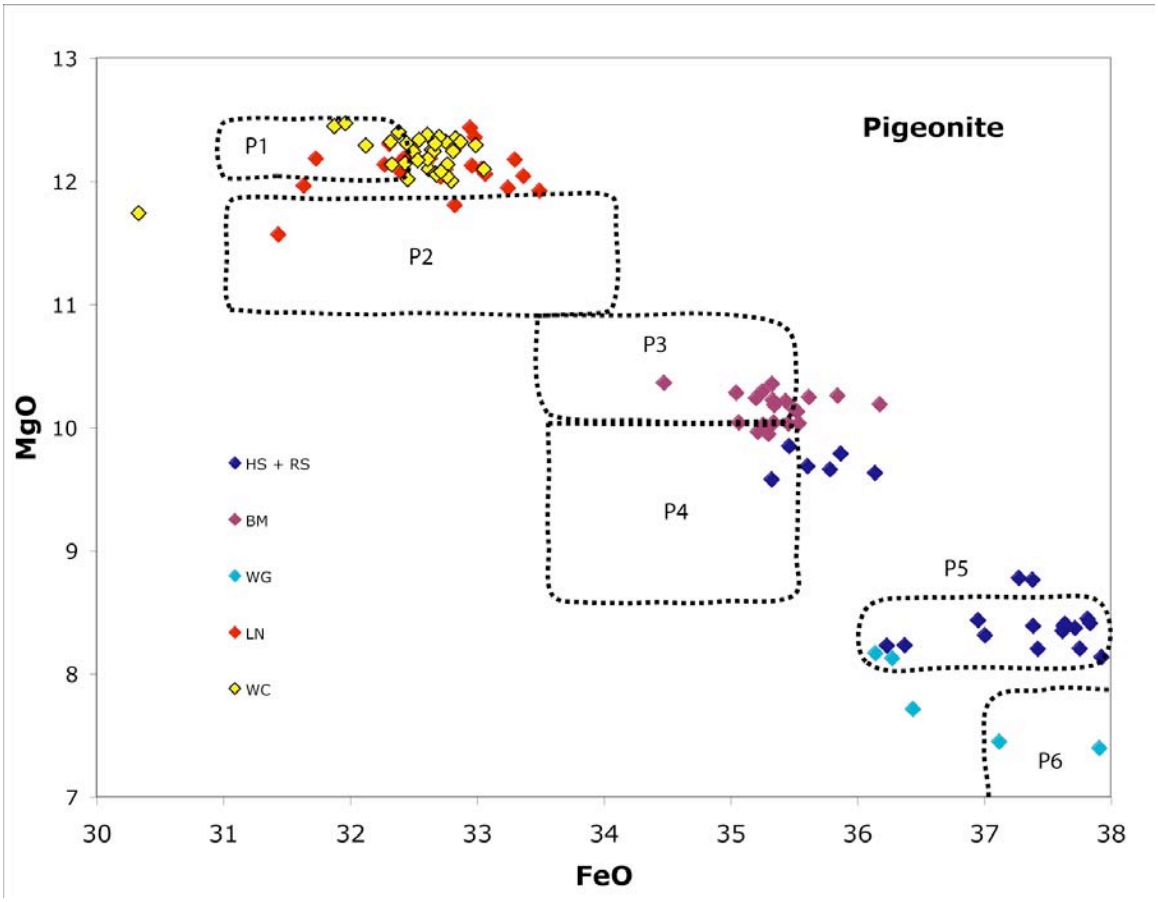

Figure 18 c: FeO vs MgO (weight percent) compositions of pigeonites for West Bennett Hills rhyolites High Springs + Rattlesnake Springs (HS + RS), Bennett Mountain (BM), Windy Gap (WG), Lower Normal (LN), and Willow Creek (WC). Data fields P1 through P6 are approximate pyroxene composition modes of the CPT from Cathey and Nash, 2003.

AUGITE	SiO_2	TiO_2	Al_2O_3	FeO	MnO	MgO	CaO	Na_2O	K_2O	sum
HS + RS	49.15	0.36	0.93	24.09	0.58	8.10	16.52	0.21	0.05	100.00
std dev	0.20	0.03	0.12	0.72	0.07	0.45	0.53	0.03	0.03	
										n = 17
FS + H	47.68	0.43	0.76	28.69	0.64	3.14	18.41	0.20	0.04	100.00
std dev	0.24	0.03	0.07	0.41	0.06	0.30	0.23	0.03	0.02	
										n = 34
WG	49.10	0.36	0.88	25.43	0.73	7.02	16.26	0.19	0.03	100.00
std dev	0.12	0.02	0.04	0.86	0.06	0.36	0.44	0.03	0.01	
										n = 4

PIGEONITE	SiO_2	TiO_2	Al_2O_3	FeO	MnO	MgO	CaO	Na_2O	K_2O	sum
HS + RS	47.93	0.23	0.47	36.92	0.94	8.74	4.65	0.05	0.07	100.00
std dev	0.26	0.03	0.04	0.89	0.06	0.62	0.47	0.02	0.08	
										n = 22
BM	48.00	0.23	0.52	35.36	0.95	10.16	4.33	0.06	0.39	100.00
std dev	0.20	0.02	0.13	0.33	0.06	0.13	0.28	0.02	0.26	
										n = 20
WG	48.43	0.25	0.53	36.21	1.03	7.72	5.74	0.06	0.04	100.00
std dev	0.26	0.02	0.07	1.54	0.07	0.35	1.48	0.02	0.01	
										n = 6
LN	49.47	0.19	0.47	32.66	1.02	12.11	3.88	0.07	0.11	100.00
std dev	0.33	0.02	0.15	0.54	0.07	0.18	0.10	0.08	0.17	
										n = 24
WC	49.19	0.22	0.51	32.52	1.02	12.21	4.24	0.05	0.04	100.00
std dev	0.27	0.02	0.04	0.48	0.06	0.16	0.42	0.02	0.02	
										n = 32

Table 3: average pyroxene compositions (in weight percent) for WBH rhyolites with standard deviations (std dev). HS + RS = High Springs + Rattlesnake Springs, FS + H = Frenchman Springs + Henley, BM = Bennett Mountain, WG = Windy Gap, LN = Lower Normal, WC = WIllow Creek.

Volcanic Glasses

Volcanic glass compositions in the West Bennett Hills rhyolites are typical of continental rhyolites: SiO_2 values range from 74 to 78 weight percent (Fig 19). TiO_2 is used because of its moderate compatibility relative to SiO_2 and its insolubility. While the compositional range of glasses is narrow, there are some instances where different units in CAT groups plot in distinct areas in SiO_2 – TiO_2 space when compared to each other. Figures 20 a – e illustrates the distinct glass compositions in CAT groups 3, 4 and 6. While these plots provide good evidence against unit-to-unit correlations for those CAT groups, the units in CAT 8 all show similar glass compositions to each other (Fig 20 f, g). Table 4 shows average glass compositions for all WBH units.

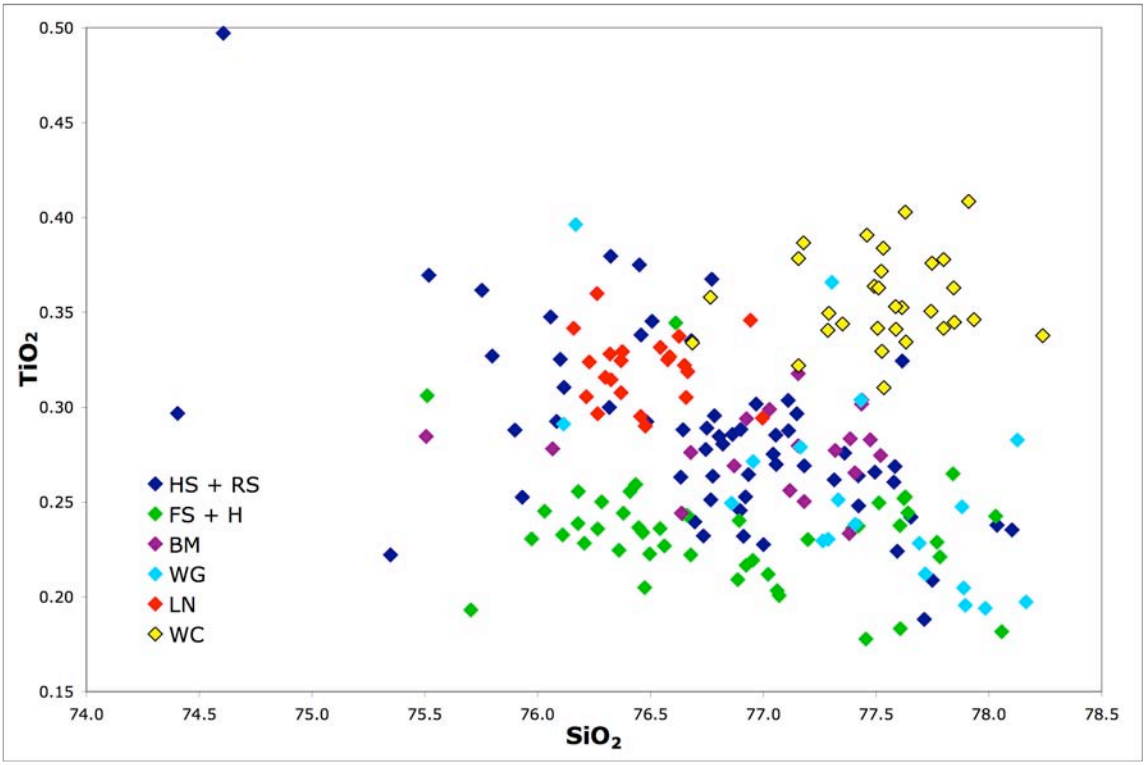

Figure 19: SiO_2 vs TiO_2 diagram of WBH volcanic glass samples collected by electron microprobe. Note the relative homogeneity of High Springs + Rattlesnake Springs (HS + RS), Windy Gap (WG), and Frenchman Springs + Henley (FS + H) samples compared to the discrete compositions of glasses from Lower Normal (LN) and Willow Creek (WC).

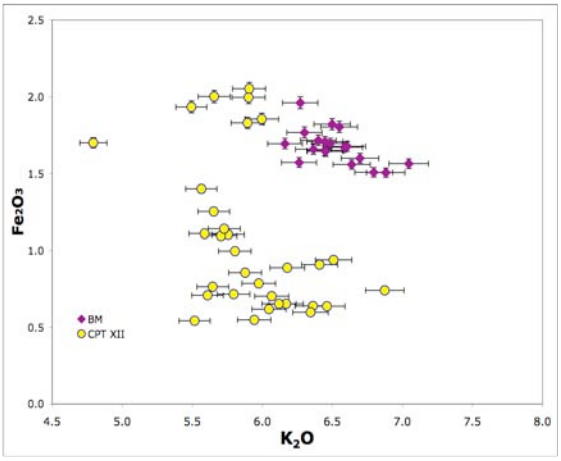

Figure 20 a

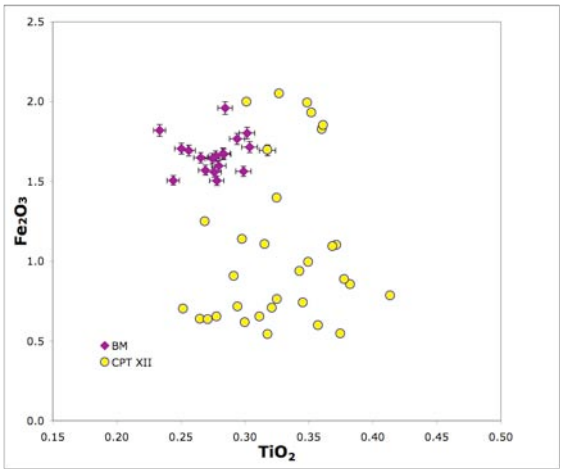

20 b

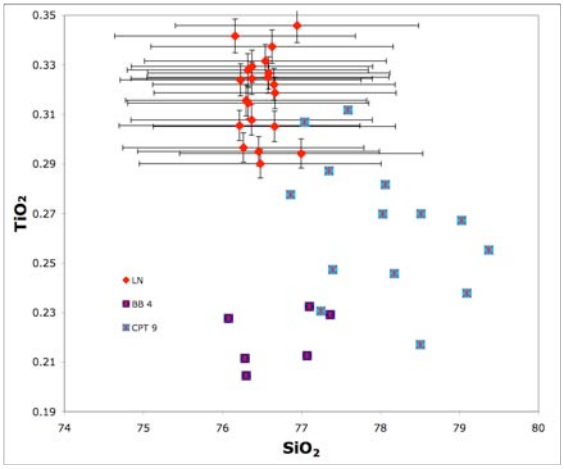

20 c

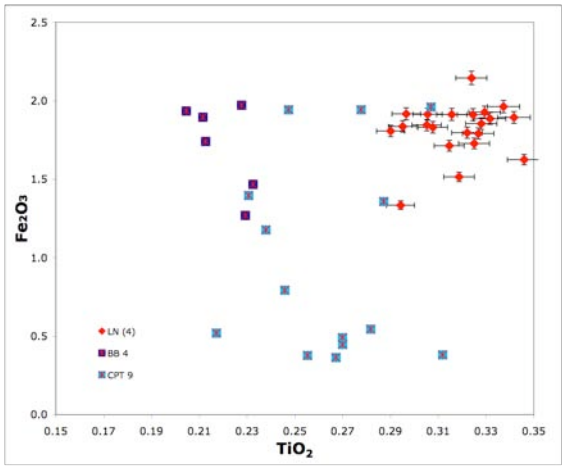

20 d

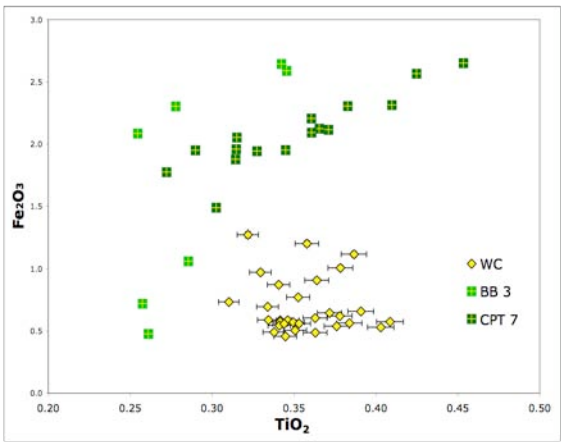

20 e

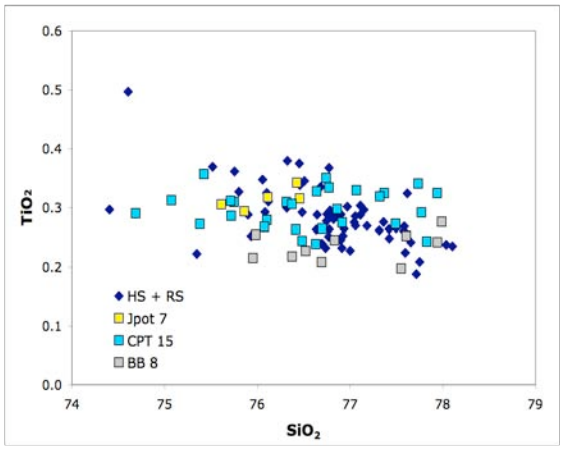

20 f

Figure 20: caption on next page

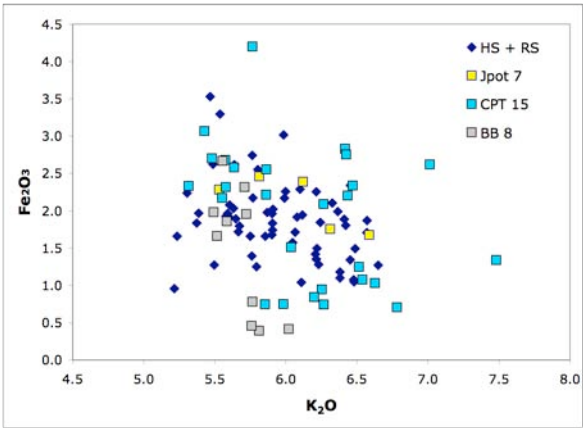

20g

Figure 20: comparison of volcanic glass compositions (in weight percent) of several WBH units and their SCSRP CAT group equivalents. West Bennett Hills (WBH) units are plotted as diamond shapes in different colors. Acronyms for the WBH units are as follows: HS + RS = High Springs + Rattlesnake Springs, BM = Bennett Mountain, LN = Lower Normal and WC = Willow Creek. Acronyms for the southern central Snake River Plain are as follows: CPT 15 = Cougar Point Tuff XV, CPT 12 = Cougar Point Tuff XII, CPT 9 = Cougar Point Tuff IX, CPT 7 = Cougar Point Tuff VII, Jpot 7 = Jackpot 7, BB 8 = Brown's Bench 8, BB 4 = Brown's Bench 4, BB 3 = Brown's Bench 3.

20 a and b: diagrams of two units from CAT group 6, Bennett Mountain and Cougar Point Tuff XII showing distinct glass composition for the two units.

20 c and d: diagrams of units in CAT group 4: Lower Normal, Cougar Point Tuff XI and Brown's Bench unit 4 that illustrate the distinct glass composition of Lower Normal from its SCSRP equivalents.

20 e: diagram of units in CAT group 3: Willow Creek, Cougar Point Tuff VII and Brown's Bench unit 3 showing differing compositions for Willow Creek when compared to its SCSRP equivalents.

20 f and g: diagrams of units in CAT group 8: High Springs + Rattlesnake Springs, Jackpot 7, Cougar Point Tuff XV, and Brown's Bench unit 8 showing the relative homogeneity of volcanic glass compositions of all four units analyzed.

GLASS	SiO_2	TiO_2	Al_2O_3	Fe_2O_3	MgO	CaO	Na_2O	K_2O	Cl	sum
HS + RS	76.76	0.29	12.00	1.86	0.05	0.29	2.77	5.95	0.02	100.00
std dev	0.73	0.05	0.28	0.53	0.05	0.22	0.26	0.38	0.01	
										n = 60
FS + H	76.85	0.23	11.91	1.99	0.03	0.27	2.24	6.44	0.04	100.00
std dev	0.65	0.03	0.19	0.56	0.02	0.17	0.41	0.66	0.02	
										n = 46
BM	77.04	0.28	11.88	1.67	0.05	0.15	2.37	6.52	0.04	100.00
std dev	0.52	0.02	0.37	0.11	0.02	0.05	0.19	0.22	0.06	
										n = 19
WG	77.46	0.25	11.74	1.46	0.02	0.05	2.46	6.54	0.03	100.00
std dev	0.62	0.06	0.28	0.81	0.02	0.11	0.32	0.42	0.01	
										n = 20
LN	76.47	0.32	12.04	1.82	0.10	0.26	2.45	6.54	0.00	100.00
std dev	0.23	0.02	0.09	0.17	0.02	0.05	0.36	0.34	0.03	
										n = 22
WC	77.53	0.36	12.23	0.69	0.02	0.05	2.18	6.89	0.01	100.00
std dev	0.33	0.02	0.16	0.22	0.02	0.07	0.38	0.27	0.03	
										n = 30

Table 4: average volcanic compositions (in weight percent) for WBH rhyolites with standard deviations (std dev). HS + RS = High Springs + Rattlesnake Springs, FS + H = Frenchman Springs + Henley, BM = Bennett Mountain, WG = Windy Gap, LN = Lower Normal, WC = WIllow Creek.

Feldspars

All West Bennett Hills rhyolites contain plagioclase phenocrysts. Approximately 50 percent of the crystals analyzed exhibited zonation from rim to core to varying degrees; the crystal with the strongest zoning was "Fspar 1" in sample #035 (Lower Normal) with An_{44} in the core and An_{32} in the rim. The majority of zoned crystals exhibit normal zoning; very few feldspars showed reverse zoning. The variation in plagioclase compositions is restricted in some units, particularly in the younger Danskin Group (Frenchman Springs = An_{23-28}, High Springs + Rattlesnake Springs = An_{26-36}), but variations can be quite substantial in the older Bennett Mountain Group (Willow Creek = An_{32-48}, Lower Normal = An_{32-44}, rhyolite of Bennett Mountain = An_{28-41}, and Windy Gap = An_{27-34}).

Sanidine crystals were found and analyzed in the High Springs + Rattlesnake Springs, Frenchman Springs and Windy Gap units. The range of orthoclase compositions in sanidine for all units is Or_{50-63}. The range of orthoclase compositions in sanidines broken down by unit are as follows: Windy Gap = Or_{53-57}, Rattlesnake Springs + High Springs = Or_{52-62}, Frenchman Springs = Or_{50-63}. Figure 21 displays the compositions of all WBH feldspars. Table 5 shows representative analyses of feldspar crystals from each unit.

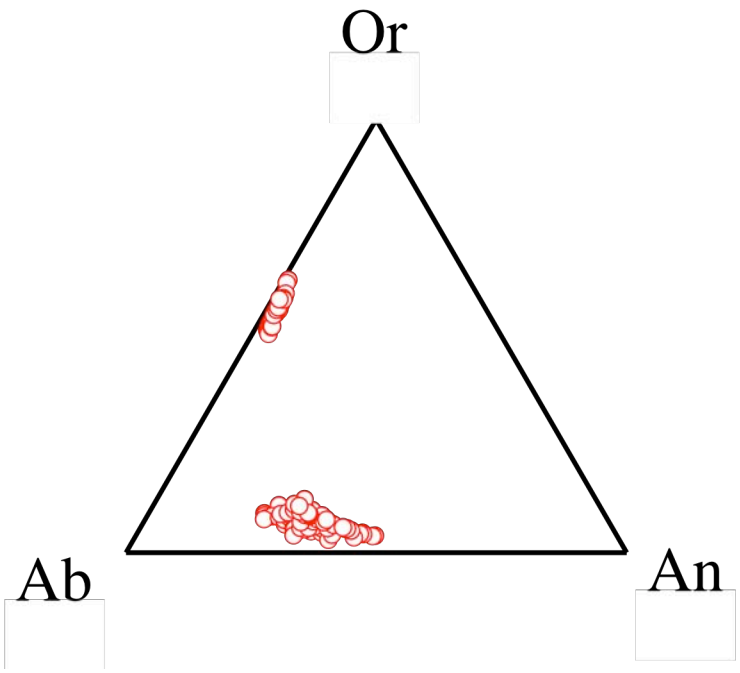

Figure 21: ternary diagram showing feldspar compositions (in mol percent) for all WBH rhyolites.

PLAG	SiO_2	Al_2O_3	BaO	FeO	CaO	Na_2O	K_20	Sum	An
HS + RS									
zoned, core	59.74	24.93	0.17	0.38	6.60	6.82	1.36	100.00	32
std dev	0.50	0.35	0.04	0.04	0.36	0.12	0.13	n = 10	
zoned, rim	60.46	24.41	0.20	0.38	5.99	7.04	1.51	100.00	29
std dev	0.42	0.24	0.03	0.05	0.35	0.17	0.13	n = 10	
Unzoned	59.37	25.16	0.15	0.39	6.97	6.71	1.24	100.00	33
std dev	0.43	0.25	0.03	0.04	0.37	0.14	0.14	n = 13	
FS									
Plag	60.89	24.06	0.24	0.34	5.54	7.47	1.46	100.00	26
std dev	0.72	0.56	0.05	0.04	0.60	0.34	0.14	n = 8	
BM									
zoned, core	58.65	25.60	0.21	0.39	7.35	6.45	1.36	100.00	36
std dev	1.34	0.96	0.07	0.01	0.98	0.28	0.32	n = 7	
zoned, rim	59.88	24.64	0.23	0.44	6.27	6.85	1.69	100.00	30
std dev	0.28	0.24	0.05	0.05	0.25	0.15	0.14	n = 8	
Unzoned	59.75	24.68	0.19	0.40	6.39	6.77	1.81	100.00	31
std dev	0.44	0.32	0.15	0.02	0.31	0.07	0.22	n = 6	
WG									
zoned, core	60.30	24.68	0.23	0.37	6.27	6.71	1.44	100.00	31
std dev	0.47	0.38	0.09	0.02	0.52	0.17	0.23	n = 4	
zoned, rim	60.81	24.36	0.23	0.36	5.82	6.86	1.56	100.00	29
std dev	0.90	0.67	0.06	0.02	0.54	0.12	0.17	n = 4	
Unzoned	60.69	24.38	0.21	0.36	6.09	6.76	1.51	100.00	30
std dev	0.53	0.41	0.06	0.02	0.50	0.21	0.22	n = 6	
LN									
zoned, core	58.37	25.94	0.12	0.42	7.83	6.35	0.98	100.00	38
std dev	1.10	0.85	0.06	0.06	0.83	0.37	0.23	n = 10	
zoned, rim	59.57	25.19	0.16	0.42	6.78	6.95	0.94	100.00	33
std dev	0.66	0.47	0.05	0.03	0.56	0.30	0.21	n = 10	
Unzoned	59.45	25.23	0.17	0.42	6.98	6.65	1.10	100.00	34
std dev	0.49	0.27	0.06	0.03	0.52	0.37	0.13	n = 7	
WC									
zoned, core	57.46	26.48	-----	0.49	8.45	6.13	0.96	100.00	41
std dev	1.81	1.26	-----	0.04	1.30	0.48	0.27	n = 8	
zoned, rim	58.99	25.39	-----	0.51	7.34	6.65	1.10	100.00	35
std dev	0.54	0.32	-----	0.04	0.33	0.28	0.11	n = 9	
Unzoned	58.95	25.47	-----	0.50	7.33	6.56	1.17	100.00	36
std dev	0.66	0.49	-----	0.04	0.51	0.29	0.16	n = 20	

Table 5: caption on next page

SANIDINE	SiO_2	Al_2O_3	BaO	FeO	CaO	Na_2O	K_20	sum	Or
HS + RS									
zoned, core	64.06	19.91	2.02	0.16	0.41	4.16	9.28	100.00	58
std dev	0.20	0.10	0.06	0.02	0.05	0.23	0.25	n = 3	
zoned rim	65.86	18.86	1.76	0.36	0.40	4.13	8.62	100.00	57
std dev	2.91	1.92	0.34	0.29	0.22	0.71	0.33	n = 4	
Unzoned	64.05	19.85	2.09	0.18	0.39	4.29	9.15	100.00	57
std dev	0.27	0.12	0.11	0.03	0.06	0.13	0.25	n = 8	
FS									
zoned, core	64.02	20.08	1.90	0.15	0.54	4.86	8.46	100.00	52
std dev	0.27	0.27	0.15	0.05	0.06	0.07	0.17	n = 5	
zoned, rim	64.12	19.66	1.89	0.21	0.39	4.45	9.28	100.00	57
std dev	0.18	0.10	0.06	0.11	0.15	0.34	0.70	n = 5	
Unzoned	63.91	20.12	1.91	0.13	0.49	4.87	8.58	100.00	52
std dev	0.25	0.08	0.19	0.02	0.05	0.08	0.15	n = 4	
WG									
zoned, core	64.06	20.14	2.06	0.19	0.63	4.56	8.37	100.00 n = 1	57
zoned, rim	64.23	19.96	1.99	0.16	0.50	4.20	8.97	100.00 n = 1	53
Unzoned	64.32	20.01	1.94	0.17	0.49	4.41	8.67	100.00	55
std dev	0.28	0.19	0.07	0.02	0.02	0.14	0.19	n = 4	

Table 5: average feldspar compositions (in weight percent) for WBH rhyolites with standard deviations (std dev). Zoned cores, rims and unzoned crystals averaged separately. HS + RS = High Springs + Rattlesnake Springs, FS + H = Frenchman Springs + Henley, BM = Bennett Mountain, WG = Windy Gap, LN = Lower Normal, WC = WIllow Creek.

LA-ICPMS trace element analyses

Trace element abundances of fresh glasses, pyroxenes and feldspars were analyzed on the same locations used in microprobe analysis to ensure proper correlation between major and trace element abundances for each sample, in addition to the normalization process for LA analyses outlined in the methods section of this study.

Distribution Coefficients

D values were calculated using average compositions of glass, augite, pigeonite, plagioclase and sanidine for each WBH unit :

D = [element X in phase (pyx or feldspar)] / [element X in melt (glass)]

Figures 22 a and b are diagrams of distribution coefficients for incompatible trivalent trace elements in pyroxenes from the WBH and other rhyolites from the literature (Bacon and Druitt 1988, Nash and Crecraft 1985, Mahood and Hildreth 1983, Streck and Grunder, 1997). The rare earth elements, plus Y^{3+}, were chosen for D value comparison and lie on the x axis, arranged by ionic radius in eightfold coordination (ionic radius data taken from Shannon, 1971). Yttrium is included in these diagrams due to its trivalent state and similar ionic radius (1.019 Å) to the rare earth elements, specifically Ho (1.015 Å) in eightfold coordination and in sixfold coordination: $^{VI}Y = 0.900$ Å, $^{VI}Ho = 0.901$ Å.These elements are assumed to be in eightfold coordination because the M2 site in pyroxenes becomes distorted and shifts from sixfold to eightfold coordination when a large cation (such as Ca^{2+} in augites and pigeonites) enters the pyroxene structure (Deer, Howie and Zussman, 1992), and it is assumed that these incompatible elements are

substituting for Ca^{2+} in the M2 site. The data taken from the literature conform to the pattern of the WBH pyroxenes with the notable exception of Mahood and Hildreth (1983) augite data (Fig 22 a), which were found to be erroneous due to chevkinite inclusions (Michael, 1988). Pigeonite data from Nash and Crecraft (1985) plot significantly higher than any WBH sample for LREE, and Bacon and Druitt's (1988) HREE D values are significantly lower than the data for WBH pigeonites (Fig 22 b).

D_{Eu} values are lower than those of neighboring REE (Sm and Nd) in both the pigeonites and augites. This is attributed to Eu having two oxidation states, one trivalent and the other divalent. As such, Eu does not behave in the same manner as the trivalent REEs. For this reason, D_{Eu} is not included in the partition coefficient diagrams. Although yttrium should behave the same way as holmium due to their identical valence and similar ionic radii (only 0.004 Å difference, Shannon, 1971), yttrium distribution coefficients in pyroxenes are lower than D_{Ho} and D_{Dy} values. This is especially noticeable in augites (Figs 22 a, 23 a). Olin (2007) found similar Y-Ho partitioning relations in Na-rich salites in the Fasnia member of the Diego Hernandez formation on Tenerife and attributed it to the eightfold site in pyroxenes preferring the REEs over Y, effectively partitioning Y from chemically similar HREEs.

D_{Lu}, due to high Lu contents with regard to other HREE, is higher than expected for the augites (Fig 22a). Streck and Grunder (1997) also found high D_{Lu} distribution coefficient data. Olin (2007) found this phenomenon also occurred in the Na-rich salites of the Fasnia phonolite and invokes Lu substituting for Fe and Mn in sixfold coordination in the M1 site. Cameron and Papike (1980) stated that the M1 site in pyroxenes is able to accept cations with an ionic radius from 0.53 Å (^{IV}Al) to 0.83 Å (^{VI}Mn). A comparison of

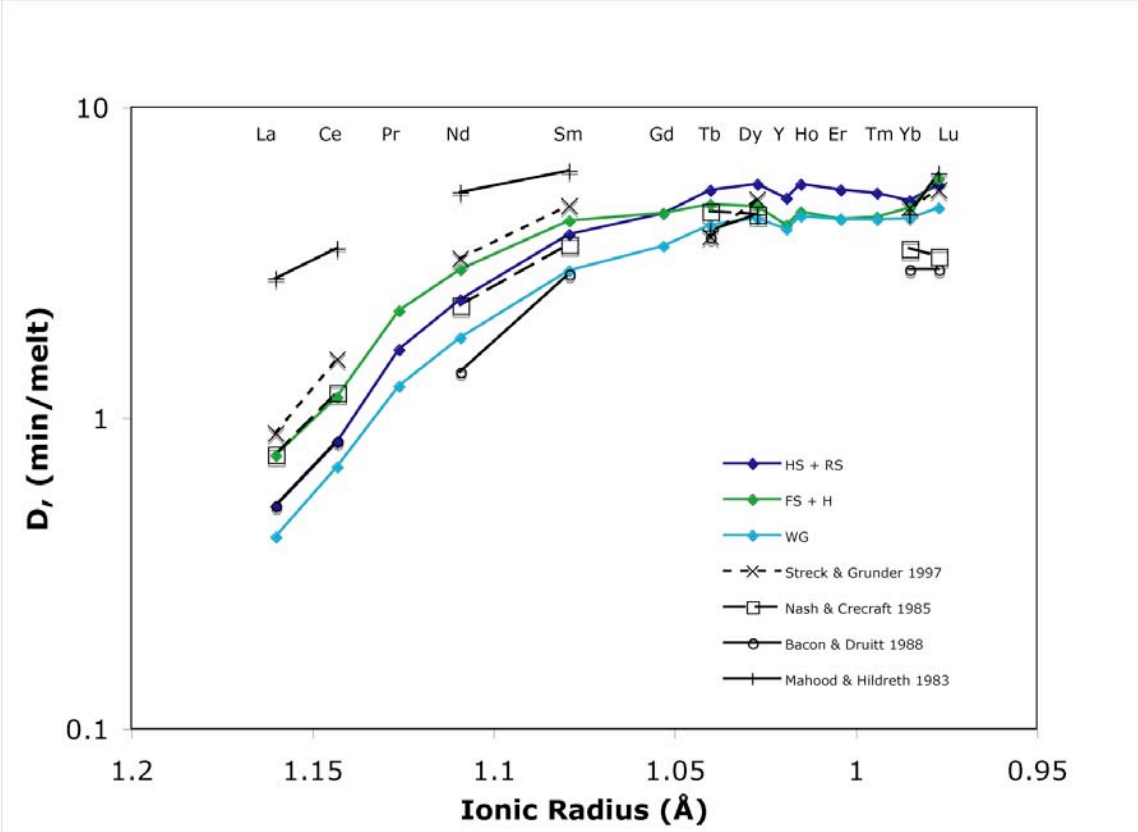

Figure 22 a: Partition coefficient (D) diagram for incompatible trivalent ions in augites for WBH rhyolites, plotted with D values from the literature.

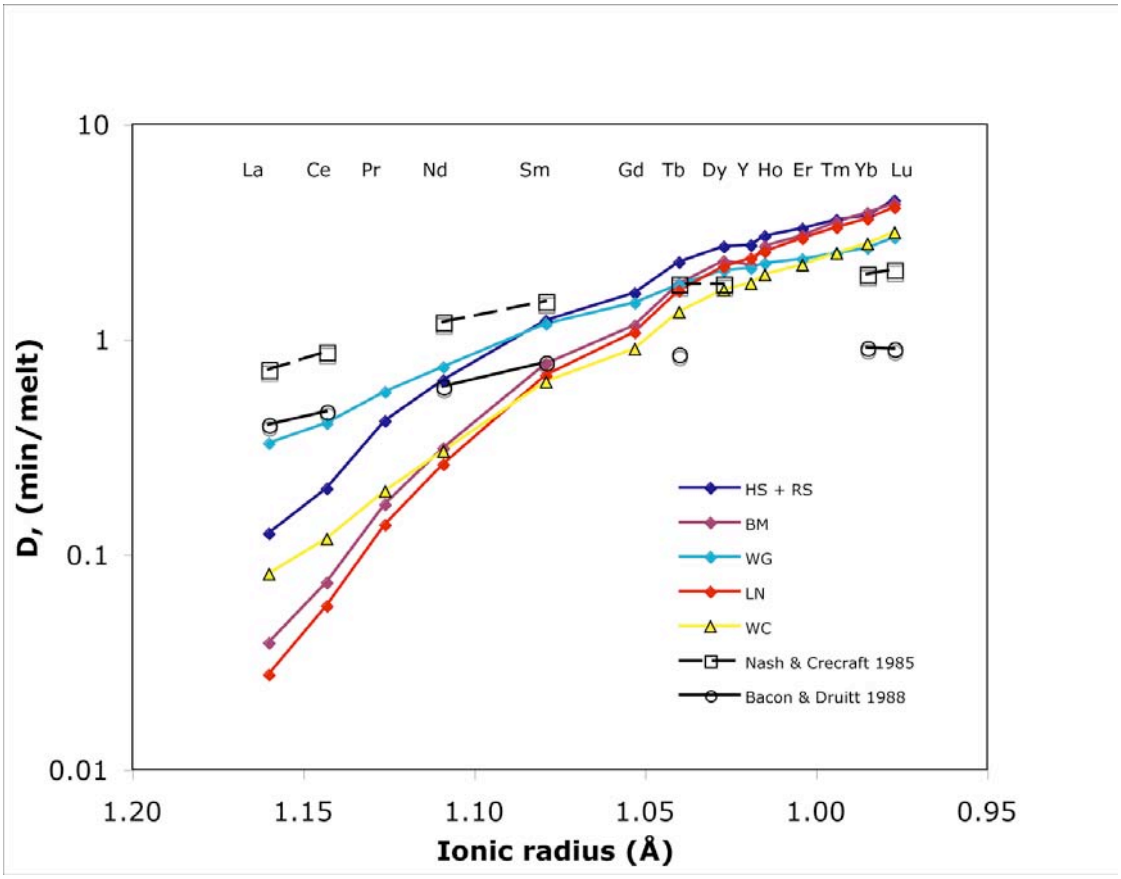

Figure 22 b: Partition coefficient (D) diagram for incompatible trivalent ions in pigeonites for WBH rhyolites, plotted with D values from the literature.

ionic radii for Lu^{3+} (0.861 Å), Mn^{2+} (0.83 Å) and Fe^{2+} (0.78 Å) in sixfold coordination indicates that Lu substituting for Fe and Mn in the M1 site is a reasonable mechanism for increased D_{Lu} values and Lu abundances relative to other HREEs.

The only High Field Strength Elements (HFSE) that are abundant enough to calculate accurate distribution coefficients for WBH pyroxenes are Zr and Ti. Figure 23 b shows this data in comparison to published data from the literature. Note that D_{Ti} for pigeonites does not exceed 0.8 for any sample.

Distribution coefficients were calculated for Sr and Ba in feldspars were calculated to compare against data from the literature and is displayed in Figures 23c and d. D_{Sr} and D_{Ba} display roughly positive correlations for both plagioclase and sanidine. The WBH data generally conforms to the literature data (Nash and Crecraft, 1985; Ewart and Griffin, 1994), with the notable exception of high D_{Sr} values for plagioclase in the WBH rhyolites. Blundy and Wood (1991) demonstrated that anorthite content (An) in plagioclase is the most important factor in determining D_{Sr} values in plagioclase. Low An values correspond to high D_{Sr} values, and Blundy and Wood (1991) stated that the highest D_{Sr} value for high silica rhyolites with An_{30-40} (approximate range for WBH plagioclases, Table 5) is approximately 13. The WBH plagioclases are in stark contrast to this data; the D_{Sr} values range from 13 to 37. Although no study has investigated the effect of orthoclase content on Sr partitioning in plagioclases, comparing the ionic radius of ^{VIII}K (1.51 Å) to the radii of ^{VIII}Ca (1.12 Å) and ^{VIII}Na (1.18 Å) implies that the plagioclase structure would expand significantly with increasing Or content. This expansion could possibly facilitate ^{VIII}Sr (ionic radius of 1.26 Å) substitution.

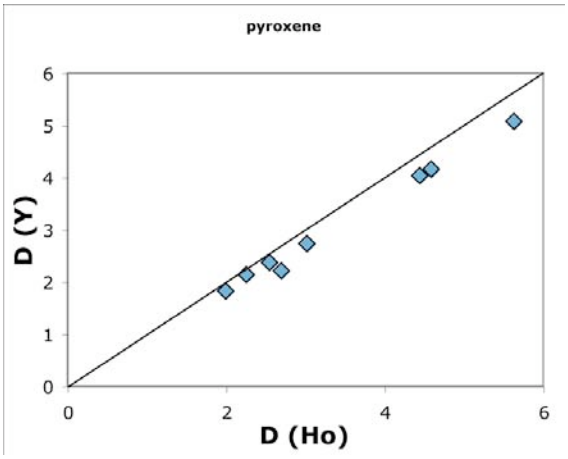

Figure 23 a

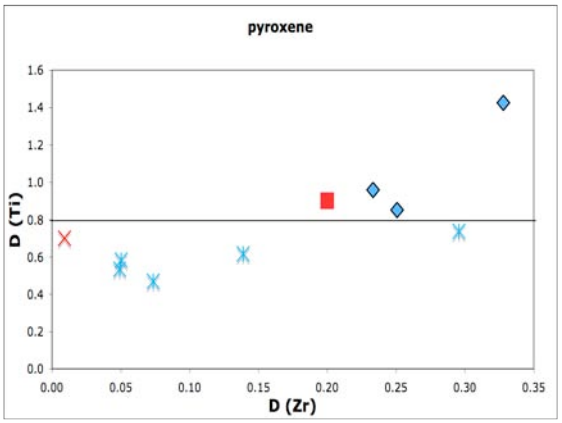

23 b

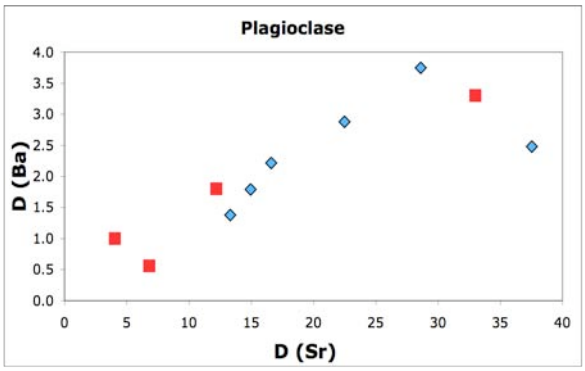

23 c

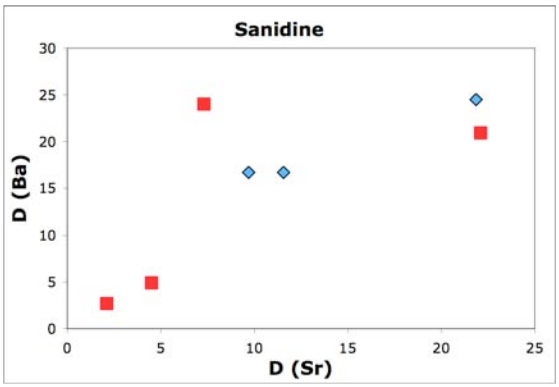

23 d

Figure 23: diagrams of distribution coefficients in the WBH rhyolites. Blue diamonds are WBH values, red boxes are data collected from the literature.

23 a: D_Y vs D_{Ho} for WBH pyroxenes, showing higher D_{Ho} values than the expected 1:1 ratio.

23 b: D_{Zr} vs D_{Ti} for WBH pyroxenes. WBH pigeonites shown in blue asterisks, WBH augites in solid blue diamonds. All points above $D_{Ti} = 0.8$ are augites. Literature data comes from Sisson, 1991 (pigeonite, plotted as a red X) and Sisson, 1994 (augite, plotted as a red box).

23 c, d: D_{Sr} vs D_{Ba} for WBH plagioclase and sanidine. Literature data comes from Nash and Crecraft, 1985 and Ewart and Griffin, 1994.

Pyroxenes

Figures 24 a and b show two distinct groups of trace element compositions, illustrating the differences in trace element abundances for the two varieties of pyroxenes in the WBH rhyolites. Augites, due to their higher Ca^{2+} abundance (~15-17 CaO weight percent), have a much greater ability to accept incompatible trace elements into the pyroxene lattice than pigeonites (~3-5 CaO weight percent). The Ca^{2+} ion is large in eightfold coordination (1.12 Å) and sixfold coordination (1.00 Å) and would therefore expand the M2 site (Deer, Howie and Zussman, 1992; Cameron and Papike, 1980). Wood and Blundy (1997) stated that CaO abundance is one of the most important factors in the ability of a pyroxene to allow substitution of incompatible trace elements, and the more CaO a pyroxene has, the more likely it is to accept trace elements.

The trace element data collected on proxenes in the WBH rhyolites reinforces the results from the glass trace element data described earlier in this study. Figures 25 a – d is a compilation of a variety of incompatible trace element diagrams showing distinct trace element compositions of the WBH rhyolite pyroxenes when compared to their SCSRP unit equivalents.

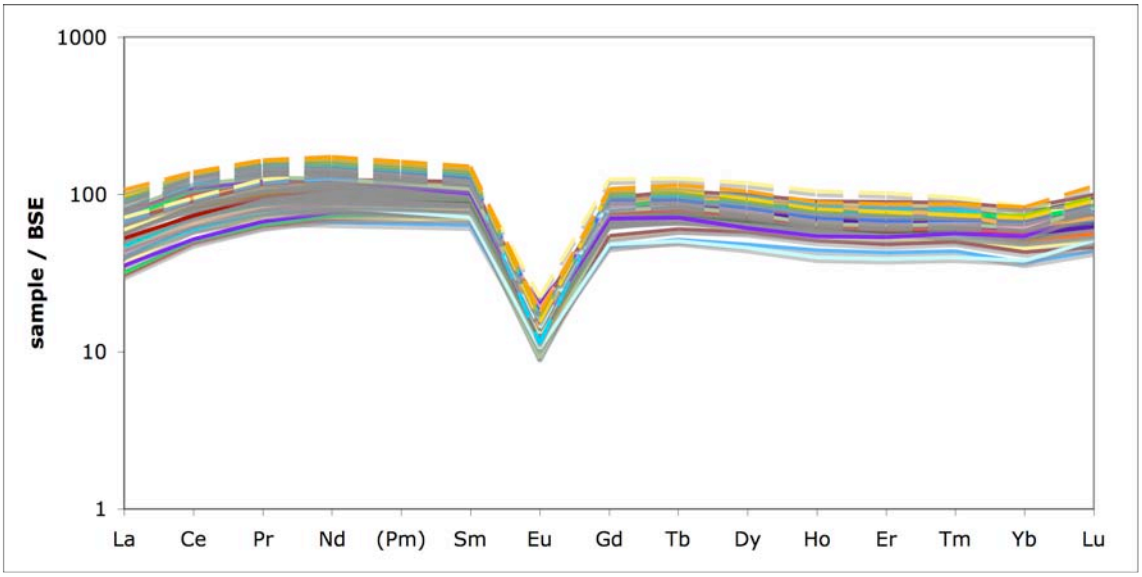

Figure 24a: REE diagram of WBH augites. Augites are overall enriched in REE relative to pigeonites and display approximately flat patterns. All samples normalized to BSE (McDonough and Sun, 1995).

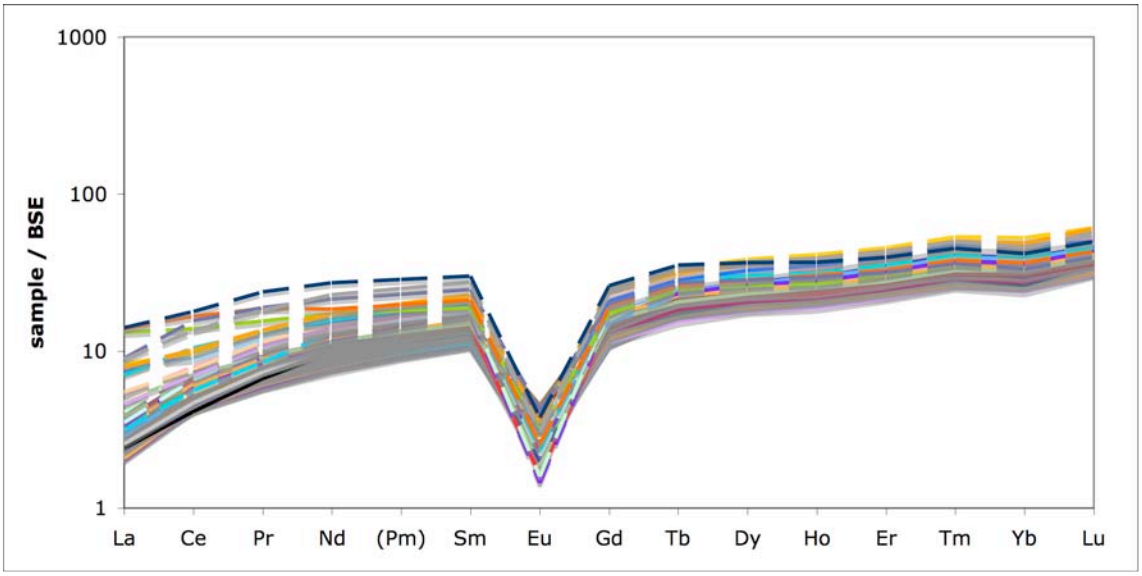

Figure 24b: REE diagram of WBH pigeonites. Pigeonites are significantly depleted in LREE relative to augites. All samples normalized to BSE (McDonough and Sun, 1995).

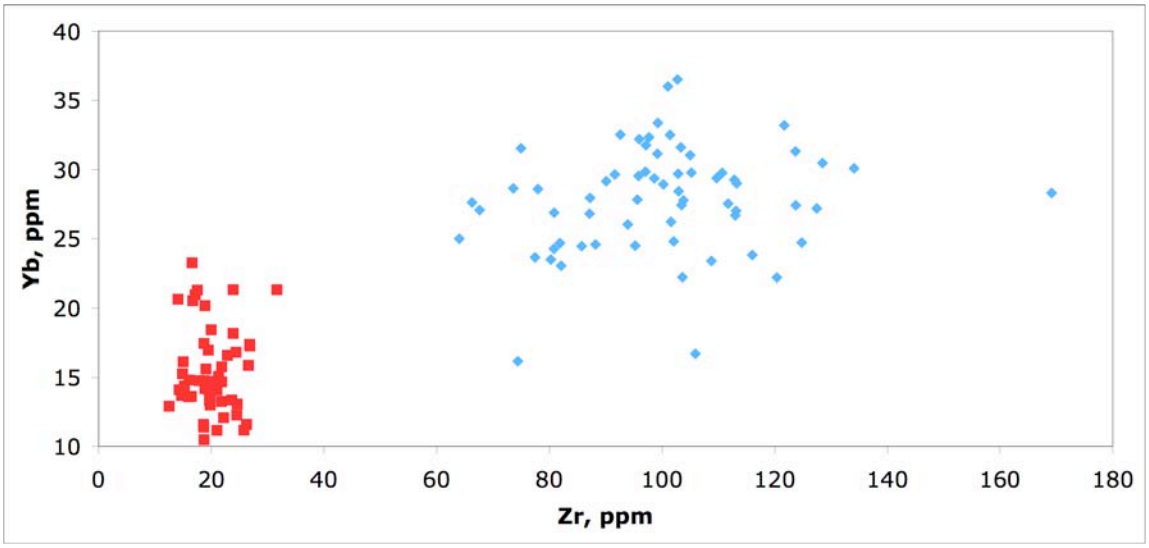

Figure 24c: Zr vs Yb diagram of all WBH pyroxenes. Note the relatively limited composition of pigeonites (red boxes) compared to the spread of augite compositions (blue diamonds).

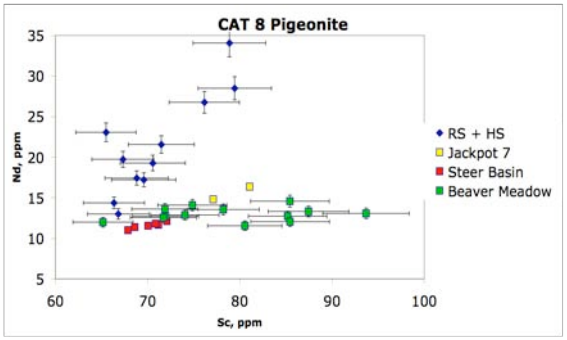

25 a

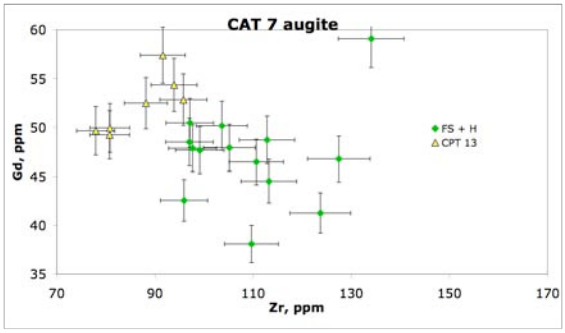

25 b

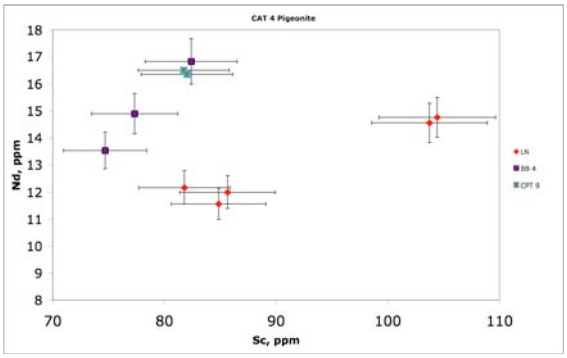

25 c

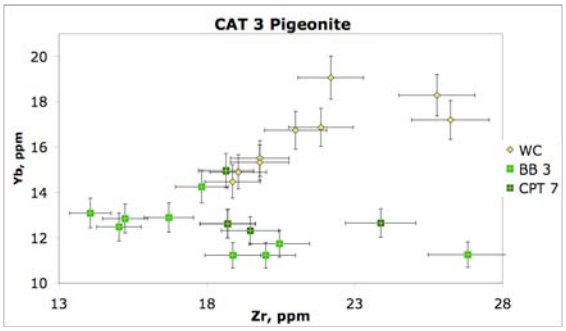

25 d

Figure 25: diagrams comparing trace element data from WBH units to their CAT group equivalents. Abbreviations for the WBH rhyolites: RS + HS = Rattlesnake Springs + High Springs, FS + H = Henley, LN = Lower Normal, WC = Willow Creek. Abbreviations for the SCSRP rhyolites: CPT 13 = Cougar Point Tuff XIII, CPT 9 = Cougar Point Tuff IX, CPT 7 = Cougar Point Tuff VII, BB 4 = Brown's Bench 4, BB 3 = Browns Bench 3.

Glasses

See Figure 26 for a rare earth element diagram of all WBH glass samples. The trace element abundances of volcanic glasses for the units in CAT Groups 3, 4 and 6 reinforce the results of the microprobe glass data, mainly that the WBH units in these CAT Groups display distinctly different trace element compositions from their SCSRP counterparts (Fig 27 a – c). The most important aspect of the addition of glass trace elements to this data set is the distinctly different compositions of incompatible trace elements for the units in CAT Groups 7 and 8. The probe glass data suggests that the units in these CAT Groups have nearly identical compositions, but the trace element analyses suggest otherwise. The units in CAT Group 7, WBH unit Frenchman Springs + Henley and SCSRP units Brown's Bench 8, Cougar Point Tuff XIII, and Lower Jackpot all plot in distinct areas in a diagram of Zr vs Y (Fig. 27 d). This diagram is the most useful in interpreting the possible N-S correlations of CAT group 7, as the units all plot quite distinct from each other in Zr vs Y space. Although the SCSRP unit Brown's Bench 8 was placed into CAT Group 8 by Bonnichsen, et al. (2008), trace element compositions of glasses show that BB 8 is closer to CAT 7 units than those in CAT 8 (Figs 25 d, e).

Although no "magic bullet" diagram could be found for the units in CAT Group 8, Figures 27e – g show a collection of diagrams utilizing several incompatible trace elements that together illustrate the subtle distinct compositions of these units. Figure 27e is a diagram of Ti vs Nd, and displays the distinct plots of SCSRP units Jackpot 7, Beaver Meadow, Cougar Point Tuff XV and Brown's Bench 8; Figure 27 f, also a Ti vs Nd diagram, shows the slight chemical distinction of Cougar Point Tuff XV from the WBH unit High Springs + Rattlesnake Springs. This is essentially the only diagram that

successfully separates the composition of the HS + RS unit from the composition of the CPT XV that could be found. This could be interpreted as a possible correlation, but further investigations are necessary before conclusive statements can be made. Figure 27 g plots Pb vs Zr and illustrates the different Pb abundances for the Steer Basin and Beaver Meadow units.

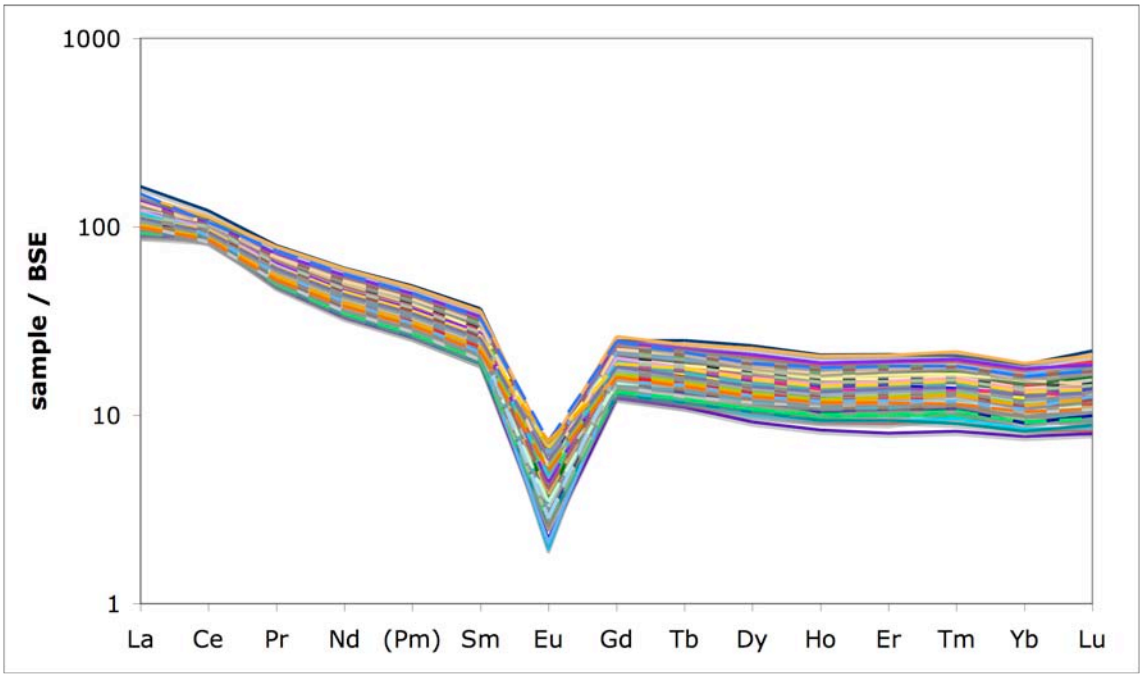

Figure 26: REE diagram for West Bennett Hills fresh glass samples. All samples normalized to BSE (McDonough and Sun, 1995).

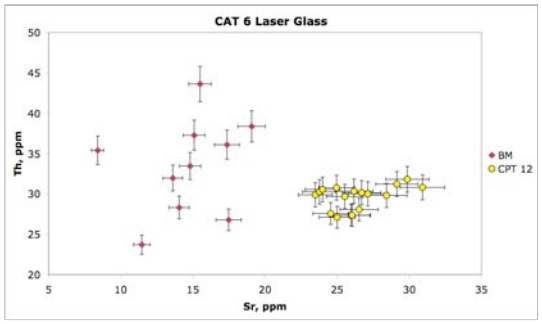

27 a

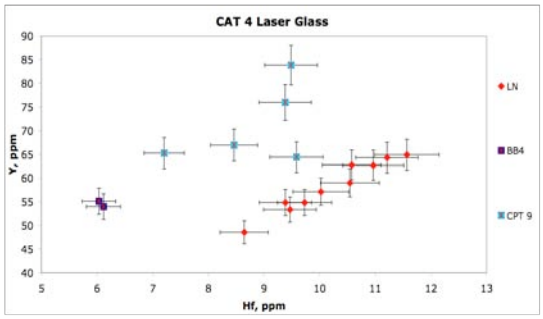

27 b

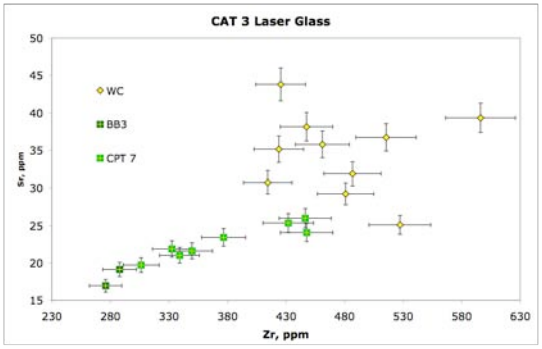

27 c

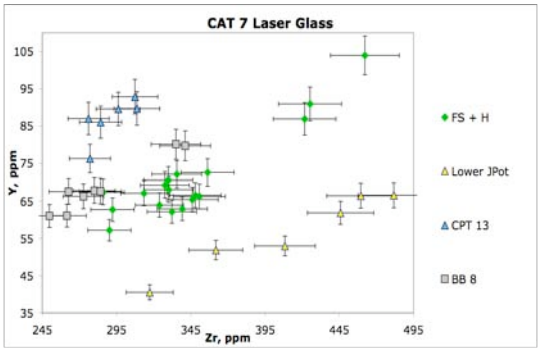

27 d

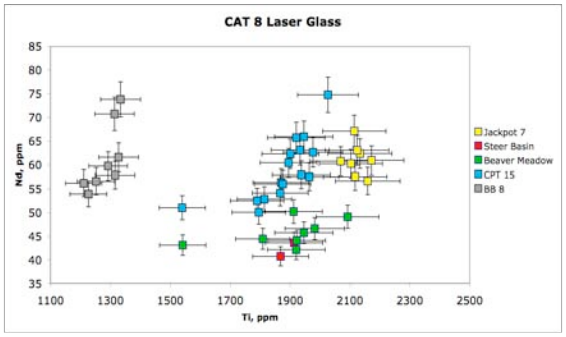

27 e

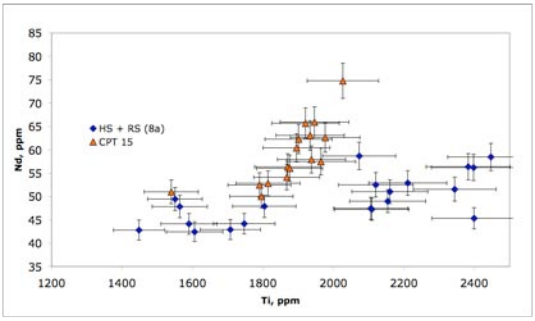

27 f

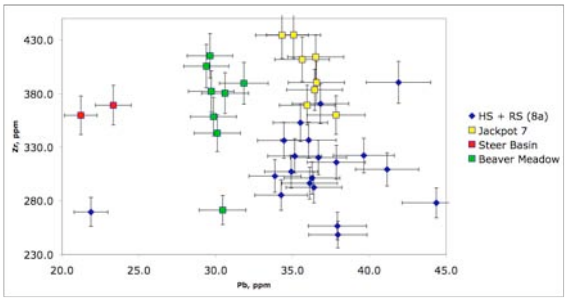

27 g

Figure 27: caption on next page

Figure 27: Glass trace element diagrams showing compositional differences between West Bennett Hills rhyolites (HS + RS = High Springs + Rattlesnake Springs, FS + H = Frenchman Springs + Henley, BM = Bennett Mountain, LN = Lower Normal, WC = Willow Creek) and their CAT group equivalents in the SCSRP (CPT 15 = Cougar Point Tuff XV, Jpot Lower = Jackpot Lower, CPT 13 = Cougar Point Tuff XIII, CPT 12 = Cougar Point Tuff XII, CPT 9 = Cougar Point Tuff XI, BB 4 = Brown's Bench 4, CPT 7 = Cougar Point Tuff VII, BB 3 = Brown's Bench 3).

Feldspars

Figure 28a is a diagram of BSE-normalized REE values for WBH feldspars. There are fewer trace elements in sufficient abundance (> 10 ppm) in the West Bennett Hills feldspars than both pyroxenes and fresh glasses. The only elements in WBH feldspars useful for geochemical comparisons are Rb, Sr, Ba, Pb, Ti, La and Ce. Considerable overlap is found among feldspars from different units, therefore making unit-to-unit comparisons difficult at best (Fig 28b). One example where data trends are distinct is Fig 28c, which shows a diagram of different Ti and Ba compositions for the West Bennett Hills unit Frenchman Springs and its SCSRP equivalent Lower Jackpot, both in CAT group 7.

Although the vast majority of feldspar trace element compositions appear to be too homogenous for unit-to-unit comparisons in the CSRP, Fig 28c illustrates that the feldspar data can be useful. Note that only two samples from the SCSRP were analyzed for trace elements in feldspars, compared to fifteen samples for both pyroxene and glass trace element analyses.

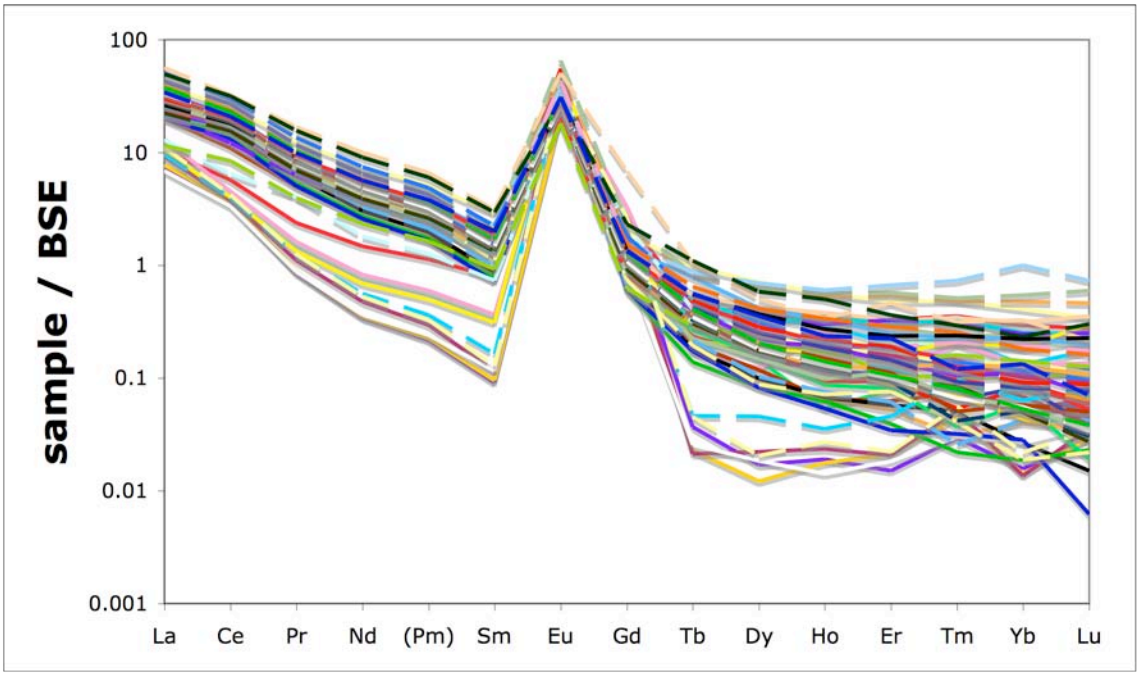

Figure 28 a: REE diagram for WBH feldspars. All samples normalized to BSE (McDonough and Sun, 1995).

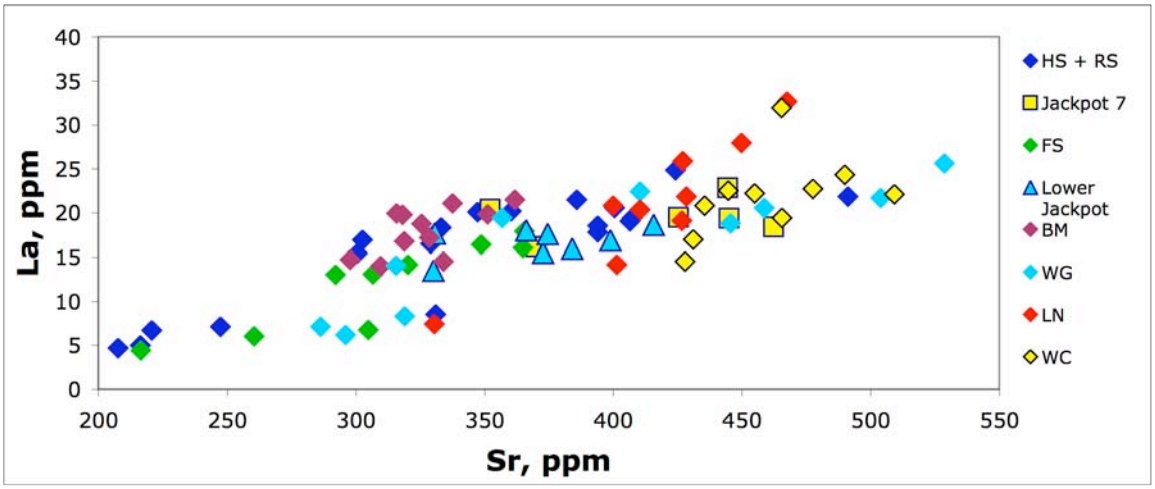

Figure 28 b: trace element diagram showing similar composition for all CSRP feldspars analyzed.

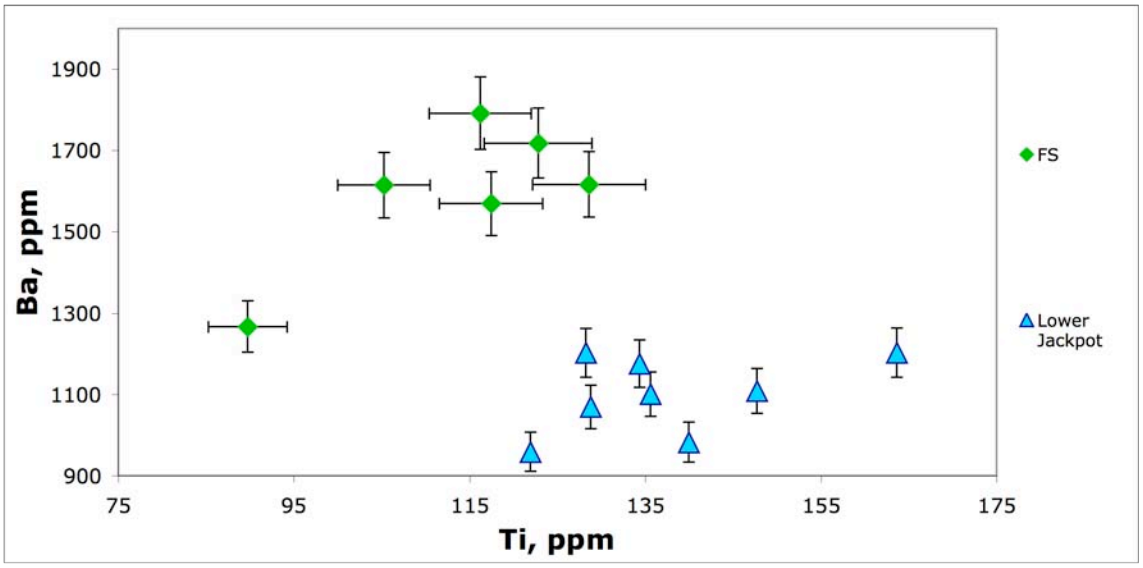

Figure 28 c: trace element diagram showing one of the rare instances where feldspar trace element compositions are distinct from unit to unit.

Chapter 4: Discussion and Conclusions

Assessment of N-S correlations in the CSRP

The data presented in Chapter 3 of this study illustrate the similar chemical compositions of the rhyolites of the southern central Snake River Plain and West Bennett Hills. Even across the CAT Groups set forth by Bonnichsen et al. (2008), the overlap of chemical compositions is significant. Comparison within each individual CAT Group reveals more pronounced compositional overlap, and quite often the distinct chemical composition of units can only be found in a single diagram or even a single trace element abundance.

All possible correlations inferred from the CAT groups investigated in this study are, on the basis of chemical composition, unlikely to demonstrate that the SCSRP rhyolites traveled as far north as the West Bennett Hills. The data in this study are not sufficient to make definitive statements regarding cross-plain N-S correlations. There is at least one possible correlation (the WBH unit High Springs and Cougar Point Tuff XV, both in CAT group 8) that requires additional investigation, particularly a radiometric age date on the High Springs, before the possibility of that correlation can be determined. In addition, the lack of comparison of the microanalytical data for the units in CAT group 5 is an issue that must be addressed in order for this problem to be solved. Table 6 shows a summary of the possible correlations investigated in this study.

The Proterozoic Yardea Dacite and Eucarro Rhyolite in southern Australia share some basic characteristics with the CSRP rhyolites: they are widespread, voluminous (> 25,000 km^3 total erupted volume), high temperature (900-1100^o C from feldspar and pyroxene thermometry) magmas with anhydrous phenocryst assemblages (Allen et al.,

CAT Group	Age Range (Ma)	units from Bruneau - Jarbidge area	units from Twin Falls area	units from WBH	Possible correlations to WBH?
8 (a & b)	10.4 - 10.7	CPT XV	BBU 8 Jackpot 7 Steer Basin Beaver Meadow	Rattlesnake Springs High Springs	HS - CPT XV possible, all others unlikely
7	10.7 - 11.0	CPT XIII	BBU 7 Lower Jackpot Big Bluff	Frenchman Springs Dive Creek Henley	unlikely
6	11.0 - 11.2	CPT XII	------	Bennett Mountain	unlikely
5	11.2 - 11.5	CPT XI, X	BBU 5, 6	Windy Gap Lower Reverse	?
4	11.5 - 11.7	CPT IX	BBU 4	Lower Normal	unlikely
3	11.7 - 11.9	CPT VII	BBU 3	Willow Creek	unlikely

Table 6: overview of the possible correlations of the CAT groups pertinent in this study (Bonnichsen et al., 2008).

2003 and references therein). Allen et al. (2003) proposed that the Yardea and Eucarro flows are correlative over an area of several 10s of kilomenters based on whole rock major element data and petrographic similarities. Twenty years ago, researchers could have made similar claims for the correlation of rhyolites in the CSRP with a data set that was only comprised of XRF data and petrographic descriptions, but the current more detailed data set for CSRP rhyolites does not allow for such claims to be made with certainty.

For the purposes of this study, units must share similar chemical compositions in all geochemical comparisons made in order for them to be deemed co-eruptive. When the units of the CAT Groups of Bonnichsen et al. (2008) are compared under the scrutiny of detailed geochemical comparisons, no firm evidence surfaces that indicates that the rhyolites of the West Bennett Hills share genetic relationships with the rhyolites of the southern central Snake River Plain. This suggests that the widespread ash-flow tuffs of the SCSRP did not extend north to the West Bennett Hills.

Implications for CSRP petrogenesis

The CSRP rhyolites share similar chemical signatures, especially whole rock major and trace elements and oxygen isotope ratios, but subtle differences in microanalytical data (microprobe major elements and laser-ablation trace elements) suggest subtle variations occurred during their petrogenesis. Three possible mechanisms for these subtle variations will be discussed: 1) individual CSRP rhyolites within a single CAT Group are actually compositionally distinct lobes of the same voluminous eruption, similar to the Bandelier tuff in northern New Mexico and the Bishop tuff in eastern

California; 2) the units are different eruptions from separate but similar systems, a mechanism that Hildreth (2004) proposed for the Long Valley region; and 3) the slight variations in the CSRP rhyolites are the products of semi-closed parts of the same system.

Studies of the Bandelier Tuff by Smith and Bailey (1966) and the Bishop Tuff by Hildreth (1979) and Smith (1979) established that large-volume intra-continental silicic tuffs can exhibit chemical zoning within a single erupted unit. The flows are the surficial manifestations of zoned magma chambers: as the eruptions began, the uppermost portion of the magma chambers were erupted and displayed the highest degree of differentiated material. As the eruptions proceeded, the more mafic portions of the chambers were eventually tapped and subsequently erupted. An important observation regarding these zoned flows is that the whole rock trace element variations are more pronounced than the whole rock major element zonation. While the possibility exists that the CSRP rhyolites are zoned with respect to trace element compositions, no consistent variations have been found in the major element composition in outcrop scale of units in the CSRP rhyolites as can be found in the Bishop & Bandelier tuffs (Smith and Bailey, 1966; Smith, 1979). If the CSRP rhyolites were erupted from a zoned magma chamber (or chambers) as the Bandelier and Bishop tuffs were, the compositional variations are significantly smaller for the CSRP rhyolites than the variations found in the Bandelier and Bishop tuffs.

Hildreth (2004) proposed a petrogenesis for the Long Valley volcanic region, eruptive center of the voluminous Bishop tuff, where the partial melting zone in the crust is not a magma "chamber" in the traditional sense, but rather an amalgamation of dikes, pods and mushy differentiated intrusions caused by direct intrusion of basaltic magma as opposed to underplating. Ductile deformation in this zone would promote extraction,

aggregation and blending of various melts, which would collect in spatially distinct pods at the top of the mush zone (Fig 29). If this scenario occurred in the central Snake River Plain, it could explain the subtle variations in chemical composition of the rhyolites within individual CAT groups. A system of multiple pods and dikes of magma underneath the Bruneau – Jarbidge region would likely have slightly differing rates and extents of crustal assimilation, crystal fractionation and magma mixing. Even if the assimilated country rock is homogenous over the entire region, these physical differences would likely impart subtle differences on the chemical compositions of the magmas generated.

If the CSRP magma chamber is a single continuous form, the possibility exists that, primarily due to heterogeneity in the surrounding country rock, chemical heterogeneity could exist in zones of the magma chamber. If isolated zones of this heterogeneous chamber are tapped during an eruption, the rhyolite would exhibit a slightly different chemical signature when compared to a rhyolite that was tapped from a different part of the magma chamber.

In order for reasonable statements to be made regarding the petrogenesis of the CSRP rhyolites, a coherent stratigraphic framework must be established that can withstand a detailed geochemical comparison of the units. Due to the massive nature of CSRP magmatism (specifically the areal extent and volume of eruptive units and the number of these massive units erupted), creating such a framework would require more radiometric age dates and a data set (including whole rock, microanalytical and oxygen isotope data) that should be at least an order of magnitude larger than the data set for this study. Although the scope of this project does not allow for definitive statements to be

made regarding the validity of cross-plain unit-to-unit correlations within the CAT Groups of Bonnichsen et al. (2008). The data presented here suggests that the widespread voluminous tuffs of the SCSRP did not propagate as far north as the West Bennett Hills.

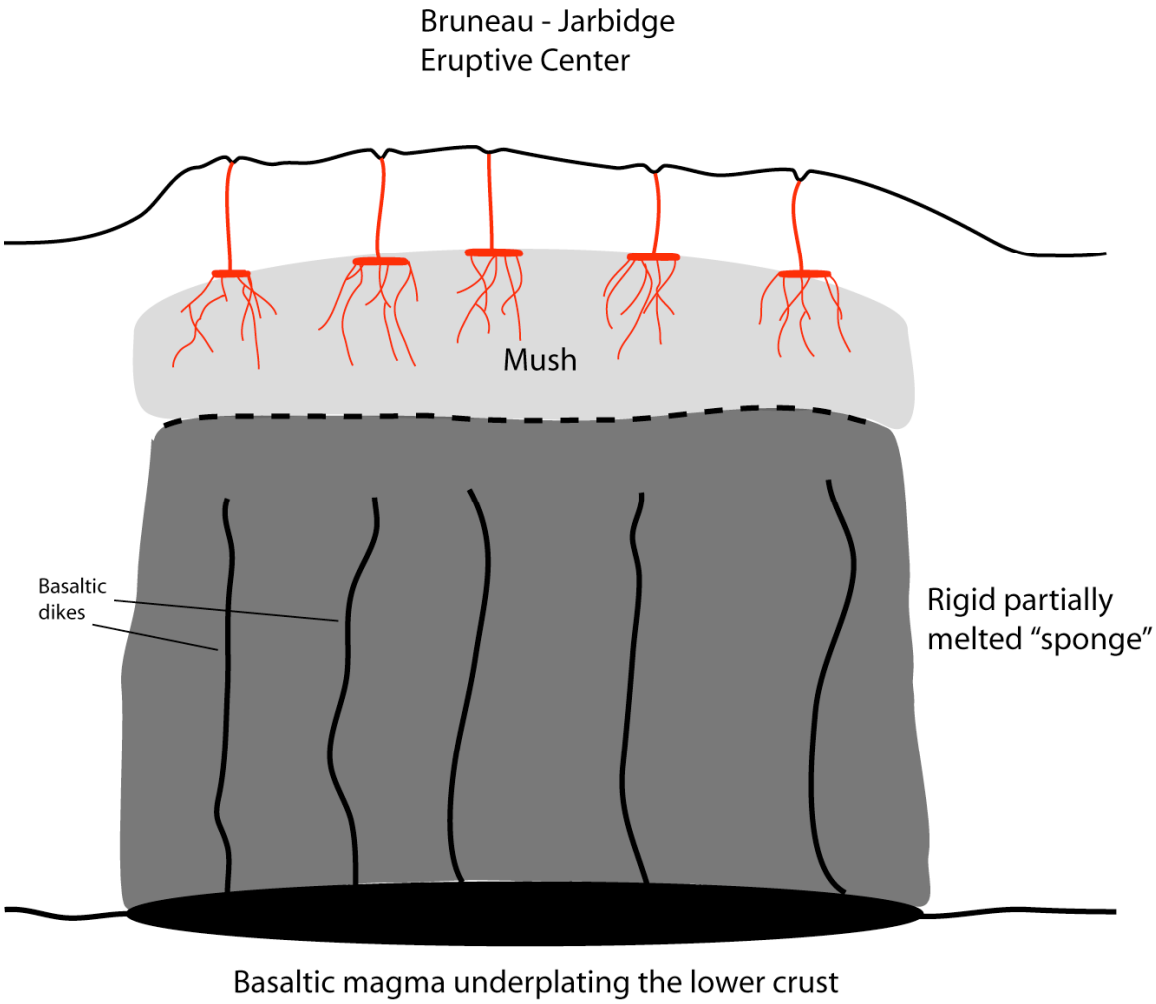

Figure 29: Cartoon illustrating a hypothetical petrogenesis for the CSRP rhyolites: basaltic magmas underplate the lower crust, heating the zone above the basaltic magma. Focused injection of basaltic dikes through the lower crust facilitate partial melting of the upper portions of the crust, and at some point the crust becomes a mush. Rhyolitic melts (shown in red) percolate through the mush and collect in spatially discreet pods at the top of the mush zone. These pods of rhyolitic magma would then erupt in spatially discrete vents, fissures and/or calderas in the Bruneau-Jarbidge eruptive center.

REFERENCES CITED

Allen, S.R., Simpson, C.J., McPhie, J., Daly, S.J., 2003, Stratigraphy, distribution and geochemistry of widespread felsic volcanic units in the Mesoproterozoic Gawler Range Volcanics, South Australia: Australia Journal of Earth Sciences, v. 50, p. 97 – 112.

Alt, D., Sears, J.M., Hyndman, D.W., 1988, Terrestrial maria; the origins of large basalt plateaus, hotspot tracks and spreading ridges: Journal of Geology, v. 96, p. 647 – 662.

Bacon, C.R., and Druitt, T.H., 1988, Compositional evolution of the zoned calcalkaline magma chamber of Mount Mazama, Crater Lake, Oregon: Contributions to Mineralogy and Petrology, v. 98, n. 2, p. 224 – 256.

Bilal, B.A., and Mueller, E., 1992, Thermodynamic study of Ce^{4+}/Ce^{3+} redox reaction in aqueous solution at elevated temperatures, 1. Reduction potential and hydrolysis equilibria of Ce^{4+} in $HClO_4$ solutions: Zeitschrift fuer Naturforschung, v. 47a, 974 – 984.

Bindeman, I.N., and Valley, J.W., 2001, Low $\delta^{18}O$ rhyolites from Yellowstone: Magmatic evolution based on analyses of zircons and individual phenocrysts: Journal of Petrology, v. 42, p. 1492 – 1517.

Blundy, J.D., and Wood, B.J., 1991, Crystal-chemical controls on the partitioning of Sr and Ba between plagioclase feldspar, silicate melts, and hydrothermal solutions: Geochimica et Cosmochimica Acta, v. 55, 193 – 209.

Blundy, J., Wood, B., 1994. Prediction of crystal-melt partition coefficients from elastic moduli: Nature, v. 372, p. 452 – 454.

Bonnichsen, B., 1982, The Bruneau – Jarbidge eruptive center, southwestern Idaho: *in* Bill Bonnichsen and R.M. Breckenridge, eds, Cenozoic Geology of Idaho: Idaho Bureau of Mines and Geology Bulletin 26, p. 237 – 254.

Bonnichsen, B., and Citron, G.P., 1982, The Cougar Point Tuff, southwestern Idaho and vicinity: *in* Bill Bonnichsen and R.M. Breckenridge, eds, Cenozoic Geology of Idaho: Idaho Bureau of Mines and Geology Bulletin 26, p. 255 – 281.

Bonnichsen, B., and Kauffman, D.F., 1987, Physical features of rhyolite lava flows in the Snake River Plain volcanic province, southwestern Idaho: Geological Society of America Special Paper 212, p. 119 – 145.

Bonnichsen, B., Godchaux, M.M., 2002, Late Miocene, Pliocene, and Pleistocene Geology of Southwestern Idaho With Emphasis on Basalts in the Bruneau-

Jarbidge, Twin Falls, and Western Snake River Plain Regions: *in* Bill Bonnichsen, C.M. White, and Michael McCurry, eds., Tectonic and Magmatic Evolution of the Snake River Plain Volcanic Province: Idaho Geological Survey Bulletin 30, p. 233 – 314.

Bonnichsen, B., Leeman, W. P., Honjo, N., McIntosh, W.C., Godchaux, M.M., 2008, Miocene silicic volcanism in southwestern Idaho: geochronology, geochemistry, and evolution of the central Snake River Plain: Bulletin of Volcanology, v. 70, p. 315 – 342.

Boroughs, S., Wolff, J., Bonnichsen, B., Godchaux, M., Larson, P., 2005, Large-volume, Low-$\delta^{18}O$ rhyolites of the central Snake River Plain, Idaho, USA: Geology, v. 33, p. 821 – 824.

Branney, M.J., Bonnichsen, B., Andrews, G.D.M., Ellis, B., Barry, T.L., McCurry, M., 2008, 'Snake River (SR)-type' volcanism at the Yellowstone hotspot track: distinctive products from unusual, high-temperature silicic super-eruptions: Bulletin of Volcanology, v. 70, p. 293 - 314

Brueseke, M.E., Hart, W.K., Heizler, M.T., 2008, Diverse mid-Miocene silicic volcanism associated with the Yellowstone-Newberry thermal anomaly: Bulletin of Volcanology, v. 70, p.343 - 360

Cameron, M., and Papike, J.J., 1980, Crystal chemistry of silicate pyroxenes: *in* Charles Prewitt, ed., Reviews in Mineralogy Volume 7: Pyroxenes, p. 5 – 92.

Camp, V.E., Ross, M.E., Hanson, W.E., 2003, Genesis of flood basalts and Basin and Range volcanic rocks from Steens Mountain to the Malheur River Gorge, Oregon: Geological Society of America Bulletin, v. 115, p. 105 – 128.

Camp, V.E., and Ross, M.E., 2004, Mantle dynamics and genesis of mafic magmatism in the intermontane Pacific Northwest: Journal of Geophysical Research, v. 109, B08204.

Cathey, H., and Nash, B. 2004. The Cougar Point Tuff: Implications for Thermochemical Zonation and Longevity of High-Temperature, Large-Volume Silicic Magmas of the Miocene Yellowstone Hotspot: Journal of Petrology 45, no. 1, p. 27-58.

Christiansen, R.L., 2001, Geology of Yellowstone Park: The Quaternary and Pliocene Yellowstone Plateau Volcanic Field of Wyoming, Idaho, and Montana: USGS Professional Paper 729-G.

Christiansen, R.L., Foulger, G.R., Evans, J.R., 2002, Upper-mantle origin of the Yellowstone hotspot: Geological Society of America Bulletin, v. 114, no. 10, p. 1245 – 1256.

Coats, R.R., 1987, Geology of Elko County, Nevada: Nevada Bureau of Mines and Geology Bulletin 101, p.1 – 111.

Eby, G.N., 1990, The A-type granitoids: a review of their occurrence and chemical characteristics and speculations on the their petrogenesis: Lithos, v. 26, p. 115-134.

Ewart, A., and W. L. Griffin, 1994, Application of proton-microprobe data to trace-element partitioning in volcanic rocks: Chemical Geology, v. 117, no. 1-4, p. 251-284.

Glen, J.M.G., Ponce, D.A., 2002, Large-scale fractures related to inception of the Yellowstone hotspot: Geological Society of America Bulletin, v. 30, no. 7, p. 647 – 650.

Hamilton, W., 1987, Plate-tectonic evolution of the western U.S.A.: Episodes, v. 10, p. 271 – 276.

Henry, C.D., and Wolff, J.A., 1992, Distinguishing strongly rheomorphic tuffs from extensive silicic lavas: Bulletin of Volcanology, v. 54, p. 171 – 186.

Hildreth, W., 1979, The Bishop Tuff: Evidence for the origin of compositional zonation in silicic magma chambers: GSA Special Paper 180, p. 43 – 75.

Hildreth, W., Christiansen, R.L., and O'Neil, J.R., 1984, Catastrophic isotopic modification of rhyolitic magma at times of caldera subsidence, Yellowstone Plateau volcanic field: Journal of Geophysical Research v. 89, p. 8339-8369.

Hildreth, W., Halliday, A.N., Christiansen, R.L., 1991, Isotopic and Chemical Evidence Concerning the Genesis and Contamination of Basaltic and Rhyolitic Magma Beneath the Yellowstone Plateau Volcanic Field: Journal of Petrology, v. 32, p. 63 – 138.

Hildreth, W., 2004, Volcanological perspectives on Long Valley, Mammoth Mountain, and Mono Craters: several contiguous but discrete systems: Journal of Volcanology and Geothermal Research, v. 136, p. 169 – 180.

Honjo, N., Bonnichsen, B., Leeman, W.P., Stormer, J.C., Jr, 1992, Mineralogy and geothermometry of high-temperature rhyolites from the central and western Snake River Plain: Bulletin of Volcanology, v. 54, p. 220 – 237.

Hooper, P.R., 1990, The timing of crustal extension and the eruption of continental flood basalts: Nature, v. 345, p. 246 – 249.

Hooper, P.R., Johnson, J., and Hawkesworth, C., 2002, A model for the origin of the western Snake River Plain as an extensional strike-slip duplex, Idaho and Oregon:

in Bill Bonnichsen, C.M. White, and Michael McCurry, eds., Tectonic and Magmatic Evolution of the Snake River Plain Volcanic Province: Idaho Geological Survey Bulletin 30, p. 59-67.

Humphreys, E., Hessler, E., Dueker, K., Farmer, G.L., Erslev, E., Atwater, T., 2003, How Laramide-Age Hydration of North American Lithosphere by the Farallon Slab Controlled Subsequent Activity in the Western United States: International Geology Review, v. 45, p. 575 – 595.

Jordan, B.T., Grunder, A.L., Duncan, R.A., Deino, A.L., 2004, Geochronology of age-progressive volcanism of the Oregon High Lava Plains: Implications for the plume interpretation of Yellowstone: Journal of Geophysical Research, vol. 109, B10202.

Mahood, G., Hildreth, W., 1983, Large partition coefficients for trace elements in high-silica rhyolites: Geochimica et Cosmochimica Acta, v. 47, p. 11 – 30.

Malde, H.E., Powers H.A., Marshall, C.H., 1963, Reconnaissance geologic map of the west-central Snake River Plain, Idaho, US Geological Survey Misc Geologic Investigations Map I-373.

McDonough, W.F., and Sun, S., 1995, The composition of the Earth: Chemical Geology, v. 120, p. 223 – 253.

Michael, P.J., 1983, Chemical differentiation of the Bishop Tuff and other high-silica magmas through crystallization process: Geology, v. 11, p. 31 – 34.

Michael, P. J., 1988, Partition coefficients for rare elements in mafic minerals of high silica rhyolites; the importance of accessory mineral inclusions: Geochimica et Cosmochimica Acta, Vol. 52, Issue 2, p. 275 - 282

Morgan, L.M., and McIntosh, W.C., 2005, Timing and development of the Heise volcanic field, Snake River Plain, Idaho, western USA: Geological Society of America Bulletin, v. 117, no. 3/4, p. 288 – 306.

Nash, W.P., and Crecraft, H.R., 1985, Partition coefficients for trace elements in silicic magmas: Geochimica et Cosmochimica Acta, v. 49, p. 2309 – 2322.

Olin, P.H., 2007, Magma Dynamics of the Phonolitic Diego Hernandez formation, Tenerife, Canary Island: Ph.D. dissertation, Washington State University.

Patino, L.C., Velbel, M.C., Price, J.R., Wade, J.A., 2003, Trace element mobility during spheroidal weathering of basalts and andesites in Hawaii and Guatemala: Chemical Geology, v. 202, p. 343 – 364.

Patino-Douce, A.E., 1997, Generation of metaluminous A-type granites by low-pressure melting of calc-alkaline granitoids: Geology, v.25, p. 743 – 746.

Pierce, K.L., Morgan, L.A., 1992, The track of the Yellowstone hot spot: Volcanism, faulting, and uplift: *in* Link, P.K., Kuntz, M.A., and Platt, L.B., eds., Regional Geology of Eastern Idaho and Western Wyoming: Geological Society of America Memoir 179.

Perkins, M.E., and Nash B.P., 2002, Explosive silicic volcanism of the Yellowstone hotspot: The ash fall record: Geological Society of America Bulletin, v. 114, no. 3, p. 367 – 381.

Rytuba, J.J., McKee, E.H., 1984, Peralkaline Ash Flow Tuffs and Calderas of the McDermitt Volcanic Field, Southeast Oregon and North Central Nevada: Journal of Geophysical Research, vol. 89, no. B10, p. 8616-8628.

Shannon, R.D., 1976, Revised Effective Ionic Radii and Systematic Studies of Interatomic Distances in Halides and Chalcogenides: Acta Crystallographica, A32, p. 751 – 767.

Sharp, Z.D., 1990, A laser-based microanalytical method for the *in situ* determination of oxygen isotope ratios of silicates and oxides: Geochimica et Cosmochimica Acta, v. 54, p. 1353- 1357.

Sisson, T.W., 1991, Pyroxene-high silica rhyolite trace element partition coefficients measured by ion microprobe: Geochimica et Cosmochimica Acta, v. 55, p. 1575 – 1585.

Sisson, T.W., 1994, Hornblende-melt trace-element partitioning measured by ion microprobe: Chemical Geology, v. 117, p. 331 – 344.

Smith, A., 1992, Back-arc convection model for Columbia River basalt genesis: Tectonophysics, v. 207 p. 269 – 285.

Smith, R.L., and Bailey, R.A., 1966, The Bandelier Tuff: A study of ash-flow eruption cycles from zoned magma chambers: Bulletin Volcanologique, v. 29, p. 83 – 104.

Smith, R.L., 1979, Ash-flow magmatism: Geological Society of America Special Paper 180, p. 5 – 27.

Streck M.J., Grunder A.L., 1997, Compositional gradients and gaps in high-silica rhyolites of the Rattlesnake Tuff, Oregon: Journal of Petrology, v. 38, p. 133–163.

Taylor, H.P., 1979, Oxygen and hydrogen isotope relationships in hydrothermal mineral deposits, *in* Barnes, H.L., ed., Geochemistry of hydrothermal ore deposits, 2nd ed.: New York, John Wiley, p. 236-277.

Valley, J.W., Kitchen, N., Kohn, M.J., Niendorf, C.R., and Spicuzza, M.J., 1995, UWG-2, a garnet standard for oxygen isotope ratios: strategies for high precision and accuracy with laser heating: Geochimica et Cosmochimica Acta, v. 59, p. 5223-5231.

Waite, G.P., Smith, R.B., Allen, R.M., 2005, Vp and Vs structure of the Yellowstone hot spot from teleseismic tomography: Evidence for an upper mantle plume: Journal of Geophysical Research, v. 111, B04303.

Whalen, J., Currie, K. Chappel, B., 1987. A-type granites: geochemical characteristics, discrimination, and petrogenesis: Contributions to Mineralogy and Petrology, v. 95, p. 407 – 419.

Wolff, J.A., Rowe, M.C., Teasdale, R., Gardner, J.N., Ramos, F.C., Heikoop, C.E., 2005, Petrogenesis of Pre-caldera Mafic Lavas, Jemez Mountains Volcanic Field (New Mexico, USA): Journal of Petrology, v.46, p. 407 – 439.

Wolff, J.A., Ramos, F.C., Hart, G.L., Patterson, J.D., Brandon, A.D., 2008, Columbia River flood basalts from a centralized crustal magmatic system: Nature Geoscience v. 1, p. 177 – 180.

Wood S., Gardner J., 1984, Silicic volcanic rocks of the Miocene Idavada group, Bennett Mountain, southwestern Idaho: Final Contract Report to Los Alamos National Laboratory

Wood, S.H., and Clemens, D.M., 2002, Geologic and Tectonic History of the Western Snake River Plain, Idaho and Oregon: *in* Bill Bonnichsen, C.M. White, and Michael McCurry, eds., Tectonic and Magmatic Evolution of the Snake River Plain Volcanic Province: Idaho Geological Survey Bulletin 30, p. 69 – 103.

Yuan, H., and Dueker, K., 2005, Teleseismic P-wave tomogram of the Yellowstone plume: Geophysical Research Letters, v. 32, L07304.

APPENDIX A

WHOLE ROCK XRF DATA

Appendix A.
WBH XRF data

UNIT	HS	HS	HS	HS	HS	HS	HS
SAMPLE	**06WS 021**	**06WS 020**	**06WS 004**	**06WS 005**	**WS 003**	**WS-017**	**WS-048**
Normalized major element oxides (wt %)							
SiO_2	73.97	73.51	72.00	74.11	71.97	73.29	70.01
TiO_2	0.40	0.58	0.59	0.40	0.625	0.537	0.735
Al_2O_3	12.78	12.84	13.18	12.62	12.87	13.02	13.98
FeO	2.79	3.74	4.18	2.82	4.32	3.65	5.13
MnO	0.04	0.02	0.04	0.05	0.058	0.019	0.092
MgO	0.25	0.13	0.29	0.21	0.40	0.09	0.41
CaO	1.35	0.99	1.62	1.46	1.63	1.16	1.90
Na_2O	2.52	2.89	3.19	2.69	3.24	3.17	2.79
K_2O	5.84	5.13	4.77	5.53	4.77	5.02	4.82
P_2O_5	0.07	0.16	0.15	0.10	0.116	0.056	0.124
XRF trace elements (ppm)							
Ni	8.4	6.4	8.2	6.0	4.0	0.1	1.9
Cr	3.2	2.6	3.4	2.7	4.1	4.1	6.1
Sc	5.8	7.7	8.3	5.0	6.7	5.9	7.2
V	10.3	21.5	25.1	10.5	22.6	20.7	24.4
Ba	1229.6	1113.0	1166.3	1274.2	1189.0	1220.7	1139.5
Rb	187.9	184.9	172.0	181.3	170.1	178.3	150.7
Sr	92.0	84.6	118.9	97.5	116.0	103.8	117.0
Zr	456.4	555.9	562.9	455.0	571.5	515.8	622.5
Y	52.8	49.4	56.0	54.4	71.6	33.6	73.7
Nb	36.9	40.2	39.1	36.2	38.1	38.9	40.5
Ga	20.4	20.5	23.2	20.7	20.0	20.6	21.3
Cu	4.6	7.8	6.1	3.9	8.0	7.4	9.5
Zn	66.1	81.2	83.7	66.6	90.2	73.7	98.2
Pb	27.6	27.1	26.1	27.4	22.7	24.2	29.4
La	81.7	76.2	77.5	76.2	81.7	87.2	92.7
Ce	147.1	129.1	146.9	145.3	144.7	80.7	163.0
Th	28.8	29.2	26.3	27.8	26.6	27.2	28.6
Nd	58.8	60.4	62.9	58.2	63.6	68.5	73.7
U	8.0	8.4	7.3	8.0	5.5	7.0	6.5

Appendix A.
WBH XRF data

UNIT	HS	HS	HS	HS	RS	RS	RS
SAMPLE	**WS-027**	**WS-028**	**WS-029**	**WS-030**	**06WS 053**	**06WS 054**	**06WS 051**
Normalized major element oxides (wt %)							
SiO_2	74.31	73.84	71.91	74.06	74.22	73.18	72.69
TiO_2	0.502	0.426	0.589	0.439	0.39	0.52	0.55
Al_2O_3	13.10	12.80	13.05	12.76	12.71	13.03	13.27
FeO	2.44	2.92	3.98	2.91	2.65	3.57	3.82
MnO	0.014	0.039	0.062	0.043	0.04	0.03	0.03
MgO	0.13	0.26	0.39	0.21	0.19	0.20	0.15
CaO	1.10	1.43	1.83	1.21	1.27	1.32	1.42
Na_2O	3.23	2.88	2.79	3.16	2.61	3.08	3.22
K_2O	5.07	5.33	5.29	5.14	5.86	4.99	4.78
P_2O_5	0.101	0.071	0.107	0.065	0.06	0.09	0.07
XRF trace elements (ppm)							
Ni	6.8	2.7	1.7	0.0	7.3	8.3	8.6
Cr	6.4	2.6	4.4	1.9	1.7	4.3	2.4
Sc	5.7	5.5	7.4	4.4	5.4	6.6	6.8
V	15.5	10.5	18.7	11.6	8.4	16.5	23.1
Ba	1267.4	1190.2	1163.6	1222.6	1191.2	1312.3	1797.7
Rb	178.5	175.8	166.1	181.1	187.8	180.8	171.0
Sr	99.7	98.4	112.1	91.9	86.7	107.5	132.8
Zr	507.5	457.3	541.7	463.4	442.2	519.7	540.0
Y	54.3	56.8	59.4	62.0	52.5	42.7	57.0
Nb	38.8	36.6	37.8	37.2	37.9	39.1	38.2
Ga	18.8	20.1	22.0	19.9	20.2	21.6	19.9
Cu	5.2	4.9	6.2	9.7	4.7	7.6	7.1
Zn	73.3	68.5	83.0	73.4	62.8	74.0	69.7
Pb	25.6	25.7	23.0	25.3	27.0	25.7	26.0
La	77.6	75.9	79.8	84.9	77.5	73.0	113.9
Ce	145.2	149.2	150.5	146.4	145.8	118.5	119.2
Th	29.6	29.1	27.3	30.3	28.0	26.8	25.8
Nd	57.8	57.9	59.7	63.3	58.4	58.4	88.9
U	8.0	7.0	8.3	6.5	6.9	7.3	5.5

Appendix A.
WBH XRF data

UNIT	RS	RS	RS	DC	DC	DC	DC
SAMPLE	**06WS 050**	**WS-061**	**WS-052**	**06WS 045**	**06WS 001**	**06WS 041**	**WS-007**
Normalized major element oxides (wt %)							
SiO_2	72.51	73.72	72.79	75.33	75.82	75.23	75.49
TiO_2	0.56	0.466	0.527	0.33	0.29	0.31	0.309
Al_2O_3	12.95	12.91	12.79	12.43	12.30	12.38	12.21
FeO	3.78	3.27	3.49	2.80	1.34	2.69	2.84
MnO	0.05	0.025	0.055	0.03	0.01	0.04	0.013
MgO	0.35	0.13	0.32	0.02	0.05	0.06	0.05
CaO	1.72	1.16	1.65	0.57	1.51	0.84	0.51
Na_2O	2.76	3.15	2.85	3.07	3.13	2.51	3.09
K_2O	5.21	5.10	5.45	5.41	5.51	5.89	5.45
P_2O_5	0.10	0.069	0.086	0.03	0.04	0.06	0.032
XRF trace elements (ppm)							
Ni	8.1	1.4	0.5	8.0	8.0	7.6	1.3
Cr	3.4	2.7	3.7	2.1	0.0	2.6	2.4
Sc	6.8	4.7	5.0	5.0	4.5	4.5	3.5
V	19.2	13.4	16.3	3.4	1.3	2.5	5.0
Ba	1172.2	1271.8	1202.2	1374.2	1178.8	1336.4	1280.9
Rb	175.3	174.8	173.4	202.3	199.9	192.5	194.2
Sr	110.2	97.0	100.3	61.9	58.1	66.5	54.6
Zr	530.8	479.9	512.7	543.7	490.5	510.5	516.4
Y	55.2	54.9	62.2	46.4	45.8	74.6	69.4
Nb	38.7	38.4	38.0	48.6	46.2	46.5	48.5
Ga	20.2	20.5	19.6	21.1	22.4	22.6	22.3
Cu	5.1	5.8	5.5	3.6	5.7	3.8	5.0
Zn	83.3	66.1	77.2	94.5	73.4	91.1	102.5
Pb	25.3	24.4	24.5	29.4	30.3	26.7	27.5
La	84.3	83.2	78.0	66.9	89.2	93.5	68.1
Ce	144.5	121.5	149.5	106.2	161.5	173.4	180.0
Th	26.4	27.6	27.3	31.7	32.9	30.4	31.1
Nd	63.8	61.7	58.3	53.5	71.1	72.6	54.3
U	5.7	6.1	6.1	6.4	6.2	8.2	5.4

Appendix A.
WBH XRF data

UNIT	DC	FS	FS	FS	FS	FS	FS
SAMPLE	**WS-023**	**06WS 059**	**06WS 058**	**06WS 056**	**WS-057**	**WS-060**	**WS-049**
Normalized major element oxides (wt %)							
SiO_2	75.67	75.21	75.30	75.35	75.43	73.81	75.38
TiO_2	0.310	0.32	0.31	0.31	0.308	0.303	0.315
Al_2O_3	12.22	12.26	12.21	12.33	12.21	12.16	12.23
FeO	2.08	2.65	2.71	2.67	2.69	2.59	2.78
MnO	0.029	0.04	0.04	0.04	0.032	0.044	0.084
MgO	0.34	0.04	0.08	0.05	0.02	0.26	0.04
CaO	0.79	0.90	0.77	0.65	0.55	2.43	0.58
Na_2O	2.73	2.55	3.16	3.18	3.03	3.14	3.17
K_2O	5.78	5.99	5.40	5.39	5.50	5.24	5.39
P_2O_5	0.055	0.03	0.03	0.04	0.234	0.032	0.035
XRF trace elements (ppm)							
Ni	16.7	8.7	7.6	9.1	0.0	0.0	0.4
Cr	13.7	1.3	2.0	3.1	2.6	2.2	1.7
Sc	4.3	5.2	3.4	5.2	4.1	4.5	3.9
V	4.4	1.7	6.0	1.8	8.4	5.0	5.7
Ba	1362.6	1259.2	1324.7	1306.2	1188.4	1304.1	1375.5
Rb	185.8	200.8	198.0	200.5	199.1	179.9	191.1
Sr	67.9	56.5	60.6	62.8	51.4	77.2	60.8
Zr	517.6	514.9	523.7	519.7	499.8	495.2	525.4
Y	68.2	66.3	68.5	70.2	73.2	75.5	54.0
Nb	47.6	47.0	48.1	47.6	48.6	45.8	48.2
Ga	22.1	21.9	22.8	21.4	21.3	21.1	21.2
Cu	5.1	2.0	3.7	4.7	6.7	6.2	3.1
Zn	88.0	93.4	95.1	85.3	83.4	72.5	93.9
Pb	30.3	30.2	26.7	28.8	27.7	29.2	26.2
La	93.7	86.4	91.4	111.3	93.6	88.8	85.8
Ce	155.7	172.3	168.3	162.2	168.9	167.0	114.0
Th	31.6	30.4	30.3	31.4	30.7	29.9	30.2
Nd	69.5	69.5	77.3	87.5	76.3	68.1	66.5
U	7.0	8.0	8.3	7.3	5.0	6.5	5.0

Appendix A.
WBH XRF data

UNIT	Hn	Hn	Hn	BM	BM	WG	WG
SAMPLE	**06WS 064**	**WS-076**	**WS-077**	**06WS 065**	**06WS 063**	**06WS 071**	**06WS 066**
Normalized major element oxides (wt %)							
SiO_2	75.96	74.98	74.95	73.86	73.25	75.17	74.57
TiO_2	0.314	0.320	0.314	0.508	0.497	0.373	0.399
Al_2O_3	12.20	12.38	12.26	12.98	12.96	12.46	12.76
FeO	2.15	2.73	2.73	3.22	3.16	2.20	2.92
MnO	0.014	0.032	0.048	0.026	0.049	0.033	0.027
MgO	0.06	0.09	0.06	0.11	0.30	0.17	0.09
CaO	0.58	0.94	0.92	0.93	1.45	0.92	0.63
Na_2O	3.13	2.75	2.70	3.03	2.75	2.50	3.03
K_2O	5.54	5.74	5.99	5.27	5.51	6.13	5.53
P_2O_5	0.050	0.031	0.034	0.069	0.085	0.044	0.051
XRF trace elements (ppm)							
Ni	3.0	0.0	0.0	3.9	3.1	2.4	2.3
Cr	1.3	1.8	2.6	2.6	2.1	0.7	3.2
Sc	4.8	3.8	4.6	5.9	6.3	5.3	5.6
V	3.2	1.3	1.6	22.1	16.4	6.4	2.5
Ba	1280.7	1275.0	1279.5	1175.0	1173.6	1000.7	1197.8
Rb	190.8	186.1	187.9	188.8	185.7	215.7	202.5
Sr	54.7	57.0	54.2	72.7	86.1	63.7	59.3
Zr	528.1	510.5	506.1	503.4	491.8	425.5	561.4
Y	50.6	82.7	80.2	71.4	52.4	57.8	68.1
Nb	47.0	47.6	46.3	38.0	37.1	40.5	46.2
Ga	24.6	21.3	21.5	19.8	19.8	18.2	19.9
Cu	3.5	4.3	2.8	5.7	6.9	3.6	5.2
Zn	90.8	94.2	90.2	65.1	66.8	56.0	65.7
Pb	29.4	30.7	28.9	23.7	26.0	25.6	29.1
La	71.7	92.5	87.8	104.2	77.4	79.1	86.3
Ce	87.8	165.4	172.5	117.7	145.5	147.0	159.6
Th	27.5	32.9	29.9	27.2	28.2	29.4	30.5
Nd	56.6	71.3	68.8	90.5	55.1	57.1	70.2
U	7.6	7.3	7.3	7.9	9.5	9.2	9.0

Appendix A.
WBH XRF data

UNIT	WG	WG	WG	WG	LR	LN	LN
SAMPLE	**06WS 067**	**06WS 068**	**06WS 069**	**06WS 070**	**06WS 072**	**06WS 035**	**06WS 034**
Normalized major element oxides (wt %)							
SiO_2	73.72	74.93	74.25	76.08	75.70	74.06	75.33
TiO_2	0.434	0.387	0.408	0.354	0.391	0.44	0.44
Al_2O_3	12.74	12.43	12.56	12.25	12.48	12.83	12.70
FeO	3.11	2.55	2.73	2.04	2.01	2.52	1.95
MnO	0.049	0.014	0.049	0.012	0.018	0.04	0.02
MgO	0.16	0.16	0.16	0.07	0.09	0.26	0.10
CaO	1.15	0.80	1.09	0.64	0.77	1.33	1.02
Na_2O	2.74	3.09	2.62	2.94	2.93	2.66	2.99
K_2O	5.83	5.60	6.06	5.58	5.56	5.78	5.38
P_2O_5	0.055	0.043	0.062	0.041	0.045	0.07	0.06
XRF trace elements (ppm)							
Ni	2.7	2.8	1.8	3.6	3.4	9.6	8.7
Cr	4.6	1.5	2.3	0.0	0.0	4.7	3.0
Sc	6.1	4.6	4.6	4.7	4.9	6.0	6.5
V	4.7	1.6	2.9	5.1	6.9	12.4	11.7
Ba	1153.7	1152.6	1195.2	1208.2	1040.6	961.2	960.9
Rb	196.7	212.5	202.3	210.4	201.9	214.1	210.3
Sr	73.7	60.4	66.8	63.3	70.1	89.0	82.1
Zr	578.5	525.4	554.6	420.6	455.6	422.2	432.8
Y	60.8	31.8	62.8	48.6	69.2	49.1	48.0
Nb	45.2	43.0	42.2	40.3	38.7	38.5	40.0
Ga	19.6	21.1	20.4	19.7	20.2	20.0	20.3
Cu	6.7	4.5	5.7	6.2	3.9	5.7	3.3
Zn	73.4	65.5	70.5	66.6	61.8	60.3	57.2
Pb	28.7	29.2	28.9	28.3	27.6	27.0	29.3
La	80.6	71.5	82.1	85.8	92.0	75.7	77.5
Ce	157.9	96.1	156.7	157.0	128.2	149.6	139.0
Th	29.1	30.3	28.7	28.6	29.6	29.2	30.3
Nd	62.1	52.4	63.6	62.4	71.0	58.3	60.0
U	8.3	6.1	7.0	10.0	7.5	6.0	8.7

Appendix A.
WBH XRF data

UNIT	LN	WC	WC	WC	WC
SAMPLE	**06WS 036**	**06WS 040**	**06WS 039**	**06WS 037**	**WS-038**
Normalized major element oxides (wt %)					
SiO_2	74.30	73.73	74.66	73.10	72.97
TiO_2	0.493	0.50	0.50	0.52	0.527
Al_2O_3	13.03	13.00	12.80	13.01	13.01
FeO	2.48	2.99	2.41	3.01	3.38
MnO	0.033	0.03	0.02	0.05	0.048
MgO	0.14	0.18	0.11	0.38	0.34
CaO	1.17	1.29	1.23	1.58	1.46
Na_2O	2.91	3.02	2.90	2.56	2.50
K_2O	5.36	5.17	5.29	5.70	5.67
P_2O_5	0.081	0.09	0.09	0.09	0.089
XRF trace elements (ppm)					
Ni	4.5	9.7	10.6	8.1	4.4
Cr	3.9	4.8	4.5	2.6	12.3
Sc	6.9	5.8	5.9	7.2	6.5
V	18.2	17.7	14.6	19.2	14.9
Ba	1178.6	969.1	1001.1	1060.7	1123.5
Rb	200.3	199.7	201.1	204.7	198.8
Sr	103.3	102.3	97.6	108.7	99.7
Zr	466.8	467.3	447.5	443.2	447.5
Y	50.2	45.5	51.4	52.0	58.5
Nb	39.0	40.3	39.0	38.4	38.6
Ga	19.6	21.0	20.0	19.8	20.3
Cu	6.7	3.8	5.4	5.1	4.8
Zn	69.0	75.5	75.4	72.9	69.2
Pb	25.6	26.2	26.7	24.9	25.7
La	83.4	67.8	80.6	75.8	80.4
Ce	125.1	107.4	136.5	145.4	144.9
Th	30.4	27.9	28.8	27.6	28.2
Nd	66.3	53.6	63.1	57.9	58.7
U	6.5	8.2	7.1	7.6	9.4

APPENDIX B

WHOLE ROCK ICP DATA

Appendix B.
WBH ICP trace element data (ppm)

UNIT	HS	HS	HS	HS	HS	HS	HS
SAMPLE	**06WS 021**	**06WS 020**	**06WS 004**	**06WS 005**	**WS 003**	**WS-017**	**WS-048**
La	78.8	75.6	77.3	79.6	85.3	88.0	99.5
Ce	148.8	129.3	144.9	147.8	147.3	81.7	171.8
Pr	16.6	16.1	16.7	16.7	18.2	19.7	21.3
Nd	58.3	57.6	60.6	58.8	66.5	71.0	78.5
Sm	11.5	11.5	12.2	11.7	13.3	13.4	15.7
Eu	1.7	1.7	2.2	1.8	2.2	2.3	2.6
Gd	10.2	10.3	11.2	10.7	12.7	9.8	14.6
Tb	1.7	1.7	1.9	1.8	2.1	1.5	2.4
Dy	10.6	10.5	11.6	11.1	13.2	7.9	14.8
Ho	2.2	2.1	2.3	2.3	2.7	1.5	3.0
Er	6.0	5.7	6.5	6.3	7.6	3.8	8.1
Tm	0.9	0.8	0.9	0.9	1.1	0.6	1.2
Yb	5.4	5.1	5.9	5.7	6.8	3.5	7.3
Lu	0.8	0.8	0.9	0.9	1.1	0.5	1.1
Ba	1230.6	1108.3	1182.7	1285.9	1236.0	1264.9	1196.5
Th	28.3	28.8	27.8	29.1	28.0	29.5	30.2
Nb	39.3	39.3	38.7	37.1	39.6	40.2	42.4
Y	58.1	53.1	60.6	59.1	72.7	33.6	75.6
Hf	12.1	13.9	14.7	12.5	14.8	13.8	16.5
Ta	2.7	2.9	2.9	2.8	2.7	2.8	2.9
U	6.7	7.2	5.7	6.7	6.4	6.4	7.1
Pb	24.6	24.9	25.3	25.9	24.4	26.2	30.1
Rb	185.0	171.7	163.7	172.1	169.6	177.2	154.8
Cs	3.4	2.6	2.7	3.3	2.6	2.8	3.0
Sr	87.8	80.2	114.4	93.5	118.7	105.0	121.1
Sc	5.7	7.1	8.0	5.5	7.7	6.5	9.1
Zr	443.9	506.5	542.8	441.3	554.8	503.6	621.3

Appendix B.
WBH ICP trace element data (ppm)

UNIT	HS	HS	HS	HS	RS	RS	RS
SAMPLE	**WS-027**	**WS-028**	**WS-029**	**WS-030**	**06WS 053**	**06WS 054**	**06WS 051**
La	82.4	79.6	81.0	87.8	79.9	76.5	115.9
Ce	149.1	150.0	151.0	153.4	148.3	122.6	123.2
Pr	17.2	16.6	17.0	18.2	16.7	16.2	25.7
Nd	60.7	58.9	61.5	65.5	59.2	58.4	91.8
Sm	12.0	11.6	12.3	12.9	11.7	11.7	17.8
Eu	2.0	1.9	2.1	1.9	1.6	2.1	3.0
Gd	10.7	10.6	11.2	11.8	10.6	10.1	14.5
Tb	1.8	1.8	1.9	2.0	1.8	1.7	2.4
Dy	10.7	10.8	11.4	12.0	11.1	10.0	13.8
Ho	2.1	2.2	2.3	2.4	2.2	2.0	2.5
Er	5.7	6.1	6.4	6.6	6.1	5.3	6.6
Tm	0.8	0.9	0.9	1.0	0.9	0.8	0.9
Yb	5.1	5.6	5.7	5.9	5.6	4.8	5.6
Lu	0.8	0.8	0.9	0.9	0.9	0.7	0.8
Ba	1319.2	1240.7	1199.6	1272.2	1212.7	1314.2	1833.3
Th	30.6	29.7	28.0	30.7	29.9	28.8	27.8
Nb	40.4	38.0	38.5	38.9	38.0	38.8	38.1
Y	54.6	57.3	60.7	62.8	58.0	46.2	63.0
Hf	13.9	12.7	14.5	13.0	12.0	13.6	14.2
Ta	2.8	2.7	2.6	2.8	2.9	2.8	2.8
U	7.8	7.2	6.9	7.2	6.8	6.6	6.0
Pb	27.1	26.3	25.1	26.5	26.3	25.5	25.7
Rb	180.5	176.8	166.5	182.7	181.7	173.2	166.5
Cs	2.7	3.2	3.1	3.4	3.4	2.4	2.5
Sr	102.6	100.6	114.5	94.2	84.6	103.9	132.5
Sc	6.1	5.4	7.4	5.4	5.3	7.2	7.9
Zr	513.0	458.8	539.9	461.4	420.9	491.2	524.5

Appendix B.
WBH ICP trace element data (ppm)

UNIT	RS	RS	RS	DC	DC	DC	DC
SAMPLE	**06WS 050**	**WS-061**	**WS-052**	**06WS 045**	**06WS 001**	**06WS 041**	**WS-007**
La	82.0	88.2	81.6	65.2	91.4	94.2	70.7
Ce	145.6	132.2	154.4	108.1	164.0	176.9	184.1
Pr	17.6	18.7	17.3	14.8	19.9	20.2	15.8
Nd	63.0	67.1	62.0	54.0	70.6	73.6	56.4
Sm	12.5	13.0	12.3	11.1	14.0	15.1	11.9
Eu	2.0	2.0	1.9	2.2	2.0	2.3	2.1
Gd	11.1	11.5	11.4	9.3	11.7	13.9	11.3
Tb	1.9	1.8	1.9	1.7	1.9	2.4	2.0
Dy	11.4	10.9	11.9	10.4	11.2	15.4	12.8
Ho	2.3	2.2	2.4	2.1	2.1	3.1	2.6
Er	6.4	5.8	6.5	5.9	5.7	8.8	7.3
Tm	0.9	0.8	1.0	0.9	0.8	1.3	1.1
Yb	5.7	5.3	6.0	5.7	4.9	7.8	7.0
Lu	0.9	0.8	0.9	0.9	0.7	1.2	1.1
Ba	1165.1	1339.7	1257.2	1390.7	1202.4	1368.8	1331.9
Th	26.7	30.4	29.7	31.1	32.4	30.6	32.1
Nb	39.3	39.7	39.5	48.6	46.5	46.8	49.0
Y	60.2	56.3	63.1	51.5	51.3	81.5	68.8
Hf	13.6	13.5	14.1	14.7	14.1	13.3	14.5
Ta	2.7	2.8	2.7	3.5	3.5	3.4	3.4
U	6.4	6.8	7.3	6.0	6.2	7.0	6.6
Pb	23.4	26.4	25.9	27.8	28.4	26.3	27.4
Rb	171.0	178.3	175.5	191.6	189.1	184.6	192.1
Cs	3.1	2.9	3.2	2.5	2.8	3.9	3.4
Sr	106.2	99.8	103.1	59.6	55.3	65.3	55.1
Sc	8.0	5.6	6.4	5.0	4.2	4.9	4.6
Zr	505.9	480.4	516.7	514.4	476.8	450.7	507.5

Appendix B.
WBH ICP trace element data (ppm)

UNIT	DC	FS	FS	FS	FS	FS	FS
SAMPLE	**WS-023**	**06WS 059**	**06WS 058**	**06WS 056**	**WS-057**	**WS-060**	**WS-049**
La	95.9	91.2	93.8	111.0	101.6	93.4	89.6
Ce	162.4	173.9	167.9	161.8	177.8	175.3	121.4
Pr	20.6	19.5	20.2	23.7	22.8	20.0	19.6
Nd	75.1	70.7	73.9	86.4	82.0	72.9	70.8
Sm	14.9	14.4	15.2	17.0	16.2	14.7	14.1
Eu	2.2	2.1	2.2	2.5	2.3	2.3	2.2
Gd	13.6	13.3	13.8	15.3	13.9	13.9	12.3
Tb	2.3	2.3	2.4	2.6	2.4	2.4	2.0
Dy	13.6	14.0	14.8	15.8	14.4	14.9	11.6
Ho	2.7	2.8	3.0	3.1	2.9	3.1	2.3
Er	7.4	7.8	8.3	8.2	8.0	8.6	6.0
Tm	1.1	1.1	1.2	1.2	1.2	1.3	0.9
Yb	6.6	7.1	7.6	7.2	7.2	7.9	5.7
Lu	1.0	1.1	1.2	1.1	1.1	1.2	0.9
Ba	1430.6	1282.6	1348.5	1320.4	1237.2	1372.0	1424.6
Th	32.1	31.3	31.4	32.1	33.4	31.9	32.4
Nb	48.9	47.9	48.4	47.6	49.5	47.8	49.7
Y	68.8	73.0	76.0	77.3	73.9	78.0	54.4
Hf	14.9	14.1	14.4	13.9	14.4	14.4	14.8
Ta	3.3	3.5	3.5	3.5	3.5	3.3	3.4
U	7.8	7.1	7.4	6.6	6.4	7.7	6.0
Pb	32.0	29.2	26.5	28.0	29.1	30.4	28.0
Rb	188.6	192.2	189.4	190.9	202.0	185.8	192.6
Cs	3.8	3.6	3.5	2.9	3.1	2.6	3.0
Sr	69.6	55.5	58.6	60.7	53.5	80.8	62.3
Sc	4.8	5.0	4.9	5.2	4.2	4.4	4.5
Zr	523.2	483.7	499.5	472.8	495.3	502.9	518.6

Appendix B.
WBH ICP trace element data (ppm)

UNIT	Hn	Hn	Hn	BM	BM	WG	WG
SAMPLE	**06WS 064**	**WS-076**	**WS-077**	**06WS 065**	**06WS 063**	**06WS 071**	**06WS 066**
La	73.2	95.87	93.42	108.8	78.4	83.5	87.3
Ce	93.5	173.41	181.52	118.9	144.3	156.5	161.5
Pr	16.3	20.66	20.19	25.4	16.4	17.6	18.4
Nd	58.7	74.46	72.99	92.9	57.3	61.6	65.6
Sm	11.9	15.17	14.97	18.1	11.2	12.2	12.9
Eu	2.1	2.14	2.14	2.2	1.7	1.4	1.8
Gd	10.1	14.17	13.86	15.3	10.0	10.6	11.5
Tb	1.7	2.48	2.42	2.4	1.7	1.8	2.0
Dy	10.3	15.53	15.31	14.2	10.3	11.1	11.8
Ho	2.1	3.18	3.14	2.8	2.1	2.3	2.4
Er	5.7	8.84	8.71	7.7	5.7	6.2	6.5
Tm	0.8	1.30	1.28	1.1	0.8	0.9	1.0
Yb	5.2	8.18	7.91	6.9	5.2	5.7	6.0
Lu	0.8	1.26	1.21	1.1	0.8	0.9	0.9
Ba	1303.6	1314	1339	1201.1	1175.2	1043.5	1202.6
Th	31.4	32.21	31.95	30.8	28.2	32.9	31.1
Nb	49.5	48.92	49.03	38.9	38.4	41.7	44.5
Y	52.1	83.49	81.96	71.1	54.7	57.3	61.1
Hf	14.9	15.02	14.96	13.9	12.4	11.7	15.1
Ta	3.4	3.35	3.36	2.8	2.7	3.1	3.1
U	7.0	7.81	8.22	7.9	6.8	7.7	7.4
Pb	28.6	30.11	29.70	26.7	24.4	28.7	28.9
Rb	197.8	190.6	192.8	189.9	187.6	222.2	197.0
Cs	2.6	3.58	3.80	2.8	3.4	4.5	3.7
Sr	58.0	58	57	74.4	85.1	66.2	75.0
Sc	5.6	4.7	4.7	7.8	6.6	6.0	7.1
Zr	520.8	524	524	487.4	453.4	389.7	558.2

Appendix B.
WBH ICP trace element data (ppm)

UNIT	WG	WG	WG	WG	LR	LN	LN
SAMPLE	**06WS 067**	**06WS 068**	**06WS 069**	**06WS 070**	**06WS 072**	**06WS 035**	**06WS 034**
La	89.9	73.7	86.6	89.4	97.0	76.9	82.0
Ce	162.2	97.7	161.3	161.0	133.5	145.3	150.2
Pr	19.2	15.4	18.2	18.5	20.8	16.2	17.2
Nd	69.1	53.4	64.5	64.7	75.4	57.1	60.4
Sm	13.9	10.1	12.9	12.6	15.2	11.1	11.9
Eu	1.9	1.6	1.7	1.5	1.8	1.5	1.5
Gd	12.4	7.8	11.5	10.7	14.0	10.0	10.3
Tb	2.1	1.2	2.0	1.8	2.3	1.7	1.7
Dy	13.0	6.7	12.1	10.9	13.8	10.3	10.7
Ho	2.6	1.2	2.5	2.1	2.8	2.0	2.1
Er	7.3	3.3	6.9	5.8	7.5	5.6	5.8
Tm	1.1	0.5	1.0	0.9	1.1	0.8	0.9
Yb	6.6	3.0	6.3	5.3	6.5	5.2	5.3
Lu	1.0	0.5	1.0	0.8	1.0	0.8	0.8
Ba	1220.9	1181.8	1225.1	1233.9	1089.3	966.3	990.0
Th	33.0	31.3	31.4	33.5	33.4	30.6	32.8
Nb	46.7	44.9	44.4	42.5	42.3	38.2	41.0
Y	67.3	30.4	63.4	51.0	71.5	54.1	54.1
Hf	15.1	13.3	14.7	11.5	12.4	11.4	11.9
Ta	3.3	3.1	3.1	3.1	3.1	2.9	3.1
U	7.8	6.3	7.5	8.0	7.7	6.8	7.5
Pb	29.4	28.0	28.4	28.6	28.7	26.6	28.2
Rb	203.1	211.7	203.7	217.1	206.5	203.2	205.6
Cs	3.5	3.2	3.8	3.8	3.4	3.6	3.4
Sr	60.8	62.3	71.3	68.4	74.1	85.6	79.4
Sc	7.1	6.2	6.8	6.2	6.5	6.0	6.5
Zr	539.1	476.9	536.4	378.0	415.6	395.5	411.3

Appendix B.
WBH ICP trace element data (ppm)

UNIT	LN	WC	WC	WC	WC
SAMPLE	**06WS 036**	**06WS 040**	**06WS 039**	**06WS 037**	**WS-038**
La	87.2	71.0	80.6	84.7	81.5
Ce	130.4	114.3	138.8	159.1	152.2
Pr	18.3	15.1	17.4	17.9	17.2
Nd	65.3	54.4	62.6	63.9	61.6
Sm	12.7	11.0	12.6	12.7	12.2
Eu	1.8	1.8	1.7	1.9	1.7
Gd	11.0	9.8	11.1	11.4	11.0
Tb	1.8	1.6	1.9	1.9	1.8
Dy	10.5	10.0	11.2	11.7	11.2
Ho	2.0	2.0	2.2	2.4	2.3
Er	5.4	5.3	5.9	6.5	6.2
Tm	0.8	0.8	0.9	0.9	0.9
Yb	4.6	4.7	5.3	5.9	5.6
Lu	0.7	0.7	0.8	0.9	0.9
Ba	1199.0	989.2	1023.5	1178.4	1186.2
Th	31.9	30.3	30.0	31.9	30.6
Nb	40.0	39.6	39.3	41.8	40.4
Y	49.4	49.2	56.8	61.6	59.8
Hf	12.6	12.2	12.1	13.0	12.8
Ta	3.0	3.0	3.0	3.1	2.9
U	6.8	6.5	6.9	7.2	7.3
Pb	27.6	26.4	26.4	28.0	27.1
Rb	200.2	192.9	193.6	214.2	203.7
Cs	3.2	3.0	3.2	3.9	3.6
Sr	108.9	99.3	94.5	114.4	103.6
Sc	7.0	7.1	7.0	7.8	6.5
Zr	447.1	430.1	426.4	461.9	457.8

APPENDIX C

MICROPROBE PYROXENE DATA

Appendix C. Pyroxene electron microprobe data

UNIT	HS	HS	HS	HS	HS	HS	HS	HS
SAMPLE	**06WS 028**	**06WS 028**	**06WS 028**	**06WS 028**	**06WS 028**	**06WS 028**	**06WS 028**	**06WS 028**
ANALYSIS	pyx2 rim	pyx4 core	pyx4 rim	pyx5 core	pyx5 rim	pyx6 rim2	pyx8 core	pyx9 core
SiO_2	47.93	47.99	48.08	47.84	47.91	48.03	47.80	47.89
TiO_2	0.23	0.20	0.23	0.25	0.22	0.20	0.22	0.27
Al_2O_3	0.43	0.41	0.43	0.39	0.43	0.49	0.46	0.46
FeO	37.62	37.64	37.75	37.93	37.42	37.39	37.38	36.95
MnO	0.95	0.86	1.01	1.02	0.94	0.99	0.97	1.01
MgO	8.35	8.41	8.20	8.14	8.20	8.39	8.76	8.44
CaO	4.39	4.41	4.21	4.36	4.77	4.35	4.31	4.86
Na_2O	0.04	0.02	0.03	0.05	0.04	0.10	0.04	0.05
K_2O	0.05	0.05	0.06	0.04	0.06	0.07	0.06	0.07
TOTAL	98.72	99.90	100.21	99.70	99.91	99.23	99.89	100.28

Appendix C. Pyroxene electron microprobe data

UNIT	HS	HS	HS	HS	HS	HS	RS	RS
SAMPLE	**06WS 028**	**06WS 028**	**06WS 028**	**06WS 028**	**06WS 028**	**06WS 028**	**06WS 052**	**06WS 052**
ANALYSIS	pyx9 rim	pyx10 rim	pyx11 core	pyx11 rim	pyx12 core2	pyx13 rim	pyx2 core	pyx4 core
SiO_2	48.14	48.38	49.22	49.14	49.22	49.32	48.32	47.96
TiO_2	0.22	0.29	0.36	0.37	0.38	0.37	0.23	0.24
Al_2O_3	0.49	0.47	0.91	0.94	0.92	1.28	0.54	0.45
FeO	36.23	35.61	23.77	23.51	23.43	24.81	35.32	37.63
MnO	0.89	0.92	0.57	0.65	0.51	0.56	0.85	0.95
MgO	8.23	9.69	8.30	8.33	8.32	7.23	9.58	8.39
CaO	5.70	4.50	16.67	16.75	16.90	16.02	5.12	4.34
Na_2O	0.06	0.06	0.15	0.21	0.21	0.26	0.03	0.02
K_2O	0.04	0.08	0.06	0.09	0.11	0.15	0.01	0.02
TOTAL	98.96	100.78	99.37	99.46	98.56	100.68	98.57	99.16

Appendix C. Pyroxene electron microprobe data

UNIT	RS	RS	RS	RS	RS	RS	RS	RS
SAMPLE	**06WS 052**	**06WS 052**	**06WS 052**	**06WS 052**	**06WS 052**	**06WS 052**	**06WS 052**	**06WS 052**
ANALYSIS	pyx4 rim	pyx5 core2	pyx5 rim	pyx9 core	pyx9 core2	pyx9 rim	pyx9 rim2	pyx12 core
SiO_2	47.72	48.13	48.41	47.69	47.70	47.93	47.89	47.39
TiO_2	0.19	0.28	0.22	0.21	0.23	0.26	0.18	0.25
Al_2O_3	0.47	0.51	0.50	0.44	0.43	0.48	0.52	0.50
FeO	37.84	35.87	35.46	37.72	37.82	36.37	37.28	37.01
MnO	0.98	0.93	0.89	1.00	0.90	0.83	1.02	0.96
MgO	8.41	9.79	9.85	8.37	8.44	8.23	8.78	8.31
CaO	4.31	4.41	4.57	4.49	4.32	5.82	4.24	5.48
Na_2O	0.03	0.06	0.05	0.05	0.04	0.05	0.04	0.05
K_2O	0.04	0.02	0.05	0.03	0.12	0.03	0.04	0.05
TOTAL	98.72	101.13	99.90	99.24	100.28	99.32	100.60	99.99

Appendix C. Pyroxene electron microprobe data

UNIT	RS	RS	RS	RS	RS	RS	RS	RS
SAMPLE	**06WS 052**	**06WS 052**	**06WS 052**	**06WS 052**	**06WS 052**	**06WS 052**	**06WS 052**	**06WS 052**
ANALYSIS	L10 core	L10 rim	pyx1 core	pyx1 rim	pyx6 rim2	pyx7 core2	pyx7 rim	pyx8 core
SiO_2	47.44	47.85	49.15	49.51	49.12	49.04	49.30	49.32
TiO_2	0.22	0.21	0.36	0.37	0.38	0.34	0.37	0.36
Al_2O_3	0.52	0.55	0.86	0.98	0.99	0.90	1.04	0.91
FeO	36.14	35.79	25.39	23.13	24.04	23.73	23.49	24.57
MnO	0.96	0.95	0.71	0.53	0.48	0.62	0.54	0.62
MgO	9.63	9.66	8.53	8.44	8.35	8.33	8.38	7.90
CaO	4.66	4.73	14.78	16.82	16.40	16.82	16.62	16.09
Na_2O	0.05	0.03	0.19	0.17	0.20	0.19	0.21	0.17
K_2O	0.37	0.24	0.02	0.04	0.02	0.02	0.05	0.06
TOTAL	99.15	99.47	98.98	99.15	100.59	99.54	99.79	99.21

Appendix C. Pyroxene electron microprobe data

UNIT	RS	RS	RS	RS	RS	RS	RS	FS
SAMPLE	**06WS 052**	**06WS 052**	**06WS 052**	**06WS 052**	**06WS 052**	**06WS 052**	**06WS 052**	**06WS 059**
ANALYSIS	pyx8 rim	pyx10 core	pyx10 rim	pyx11 core	pyx11 rim	pyx13 core2	pyx13 rim	pyx1 core
SiO_2	49.17	49.19	49.29	49.01	49.03	48.68	48.82	47.08
TiO_2	0.28	0.38	0.39	0.35	0.35	0.35	0.36	0.42
Al_2O_3	0.72	0.96	1.03	0.91	0.90	0.81	0.82	0.76
FeO	24.50	23.88	23.45	23.81	23.70	25.52	24.84	29.36
MnO	0.53	0.47	0.66	0.64	0.62	0.62	0.58	0.62
MgO	7.44	8.36	8.26	8.32	8.47	7.39	7.32	2.94
CaO	17.09	16.51	16.66	16.70	16.70	16.39	16.98	18.57
Na_2O	0.23	0.23	0.23	0.21	0.18	0.19	0.25	0.22
K_2O	0.04	0.03	0.03	0.05	0.04	0.05	0.05	0.03
TOTAL	98.78	100.62	100.58	100.13	100.11	100.29	99.76	99.93

Appendix C. Pyroxene electron microprobe data

UNIT	FS	FS	FS	FS	FS	FS	FS	FS
SAMPLE	**06WS 059**	**06WS 059**	**06WS 059**	**06WS 059**	**06WS 059**	**06WS 059**	**06WS 059**	**06WS 059**
ANALYSIS	pyx1 rim	pyx2 core	pyx2 rim 2	pyx3 core	pyx4 core	pyx4 rim	pyx5 core	pyx6 rim
SiO_2	47.44	47.44	48.46	48.02	47.70	47.87	48.11	47.72
TiO_2	0.41	0.46	0.42	0.42	0.50	0.45	0.46	0.40
Al_2O_3	0.76	0.77	0.80	0.70	0.77	0.78	0.78	0.72
FeO	29.42	28.28	27.63	27.62	28.32	28.31	28.42	28.42
MnO	0.68	0.73	0.57	0.69	0.61	0.71	0.56	0.66
MgO	2.69	3.76	3.83	3.97	3.75	3.01	3.02	3.03
CaO	18.36	18.34	18.14	18.36	18.12	18.59	18.46	18.80
Na_2O	0.19	0.20	0.13	0.16	0.18	0.23	0.18	0.21
K_2O	0.03	0.02	0.02	0.05	0.04	0.05	0.02	0.03
TOTAL	99.10	99.31	98.54	98.88	98.58	98.59	98.63	99.05

Appendix C. Pyroxene electron microprobe data

UNIT	FS	FS	FS	FS	FS	FS	FS	FS
SAMPLE	**06WS 059**	**06WS 059**	**06WS 059**	**06WS 059**	**06WS 059**	**06WS 059**	**06WS 059**	**06WS 059**
ANALYSIS	pyx7 core	pyx7 rim	pyx8 core	pyx8 core 2	pyx9 core	pyx9 rim	pyx11 rim	pyx13 core
SiO_2	47.58	47.31	47.48	47.74	47.64	47.74	47.79	47.28
TiO_2	0.40	0.41	0.44	0.47	0.45	0.39	0.43	0.45
Al_2O_3	0.70	0.76	0.91	1.07	0.82	0.78	0.76	0.74
FeO	28.66	28.99	28.75	28.99	28.30	28.84	28.47	29.01
MnO	0.64	0.70	0.57	0.56	0.72	0.71	0.67	0.73
MgO	3.05	3.06	3.24	3.15	3.56	2.88	3.12	2.93
CaO	18.71	18.52	18.39	17.69	18.27	18.39	18.53	18.64
Na_2O	0.23	0.22	0.19	0.20	0.20	0.23	0.17	0.16
K_2O	0.02	0.02	0.04	0.12	0.04	0.04	0.06	0.07
TOTAL	99.73	99.40	99.82	99.19	99.40	99.18	99.20	99.66

Appendix C. Pyroxene electron microprobe data

UNIT	FS	FS	Hn	Hn	Hn	Hn	Hn	Hn
SAMPLE	**06WS 059**	**06WS 059**	**07WS 077**	**07WS 077**	**07WS 077**	**07WS 077**	**07WS 077**	**07WS 077**
ANALYSIS	pyx13 rim	pyx 14 rim	1c	1r	2c	2r	3c	3r
SiO_2	47.71	47.69	47.77	47.73	47.64	47.52	47.63	47.72
TiO_2	0.42	0.40	0.39	0.39	0.44	0.49	0.46	0.43
Al_2O_3	0.73	0.76	0.72	0.74	0.69	0.74	0.76	0.79
FeO	28.28	28.55	28.87	28.76	28.87	29.19	28.57	28.70
MnO	0.67	0.65	0.59	0.59	0.63	0.58	0.72	0.56
MgO	3.01	3.00	3.12	3.05	2.97	2.77	3.25	3.25
CaO	18.95	18.70	18.24	18.54	18.50	18.48	18.40	18.35
Na_2O	0.19	0.21	0.24	0.18	0.22	0.20	0.18	0.18
K_2O	0.05	0.04	0.05	0.03	0.03	0.03	0.03	0.03
TOTAL	99.38	99.48	100.64	100.48	100.53	100.20	98.61	98.19

Appendix C. Pyroxene electron microprobe data

UNIT	Hn	Hn	Hn	Hn	Hn	Hn	Hn	Hn
SAMPLE	**07WS 077**	**07WS 077**	**07WS 077**	**07WS 077**	**07WS 077**	**07WS 077**	**07WS 077**	**07WS 077**
ANALYSIS	4c	4r	5c	5r	6c	6r	7c	8c
SiO_2	47.64	47.69	47.67	47.62	47.72	47.71	47.64	47.73
TiO_2	0.47	0.42	0.44	0.45	0.46	0.43	0.44	0.40
Al_2O_3	0.76	0.75	0.72	0.78	0.78	0.74	0.74	0.69
FeO	28.74	28.80	28.94	29.22	28.66	28.91	28.85	29.00
MnO	0.61	0.53	0.71	0.64	0.66	0.61	0.67	0.61
MgO	3.11	2.99	3.13	2.90	3.20	2.94	3.09	2.98
CaO	18.38	18.55	18.11	18.18	18.24	18.41	18.26	18.28
Na_2O	0.26	0.22	0.24	0.18	0.22	0.20	0.25	0.22
K_2O	0.03	0.04	0.04	0.03	0.05	0.05	0.06	0.10
TOTAL	99.41	98.85	99.52	99.59	98.61	97.89	100.55	99.84

Appendix C. Pyroxene electron microprobe data

UNIT	Hn	BM	BM	BM	BM	BM	BM	BM
SAMPLE	07WS 077	06WS 062	06WS 062	06WS 062	06WS 062	06WS 062	06WS 062	06WS 062
ANALYSIS	8r	1 c	1 r	2 c	2 r	3 c	3 r	4 c
SiO_2	47.75	48.09	47.88	47.78	47.63	47.85	47.97	48.09
TiO_2	0.45	0.21	0.22	0.25	0.18	0.22	0.22	0.23
Al_2O_3	0.73	0.50	0.47	0.47	0.43	0.58	0.48	0.50
FeO	28.82	35.06	35.05	35.21	35.50	35.34	35.46	35.53
MnO	0.53	0.88	0.95	0.94	0.91	0.97	0.92	0.89
MgO	3.07	10.04	10.28	9.96	10.15	10.04	10.03	10.13
CaO	18.41	4.69	4.28	4.27	4.29	4.35	4.38	4.41
Na_2O	0.20	0.09	0.05	0.03	0.10	0.06	0.07	0.04
K_2O	0.05	0.44	0.83	1.08	0.81	0.60	0.48	0.19
TOTAL	99.40	100.46	100.97	100.76	100.57	100.37	99.80	99.65

Appendix C. Pyroxene electron microprobe data

UNIT	BM	BM	BM	BM	BM	BM	BM	BM
SAMPLE	**06WS 062**	**06WS 062**	**06WS 062**	**06WS 062**	**06WS 062**	**06WS 062**	**06WS 062**	**06WS 062**
ANALYSIS	4 r	5 c	5 r	6 c	6 r	7 c	7 r	8 c
SiO_2	48.13	47.88	48.19	48.06	48.01	48.03	48.44	48.14
TiO_2	0.22	0.24	0.20	0.25	0.24	0.26	0.22	0.23
Al_2O_3	0.45	0.49	0.48	0.53	0.47	0.49	1.03	0.46
FeO	35.25	35.33	35.26	34.47	35.43	36.18	35.30	35.54
MnO	1.01	0.94	1.13	0.98	0.91	0.90	0.83	1.01
MgO	10.29	10.35	10.02	10.36	10.21	10.19	9.95	10.03
CaO	4.31	4.38	4.26	5.15	4.47	3.69	3.85	4.34
Na_2O	0.06	0.07	0.05	0.12	0.09	0.09	0.05	0.04
K_2O	0.28	0.31	0.41	0.08	0.17	0.18	0.33	0.21
TOTAL	100.79	100.41	100.07	100.26	98.76	98.80	99.50	100.19

Appendix C. Pyroxene electron microprobe data

UNIT	BM	BM	BM	BM	BM	WG	WG	WG
SAMPLE	**06WS 062**	**06WS 062**	**06WS 062**	**06WS 062**	**06WS 062**	**06WS 069**	**06WS 069**	**06WS 069**
ANALYSIS	8 r	9 c	9 r	10 c	10 r	pyx 2	pyx 3 right	pyx 5
SiO_2	48.08	47.70	48.10	48.25	47.71	48.55	48.06	48.53
TiO_2	0.26	0.24	0.26	0.23	0.23	0.26	0.24	0.29
Al_2O_3	0.68	0.48	0.45	0.47	0.48	0.54	0.43	0.62
FeO	35.20	35.62	35.33	35.35	35.84	36.28	37.91	33.37
MnO	1.00	0.95	0.96	0.95	0.97	0.99	1.13	0.95
MgO	10.24	10.25	10.22	10.18	10.26	8.13	7.40	7.44
CaO	4.29	4.37	4.21	4.32	4.25	5.17	4.79	8.69
Na_2O	0.04	0.07	0.05	0.06	0.09	0.06	0.04	0.09
K_2O	0.22	0.33	0.42	0.19	0.17	0.03	0.02	0.03
TOTAL	100.81	100.42	100.33	100.50	100.37	97.71	98.78	98.37

Appendix C. Pyroxene electron microprobe data

UNIT	WG	WG	WG	WG	WG	WG	WG	LN
SAMPLE	**06WS 069**	**06WS 069**	**06WS 069**	**06WS 069**	**06WS 069**	**06WS 069**	**06WS 069**	**06WS 035**
ANALYSIS	pyx6	pyx 8	pyx 10	pyx 3 left	pyx 5a	pyx 7	pyx 9	pyx1 core
SiO_2	48.39	48.81	48.24	48.99	48.99	49.21	49.21	48.99
TiO_2	0.23	0.26	0.23	0.37	0.33	0.38	0.36	0.19
Al_2O_3	0.48	0.58	0.51	0.90	0.83	0.91	0.86	0.44
FeO	37.12	36.14	36.44	25.93	25.64	24.17	26.00	33.49
MnO	1.10	1.01	1.01	0.73	0.65	0.81	0.73	0.99
MgO	7.45	8.17	7.71	6.81	6.81	7.57	6.90	11.92
CaO	5.11	4.92	5.76	16.07	16.50	16.73	15.75	3.90
Na_2O	0.08	0.06	0.05	0.16	0.21	0.21	0.16	0.04
K_2O	0.03	0.06	0.05	0.03	0.03	0.03	0.04	0.03
TOTAL	98.47	97.92	98.86	98.62	99.07	99.05	98.60	100.21

Appendix C. Pyroxene electron microprobe data

UNIT	LN	LN	LN	LN	LN	LN	LN	LN
SAMPLE	**06WS 035**	**06WS 035**	**06WS 035**	**06WS 035**	**06WS 035**	**06WS 035**	**06WS 035**	**06WS 035**
ANALYSIS	pyx1 rim	pyx2 rim	pyx3 rim	pyx4 rim	pyx5 rim	pyx6 core	pyx6 rim	pyx7 core
SiO_2	49.33	49.25	49.05	49.15	49.81	48.93	49.08	49.57
TiO_2	0.21	0.21	0.20	0.20	0.18	0.23	0.24	0.16
Al_2O_3	0.44	0.43	0.40	0.41	0.41	0.46	0.47	0.36
FeO	33.04	32.84	32.98	33.37	32.63	33.30	33.24	32.96
MnO	1.01	1.06	0.99	0.98	0.97	0.96	1.10	1.04
MgO	12.10	12.29	12.36	12.04	12.18	12.17	11.94	12.12
CaO	3.81	3.77	3.91	3.80	3.72	3.92	3.81	3.74
Na_2O	0.04	0.09	0.02	0.03	0.06	0.00	0.07	0.02
K_2O	0.03	0.07	0.09	0.03	0.04	0.03	0.05	0.03
TOTAL	99.55	100.42	100.30	100.23	97.95	100.66	100.60	100.09

Appendix C. Pyroxene electron microprobe data

UNIT	LN	LN	LN	LN	LN	LN	LN	LN
SAMPLE	**06WS 035**	**06WS 035**	**06WS 035**	**06WS 035**	**06WS 035**	**06WS 035**	**06WS 035**	**06WS 035**
ANALYSIS	pyx7 rim	pyx9 core	pyx9 rim	LP 1 rim	LP 1 core	LP 2 rim	LP 2 core	LP 3 rim
SiO_2	49.38	49.18	49.22	50.01	49.43	49.62	49.53	49.51
TiO_2	0.18	0.15	0.22	0.18	0.21	0.17	0.17	0.16
Al_2O_3	0.41	0.41	0.41	0.68	0.45	0.46	0.45	0.51
FeO	33.07	32.95	32.84	31.63	32.40	32.75	32.42	32.34
MnO	0.98	0.94	1.09	1.06	1.01	0.95	1.21	1.06
MgO	12.06	12.43	12.28	11.96	12.07	12.10	12.18	12.13
CaO	3.84	3.92	3.85	3.83	3.91	3.86	3.95	3.79
Na_2O	0.05	0.00	0.04	0.13	0.09	0.06	0.05	0.06
K_2O	0.03	0.02	0.05	0.51	0.42	0.03	0.04	0.44
TOTAL	100.50	99.68	99.45	98.66	98.16	98.60	98.65	98.73

Appendix C. Pyroxene electron microprobe data

UNIT	LN	LN	LN	LN	LN	LN	LN	WC
SAMPLE	**06WS 035**	**06WS 035**	**06WS 035**	**06WS 035**	**06WS 035**	**06WS 035**	**06WS 035**	**06WS 037**
ANALYSIS	LP 3 core	LP 4 rim	LP 4 core	LP 5 rim	LP 5 core	LP 6 rim	LP 6 rim 2	pyx1 core
SiO_2	49.83	49.50	50.16	49.65	49.72	49.82	49.58	48.87
TiO_2	0.20	0.18	0.22	0.23	0.18	0.17	0.21	0.18
Al_2O_3	1.10	0.51	0.48	0.40	0.41	0.42	0.45	0.50
FeO	31.43	32.31	31.73	32.83	32.71	32.40	32.27	32.83
MnO	0.92	1.06	1.00	1.03	0.90	1.05	1.16	0.98
MgO	11.56	12.30	12.18	11.81	12.04	12.15	12.13	12.34
CaO	4.05	4.04	4.15	3.92	3.93	3.90	3.91	4.20
Na_2O	0.37	0.07	0.05	0.11	0.07	0.04	0.21	0.06
K_2O	0.54	0.03	0.04	0.02	0.03	0.06	0.08	0.04
TOTAL	99.46	99.15	97.18	98.65	99.05	98.46	97.47	99.31

Appendix C. Pyroxene electron microprobe data

UNIT	WC	WC	WC	WC	WC	WC	WC	WC
SAMPLE	06WS 037	06WS 037	06WS 037	06WS 037	06WS 037	06WS 037	06WS 037	06WS 037
ANALYSIS	pyx1 rim	pyx2 core	pyx2 rim	pyx3 core	pyx3 rim	pyx4 core	pyx4 rim	pyx5 core
SiO_2	49.09	48.81	49.10	49.24	49.48	49.17	49.00	48.86
TiO_2	0.21	0.22	0.22	0.21	0.24	0.23	0.23	0.20
Al_2O_3	0.53	0.52	0.61	0.51	0.40	0.50	0.48	0.48
FeO	32.61	32.81	32.65	32.45	32.62	32.54	32.75	32.70
MnO	0.98	1.03	1.04	1.05	0.94	0.98	1.00	1.08
MgO	12.38	12.24	12.25	12.31	12.10	12.33	12.32	12.36
CaO	4.14	4.16	4.03	4.13	4.14	4.16	4.12	4.22
Na_2O	0.03	0.09	0.07	0.04	0.02	0.02	0.03	0.07
K_2O	0.04	0.10	0.03	0.06	0.05	0.07	0.07	0.03
TOTAL	98.93	99.56	100.00	99.17	98.61	99.55	99.58	99.87

Appendix C. Pyroxene electron microprobe data

UNIT	WC	WC	WC	WC	WC	WC	WC	WC
SAMPLE	06WS 037	06WS 037	06WS 037	06WS 037	06WS 037	06WS 037	06WS 037	06WS 037
ANALYSIS	pyx5 rim	pyx6 core	pyx6 rim1	pyx6 rim2	pyx7 core	pyx7 rim	pyx9 core	pyx9 rim
SiO_2	49.26	48.81	49.43	49.11	49.54	49.31	49.21	49.48
TiO_2	0.25	0.23	0.26	0.22	0.25	0.21	0.21	0.26
Al_2O_3	0.52	0.47	0.64	0.55	0.50	0.48	0.48	0.48
FeO	32.67	32.87	30.33	32.38	32.45	32.32	32.66	32.44
MnO	1.02	1.01	0.96	1.12	0.93	1.00	1.04	0.98
MgO	12.06	12.32	11.74	12.39	12.01	12.32	12.24	12.14
CaO	4.13	4.22	6.51	4.13	4.23	4.30	4.12	4.15
Na_2O	0.07	0.05	0.09	0.05	0.06	0.03	0.01	0.05
K_2O	0.03	0.03	0.04	0.04	0.03	0.04	0.03	0.03
TOTAL	99.56	99.96	99.72	99.42	99.01	98.53	99.06	99.19

Appendix C. Pyroxene electron microprobe data

UNIT	WC	WC	WC	WC	WC	WC	WC	WC
SAMPLE	06WS 037	06WS 037	06WS 037	06WS 037	06WS 037	06WS 037	06WS 037	06WS 037
ANALYSIS	pyx10 core	pyx10 rim	pyx11 rim	pyx12 core	pyx12 rim	pyx13 core	pyx13 rim	pyx14 core
SiO_2	49.16	49.17	49.39	48.92	49.05	48.78	48.97	48.63
TiO_2	0.21	0.25	0.19	0.23	0.23	0.21	0.24	0.25
Al_2O_3	0.50	0.52	0.48	0.51	0.54	0.53	0.54	0.51
FeO	32.80	32.50	32.68	32.77	32.61	32.99	32.67	33.05
MnO	0.98	1.08	1.02	1.08	1.15	1.07	0.98	1.13
MgO	12.00	12.24	12.05	12.13	12.18	12.29	12.30	12.10
CaO	4.27	4.18	4.09	4.27	4.17	4.07	4.20	4.23
Na_2O	0.05	0.03	0.05	0.06	0.05	0.03	0.06	0.05
K_2O	0.02	0.03	0.04	0.02	0.03	0.02	0.03	0.03
TOTAL	99.35	100.22	99.12	99.75	100.62	99.84	100.01	99.94

Appendix C. Pyroxene electron microprobe data

UNIT	WC	WC	WC	WC	WC	WC	WC
SAMPLE	**06WS 037**	**06WS 037**	**06WS 037**	**06WS 037**	**06WS 037**	**06WS 037**	**06WS 037**
ANALYSIS	pyx14 rim 2	pyx15 core	pyx15 rim	LP 8 rim	LP 8 core	LP 9 rim	LP 9 core
SiO_2	49.69	49.22	49.36	49.45	49.37	49.54	49.53
TiO_2	0.20	0.24	0.25	0.27	0.21	0.22	0.19
Al_2O_3	0.51	0.49	0.51	0.52	0.49	0.47	0.55
FeO	31.88	32.77	32.54	31.97	32.72	32.33	32.12
MnO	0.96	1.06	1.02	1.04	1.07	0.95	1.01
MgO	12.44	12.04	12.17	12.47	12.07	12.13	12.29
CaO	4.25	4.13	4.07	4.20	4.01	4.30	4.19
Na_2O	0.04	0.02	0.04	0.06	0.04	0.03	0.09
K_2O	0.04	0.03	0.04	0.03	0.02	0.03	0.03
TOTAL	98.79	100.63	100.20	99.18	98.57	98.97	99.60

APPENDIX D

MICROPROBE VOLCANIC GLASS DATA

Appendix D. Glass electron microprobe data

UNIT	HS	HS	HS	HS	HS	HS
SAMPLE	**06WS 028**	**06WS 028**	**06WS 028**	**06WS 028**	**06WS 028**	**06WS 028**
ANALYSIS	1 a	1 b	2 a	2 b	2 b	3 a
SiO_2	76.93	76.73	76.32	75.35	77.59	77.58
TiO_2	0.26	0.23	0.30	0.22	0.22	0.26
Al_2O_3	11.86	12.08	12.03	11.72	11.98	12.13
Fe_2O_3	1.68	1.84	2.29	3.02	1.10	1.08
MgO	0.05	0.02	0.03	0.30	0.01	0.04
CaO	0.26	0.20	0.19	1.20	0.06	0.08
Na_2O	3.04	2.63	2.72	2.21	2.64	2.33
K_2O	5.90	6.24	6.10	5.98	6.38	6.48
Cl^-	0.01	0.01	0.03	0.00	0.01	0.02
TOTAL	96.80	96.93	96.35	96.30	95.91	94.81

Appendix D. Glass electron microprobe data

UNIT	HS	HS	HS	HS	HS	HS
SAMPLE	**06WS 028**	**06WS 028**	**06WS 028**	**06WS 028**	**06WS 028**	**06WS 028**
ANALYSIS	3 b	3 c	4 a	4 b	4 c	5 a
SiO_2	77.58	77.75	76.78	77.65	76.75	77.04
TiO_2	0.27	0.21	0.26	0.24	0.29	0.28
Al_2O_3	12.05	12.00	11.83	11.80	11.88	11.84
Fe_2O_3	1.04	1.05	1.87	1.35	1.89	1.95
MgO	0.03	0.01	0.09	0.04	0.03	0.04
CaO	0.11	0.06	0.28	0.13	0.16	0.03
Na_2O	2.78	2.44	2.29	2.55	2.56	2.68
K_2O	6.11	6.48	6.57	6.21	6.41	6.12
Cl^-	0.03	0.01	0.02	0.02	0.04	0.04
TOTAL	95.62	95.80	95.17	95.43	95.85	95.89

Appendix D. Glass electron microprobe data

UNIT	HS	HS	HS	HS	HS	HS
SAMPLE	**06WS 028**	**06WS 028**	**06WS 028**	**06WS 028**	**06WS 028**	**06WS 028**
ANALYSIS	5 b	5 c	6 a	6 b	6 c	7 a
SiO_2	76.77	78.04	77.71	77.00	76.64	76.10
TiO_2	0.37	0.24	0.19	0.23	0.29	0.33
Al_2O_3	11.55	11.99	11.93	12.33	11.96	12.72
Fe_2O_3	2.34	0.96	1.18	1.34	2.10	1.66
MgO	-0.01	0.04	0.00	0.01	0.03	0.02
CaO	0.01	0.45	0.05	0.11	0.12	0.66
Na_2O	2.45	3.08	2.57	2.53	2.52	3.25
K_2O	6.45	5.22	6.38	6.45	6.33	5.24
Cl^-	0.06	0.00	-0.01	-0.01	0.02	0.03
TOTAL	95.79	98.42	95.11	95.33	94.72	96.87

Appendix D. Glass electron microprobe data

UNIT	HS	HS	HS	HS	HS	HS
SAMPLE	**06WS 028**	**06WS 028**	**06WS 028**	**06WS 028**	**06WS 028**	**06WS 028**
ANALYSIS	7 b	7 c	8 a	8 b	8 c	9 a
SiO_2	75.90	77.62	76.86	77.36	77.42	76.70
TiO_2	0.29	0.32	0.29	0.28	0.26	0.24
Al_2O_3	12.77	11.49	11.94	11.95	11.93	11.86
Fe_2O_3	1.72	1.84	1.71	1.28	1.27	1.99
MgO	0.00	0.03	0.03	0.05	-0.01	0.06
CaO	0.62	0.05	0.09	0.05	0.12	0.28
Na_2O	3.00	2.71	2.50	2.78	2.32	2.49
K_2O	5.67	5.91	6.57	6.23	6.65	6.37
Cl^-	0.04	0.03	0.02	0.02	0.04	0.02
TOTAL	96.87	96.19	96.24	96.07	95.48	95.58

Appendix D. Glass electron microprobe data

UNIT	HS	HS	HS	HS	HS	HS
SAMPLE	**06WS 028**	**06WS 028**	**06WS 028**	**06WS 028**	**06WS 028**	**06WS 028**
ANALYSIS	9 b	9 c	10 a	10 b	10 c	11 a
SiO_2	76.92	76.82	76.80	76.91	76.77	77.31
TiO_2	0.25	0.28	0.28	0.23	0.25	0.26
Al_2O_3	12.00	11.93	11.93	11.77	12.00	11.82
Fe_2O_3	1.84	1.89	1.80	1.92	1.71	1.66
MgO	0.05	0.05	0.05	0.06	0.06	0.04
CaO	0.42	0.33	0.07	0.13	0.18	0.15
Na_2O	3.11	3.05	2.62	2.88	2.94	2.88
K_2O	5.37	5.65	6.42	6.08	6.07	5.86
Cl^-	0.03	0.00	0.02	0.02	0.02	0.02
TOTAL	96.56	96.58	97.32	97.39	97.53	97.05

Appendix D. Glass electron microprobe data

UNIT	HS	HS	RS	RS	RS	RS
SAMPLE	**06WS 028**	**06WS 028**	**06WS 052**	**06WS 052**	**06WS 052**	**06WS 052**
ANALYSIS	11 b	11 c	1 a	1 b	1 c	2 a
SiO_2	76.97	76.74	76.45	77.18	77.15	76.32
TiO_2	0.30	0.28	0.38	0.27	0.30	0.38
Al_2O_3	11.75	12.03	11.80	11.87	12.01	11.89
Fe_2O_3	2.03	1.93	2.55	1.66	1.50	2.62
MgO	0.06	0.05	0.05	0.04	0.06	0.04
CaO	0.24	0.32	0.26	0.31	0.23	0.30
Na_2O	2.98	3.05	2.69	2.90	2.52	2.78
K_2O	5.63	5.58	5.80	5.75	6.22	5.64
Cl^-	0.03	0.01	0.02	0.01	0.02	0.04
TOTAL	97.10	96.87	96.53	96.21	96.45	96.42

Appendix D. Glass electron microprobe data

UNIT	RS	RS	RS	RS	RS	RS
SAMPLE	**06WS 052**	**06WS 052**	**06WS 052**	**06WS 052**	**06WS 052**	**06WS 052**
ANALYSIS	2 b	2 c	3 a	3 b	3 c	4 b
SiO_2	75.93	77.11	76.06	76.12	77.42	74.61
TiO_2	0.25	0.29	0.35	0.31	0.25	0.50
Al_2O_3	12.90	11.72	12.14	12.18	11.86	12.39
Fe_2O_3	1.49	1.96	2.26	2.17	1.42	3.30
MgO	0.04	0.07	0.04	0.08	0.04	0.05
CaO	0.42	0.35	0.29	0.45	0.24	0.47
Na_2O	2.47	2.88	2.64	2.89	2.53	3.13
K_2O	6.49	5.59	6.21	5.77	6.21	5.54
Cl^-	0.01	0.03	0.02	0.04	0.03	0.03
TOTAL	96.63	96.64	96.08	95.35	95.13	96.76

Appendix D. Glass electron microprobe data

UNIT	RS	RS	RS	RS	RS	RS
SAMPLE	**06WS 052**	**06WS 052**	**06WS 052**	**06WS 052**	**06WS 052**	**06WS 052**
ANALYSIS	4 c	5 a	5 b	5 c	6 a	6 b
SiO_2	76.90	75.80	78.10	76.08	77.06	76.46
TiO_2	0.29	0.33	0.24	0.29	0.29	0.34
Al_2O_3	12.18	12.57	11.58	12.30	11.71	11.87
Fe_2O_3	1.57	1.80	1.25	2.24	1.96	2.17
MgO	0.04	0.04	0.06	0.05	0.09	0.05
CaO	0.39	0.48	0.23	0.59	0.30	0.33
Na_2O	2.55	3.29	2.73	3.13	2.65	2.76
K_2O	6.05	5.67	5.79	5.30	5.90	5.99
Cl^-	0.04	0.02	0.02	0.02	0.04	0.04
TOTAL	96.40	96.31	96.05	96.73	96.73	96.42

Appendix D. Glass electron microprobe data

UNIT	RS	RS	RS	RS	RS	RS
SAMPLE	**06WS 052**	**06WS 052**	**06WS 052**	**06WS 052**	**06WS 052**	**06WS 052**
ANALYSIS	6 c	7 a	7 b	7 c	8 a	8 b
SiO_2	76.48	76.68	77.50	75.75	77.06	76.63
TiO_2	0.29	0.34	0.27	0.36	0.27	0.26
Al_2O_3	12.11	11.64	12.11	12.03	11.79	12.25
Fe_2O_3	1.93	2.26	1.28	2.74	1.98	1.74
MgO	0.07	0.04	0.04	0.06	0.03	0.07
CaO	0.50	0.32	0.31	0.30	0.25	0.37
Na_2O	3.00	2.70	2.99	2.97	2.71	2.75
K_2O	5.60	6.00	5.50	5.76	5.87	5.91
Cl^-	0.02	0.03	0.02	0.02	0.03	0.01
TOTAL	96.47	96.08	96.33	96.50	96.01	96.13

Appendix D. Glass electron microprobe data

UNIT	RS	RS	RS	RS	RS	RS
SAMPLE	**06WS 052**	**06WS 052**	**06WS 052**	**06WS 052**	**06WS 052**	**06WS 052**
ANALYSIS	8 c	9 b	9 c	10 a	10 b	10 c
SiO_2	76.78	77.11	76.51	74.40	75.52	76.90
TiO_2	0.30	0.30	0.35	0.30	0.37	0.25
Al_2O_3	11.95	11.69	12.20	11.99	12.32	12.38
Fe_2O_3	2.02	2.08	1.97	3.53	2.62	1.39
MgO	0.04	0.04	0.01	0.25	0.06	0.04
CaO	0.29	0.29	0.32	1.01	0.55	0.31
Na_2O	2.69	2.87	3.24	3.02	3.06	2.95
K_2O	5.91	5.60	5.39	5.47	5.49	5.76
Cl^-	0.02	0.02	0.02	0.04	0.02	0.03
TOTAL	95.78	96.52	96.72	96.05	95.24	94.47

Appendix D. Glass electron microprobe data

UNIT	FS	FS	FS	FS	FS	FS
SAMPLE	**06WS 059**	**06WS 059**	**06WS 059**	**06WS 059**	**06WS 059**	**06WS 059**
ANALYSIS	1 a	1 b	1 c	2 a	2 b	2 c
SiO_2	76.11	76.54	76.66	77.39	75.70	76.36
TiO_2	0.23	0.24	0.24	0.24	0.19	0.22
Al_2O_3	11.91	12.05	11.85	11.81	11.78	11.99
Fe_2O_3	2.29	2.00	1.64	1.26	2.61	2.11
MgO	0.01	0.02	0.03	0.04	0.07	0.00
CaO	0.16	0.14	0.18	-0.04	0.66	0.17
Na_2O	2.63	2.17	2.05	2.59	2.85	2.68
K_2O	6.61	6.81	7.32	6.66	6.12	6.43
Cl^-	0.04	0.04	0.04	0.03	0.03	0.02
TOTAL	95.40	95.74	95.84	95.27	96.84	96.16

Appendix D. Glass electron microprobe data

UNIT	FS	FS	FS	FS	FS	FS
SAMPLE	**06WS 059**	**06WS 059**	**06WS 059**	**06WS 059**	**06WS 059**	**06WS 059**
ANALYSIS	3 a	3 b	3 c	4 a	4 b	4 c
SiO_2	75.97	76.46	76.28	76.89	77.07	76.43
TiO_2	0.23	0.23	0.25	0.21	0.20	0.26
Al_2O_3	12.04	11.91	11.78	11.89	11.90	12.22
Fe_2O_3	2.27	1.93	2.19	1.85	1.64	1.71
MgO	0.04	0.00	0.03	0.04	-0.01	0.05
CaO	0.43	0.24	0.17	0.15	0.04	0.20
Na_2O	2.63	2.83	2.09	1.45	1.81	2.34
K_2O	6.37	6.34	7.20	7.47	7.32	6.76
Cl^-	0.02	0.05	0.02	0.06	0.03	0.03
TOTAL	95.83	95.78	95.93	95.16	95.16	94.91

Appendix D. Glass electron microprobe data

UNIT	FS	FS	FS	FS	FS	FS
SAMPLE	**06WS 059**	**06WS 059**	**06WS 059**	**06WS 059**	**06WS 059**	**06WS 059**
ANALYSIS	5 a	5 b	5 c	6 a	6 b	6 c
SiO_2	76.47	76.38	76.45	76.95	76.92	75.51
TiO_2	0.20	0.24	0.24	0.22	0.22	0.31
Al_2O_3	11.71	11.93	11.78	12.06	11.96	11.96
Fe_2O_3	2.35	2.02	2.25	1.39	1.57	2.88
MgO	0.07	0.03	0.02	0.01	0.03	0.05
CaO	0.17	0.18	0.51	0.04	0.06	0.08
Na_2O	1.67	2.73	2.76	2.70	2.00	2.04
K_2O	7.30	6.45	5.96	6.57	7.18	7.13
Cl^-	0.05	0.03	0.05	0.05	0.06	0.04
TOTAL	95.67	96.24	96.40	94.83	95.09	95.71

Appendix D. Glass electron microprobe data

UNIT	FS	FS	FS	FS	FS	FS
SAMPLE	**06WS 059**	**06WS 059**	**06WS 059**	**06WS 059**	**06WS 059**	**06WS 059**
ANALYSIS	7 a	7 b	7 c	8 a	8 b	8 c
SiO_2	76.56	76.41	76.18	77.02	76.68	76.03
TiO_2	0.23	0.26	0.26	0.21	0.22	0.25
Al_2O_3	12.00	12.07	11.92	11.97	11.97	11.98
Fe_2O_3	1.79	1.87	2.04	1.25	1.60	2.54
MgO	0.02	0.03	0.01	0.00	0.06	0.04
CaO	0.33	0.25	0.31	0.05	0.07	0.40
Na_2O	2.87	3.03	2.22	2.48	2.43	1.55
K_2O	6.17	6.03	7.03	6.98	6.86	7.18
Cl^-	0.04	0.05	0.05	0.04	0.11	0.04
TOTAL	94.73	94.70	95.08	95.31	95.41	95.43

Appendix D. Glass electron microprobe data

UNIT	FS	FS	FS	FS	FS	FS
SAMPLE	**06WS 059**	**06WS 059**	**06WS 059**	**06WS 059**	**06WS 059**	**06WS 059**
ANALYSIS	9 a	9 b	9 c	10 a	10 b	10 c
SiO_2	76.21	76.26	76.64	77.06	77.45	76.18
TiO_2	0.23	0.24	0.24	0.20	0.18	0.24
Al_2O_3	11.93	12.06	11.88	12.28	12.12	11.83
Fe_2O_3	2.52	1.87	1.94	0.88	0.80	2.17
MgO	0.04	0.04	0.03	0.02	0.04	0.02
CaO	0.20	0.25	0.17	0.17	-0.04	0.12
Na_2O	1.80	2.47	2.79	2.10	2.30	2.19
K_2O	7.05	6.78	6.30	7.23	7.11	7.25
Cl^-	0.03	0.03	0.01	0.06	0.04	0.02
TOTAL	95.45	96.24	95.56	95.41	95.65	95.53

Appendix D. Glass electron microprobe data

UNIT	Hn	Hn	Hn	Hn	Hn	Hn
SAMPLE	**07WS 077**	**07WS 077**	**07WS 077**	**07WS 077**	**07WS 077**	**07WS 077**
ANALYSIS	1a	1b	2a	2b	3a	3b
SiO_2	77.51	77.20	77.78	77.61	78.03	77.84
TiO_2	0.25	0.23	0.22	0.18	0.24	0.26
Al_2O_3	12.31	12.17	12.15	12.22	11.47	11.54
Fe_2O_3	1.75	2.24	1.69	1.60	2.02	1.92
MgO	0.01	0.04	0.02	0.01	0.03	0.02
CaO	0.44	0.47	0.25	0.46	0.42	0.47
Na_2O	2.06	1.87	2.00	2.20	2.32	2.29
K_2O	5.62	5.76	5.86	5.67	5.43	5.60
Cl^-	0.06	0.03	0.03	0.04	0.03	0.06
TOTAL	96.92	96.89	97.73	97.72	99.34	98.53

Appendix D. Glass electron microprobe data

UNIT	Hn	Hn	Hn	Hn	Hn	Hn
SAMPLE	**07WS 077**	**07WS 077**	**07WS 077**	**07WS 077**	**07WS 077**	**07WS 077**
ANALYSIS	4a	4b	5a	5b	6a	6b
SiO_2	77.61	78.06	77.77	77.42	76.50	76.89
TiO_2	0.24	0.18	0.23	0.24	0.22	0.24
Al_2O_3	11.79	11.84	11.88	11.91	11.43	11.61
Fe_2O_3	2.01	1.62	1.75	1.96	3.84	3.06
MgO	0.05	0.05	0.03	0.03	0.02	0.03
CaO	0.59	0.48	0.32	0.41	0.51	0.43
Na_2O	2.36	2.35	1.96	1.28	2.24	1.85
K_2O	5.33	5.39	6.06	6.74	5.20	5.87
Cl^-	0.03	0.04	0.01	0.01	0.04	0.02
TOTAL	99.30	99.12	99.65	98.61	100.15	100.31

Appendix D. Glass electron microprobe data

UNIT	Hn	Hn	Hn	Hn	BM	BM
SAMPLE	07WS 077	07WS 077	07WS 077	07WS 077	06WS 062	06WS 062
ANALYSIS	7a	7b	8a	8b	1 a	1 b
SiO_2	77.62	77.63	76.61	77.64	77.18	77.15
TiO_2	0.25	0.25	0.34	0.24	0.25	0.28
Al_2O_3	11.87	11.78	11.68	11.71	11.81	11.85
Fe_2O_3	1.75	1.79	3.23	2.18	1.71	1.60
MgO	0.02	0.04	0.02	0.00	0.06	0.04
CaO	0.42	0.35	0.34	0.32	0.16	0.16
Na_2O	2.35	1.56	2.05	2.26	2.36	2.19
K_2O	5.68	6.58	5.70	5.61	6.45	6.70
Cl^-	0.03	0.03	0.03	0.03	0.03	0.03
TOTAL	100.03	98.91	100.19	100.28	95.09	94.76

Appendix D. Glass electron microprobe data

UNIT	BM	BM	BM	BM	BM	BM
SAMPLE	**06WS 062**	**06WS 062**	**06WS 062**	**06WS 062**	**06WS 062**	**06WS 062**
ANALYSIS	1 c	3 a	3 b	4 a	4 b	5 a
SiO_2	76.93	77.39	76.68	77.47	77.41	76.87
TiO_2	0.29	0.28	0.28	0.28	0.27	0.27
Al_2O_3	11.86	11.72	12.17	11.73	11.68	12.05
Fe_2O_3	1.77	1.67	1.56	1.68	1.65	1.57
MgO	0.08	0.08	0.04	0.03	0.07	0.03
CaO	0.17	0.12	0.13	0.09	0.11	0.29
Na_2O	2.57	2.12	2.47	2.08	2.37	2.63
K_2O	6.30	6.58	6.64	6.61	6.45	6.26
Cl^-	0.05	0.03	0.03	0.02	0.01	0.03
TOTAL	95.25	95.97	95.26	95.07	95.30	95.10

Appendix D. Glass electron microprobe data

UNIT	BM	BM	BM	BM	BM	BM
SAMPLE	**06WS 062**	**06WS 062**	**06WS 062**	**06WS 062**	**06WS 062**	**06WS 062**
ANALYSIS	5 b	6 a	6 b	7 a	7 b	8 a
SiO_2	77.38	77.03	76.64	77.15	77.32	77.52
TiO_2	0.23	0.30	0.24	0.32	0.28	0.27
Al_2O_3	11.55	11.75	12.42	11.68	11.85	11.47
Fe_2O_3	1.82	1.56	1.51	1.69	1.66	1.64
MgO	0.07	0.03	0.02	0.05	0.04	0.04
CaO	0.16	0.06	0.13	0.15	0.14	0.16
Na_2O	2.26	2.19	2.18	2.46	2.30	2.43
K_2O	6.50	7.04	6.80	6.48	6.36	6.45
Cl^-	0.03	0.04	0.06	0.01	0.04	0.01
TOTAL	96.36	96.03	96.70	95.06	95.60	95.06

Appendix D. Glass electron microprobe data

UNIT	BM	BM	BM	BM	BM	WG
SAMPLE	**06WS 062**	**06WS 062**	**06WS 062**	**06WS 062**	**06WS 062**	**06WS 069**
ANALYSIS	8 b	9 a	9 b	10 a	10 b	1a
SiO_2	76.07	75.51	77.44	77.12	77.43	77.29
TiO_2	0.28	0.28	0.30	0.26	0.30	0.23
Al_2O_3	12.54	12.81	11.44	11.80	11.54	11.93
Fe_2O_3	1.50	1.96	1.72	1.69	1.80	1.47
MgO	0.01	0.09	0.05	0.09	0.08	0.02
CaO	0.18	0.25	0.14	0.19	0.13	0.07
Na_2O	2.59	2.55	2.49	2.68	2.10	2.51
K_2O	6.88	6.27	6.40	6.16	6.55	6.46
Cl^-	-0.04	0.28	0.02	0.02	0.05	0.03
TOTAL	95.64	95.91	95.48	97.59	94.79	95.93

Appendix D. Glass electron microprobe data

UNIT	WG	WG	WG	WG	WG	WG
SAMPLE	**06WS 069**	**06WS 069**	**06WS 069**	**06WS 069**	**06WS 069**	**06WS 069**
ANALYSIS	1b	2a	2b	3a	3b	4a
SiO_2	77.33	77.43	77.98	77.26	77.69	77.89
TiO_2	0.25	0.30	0.19	0.23	0.23	0.20
Al_2O_3	11.70	11.58	12.09	12.34	12.02	11.87
Fe_2O_3	1.35	1.46	0.61	0.84	1.16	0.70
MgO	0.02	0.02	0.03	-0.03	0.02	0.05
CaO	0.05	0.02	-0.02	0.08	0.38	-0.02
Na_2O	2.85	2.33	2.79	2.56	2.86	2.25
K_2O	6.40	6.83	6.32	6.70	5.63	7.03
Cl^-	0.04	0.02	0.01	0.01	0.01	0.03
TOTAL	95.96	96.09	95.34	95.82	97.21	96.21

Appendix D. Glass electron microprobe data

UNIT	WG	WG	WG	WG	WG	WG
SAMPLE	**06WS 069**	**06WS 069**	**06WS 069**	**06WS 069**	**06WS 069**	**06WS 069**
ANALYSIS	4b	5a	5b	6a	6b	7a
SiO_2	78.51	77.41	77.16	78.13	77.89	76.96
TiO_2	0.20	0.24	0.28	0.28	0.20	0.27
Al_2O_3	11.77	11.46	11.29	11.49	12.08	11.65
Fe_2O_3	0.47	1.73	2.22	1.21	0.57	2.26
MgO	0.00	0.02	0.01	0.03	0.06	0.01
CaO	-0.06	0.00	0.08	-0.10	-0.01	0.21
Na_2O	2.11	2.08	2.51	1.93	2.78	2.73
K_2O	6.97	7.03	6.39	7.02	6.39	5.89
Cl^-	0.04	0.03	0.06	0.01	0.04	0.02
TOTAL	95.86	96.10	95.37	96.55	96.13	95.81

Appendix D. Glass electron microprobe data

UNIT	WG	WG	WG	WG	WG	WG
SAMPLE	**06WS 069**	**06WS 069**	**06WS 069**	**06WS 069**	**06WS 069**	**06WS 069**
ANALYSIS	7b	8a	8b	9a	9b	10a
SiO_2	76.17	76.12	77.88	78.16	77.72	77.30
TiO_2	0.40	0.29	0.25	0.20	0.21	0.37
Al_2O_3	11.46	11.63	11.72	11.73	12.09	11.40
Fe_2O_3	3.08	2.93	1.21	0.76	0.55	2.15
MgO	0.04	0.07	0.01	0.01	0.01	0.04
CaO	0.11	0.19	-0.03	-0.02	-0.05	-0.03
Na_2O	2.44	2.88	1.82	2.52	2.58	2.19
K_2O	6.27	5.87	7.11	6.59	6.86	6.55
Cl^-	0.03	0.03	0.04	0.06	0.04	0.04
TOTAL	95.88	96.20	95.36	95.24	95.21	95.91

Appendix D. Glass electron microprobe data

UNIT	WG	LN	LN	LN	LN	LN
SAMPLE	**06WS 069**	**06WS 035**	**06WS 035**	**06WS 035**	**06WS 035**	**06WS 035**
ANALYSIS	10b	1 a	1 b	1 c	2 a	2 b
SiO_2	76.86	76.48	76.23	76.22	76.66	76.58
TiO_2	0.25	0.29	0.32	0.31	0.31	0.33
Al_2O_3	11.45	11.98	11.91	12.17	11.89	12.14
Fe_2O_3	2.38	1.81	2.15	1.91	1.84	1.73
MgO	0.02	0.11	0.08	0.13	0.13	0.07
CaO	0.15	0.28	0.28	0.30	0.27	0.22
Na_2O	2.41	2.62	2.41	2.52	2.25	2.16
K_2O	6.44	6.38	6.61	6.52	6.71	6.82
Cl^-	0.03	0.05	0.02	-0.06	-0.05	-0.04
TOTAL	95.84	95.49	95.41	95.57	95.03	95.08

Appendix D. Glass electron microprobe data

UNIT	LN	LN	LN	LN	LN	LN
SAMPLE	**06WS 035**	**06WS 035**	**06WS 035**	**06WS 035**	**06WS 035**	**06WS 035**
ANALYSIS	3 a	3 b	4 a	4 b	5 a	5 b
SiO_2	76.30	76.46	76.65	76.59	76.94	76.63
TiO_2	0.32	0.30	0.32	0.33	0.35	0.34
Al_2O_3	12.07	12.07	12.02	11.93	11.96	11.96
Fe_2O_3	1.91	1.84	1.80	1.79	1.62	1.96
MgO	0.08	0.11	0.08	0.09	0.07	0.11
CaO	0.24	0.18	0.23	0.31	0.17	0.22
Na_2O	2.32	2.25	2.89	2.86	2.52	1.69
K_2O	6.79	6.82	6.02	6.11	6.35	7.07
Cl^-	-0.02	-0.01	-0.01	0.00	0.02	0.02
TOTAL	95.67	95.56	95.62	95.49	95.70	95.16

Appendix D. Glass electron microprobe data

UNIT	LN	LN	LN	LN	LN	LN
SAMPLE	**06WS 035**	**06WS 035**	**06WS 035**	**06WS 035**	**06WS 035**	**06WS 035**
ANALYSIS	6 a	6 b	7 a	7 b	8 a	8 b
SiO_2	76.54	76.37	76.16	76.66	76.26	76.32
TiO_2	0.33	0.32	0.34	0.32	0.36	0.33
Al_2O_3	11.93	12.12	12.19	12.07	12.10	12.02
Fe_2O_3	1.89	1.91	1.89	1.51	1.79	1.85
MgO	0.13	0.10	0.10	0.09	0.13	0.11
CaO	0.30	0.28	0.33	0.30	0.27	0.34
Na_2O	2.34	1.73	2.87	2.43	2.61	2.78
K_2O	6.50	7.15	6.09	6.60	6.48	6.23
Cl^-	0.03	0.01	0.01	0.02	0.01	0.02
TOTAL	94.08	94.30	93.95	93.82	95.32	94.51

Appendix D. Glass electron microprobe data

UNIT	LN	LN	LN	LN	LN	WC
SAMPLE	**06WS 035**	**06WS 035**	**06WS 035**	**06WS 035**	**06WS 035**	**06WS 037**
ANALYSIS	9 a	9 b	10 a	10 b	10 c	1 a
SiO_2	76.33	76.37	77.00	76.37	76.26	77.51
TiO_2	0.31	0.31	0.29	0.33	0.30	0.34
Al_2O_3	12.01	12.13	12.12	12.07	11.97	12.27
Fe_2O_3	1.71	1.83	1.34	1.93	1.92	0.59
MgO	0.12	0.12	0.09	0.10	0.13	0.03
CaO	0.29	0.31	0.16	0.23	0.32	0.08
Na_2O	2.60	2.69	2.85	1.78	2.69	2.81
K_2O	6.62	6.22	6.15	7.19	6.42	6.33
Cl^-	0.01	0.04	0.01	0.01	0.00	0.03
TOTAL	95.05	95.21	94.83	95.03	95.41	94.99

Appendix D. Glass electron microprobe data

UNIT	WC	WC	WC	WC	WC	WC
SAMPLE	**06WS 037**	**06WS 037**	**06WS 037**	**06WS 037**	**06WS 037**	**06WS 037**
ANALYSIS	1 b	1 c	2 a	2 b	2 c	3 a
SiO_2	77.53	77.46	77.80	77.75	77.80	77.84
TiO_2	0.38	0.39	0.38	0.38	0.34	0.36
Al_2O_3	12.26	12.19	12.09	12.35	12.07	12.18
Fe_2O_3	0.56	0.66	0.62	0.54	0.58	0.49
MgO	0.01	0.03	0.02	0.01	0.01	0.04
CaO	0.00	0.01	0.02	0.01	0.00	0.01
Na_2O	2.13	2.37	0.96	1.96	2.31	2.17
K_2O	7.08	6.86	7.03	7.00	6.86	6.89
Cl^-	0.03	0.03	0.02	0.02	0.04	0.02
TOTAL	95.09	95.19	94.99	94.94	95.43	94.50

Appendix D. Glass electron microprobe data

UNIT	WC	WC	WC	WC	WC	WC
SAMPLE	06WS 037	06WS 037	06WS 037	06WS 037	06WS 037	06WS 037
ANALYSIS	3 b	3 c	4 a	4 b	4 c	5 a
SiO_2	77.53	76.77	78.24	77.93	77.52	77.59
TiO_2	0.33	0.36	0.34	0.35	0.37	0.34
Al_2O_3	12.21	12.31	12.04	12.09	12.11	12.28
Fe_2O_3	0.97	1.20	0.49	0.59	0.65	0.55
MgO	0.01	0.05	0.01	-0.01	0.05	0.05
CaO	0.02	0.14	0.03	0.01	0.05	0.03
Na_2O	1.72	2.65	1.71	2.32	2.12	2.63
K_2O	7.17	6.54	7.11	6.71	7.13	6.53
Cl^-	0.03	-0.01	0.02	0.01	0.01	0.02
TOTAL	94.67	95.54	95.02	95.03	94.97	95.60

Appendix D. Glass electron microprobe data

UNIT	WC	WC	WC	WC	WC	WC
SAMPLE	06WS 037	06WS 037	06WS 037	06WS 037	06WS 037	06WS 037
ANALYSIS	5 b	5 c	6 a	6 b	6 c	7 a
SiO_2	77.29	77.16	77.74	77.91	77.49	77.35
TiO_2	0.34	0.32	0.35	0.41	0.36	0.34
Al_2O_3	12.36	12.16	12.24	12.20	12.16	12.41
Fe_2O_3	0.87	1.27	0.51	0.57	0.91	0.56
MgO	0.01	0.02	0.00	0.02	0.07	0.04
CaO	0.07	0.05	0.05	0.03	0.04	0.03
Na_2O	2.95	1.97	2.41	1.74	1.81	2.65
K_2O	6.08	7.04	6.69	7.08	7.13	6.61
Cl^-	0.02	0.01	0.02	0.04	0.02	0.01
TOTAL	96.00	95.06	94.69	94.73	95.08	95.07

Appendix D. Glass electron microprobe data

UNIT	WC	WC	WC	WC	WC	WC
SAMPLE	06WS 037	06WS 037	06WS 037	06WS 037	06WS 037	06WS 037
ANALYSIS	7 b	7 c	8 a	8 b	8 c	9 a
SiO_2	77.18	77.61	77.63	77.29	77.51	76.69
TiO_2	0.39	0.35	0.40	0.35	0.36	0.33
Al_2O_3	11.90	12.20	12.16	12.41	12.24	12.88
Fe_2O_3	1.12	0.77	0.53	0.57	0.61	0.70
MgO	0.07	0.02	-0.02	-0.01	0.03	0.02
CaO	0.21	0.02	0.04	0.09	0.01	0.35
Na_2O	2.31	2.17	2.38	2.33	2.08	2.34
K_2O	6.81	6.83	6.98	6.97	7.15	6.67
Cl^-	0.03	0.03	-0.09	0.00	0.01	0.02
TOTAL	95.19	95.02	95.05	95.28	95.08	94.94

Appendix D. Glass electron microprobe data

UNIT	WC	WC	WC	WC	WC
SAMPLE	06WS 037	06WS 037	06WS 037	06WS 037	06WS 037
ANALYSIS	9 b	9 c	10 a	10 b	10 c
SiO_2	77.63	77.59	77.53	77.85	77.16
TiO_2	0.33	0.35	0.31	0.34	0.38
Al_2O_3	12.29	12.23	12.17	12.23	12.26
Fe_2O_3	0.59	0.56	0.73	0.46	1.01
MgO	0.00	0.01	0.03	0.00	0.01
CaO	0.06	0.03	0.01	0.02	0.00
Na_2O	1.90	2.11	2.12	2.09	2.20
K_2O	7.18	7.10	7.11	7.02	6.93
Cl^-	0.02	0.02	-0.02	-0.01	0.04
TOTAL	95.38	94.88	95.40	94.85	94.88

APPENDIX E

MICROPROBE FELDSPAR DATA

Appendix E. Feldspar electron microprobe data

UNIT	HS	HS	HS	HS	HS	HS
SAMPLE	**06WS 028**	**06WS 028**	**06WS 028**	**06WS 028**	**06WS 028**	**06WS 028**
ANALYSIS	fspar1 core	fspar1 rim	fspar2 core	fspar2 rim	fspar3 core	fspar3 rim
SiO_2	59.29	60.26	60.66	61.08	59.37	60.57
Al_2O_3	25.17	24.48	24.19	24.11	25.18	24.39
BaO	0.14	0.18	0.18	0.21	0.20	0.23
FeO	0.37	0.41	0.31	0.33	0.36	0.31
CaO	6.90	5.98	6.01	5.41	6.81	5.90
Na_2O	6.87	7.28	7.05	7.32	6.84	7.00
K_20	1.27	1.42	1.61	1.55	1.25	1.60
total	99.77	100.62	99.08	100.36	99.67	99.63

Appendix E. Feldspar electron microprobe data

UNIT	HS	HS	HS	HS	HS	HS
SAMPLE	**06WS 028**	**06WS 028**	**06WS 028**	**06WS 028**	**06WS 028**	**06WS 028**
ANALYSIS	fspar6 core	fspar6 rim	fspar7 core	fspar7 rim	fspar8 rim	fspar10 core
SiO_2	59.31	59.98	59.35	60.40	60.60	60.11
Al_2O_3	25.24	24.54	24.97	24.59	24.51	24.61
BaO	0.13	0.19	0.16	0.14	0.18	0.28
FeO	0.41	0.45	0.44	0.40	0.35	0.41
CaO	6.87	6.20	6.86	6.17	5.84	6.13
Na_2O	6.71	6.94	6.73	6.95	7.05	6.98
K_20	1.32	1.69	1.49	1.35	1.47	1.48
total	99.11	99.77	99.84	99.66	100.50	99.87

Appendix E. Feldspar electron microprobe data

UNIT	HS	HS	HS	HS	HS	HS
SAMPLE	**06WS 028**	**06WS 028**	**06WS 028**	**06WS 028**	**06WS 028**	**06WS 028**
ANALYSIS	fspar10 rim	fspar12 core	fspar12 rim	L9 core	L9 rim	L10 core
SiO_2	59.63	60.19	60.65	59.03	59.05	59.62
Al_2O_3	24.93	24.75	24.45	25.22	25.43	24.89
BaO	0.22	0.15	0.16	0.15	0.13	0.18
FeO	0.40	0.36	0.35	0.46	0.41	0.41
CaO	6.75	6.37	5.66	7.08	7.30	6.79
Na_2O	6.74	6.82	7.13	6.67	6.53	6.59
K_20	1.33	1.37	1.62	1.38	1.15	1.52
total	99.67	100.52	100.09	100.56	100.02	100.77

Appendix E. Feldspar electron microprobe data

UNIT	HS	HS	HS	HS	HS	HS
SAMPLE	**06WS 028**	**06WS 028**	**06WS 028**	**06WS 028**	**06WS 028**	**06WS 028**
ANALYSIS	L10 rim	fspar4 core	fspar4 rim	fspar5 core	fspar5 rim	fspar9 core
SiO_2	59.60	64.25	64.32	63.87	64.01	64.07
Al_2O_3	24.99	19.78	19.67	19.90	19.77	19.81
BaO	0.16	2.14	1.98	2.11	2.06	2.08
FeO	0.35	0.16	0.15	0.18	0.19	0.23
CaO	6.89	0.39	0.47	0.44	0.37	0.38
Na_2O	6.79	4.52	4.35	4.27	4.15	4.42
K_20	1.22	8.76	9.05	9.24	9.46	9.01
total	100.06	100.17	98.79	98.67	98.44	99.64

Appendix E. Feldspar electron microprobe data

UNIT	HS	HS	HS	RS	RS	RS
SAMPLE	**06WS 028**	**06WS 028**	**06WS 028**	**06WS 052**	**06WS 052**	**06WS 052**
ANALYSIS	fspar9 rim	fspar11 core	fspar11 rim	fspar2 core	fspar2 rim	fspar3 rim
SiO_2	64.35	63.56	63.93	59.69	60.74	59.04
Al_2O_3	19.87	20.02	20.01	25.11	24.30	25.23
BaO	1.99	2.32	2.00	0.15	0.20	0.19
FeO	0.20	0.16	0.18	0.35	0.41	0.44
CaO	0.39	0.42	0.27	6.70	5.97	7.03
Na_2O	4.28	4.15	4.23	6.75	6.90	6.75
K_20	8.93	9.37	9.39	1.25	1.48	1.32
total	100.69	99.39	98.86	99.64	99.93	100.65

Appendix E. Feldspar electron microprobe data

UNIT	RS	RS	RS	RS	RS	RS
SAMPLE	**06WS 052**	**06WS 052**	**06WS 052**	**06WS 052**	**06WS 052**	**06WS 052**
ANALYSIS	fspar4 core	fspar4 rim	fspar6 core	fspar6 rim	fspar7 core	fspar7 rim
SiO_2	59.26	60.58	60.13	60.76	59.17	59.30
Al_2O_3	25.28	24.20	24.79	24.14	25.26	25.29
BaO	0.14	0.25	0.18	0.21	0.12	0.13
FeO	0.41	0.43	0.36	0.31	0.42	0.44
CaO	7.04	6.03	6.33	5.84	7.25	7.14
Na_2O	6.69	7.07	6.81	7.08	6.70	6.48
K_20	1.18	1.44	1.39	1.66	1.09	1.21
total	100.37	99.70	99.50	99.51	99.94	99.61

Appendix E. Feldspar electron microprobe data

UNIT	RS	RS	RS	RS	RS	RS
SAMPLE	**06WS 052**	**06WS 052**	**06WS 052**	**06WS 052**	**06WS 052**	**06WS 052**
ANALYSIS	fspar9 core	fspar10 rim2	fspar11 core	fspar12 core	fspar12 rim	fspar5 core
SiO_2	59.25	59.36	58.96	59.26	59.53	63.96
Al_2O_3	25.22	25.19	25.47	25.22	25.11	19.99
BaO	0.15	0.13	0.19	0.10	0.15	2.07
FeO	0.34	0.39	0.35	0.36	0.37	0.14
CaO	7.09	7.13	7.21	7.07	6.84	0.41
Na_2O	6.76	6.68	6.69	6.77	6.82	4.07
K_20	1.19	1.11	1.13	1.22	1.16	9.36
total	98.84	100.17	99.52	100.75	99.88	99.06

Appendix E. Feldspar electron microprobe data

UNIT	**RS**	**RS**	**RS**	**RS**	**RS**	**RS**
SAMPLE	**06WS 052**	**06WS 052**	**06WS 052**	**06WS 052**	**06WS 052**	**06WS 052**
ANALYSIS	fspar5 rim	fspar5 rim2	fspar8 core	fspar8 rim	fspar13 rim	fspar13 rim2
SiO_2	69.22	64.32	64.28	64.19	63.93	64.17
Al_2O_3	16.65	19.70	19.80	19.85	19.95	20.08
BaO	1.37	1.94	1.95	1.98	2.05	1.95
FeO	0.69	0.20	0.15	0.17	0.18	0.22
CaO	0.15	0.43	0.36	0.47	0.46	0.57
Na_2O	3.33	4.39	3.98	4.38	4.42	4.67
K_20	8.58	9.01	9.48	8.97	9.01	8.32
total	98.94	99.50	99.68	99.37	99.33	99.36

Appendix E. Feldspar electron microprobe data

UNIT	FS	FS	FS	FS	FS	FS
SAMPLE	**06WS 052**	**06WS 059**	**06WS 059**	**06WS 059**	**06WS 059**	**06WS 059**
ANALYSIS	fspar5 core	fspar6 core	fspar6 rim	fspar7 core	fspar9 core	fspar9 rim
SiO_2	60.57	60.65	61.74	60.62	61.36	61.81
Al_2O_3	24.42	24.30	23.41	24.26	23.41	23.62
BaO	0.19	0.25	0.22	0.20	0.34	0.26
FeO	0.35	0.33	0.27	0.32	0.38	0.35
CaO	5.61	5.67	4.93	5.52	5.26	4.85
Na_2O	7.31	7.34	7.90	7.54	7.73	7.76
K_20	1.55	1.46	1.52	1.54	1.51	1.34
total	100.49	99.65	100.19	100.78	99.85	100.03

Appendix E. Feldspar electron microprobe data

UNIT	FS	FS	FS	FS	FS	FS
SAMPLE	**06WS 059**	**06WS 059**	**06WS 059**	**06WS 059**	**06WS 059**	**06WS 059**
ANALYSIS	fspar10 core	fspar13 core	fspar1 core	fspar1 rim	fspar3 core	fspar3 rim
SiO_2	60.72	59.64	63.59	63.90	64.19	63.98
Al_2O_3	24.02	25.02	20.22	20.12	20.01	20.12
BaO	0.21	0.24	2.14	1.92	1.68	1.91
FeO	0.39	0.32	0.15	0.12	0.12	0.12
CaO	5.75	6.77	0.55	0.43	0.46	0.50
Na_2O	7.33	6.83	4.85	4.78	4.88	4.96
K_20	1.58	1.18	8.50	8.74	8.66	8.41
total	100.68	100.18	98.18	99.21	100.23	100.38

Appendix E. Feldspar electron microprobe data

UNIT	FS	FS	FS	FS	FS	FS
SAMPLE	**06WS 059**	**06WS 059**	**06WS 059**	**06WS 059**	**06WS 059**	**06WS 059**
ANALYSIS	fspar4 core	fspar4 rim	fspar8 core	fspar8 rim	fspar11 core	fspar11 rim
SiO_2	63.77	63.85	63.70	64.13	64.09	64.17
Al_2O_3	20.33	19.64	20.11	19.68	20.11	19.53
BaO	1.90	1.85	2.14	1.90	1.76	1.94
FeO	0.19	0.16	0.19	0.39	0.12	0.15
CaO	0.52	0.18	0.48	0.45	0.50	0.39
Na_2O	4.81	3.92	4.89	4.53	4.78	4.62
K_20	8.47	10.40	8.49	8.93	8.64	9.20
total	100.50	100.51	99.57	99.10	99.73	99.36

Appendix E. Feldspar electron microprobe data

UNIT	FS	FS	FS	FS	BM	BM
SAMPLE	**06WS 059**	**06WS 059**	**06WS 059**	**06WS 059**	**06WS 062**	**06WS 062**
ANALYSIS	fspar12 core	fspar12 core 2	fspar14 core	fspar14 rim	1 c	1 r
SiO_2	64.32	64.34	64.20	64.10	59.20	59.39
Al_2O_3	19.62	19.66	20.21	19.81	25.14	24.94
BaO	1.91	1.82	1.79	1.95	0.00	0.00
FeO	0.15	0.13	0.06	0.19	0.37	0.42
CaO	0.56	0.36	0.62	0.60	6.70	6.75
Na_2O	4.89	4.36	4.94	4.82	6.80	6.70
K_20	8.54	9.33	8.18	8.53	1.76	1.74
total	99.22	98.85	99.56	99.50	100.16	99.01

Appendix E. Feldspar electron microprobe data

UNIT	BM	BM	BM	BM	BM	BM
SAMPLE	**06WS 062**	**06WS 062**	**06WS 062**	**06WS 062**	**06WS 062**	**06WS 062**
ANALYSIS	2 c	2 r	3 c	3 r	4 c	4 r
SiO_2	58.31	59.72	59.56	59.89	57.41	59.85
Al_2O_3	25.75	24.69	24.92	24.52	26.51	24.70
BaO	0.11	0.25	0.29	0.24	0.16	0.17
FeO	0.42	0.43	0.40	0.40	0.38	0.43
CaO	7.32	6.33	6.66	6.09	8.52	6.48
Na_2O	6.57	6.76	6.70	7.07	6.04	6.85
K_20	1.53	1.81	1.47	1.80	0.98	1.53
total	99.96	99.68	100.68	100.35	100.29	99.65

Appendix E. Feldspar electron microprobe data

UNIT	BM	BM	BM	BM	BM	BM
SAMPLE	**06WS 062**	**06WS 062**	**06WS 062**	**06WS 062**	**06WS 062**	**06WS 062**
ANALYSIS	5 c	5 r	6 c	6 r	7 c	7 r
SiO_2	58.61	60.12	60.31	60.16	58.25	59.76
Al_2O_3	25.70	24.40	24.31	24.39	25.74	24.84
BaO	0.24	0.26	0.26	0.36	0.25	0.23
FeO	0.38	0.55	0.42	0.38	0.39	0.47
CaO	7.40	5.89	6.02	6.11	7.55	6.58
Na_2O	6.46	7.02	6.80	6.87	6.47	6.62
K_20	1.22	1.75	1.87	1.73	1.35	1.50
total	99.95	99.95	100.29	99.47	100.17	99.66

Appendix E. Feldspar electron microprobe data

UNIT	BM	BM	BM	BM	BM	BM
SAMPLE	**06WS 062**	**06WS 062**	**06WS 062**	**06WS 062**	**06WS 062**	**06WS 062**
ANALYSIS	8 c	8 r	9 c	9 r 1	9 r 2	10 c
SiO_2	59.89	59.52	57.29	59.79	59.47	61.14
Al_2O_3	24.73	24.55	26.69	24.70	25.02	23.86
BaO	0.22	0.28	0.14	0.30	0.21	0.25
FeO	0.39	0.41	0.40	0.41	0.42	0.39
CaO	6.53	6.24	8.33	6.22	6.55	5.66
Na_2O	6.68	6.80	6.12	6.92	6.72	6.79
K_20	1.56	2.20	1.02	1.65	1.61	1.92
total	100.20	99.40	99.08	99.35	98.75	100.55

Appendix E. Feldspar electron microprobe data

UNIT	BM	WG	WG	WG	WG	WG
SAMPLE	**06WS 062**	**06WS 069**	**06WS 069**	**06WS 069**	**06WS 069**	**06WS 069**
ANALYSIS	10 r	fspar 1 rim	fspar 1 core	fspar 2 rim	fspar 2 core	fspar 3 rim
SiO_2	60.40	60.56	60.53	61.15	60.03	61.75
Al_2O_3	24.29	24.46	24.26	24.14	24.84	23.63
BaO	0.16	0.13	0.27	0.25	0.23	0.22
FeO	0.38	0.36	0.38	0.34	0.39	0.38
CaO	6.04	6.15	6.33	5.45	6.39	5.44
Na_2O	6.85	6.95	6.84	7.02	6.78	6.87
K_20	1.88	1.39	1.39	1.65	1.34	1.72
total	100.30	99.80	100.39	100.06	100.60	99.94

Appendix E. Feldspar electron microprobe data

UNIT	WG	WG	WG	WG	WG	WG
SAMPLE	06WS 069	06WS 069	06WS 069	06WS 069	06WS 069	06WS 069
ANALYSIS	fspar 3 core	fspar 4 rim	fspar 4 core	fspar 7 rim	fspar 7 core	fspar 9 rim
SiO_2	60.10	60.46	60.00	59.60	61.00	60.74
Al_2O_3	24.79	24.61	25.01	25.22	24.13	24.45
BaO	0.23	0.18	0.18	0.17	0.34	0.30
FeO	0.36	0.38	0.35	0.36	0.35	0.36
CaO	6.43	6.38	6.68	6.59	5.53	5.79
Na_2O	6.72	6.58	6.45	6.74	6.87	6.81
K_20	1.37	1.40	1.33	1.32	1.78	1.56
total	99.96	99.93	99.78	99.67	99.85	99.18

Appendix E. Feldspar electron microprobe data

UNIT	WG	WG	WG	WG	WG	WG
SAMPLE	**06WS 069**	**06WS 069**	**06WS 069**	**06WS 069**	**06WS 069**	**06WS 069**
ANALYSIS	fspar 9 core	fspar 10 rim	fspar 10 core	fspar 5 rim	fspar 5 core	fspar 6 rim
SiO_2	60.07	61.11	61.49	64.23	64.06	64.62
Al_2O_3	24.97	24.05	23.87	19.96	20.14	19.73
BaO	0.11	0.23	0.28	1.99	2.06	1.95
FeO	0.37	0.34	0.34	0.16	0.19	0.18
CaO	6.74	5.58	5.39	0.50	0.63	0.51
Na_2O	6.47	6.96	6.79	4.20	4.56	4.41
K_20	1.27	1.72	1.85	8.97	8.37	8.59
total	99.80	100.14	100.67	98.65	99.62	99.25

Appendix E. Feldspar electron microprobe data

UNIT	WG	WG	WG	LN	LN	LN
SAMPLE	**06WS 069**	**06WS 069**	**06WS 069**	**06WS 035**	**06WS 035**	**06WS 035**
ANALYSIS	fspar 6 core	fspar 8 rim	fspar 8 core	fspar1 core	fspar1 rim	fspar2 core
SiO_2	64.27	63.95	64.42	56.45	59.51	57.03
Al_2O_3	20.06	20.18	20.05	27.23	25.10	27.07
BaO	1.95	2.02	1.84	0.04	0.19	0.15
FeO	0.15	0.17	0.17	0.41	0.40	0.40
CaO	0.48	0.47	0.50	9.24	6.64	8.86
Na_2O	4.60	4.27	4.34	5.86	7.22	5.89
K_20	8.49	8.94	8.67	0.77	0.94	0.60
total	99.72	98.84	98.78	99.11	99.44	100.53

Appendix E. Feldspar electron microprobe data

UNIT	**LN**	**LN**	**LN**	**LN**	**LN**	**LN**
SAMPLE	**06WS 035**	**06WS 035**	**06WS 035**	**06WS 035**	**06WS 035**	**06WS 035**
ANALYSIS	fspar2 rim	fspar3 rim	fspar4 core	fspar4 rim	fspar5 core	fspar5 rim
SiO_2	58.63	59.76	59.36	60.08	58.93	60.39
Al_2O_3	25.94	25.01	25.04	24.88	25.54	24.68
BaO	0.20	0.18	0.21	0.17	0.11	0.14
FeO	0.41	0.45	0.41	0.42	0.44	0.41
CaO	7.44	6.42	6.95	6.27	7.33	6.29
Na_2O	6.57	7.12	6.70	7.20	6.47	7.15
K_20	0.80	1.07	1.33	0.97	1.18	0.94
total	100.33	100.18	99.53	99.70	100.85	99.96

Appendix E. Feldspar electron microprobe data

UNIT	LN	LN	LN	LN	LN	LN
SAMPLE	**06WS 035**	**06WS 035**	**06WS 035**	**06WS 035**	**06WS 035**	**06WS 035**
ANALYSIS	fspar6 core	fspar6 rim	fspar7 core	fspar7 rim	fspar8 core	fspar8 rim
SiO_2	59.76	59.73	58.70	58.37	58.76	59.62
Al_2O_3	24.77	24.99	25.80	26.15	25.70	25.01
BaO	0.07	0.19	0.05	0.07	0.10	0.20
FeO	0.58	0.40	0.38	0.35	0.42	0.47
CaO	6.84	6.55	7.63	7.96	7.53	6.61
Na_2O	7.04	7.43	6.38	6.57	6.34	7.05
K_20	0.94	0.71	1.06	0.52	1.15	1.03
total	100.04	99.44	100.56	101.37	100.33	99.94

Appendix E. Feldspar electron microprobe data

UNIT	LN	LN	LN	LN	LN	LN
SAMPLE	**06WS 035**	**06WS 035**	**06WS 035**	**06WS 035**	**06WS 035**	**06WS 035**
ANALYSIS	fspar9 core	fspar9 rim	fspar10 core	fspar10 rim	LF 7 rim	LF 7 core
SiO_2	59.16	59.70	57.22	59.30	59.63	59.57
Al_2O_3	25.36	24.99	26.81	25.15	25.14	25.16
BaO	0.16	0.13	0.12	0.23	0.22	0.15
FeO	0.40	0.44	0.37	0.43	0.37	0.42
CaO	7.30	6.69	8.67	7.11	6.56	6.86
Na_2O	6.45	6.86	5.94	6.70	7.07	6.84
K_20	1.16	1.20	0.88	1.07	0.99	1.00
total	100.40	100.25	99.81	100.58	100.51	100.49

Appendix E. Feldspar electron microprobe data

UNIT	LN	LN	LN	LN	LN	LN
SAMPLE	**06WS 035**	**06WS 035**	**06WS 035**	**06WS 035**	**06WS 035**	**06WS 035**
ANALYSIS	LF 8 rim	LF 8 core	LF 9 rim	LF 9 mid	LF 10 rim	LF 10 core
SiO_2	59.77	59.90	60.35	58.35	58.88	58.63
Al_2O_3	24.99	25.10	24.96	26.05	25.59	25.65
BaO	0.22	0.19	0.09	0.19	0.06	0.20
FeO	0.39	0.40	0.43	0.39	0.44	0.46
CaO	6.83	6.78	6.24	7.93	7.64	7.77
Na_2O	6.57	6.33	6.75	6.38	6.41	6.20
K_20	1.24	1.31	1.18	0.72	0.99	1.09
total	100.69	100.65	100.27	99.76	100.50	100.15

Appendix E. Feldspar electron microprobe data

UNIT	WC	WC	WC	WC	WC	WC
SAMPLE	06WS 037	06WS 037	06WS 037	06WS 037	06WS 037	06WS 037
ANALYSIS	fspar1 core	fspar1 rim	fspar2 core	fspar2 rim	fspar3 core	fspar3 rim
SiO_2	56.73	58.65	55.65	59.29	59.29	59.22
Al_2O_3	26.93	25.54	27.72	25.22	25.06	25.13
BaO	- - -	- - -	- - -	- - -	- - -	- - -
FeO	0.50	0.49	0.49	0.57	0.52	0.56
CaO	9.01	7.52	9.91	7.17	7.05	7.10
Na_2O	6.00	6.63	5.55	6.69	6.63	6.76
K_20	0.82	1.17	0.68	1.05	1.46	1.23
total	99.54	99.81	100.57	99.49	100.40	99.75

Appendix E. Feldspar electron microprobe data

UNIT	WC	WC	WC	WC	WC	WC
SAMPLE	**06WS 037**	**06WS 037**	**06WS 037**	**06WS 037**	**06WS 037**	**06WS 037**
ANALYSIS	fspar4 core	fspar4 rim	fspar5 core	fspar5 rim	fspar7 core	fspar7 rim
SiO_2	59.10	58.88	55.42	58.33	58.78	59.08
Al_2O_3	25.16	25.43	28.07	25.76	25.42	25.36
BaO	- - -	- - -	- - -	- - -	- - -	- - -
FeO	0.48	0.49	0.47	0.49	0.50	0.53
CaO	7.25	7.33	9.80	7.71	7.51	7.21
Na_2O	6.76	6.81	5.58	6.70	6.62	6.55
K_20	1.26	1.06	0.67	1.01	1.17	1.27
total	99.71	99.23	100.53	100.20	99.84	99.55

Appendix E. Feldspar electron microprobe data

UNIT	WC	WC	WC	WC	WC	WC
SAMPLE	**06WS 037**	**06WS 037**	**06WS 037**	**06WS 037**	**06WS 037**	**06WS 037**
ANALYSIS	fspar8 core	fspar8 rim	fspar9 core	fspar9 rim	fspar10 core	fspar10 rim
SiO_2	58.77	58.65	57.12	59.08	59.85	59.47
Al_2O_3	25.60	25.63	26.67	25.34	24.97	25.25
BaO	- - -	- - -	- - -	- - -	- - -	- - -
FeO	0.50	0.48	0.50	0.50	0.48	0.50
CaO	7.44	7.49	8.59	7.29	6.71	6.92
Na_2O	6.51	6.64	6.16	6.61	6.57	6.68
K_20	1.19	1.10	0.96	1.17	1.41	1.19
total	99.97	99.74	100.46	99.92	99.72	100.19

Appendix E. Feldspar electron microprobe data

UNIT	WC	WC	WC	WC	WC	WC
SAMPLE	**06WS 037**	**06WS 037**	**06WS 037**	**06WS 037**	**06WS 037**	**06WS 037**
ANALYSIS	fspar11 rim	fspar12 core	fspar13 core	fspar13 rim	fspar13 rim 2	fspar13 rim 3
SiO_2	58.92	59.72	56.53	56.22	58.90	58.78
Al_2O_3	25.29	24.98	27.34	27.23	25.47	25.51
BaO	- - -	- - -	- - -	- - -	- - -	- - -
FeO	0.55	0.52	0.50	0.58	0.55	0.51
CaO	7.29	6.58	9.16	9.41	7.25	7.43
Na_2O	7.07	6.81	5.69	5.80	6.61	6.56
K_20	0.88	1.39	0.78	0.75	1.22	1.21
total	99.77	99.78	99.95	99.64	100.38	100.06

Appendix E. Feldspar electron microprobe data

UNIT	WC	WC	WC	WC	WC	WC
SAMPLE	**06WS 037**	**06WS 037**	**06WS 037**	**06WS 037**	**06WS 037**	**06WS 037**
ANALYSIS	fspar14 core	fspar14 rim	fspar15 core	fspar15 rim	fspar15 rim 2	fspar16 core
SiO_2	59.10	58.87	59.15	60.09	59.01	59.30
Al_2O_3	25.55	25.60	25.33	24.67	25.48	25.27
BaO	- - -	- - -	- - -	- - -	- - -	- - -
FeO	0.53	0.56	0.47	0.51	0.47	0.47
CaO	7.04	7.44	7.22	6.59	7.49	6.98
Na_2O	6.50	6.43	6.61	7.27	6.42	6.78
K_20	1.28	1.11	1.23	0.87	1.13	1.19
total	99.68	100.04	100.04	100.62	100.18	100.24

Appendix E. Feldspar electron microprobe data

UNIT	WC	WC	WC	WC	WC	WC
SAMPLE	06WS 037	06WS 037	06WS 037	06WS 037	06WS 037	06WS 037
ANALYSIS	fspar16 rim	fspar17 core	fspar17 rim	LF 9 rim	LF 9 core	LF 10 rim
SiO_2	58.37	58.71	58.70	59.21	60.11	59.40
Al_2O_3	25.69	25.57	25.66	25.39	24.62	25.32
BaO	- - -	- - -	- - -	0.18	0.15	0.15
FeO	0.53	0.49	0.47	0.45	0.48	0.41
CaO	7.65	7.57	7.34	7.39	6.71	7.36
Na_2O	6.67	6.51	6.72	6.21	6.56	6.32
K_20	1.08	1.14	1.10	1.18	1.37	1.05
total	100.10	99.93	100.28	100.11	99.43	100.80

Appendix E. Feldspar electron microprobe data

UNIT	**WC**
SAMPLE	**06WS 037**
ANALYSIS	LF 10 core
SiO_2	59.13
Al_2O_3	25.57
BaO	0.16
FeO	0.41
CaO	7.45
Na_2O	6.13
K_20	1.15
total	100.56

APPENDIX F

LA-ICP-MS PYROXENE DATA

Appendix G.
WBH pyroxene LA-ICP-MS trace element analyses (ppm)

UNIT	HS	HS	HS	HS	HS	HS	HS
SAMPLE	06WS028	06WS028	06WS028	06WS028	06WS028	06WS028	06WS028
ANALYSIS	pyx 1	pyx 2	pyx 3	pyx 4	pyx 5	pyx 6	pyx 7
Sc	70.6	69.6	66.3	157.2	146.9	139.0	107.6
Ti	1101.8	1094.1	1121.3	1800.0	1707.1	1927.6	1525.1
Rb	2.1	1.3	2.8	1.0	0.8	2.7	17.0
Sr	1.8	1.4	1.8	12.5	12.2	271.2	10.9
Y	142.0	136.8	108.1	289.6	268.2	318.0	234.8
Zr	20.2	19.3	24.9	87.4	80.0	69.5	68.1
Nb	0.4	0.3	0.7	0.4	0.7	1.6	4.0
Cs	0.1	0.1	0.1	0.0	0.0	0.1	0.3
Ba	0.6	0.4	6.7	1.3	1.4	5610.2	16.1
La	4.7	3.4	3.1	27.1	29.6	47.9	30.5
Ce	16.3	13.3	11.9	100.9	117.4	176.5	125.4
Pr	3.4	2.8	2.3	19.5	21.4	30.2	20.7
Nd	19.3	17.2	14.4	103.4	113.2	149.7	101.2
Sm	7.9	7.6	6.1	33.4	35.9	45.3	31.1
Eu	0.5	0.5	0.4	2.0	2.1	2.0	1.4
Gd	11.3	10.5	8.5	34.9	36.7	46.0	29.6
Tb	2.8	2.7	2.0	7.2	7.4	9.0	6.0
Dy	22.0	21.2	15.6	46.2	46.9	57.4	38.7
Ho	5.3	5.1	3.8	9.4	9.5	11.4	7.6
Er	17.3	17.1	12.2	27.3	26.4	31.8	21.0
Tm	3.2	3.2	2.2	4.3	4.1	5.0	3.4
Yb	20.5	20.6	14.4	23.5	23.1	28.1	18.9
Lu	3.4	3.5	2.6	3.9	3.8	4.7	3.1
Hf	0.8	0.8	1.0	3.2	3.0	2.9	2.3
Ta	0.0	0.0	0.0	0.0	0.0	0.0	0.2
Pb^{206}	1.0	1.4	25.6	1.0	9.1	3.8	7.5
Pb^{207}	1.0	0.9	25.8	1.2	9.6	4.1	7.8
Pb^{208}	1.2	1.0	24.7	1.0	8.9	3.5	8.0
Th	0.5	0.3	0.2	0.2	0.2	1.2	1.7
U	0.1	0.1	0.1	0.1	0.0	0.4	0.6

Appendix G.
WBH pyroxene LA-ICP-MS trace element analyses (ppm)

UNIT	HS	HS	RS	RS	RS	RS	RS
SAMPLE	06WS028	06WS028	06WS052	06WS052	06WS052	06WS052	06WS052
ANALYSIS	pyx 8	pyx 9	pyx 1	pyx 2	pyx 3	pyx 4	pyx 5
Sc	65.5	67.3	68.8	71.5	76.1	121.8	141.0
Ti	1078.5	1078.1	1072.0	1196.2	1191.8	1534.6	1589.7
Rb	0.9	2.4	1.1	0.8	0.6	0.6	0.4
Sr	1.8	2.0	1.1	1.9	2.8	11.1	11.5
Y	142.7	144.4	143.5	126.1	130.5	218.5	321.3
Zr	18.1	18.7	196.7	24.0	30.1	68.1	75.8
Nb	0.3	0.5	0.3	0.4	0.3	0.3	0.2
Cs	0.0	0.1	0.0	0.0	0.0	0.0	0.0
Ba	1.0	1.5	2.6	2.8	1.2	4.4	1.1
La	9.0	4.5	2.9	8.5	5.8	23.6	37.3
Ce	27.8	17.6	13.6	23.2	26.1	101.4	146.7
Pr	4.7	3.4	2.8	3.9	4.8	17.5	25.8
Nd	23.1	19.7	17.4	21.6	26.8	89.6	129.1
Sm	8.5	8.4	7.7	7.7	10.0	28.3	40.0
Eu	0.4	0.4	0.4	0.5	0.6	1.9	2.0
Gd	10.5	10.3	10.3	9.4	10.9	28.8	40.4
Tb	2.6	2.7	2.7	2.4	2.7	6.0	8.3
Dy	19.0	20.5	20.1	17.7	19.1	39.7	53.5
Ho	4.5	4.7	4.8	4.0	4.4	8.0	10.7
Er	14.4	15.4	15.8	13.3	13.9	22.7	30.0
Tm	2.6	2.8	2.8	2.4	2.4	3.5	4.6
Yb	16.1	17.4	18.2	14.8	14.7	20.0	25.4
Lu	2.9	3.1	3.3	2.6	2.7	3.5	4.3
Hf	0.7	0.6	3.1	0.9	1.1	2.6	2.8
Ta	0.0	0.0	0.0	0.0	0.0	0.0	0.0
Pb^{206}	2.3	1.5	0.7	0.9	1.5	1.5	0.6
Pb^{207}	2.3	1.7	0.7	1.1	1.6	1.6	0.6
Pb^{208}	2.1	1.7	0.7	0.9	1.4	1.5	0.6
Th	0.4	0.2	0.2	0.3	0.1	0.2	0.1
U	0.1	0.1	0.1	0.1	0.0	0.1	0.0

Appendix G.
WBH pyroxene LA-ICP-MS trace element analyses (ppm)

UNIT	RS	RS	RS	RS	RS	FS	FS
SAMPLE	06WS052	06WS052	06WS052	06WS052	06WS052	06WS-059	06WS-059
ANALYSIS	pyx 6	pyx 7	pyx 8	pyx 9	pyx 10	pyx 1	pyx 2
Sc	79.4	135.9	161.8	78.9	66.8	197.5	197.8
Ti	1598.3	1657.0	1849.8	1126.9	1249.3	2241.2	2131.8
Rb	2.3	0.2	2.2	2.3	0.5	8.5	8.3
Sr	2.6	12.8	16.4	2.3	0.9	15.5	19.2
Y	173.0	266.3	322.0	165.4	109.8	365.5	319.0
Zr	24.5	78.9	95.3	24.8	23.6	134.1	113.2
Nb	1.5	0.3	0.6	0.6	0.5	1.2	1.6
Cs	0.1	0.0	0.2	0.1	0.0	0.2	0.3
Ba	17.4	2.1	95.2	4.5	1.4	7.8	9.7
La	5.7	35.0	40.4	9.1	2.2	69.3	61.4
Ce	22.6	141.2	142.7	29.9	9.9	231.3	203.3
Pr	4.6	24.0	26.0	6.0	2.1	42.0	37.0
Nd	28.5	120.1	138.5	34.1	13.0	216.5	181.4
Sm	11.1	36.6	43.2	12.2	5.9	60.9	49.0
Eu	0.5	2.2	2.4	0.6	0.4	2.7	2.5
Gd	13.2	36.6	43.6	14.2	7.7	59.1	44.5
Tb	3.4	7.5	8.7	3.5	2.0	11.4	8.7
Dy	25.0	47.9	55.4	24.6	15.3	70.4	54.4
Ho	5.8	9.4	11.2	5.5	3.5	13.3	10.7
Er	19.0	25.9	30.9	17.3	11.8	38.0	29.2
Tm	3.4	4.0	4.8	3.1	2.2	5.9	4.5
Yb	20.2	22.4	25.5	18.4	13.0	36.5	27.9
Lu	3.7	3.8	4.5	3.4	2.4	7.6	6.2
Hf	1.0	3.0	3.6	1.0	0.8	5.9	4.6
Ta	0.1	0.0	0.0	0.0	0.0	0.0	0.0
Pb^{206}	3.6	2.0	1.1	0.6	0.8	4.3	4.4
Pb^{207}	4.3	2.6	0.9	0.5	0.8	4.1	4.3
Pb^{208}	4.0	2.1	0.9	0.5	0.8	4.5	4.1
Th	0.3	0.3	0.8	0.7	0.2	1.0	1.5
U	0.1	0.1	0.2	0.1	0.1	0.3	0.3

Appendix G.
WBH pyroxene LA-ICP-MS trace element analyses (ppm)

UNIT	FS	FS	FS	FS	FS	FS	FS
SAMPLE	06WS-059	06WS-059	06WS-059	06WS-059	06WS-059	06WS-059	06WS-059
ANALYSIS	pyx 3	pyx 4	pyx 5	pyx 6	pyx 7	pyx 8	pyx 9
Sc	156.7	192.2	175.1	217.8	208.2	197.5	179.4
Ti	2571.4	2117.2	2049.0	2263.0	2161.2	1989.9	1867.4
Rb	128.2	2.4	3.8	8.1	3.8	1.3	5.0
Sr	22.7	19.9	18.0	20.6	19.3	17.8	16.7
Y	203.3	301.5	299.7	336.5	327.0	323.9	278.7
Zr	169.1	109.7	110.7	123.7	112.8	105.2	95.9
Nb	11.6	0.4	0.7	0.7	0.5	0.4	0.5
Cs	3.5	0.0	0.1	0.3	0.2	0.0	0.2
Ba	58.7	1.1	4.4	8.3	5.0	2.6	5.2
La	45.7	51.9	60.3	53.2	61.2	58.8	51.6
Ce	134.9	183.7	216.5	167.0	211.8	208.9	193.8
Pr	22.0	30.5	37.5	29.6	37.1	36.0	32.4
Nd	104.4	151.2	181.7	149.7	183.8	176.7	157.0
Sm	28.9	41.1	50.1	42.2	51.9	50.1	44.1
Eu	1.6	2.2	2.7	2.4	2.8	2.6	2.5
Gd	26.1	38.1	46.5	41.3	48.7	47.9	42.6
Tb	5.0	7.1	8.7	7.8	9.3	9.3	8.2
Dy	30.7	41.1	52.4	49.1	57.8	57.0	50.9
Ho	5.9	8.1	10.2	9.5	10.9	10.9	9.6
Er	17.0	23.4	28.3	25.9	30.4	30.9	27.8
Tm	2.7	3.8	4.5	4.1	4.9	4.8	4.4
Yb	16.7	23.8	27.5	24.5	29.7	29.1	26.8
Lu	3.4	5.4	5.9	5.1	6.3	6.0	5.5
Hf	4.0	4.3	4.5	4.0	4.5	4.2	3.9
Ta	0.0	0.0	0.0	0.0	0.0	0.0	0.0
Pb^{206}	7.0	1.4	2.8	2.7	2.0	1.3	2.9
Pb^{207}	7.3	1.6	2.5	2.5	2.0	1.3	2.7
Pb^{208}	7.4	1.6	2.5	2.7	1.9	1.4	2.7
Th	1.3	0.3	0.6	0.6	0.7	0.4	0.5
U	0.8	0.0	0.0	0.0	0.0	0.0	0.0

Appendix G.
WBH pyroxene LA-ICP-MS trace element analyses (ppm)

UNIT	Hn	Hn	Hn	Hn	Hn	Hn	BM
SAMPLE	07 WS 077	07WS 077	8 WS 077	07WS 078	9 WS 077	07WS 077	06WS 062
ANALYSIS	pyx 1	pyx 2	pyx 3	pyx 4	pyx 5	pyx 6	pyx 1
Sc	158.6	165.4	175.1	180.9	178.6	166.5	92.0
Ti	1912.6	1854.7	1937.1	1925.4	1967.6	1933.9	1296.7
Rb	0.1	2.1	2.1	0.9	1.9	1.6	1.6
Sr	16.1	17.3	19.6	18.2	17.9	18.1	1.6
Y	287.6	271.7	271.7	275.5	290.8	273.4	167.6
Zr	97.1	97.0	99.1	97.7	103.6	127.4	26.9
Nb	0.4	0.8	0.5	0.4	0.8	0.9	0.8
Cs	0.0	0.1	0.3	0.2	0.1	0.1	0.1
Ba	1.2	7.0	6.4	3.1	6.1	5.4	4.9
La	59.1	56.9	57.3	55.9	62.3	56.0	5.4
Ce	227.1	217.1	212.3	208.1	228.2	214.3	16.2
Pr	38.8	37.1	36.2	35.8	38.8	36.1	3.4
Nd	187.0	179.6	175.0	174.4	188.1	173.9	21.6
Sm	52.2	50.0	49.0	49.4	51.9	48.7	9.3
Eu	2.7	2.6	2.9	2.8	2.7	2.7	0.5
Gd	50.5	48.5	47.7	47.9	50.2	46.8	13.7
Tb	9.1	8.8	8.7	8.8	9.1	8.4	3.4
Dy	54.7	52.7	51.4	52.9	55.1	50.2	25.8
Ho	10.6	10.1	9.9	10.2	10.6	9.6	6.1
Er	30.0	28.4	28.1	28.5	29.8	27.3	19.9
Tm	4.6	4.4	4.3	4.5	4.6	4.2	3.6
Yb	30.1	29.0	28.3	29.4	29.8	27.4	23.2
Lu	5.9	5.7	5.6	5.8	5.9	5.4	4.1
Hf	4.3	4.2	4.2	4.1	4.4	4.5	1.1
Ta	0.0	0.0	0.0	0.0	0.0	0.0	0.0
Pb^{206}	1.1	1.5	2.8	1.1	1.9	1.2	0.5
Pb^{207}	1.0	1.5	2.9	1.1	1.8	1.2	0.5
Pb^{208}	1.1	1.4	3.0	1.1	2.0	1.2	0.6
Th	0.3	0.5	0.9	0.2	0.8	0.9	0.5
U	0.0	0.1	0.0	0.0	0.0	0.0	0.0

Appendix G.
WBH pyroxene LA-ICP-MS trace element analyses (ppm)

UNIT	BM	BM	BM	BM	BM	BM	BM
SAMPLE	06WS 062	06WS 062	06WS 062	06WS 062	06WS 062	06WS 062	06WS 062
ANALYSIS	pyx 2	pyx 3	pyx 4	pyx 5	pyx 6	pyx 7	pyx 8
Sc	91.1	80.7	68.5	74.8	72.9	67.2	70.8
Ti	1273.6	1151.3	1055.2	1097.6	1091.9	972.6	1038.1
Rb	1.4	1.8	1.7	0.3	0.8	0.6	0.4
Sr	1.2	1.0	1.1	0.9	1.0	0.6	0.6
Y	158.9	142.8	117.5	129.9	127.6	104.4	121.0
Zr	26.6	24.4	22.9	21.0	21.8	17.1	19.7
Nb	0.6	0.6	0.8	0.3	0.5	0.4	0.4
Cs	0.0	0.1	0.1	0.0	0.0	0.0	0.0
Ba	2.3	1.9	4.4	0.6	1.5	1.6	0.6
La	3.6	2.3	2.2	3.0	2.5	1.6	1.9
Ce	12.9	8.7	10.1	13.0	12.1	8.2	9.6
Pr	2.9	1.9	2.1	2.7	2.5	1.7	2.1
Nd	18.6	12.5	13.7	17.0	15.6	11.2	13.3
Sm	8.2	6.2	6.4	7.3	6.9	5.2	6.2
Eu	0.5	0.4	0.4	0.4	0.4	0.3	0.4
Gd	12.4	9.0	8.8	10.0	9.5	7.5	8.4
Tb	3.0	2.5	2.3	2.5	2.4	2.0	2.2
Dy	23.3	18.8	17.9	19.5	19.3	15.4	16.8
Ho	5.5	4.4	4.2	4.5	4.5	3.7	4.0
Er	18.8	15.2	14.0	15.1	15.0	12.3	12.8
Tm	3.4	2.8	2.6	2.7	2.6	2.2	2.3
Yb	21.3	17.3	15.9	16.8	16.6	14.1	14.7
Lu	3.9	3.1	2.9	3.1	3.1	2.7	2.8
Hf	1.2	0.9	0.9	0.9	0.9	0.7	0.7
Ta	0.0	0.0	0.0	0.0	0.0	0.0	0.0
Pb^{206}	0.8	1.0	3.5	1.1	1.8	0.8	0.2
Pb^{207}	0.7	0.9	3.9	0.9	1.8	0.8	0.3
Pb^{208}	0.7	0.8	3.6	0.8	1.7	0.9	0.3
Th	0.3	0.2	0.5	0.1	0.2	0.1	0.0
U	2.8	0.0	- - -	- - -	- - -	- - -	- - -

Appendix G.
WBH pyroxene LA-ICP-MS trace element analyses (ppm)

UNIT	BM	WG	WG	WG	WG	WG	WG
SAMPLE	06WS 062	06WS-069	06WS-069	06WS-069	06WS-069	06WS-069	06WS-069
ANALYSIS	pyx 9	pyx 1	pyx 2	pyx 3	pyx 4	pyx 5	pyx 6
Sc	93.9	180.3	44.3	149.4	133.4	55.5	180.7
Ti	1295.1	1918.0	1539.2	1584.9	1653.0	1331.4	1788.3
Rb	0.7	3.3	107.4	4.3	30.0	94.2	0.5
Sr	0.9	14.6	5.6	8.6	10.0	17.4	13.2
Y	161.7	259.7	94.0	260.2	238.4	123.9	303.2
Zr	24.6	120.4	186.3	81.9	108.8	212.0	102.9
Nb	0.3	0.8	24.5	1.6	7.0	27.1	0.7
Cs	0.0	0.4	1.9	0.3	0.9	1.6	0.0
Ba	0.7	4.8	145.2	6.8	39.6	429.1	1.9
La	3.0	30.1	37.7	27.1	40.9	41.7	34.4
Ce	11.8	108.3	87.5	102.8	122.4	105.7	132.9
Pr	2.7	19.9	10.3	19.0	20.2	13.3	24.5
Nd	17.9	105.7	42.3	99.8	101.2	57.6	128.8
Sm	8.3	33.7	10.7	32.2	30.6	15.5	41.3
Eu	0.5	2.6	0.5	1.7	1.4	1.1	2.5
Gd	11.4	39.2	12.4	36.4	35.5	17.2	45.4
Tb	3.0	7.7	2.5	7.3	6.8	3.2	8.8
Dy	23.6	50.8	17.9	49.2	44.3	22.1	57.7
Ho	5.4	10.4	3.9	10.1	9.2	4.7	11.6
Er	18.3	30.1	12.8	29.9	27.7	14.2	32.8
Tm	3.3	4.8	2.2	4.8	4.4	2.3	5.1
Yb	21.0	27.2	13.7	28.6	26.9	14.3	29.5
Lu	4.0	4.7	2.5	5.0	4.8	2.5	5.2
Hf	1.0	5.5	7.0	3.7	4.8	6.9	4.7
Ta	0.0	0.0	1.7	0.1	0.5	1.7	0.1
Pb^{206}	0.3	0.8	16.3	1.3	5.0	19.5	0.8
Pb^{207}	0.3	0.8	16.0	1.1	5.0	19.3	0.8
Pb^{208}	0.3	0.8	16.5	1.1	5.0	20.1	0.8
Th	0.1	0.5	13.9	0.7	4.6	14.8	0.3
U	- - -	- - -	- - -	- - -	- - -	- - -	- - -

Appendix G.
WBH pyroxene LA-ICP-MS trace element analyses (ppm)

UNIT	WG	WG	WG	LN	LN	LN	LN
SAMPLE	06WS-069	06WS-069	06WS-069	06WS-035	06WS-035	06WS-035	06WS-035
ANALYSIS	pyx 7	pyx 8	pyx 9	pyx 1	pyx 2	pyx 3	pyx 4
Sc	114.1	206.0	102.1	84.8	104.4	103.7	85.6
Ti	1438.6	2001.3	1195.6	1015.9	1279.6	1151.5	1007.3
Rb	0.9	1.2	9.3	1.4	2.4	0.9	0.2
Sr	2.6	12.3	99.3	1.0	1.7	1.0	0.6
Y	182.9	384.7	211.6	125.8	159.5	155.2	126.1
Zr	51.0	112.5	85.0	16.5	23.6	19.5	14.9
Nb	1.4	1.0	3.2	0.4	2.8	0.6	0.3
Cs	0.1	0.1	0.7	0.1	0.2	0.1	0.0
Ba	4.2	2.8	350.8	3.4	7.5	4.2	0.2
La	5.1	40.4	25.6	1.5	2.2	2.3	1.8
Ce	17.0	136.9	72.7	7.5	9.0	9.1	8.9
Pr	3.5	27.6	13.1	1.8	2.1	2.1	1.8
Nd	21.7	153.5	72.2	11.6	14.8	14.6	12.0
Sm	9.2	49.7	24.1	5.7	7.0	7.2	6.0
Eu	0.6	2.5	2.0	0.3	0.4	0.4	0.3
Gd	13.4	57.9	28.3	8.7	10.8	10.3	8.5
Tb	3.1	11.3	5.7	2.3	2.9	2.7	2.2
Dy	24.9	75.2	40.9	17.7	21.8	21.2	17.2
Ho	5.8	15.2	8.5	4.2	5.4	5.2	4.0
Er	19.0	45.2	25.9	14.5	18.2	17.7	14.0
Tm	3.4	7.1	4.2	2.8	3.3	3.1	2.5
Yb	21.3	40.6	24.8	16.5	20.4	19.4	15.6
Lu	4.1	7.4	4.6	3.1	3.8	3.7	2.9
Hf	1.9	5.6	3.5	0.6	0.8	0.8	0.6
Ta	0.1	0.1	0.2	0.0	0.1	0.0	0.0
Pb^{206}	0.4	1.1	3.7	1.7	0.8	1.0	0.2
Pb^{207}	0.3	0.9	3.4	1.8	0.6	1.2	0.2
Pb^{208}	0.3	0.9	3.4	1.4	0.7	1.0	0.2
Th	0.3	0.6	2.9	0.0	0.2	0.0	0.0
U	- - -	- - -	- - -	- - -	- - -	- - -	- - -

Appendix G.
WBH pyroxene LA-ICP-MS trace element analyses (ppm)

UNIT	LN	WC	WC	WC	WC	WC	WC
SAMPLE	06WS-035	06WS-037	06WS-037	06WS-037	06WS-037	06WS-037	06WS-037
ANALYSIS	pyx 5	pyx 1	pyx 2	pyx 3	pyx 4	pyx 5	pyx 6
Sc	81.8	95.2	97.4	94.6	91.3	92.3	85.0
Ti	996.6	1180.6	1192.2	1171.1	1114.9	1202.3	1089.6
Rb	0.7	0.8	0.6	2.1	0.2	0.0	0.1
Sr	0.8	1.3	1.3	1.7	0.8	0.8	0.8
Y	125.3	128.4	137.7	137.6	128.9	128.3	114.7
Zr	16.6	22.2	25.8	26.2	21.0	21.9	19.8
Nb	0.4	0.5	0.5	0.8	0.3	0.3	0.2
Cs	0.0	0.0	0.0	0.1	0.0	0.0	0.0
Ba	3.8	2.1	2.5	5.7	0.6	0.5	0.6
La	1.9	1.7	2.5	5.2	1.6	1.9	2.2
Ce	9.1	7.8	10.1	14.9	6.9	9.3	9.5
Pr	1.9	1.9	2.3	3.0	1.7	2.1	2.0
Nd	12.2	13.3	15.2	17.2	12.2	13.5	12.5
Sm	5.8	6.4	7.1	7.3	5.6	6.4	6.0
Eu	0.3	0.5	0.5	0.5	0.4	0.5	0.4
Gd	8.1	9.8	10.5	10.2	8.9	9.3	8.4
Tb	2.2	2.5	2.6	2.5	2.2	2.4	2.1
Dy	16.9	19.2	20.1	19.0	17.1	18.0	16.1
Ho	4.1	4.8	4.9	4.5	4.3	4.4	4.0
Er	13.9	16.3	16.1	15.5	14.7	14.6	13.5
Tm	2.5	3.0	2.9	2.8	2.8	2.7	2.5
Yb	15.7	19.1	18.3	17.2	16.7	16.9	15.5
Lu	2.9	3.3	3.3	3.2	3.1	3.1	2.8
Hf	0.7	0.9	1.0	1.0	0.9	1.0	0.8
Ta	0.0	0.0	0.0	0.0	0.0	0.0	0.0
Pb^{206}	0.6	3.1	-0.2	0.6	0.3	1.0	0.8
Pb^{207}	0.5	3.5	-0.5	0.2	0.5	1.1	0.9
Pb^{208}	0.6	3.3	-1.1	-0.1	0.2	1.2	0.8
Th	0.2	0.2	0.3	0.5	0.0	0.0	0.0
U	- - -	- - -	- - -	- - -	- - -	- - -	- - -

Appendix G.
WBH pyroxene
LA-ICP-MS
trace element
analyses
(ppm)

UNIT	WC	WC	WC	WC
SAMPLE	06WS-037	06WS-037	06WS-037	06WS-037
ANALYSIS	pyx 7	pyx 8	pyx 9	pyx 10
Sc	83.7	84.7	43.9	82.2
Ti	1075.5	1024.1	1259.7	1079.1
Rb	0.0	0.0	84.3	-0.1
Sr	0.7	0.6	9.7	0.7
Y	113.4	116.9	95.9	117.4
Zr	19.1	18.9	156.4	19.8
Nb	0.2	0.2	19.7	0.3
Cs	0.0	0.0	1.5	0.0
Ba	0.3	0.1	3.8	0.4
La	2.1	1.5	40.9	1.8
Ce	9.1	7.8	102.4	8.5
Pr	2.0	1.7	11.8	1.9
Nd	12.3	11.0	48.9	12.2
Sm	5.7	5.6	11.2	5.7
Eu	0.4	0.3	0.6	0.4
Gd	8.2	7.9	12.0	8.7
Tb	2.1	2.1	2.1	2.2
Dy	15.5	15.7	14.2	17.0
Ho	3.7	3.7	3.2	4.1
Er	12.5	12.8	9.7	13.7
Tm	2.3	2.3	1.7	2.3
Yb	14.9	14.5	9.7	15.3
Lu	2.7	2.7	1.7	2.8
Hf	0.7	0.7	4.3	0.8
Ta	0.0	0.0	1.2	0.0
Pb^{206}	0.5	0.1	14.1	0.7
Pb^{207}	0.4	0.1	14.3	1.9
Pb^{208}	0.4	0.1	14.1	1.5
Th	0.1	0.0	10.8	0.1
U	- - -	- - -	- - -	- - -

APPENDIX G

LA-ICP-MS VOLCANIC GLASS DATA

Appendix G.
WBH glass
LA-ICP-MS
trace element
analyses
(ppm)

UNIT	HS	HS	HS	HS	HS	HS	HS
SAMPLE	06WS-028	06WS-028	06WS-028	06WS-028	06WS-028	06WS-028	06WS-028
ANALYSIS	Glass 1	Glass 2	Glass 3	Glass 4	Glass 5	Glass 6	Glass 7
Sc	4.0	4.1	4.5	2.1	5.3	4.0	5.4
Ti	1447.9	1746.9	1707.4	1606.0	2073.1	1803.8	2399.0
Rb	264.5	278.0	292.7	301.7	147.4	300.2	247.4
Sr	26.7	22.8	11.8	13.7	36.2	19.8	39.5
Y	44.8	52.5	47.2	46.4	64.3	53.1	51.5
Zr	248.5	296.5	285.4	269.7	390.5	303.1	353.0
Nb	47.6	56.0	53.5	53.2	66.7	55.6	55.2
Cs	4.0	4.5	4.6	4.7	4.9	4.5	3.9
Ba	624.1	557.9	389.4	443.7	679.5	582.4	844.1
La	57.6	63.8	60.4	59.1	75.7	64.7	60.1
Ce	141.4	148.3	145.8	149.6	179.6	156.8	142.4
Pr	12.3	13.0	12.5	12.5	16.5	13.6	12.7
Nd	42.8	44.2	42.9	42.4	58.7	47.9	45.3
Sm	8.1	8.2	8.2	8.0	11.1	9.0	8.6
Eu	0.6	0.5	0.4	0.5	0.8	0.6	0.9
Gd	7.5	6.8	7.6	7.3	9.8	8.4	7.7
Tb	1.2	1.1	1.2	1.2	1.7	1.4	1.3
Dy	7.7	6.8	7.7	7.3	10.4	8.4	7.9
Ho	1.5	1.4	1.5	1.4	2.1	1.7	1.6
Er	4.5	3.9	4.5	4.4	6.1	5.2	4.7
Tm	0.7	0.7	0.7	0.7	1.0	0.8	0.8
Yb	4.3	3.7	4.2	4.1	5.4	4.7	4.5
Lu	0.6	0.6	0.6	0.6	0.9	0.7	0.7
Hf	7.4	6.9	7.8	6.8	11.1	8.1	9.0
Ta	2.7	2.5	2.9	2.5	3.5	3.0	2.6
Pb^{206}	38.7	35.9	34.7	25.9	42.6	37.5	35.9
Pb^{207}	36.7	36.1	34.1	20.4	40.5	27.1	35.8
Pb^{208}	38.5	36.3	33.9	19.3	42.6	36.9	34.9
Th	27.5	23.5	25.5	17.7	36.6	26.6	23.8
U	10.6	8.7	9.4	7.0	12.4	10.0	9.0

Appendix G.
WBH glass
LA-ICP-MS
trace element
analyses
(ppm)

UNIT	HS	HS	HS	RS	RS	RS	RS
SAMPLE	06WS-028	06WS-028	06WS-028	06WS-052	06WS-052	06WS-052	06WS-052
ANALYSIS	Glass 8	Glass 9	Glass 10	Glass 1	Glass 2	Glass 3	Glass 4
Sc	4.6	4.6	4.3	6.9	6.2	7.9	5.6
Ti	1550.4	1589.9	1563.8	2344.2	2211.0	2446.9	2108.8
Rb	293.8	304.2	281.2	244.3	238.0	254.2	226.8
Sr	6.9	34.7	8.4	25.2	24.9	28.7	28.9
Y	53.8	48.8	51.2	58.8	60.0	67.5	53.1
Zr	292.6	256.5	278.2	336.6	320.4	370.6	307.3
Nb	53.4	56.0	53.5	55.1	55.1	62.7	53.3
Cs	4.4	4.8	4.5	3.9	3.9	4.6	3.9
Ba	351.5	1047.8	371.1	582.0	613.1	709.0	655.4
La	68.5	61.9	66.4	65.5	68.3	76.0	63.5
Ce	159.1	156.5	157.8	159.5	163.4	183.0	152.4
Pr	14.2	13.0	13.8	14.5	14.7	16.3	13.4
Nd	49.4	44.1	47.8	51.5	52.9	58.5	47.2
Sm	9.2	8.0	9.0	10.0	10.4	11.4	9.4
Eu	0.4	0.5	0.4	0.8	0.8	0.9	0.7
Gd	8.2	7.4	8.0	8.5	8.7	9.8	7.6
Tb	1.3	1.2	1.4	1.4	1.5	1.7	1.3
Dy	8.3	6.7	8.4	8.7	9.2	9.9	8.5
Ho	1.6	1.4	1.7	1.8	1.8	2.0	1.7
Er	5.0	4.1	5.1	5.0	5.4	5.5	4.8
Tm	0.7	0.7	0.9	0.8	0.8	0.9	0.8
Yb	4.6	3.7	4.7	4.5	5.0	5.2	4.7
Lu	0.7	0.6	0.7	0.7	0.8	0.8	0.7
Hf	7.7	5.9	8.4	8.1	8.5	9.1	7.6
Ta	2.7	2.5	3.0	2.5	2.7	2.7	2.4
Pb^{206}	36.8	37.7	43.6	37.0	38.7	37.4	35.0
Pb^{207}	36.6	37.6	45.0	35.4	37.8	35.9	35.0
Pb^{208}	35.7	38.5	44.5	35.7	33.6	37.1	34.7
Th	26.4	23.4	31.9	22.5	24.7	24.0	22.2
U	10.0	10.0	11.7	9.9	9.7	9.2	9.3

Appendix G.
WBH glass
LA-ICP-MS
trace element
analyses
(ppm)

UNIT	RS	RS	RS	RS	RS	RS	FS
SAMPLE	06WS-052	06WS-052	06WS-052	06WS-052	06WS-052	06WS-052	06WS-059
ANALYSIS	Glass 5	Glass 6	Glass 7	Glass 8	Glass 9	Glass 10	Glass 1
Sc	7.5	5.9	6.0	5.7	7.8	6.9	4.6
Ti	2382.3	2120.0	2160.1	2106.0	2397.8	2154.2	1511.5
Rb	224.0	235.5	239.1	233.1	212.2	243.3	269.6
Sr	39.2	23.4	23.0	32.5	35.6	22.8	15.1
Y	62.4	59.4	56.9	51.7	63.7	54.8	72.6
Zr	336.3	322.3	321.8	301.3	309.3	315.9	356.3
Nb	54.5	53.8	55.9	53.2	51.5	56.8	62.7
Cs	3.9	4.0	4.1	4.0	3.6	4.2	4.9
Ba	785.4	617.1	608.9	830.1	718.1	614.6	489.0
La	70.6	67.1	67.1	61.6	66.3	65.3	80.5
Ce	157.5	162.4	163.5	156.3	162.3	163.3	185.4
Pr	15.4	14.7	14.4	13.5	15.1	14.2	16.1
Nd	56.4	52.5	51.0	47.5	56.2	49.0	58.0
Sm	10.9	10.1	9.8	8.7	11.7	9.5	11.1
Eu	1.0	0.8	0.7	0.8	1.0	0.8	0.8
Gd	8.9	8.6	8.1	7.7	9.3	8.1	9.8
Tb	1.5	1.5	1.5	1.3	1.7	1.4	1.7
Dy	9.7	9.5	9.0	8.1	10.7	8.6	10.8
Ho	1.9	1.8	1.8	1.6	2.1	1.8	2.1
Er	5.6	5.4	5.1	4.7	6.1	5.1	6.6
Tm	0.8	0.9	0.8	0.8	0.9	0.8	1.0
Yb	5.1	5.1	4.9	4.5	6.0	4.8	5.5
Lu	0.8	0.8	0.7	0.7	0.9	0.7	0.9
Hf	8.5	8.8	7.9	7.6	8.5	8.3	9.9
Ta	2.5	2.8	2.5	2.6	2.7	2.6	3.1
Pb^{206}	34.6	38.9	35.2	37.9	40.3	38.8	42.3
Pb^{207}	35.1	39.0	34.7	34.5	41.2	37.0	42.7
Pb^{208}	33.7	41.0	35.5	36.4	42.0	37.8	41.8
Th	22.3	25.8	22.0	21.6	24.8	22.9	27.4
U	9.2	10.3	9.7	9.4	10.5	10.1	9.9

Appendix G.
WBH glass
LA-ICP-MS
trace element
analyses
(ppm)

UNIT	FS	FS	FS	FS	FS	FS	FS
SAMPLE	06WS-059	06WS-059	06WS-059	06WS-059	06WS-059	06WS-059	06WS-059
ANALYSIS	Glass 2	Glass 3	Glass 4	Glass 5	Glass 6	Glass 7	Glass 8
Sc	5.0	5.0	4.7	5.1	4.6	3.8	5.4
Ti	1515.3	1460.0	1519.6	1568.5	1480.3	1487.2	1423.6
Rb	287.0	277.7	300.6	309.9	256.2	270.1	252.4
Sr	9.5	7.7	7.2	9.1	14.8	9.6	18.5
Y	86.9	69.3	62.7	103.9	90.9	72.1	68.1
Zr	421.7	327.6	292.3	462.2	425.3	335.6	330.2
Nb	63.6	58.3	59.5	66.9	61.2	58.3	57.0
Cs	4.5	4.4	5.0	4.9	4.5	4.0	4.4
Ba	364.4	360.6	285.7	428.6	467.6	448.2	494.7
La	90.3	76.0	66.2	106.1	92.9	74.6	73.4
Ce	187.7	176.4	171.2	204.2	187.5	177.1	166.4
Pr	18.0	16.0	14.4	20.2	18.2	15.8	14.8
Nd	65.4	57.9	51.1	75.4	67.6	57.5	52.4
Sm	12.9	11.3	9.9	14.9	13.1	11.4	10.5
Eu	0.7	0.5	0.6	1.0	0.8	0.7	0.6
Gd	12.0	9.9	8.7	13.5	12.2	10.0	8.9
Tb	2.1	1.8	1.5	2.5	2.2	1.8	1.6
Dy	13.6	11.1	9.5	15.7	13.6	11.0	10.0
Ho	2.7	2.2	1.9	3.1	2.7	2.2	2.0
Er	7.9	6.4	5.6	9.2	8.0	6.4	6.0
Tm	1.2	1.0	0.9	1.4	1.2	1.0	1.0
Yb	7.2	5.9	5.2	8.2	6.8	5.8	5.3
Lu	1.2	1.0	0.8	1.5	1.2	1.0	0.9
Hf	12.2	9.9	8.4	13.8	12.3	9.7	9.9
Ta	3.6	3.1	2.9	3.6	3.6	3.0	3.0
Pb^{206}	38.4	39.9	44.4	41.1	36.5	37.4	35.7
Pb^{207}	37.9	38.6	44.6	40.7	36.3	36.7	35.1
Pb^{208}	39.3	40.5	44.8	39.5	37.5	37.4	36.0
Th	34.0	26.9	24.3	34.5	34.3	26.4	27.0
U	10.2	10.2	10.7	10.3	9.4	9.7	9.6

Appendix G.
WBH glass
LA-ICP-MS
trace element
analyses
(ppm)

UNIT	FS	FS	Hn	Hn	Hn	Hn	Hn
SAMPLE	06WS-059	06WS-059	07WS-077	07WS-077	07WS-077	07WS-077	07WS-077
ANALYSIS	Glass 9	Glass 10	Glass 1	Glass 2	Glass 3	Glass 4	Glass 5
Sc	4.2	4.8	4.7	5.2	5.0	5.0	4.9
Ti	1506.1	1394.9	1373.1	1469.8	1372.1	1414.1	1352.2
Rb	289.0	283.8	251.3	251.2	252.1	253.0	256.9
Sr	9.6	5.9	10.9	13.0	14.6	15.0	9.2
Y	67.1	63.9	65.4	70.6	66.6	57.2	62.2
Zr	313.5	323.9	346.1	329.9	348.0	290.2	332.3
Nb	59.6	57.3	59.5	60.0	59.0	57.2	59.1
Cs	4.7	5.3	4.0	4.1	3.8	4.0	4.2
Ba	351.2	220.6	439.4	499.3	534.5	480.5	368.2
La	71.9	69.3	72.4	75.9	71.4	64.0	69.3
Ce	180.2	166.5	168.5	180.6	166.1	158.9	169.6
Pr	15.4	14.3	15.7	17.0	15.3	14.0	15.4
Nd	54.6	51.3	56.2	61.7	54.6	49.5	54.2
Sm	10.6	9.7	11.0	11.9	10.6	9.4	10.7
Eu	0.8	0.7	0.7	1.0	0.8	0.8	0.6
Gd	9.3	8.7	10.0	11.1	9.5	8.6	9.7
Tb	1.7	1.5	1.7	1.9	1.6	1.5	1.7
Dy	10.3	9.6	10.5	11.3	10.1	8.8	10.0
Ho	2.1	2.0	2.1	2.3	2.1	1.8	2.0
Er	6.0	5.7	6.3	6.8	6.3	5.4	6.0
Tm	0.9	0.9	1.0	1.1	1.0	0.8	0.9
Yb	5.4	5.1	5.7	6.4	5.7	5.0	5.6
Lu	0.9	0.9	0.9	1.0	0.9	0.8	0.9
Hf	9.0	9.2	10.2	9.7	9.9	8.2	9.6
Ta	3.0	3.1	3.3	3.2	3.2	2.9	3.3
Pb^{206}	42.9	40.5	36.4	46.9	42.6	37.8	38.4
Pb^{207}	42.7	40.4	36.5	46.0	43.1	38.2	37.9
Pb^{208}	44.1	41.5	37.0	46.4	43.3	37.8	38.5
Th	25.9	26.0	28.4	26.6	28.5	24.1	27.6
U	10.5	9.7	9.5	10.0	9.6	10.2	10.0

Appendix G.
WBH glass
LA-ICP-MS
trace element
analyses
(ppm)

UNIT	Hn	Hn	Hn	BM	BM	BM	BM
SAMPLE	07WS-077	07WS-077	07WS-077	06WS-063	06WS-063	06WS-063	06WS-063
ANALYSIS	Glass 6	Glass 7	Glass 8	Glass 1	Glass 2	Glass 3	Glass 4
Sc	5.3	5.3	5.0	6.7	8.3	7.7	6.9
Ti	1352.2	1354.8	1458.0	1795.2	2201.9	1888.9	1956.3
Rb	239.6	250.8	266.0	308.2	268.6	284.8	283.6
Sr	16.3	11.9	11.6	8.4	19.1	15.5	14.0
Y	66.2	62.9	67.4	61.8	65.0	81.1	55.8
Zr	350.8	339.2	285.9	443.8	495.5	556.8	418.2
Nb	58.3	59.2	57.2	59.0	60.3	59.9	56.8
Cs	3.8	4.1	4.1	4.7	4.4	4.4	4.1
Ba	545.5	446.6	438.6	267.8	671.8	536.5	478.2
La	71.9	70.1	72.3	76.4	78.9	94.0	68.1
Ce	164.5	167.3	176.2	168.3	154.7	177.3	151.9
Pr	15.5	15.1	16.1	15.5	15.7	18.0	13.6
Nd	55.5	53.7	58.7	53.6	57.0	66.0	47.4
Sm	10.7	10.1	11.4	9.9	10.5	12.5	8.8
Eu	0.9	0.7	1.0	0.3	0.7	0.5	0.4
Gd	10.0	9.5	10.1	9.6	9.7	11.9	8.3
Tb	1.7	1.6	1.7	1.5	1.6	2.0	1.3
Dy	10.3	9.8	10.5	9.7	9.5	12.2	8.1
Ho	2.1	2.0	2.0	1.9	1.9	2.4	1.5
Er	6.3	5.8	6.0	5.9	5.7	7.3	4.7
Tm	0.9	0.9	0.9	0.9	0.9	1.2	0.7
Yb	5.7	5.4	5.9	5.2	4.8	6.4	4.0
Lu	0.9	0.9	0.8	0.8	0.8	1.1	0.7
Hf	10.2	9.7	8.0	11.9	12.9	16.0	10.3
Ta	3.3	3.2	2.8	3.6	3.6	4.1	3.0
Pb^{206}	62.1	41.8	41.1	35.5	33.8	33.4	31.6
Pb^{207}	61.7	41.0	40.8	36.1	33.9	33.0	30.7
Pb^{208}	61.6	41.9	40.7	37.1	35.5	34.6	31.0
Th	28.8	26.9	22.9	35.4	38.4	43.6	28.3
U	9.2	9.5	10.0	9.7	9.8	9.5	8.2

Appendix G.
WBH glass
LA-ICP-MS
trace element
analyses
(ppm)

UNIT	BM	BM	BM	BM	BM	BM	WG
SAMPLE	06WS-063	06WS-063	06WS-063	06WS-063	06WS-063	06WS-063	06WS-069
ANALYSIS	Glass 5	Glass 6	Glass 7	Glass 8	Glass 9	Glass 10	Glass 1
Sc	6.2	6.2	6.8	5.7	7.1	6.8	6.6
Ti	1926.6	1770.3	2314.7	1767.8	1923.2	2080.5	1884.0
Rb	288.6	295.7	285.1	265.8	266.2	292.6	246.3
Sr	13.6	11.5	17.5	14.8	17.4	15.1	22.5
Y	52.1	44.7	48.2	55.3	72.7	81.7	79.1
Zr	394.4	341.1	379.7	412.8	513.8	582.3	498.7
Nb	58.2	54.1	59.9	51.8	55.0	64.0	61.5
Cs	4.4	4.6	4.4	4.1	3.6	4.5	3.9
Ba	438.9	370.7	550.2	515.2	539.3	401.3	582.6
La	65.7	57.7	60.6	65.7	79.4	85.1	84.9
Ce	156.2	148.3	148.5	139.0	150.8	148.6	172.1
Pr	13.7	12.1	12.4	13.0	15.2	14.4	18.2
Nd	47.7	41.2	42.3	44.5	54.4	49.9	68.7
Sm	8.8	7.6	7.6	8.0	10.2	8.7	13.5
Eu	0.4	0.3	0.4	0.7	0.5	0.3	0.8
Gd	8.3	6.7	7.0	7.7	9.6	8.2	13.0
Tb	1.4	1.1	1.1	1.2	1.6	1.4	2.2
Dy	8.1	6.2	7.0	7.8	9.6	8.6	13.8
Ho	1.6	1.2	1.4	1.7	1.9	1.8	2.7
Er	4.8	3.5	4.1	5.0	5.7	5.2	8.4
Tm	0.8	0.6	0.6	0.8	0.9	0.8	1.3
Yb	4.4	3.4	3.6	4.5	5.1	4.7	7.6
Lu	0.7	0.5	0.6	0.7	0.9	0.8	1.3
Hf	10.8	7.8	8.4	11.6	13.0	12.9	16.4
Ta	3.3	2.4	2.8	3.3	3.3	3.3	4.1
Pb^{206}	39.7	32.4	32.4	34.3	27.7	28.2	39.5
Pb^{207}	39.5	32.8	32.5	34.5	26.9	28.7	37.6
Pb^{208}	40.2	33.2	31.8	36.0	27.7	29.3	39.8
Th	32.0	23.7	26.8	33.4	36.1	37.3	40.1
U	10.7	8.8	9.2	9.2	7.9	8.0	10.6

Appendix G.
WBH glass
LA-ICP-MS
trace element
analyses
(ppm)

UNIT	WG	WG	WG	WG	WG	WG	WG
SAMPLE	06WS-069	06WS-069	06WS-069	06WS-069	06WS-069	06WS-069	06WS-069
ANALYSIS	Glass 2	Glass 3	Glass 4	Glass 5	Glass 6	Glass 7	Glass 8
Sc	6.0	5.2	6.0	6.5	6.1	5.1	5.6
Ti	1643.2	1839.6	1821.2	1991.0	1939.6	1721.7	1918.4
Rb	226.6	246.7	248.7	232.0	224.7	262.4	231.2
Sr	23.7	20.6	31.2	27.1	27.9	26.1	26.9
Y	75.3	71.5	76.5	89.2	74.2	62.8	68.4
Zr	446.5	461.8	490.4	503.6	483.6	399.4	427.5
Nb	56.2	62.8	63.7	66.1	64.1	61.6	67.1
Cs	3.9	4.6	4.1	3.9	3.9	4.2	4.2
Ba	642.5	557.2	825.3	787.4	776.8	696.4	802.2
La	87.4	86.5	89.0	94.4	85.4	74.5	79.5
Ce	165.2	172.0	175.0	188.3	170.5	167.9	177.3
Pr	17.3	17.8	18.2	19.8	17.5	16.1	17.4
Nd	64.4	65.0	68.9	74.7	65.1	58.3	64.2
Sm	12.6	12.7	13.6	14.5	13.0	11.1	12.4
Eu	0.7	0.6	1.0	1.0	1.0	0.8	1.0
Gd	11.9	12.2	13.3	14.2	12.4	10.3	11.7
Tb	2.0	2.0	2.2	2.3	2.0	1.8	1.9
Dy	12.2	12.6	14.1	15.2	12.6	11.1	12.8
Ho	2.4	2.5	2.8	3.1	2.6	2.2	2.6
Er	7.2	7.7	8.4	9.1	7.7	6.6	7.8
Tm	1.1	1.2	1.3	1.5	1.2	1.0	1.2
Yb	6.7	7.0	7.8	8.3	7.0	6.0	7.3
Lu	1.2	1.2	1.2	1.4	1.2	1.0	1.2
Hf	13.6	15.4	16.2	16.5	16.1	12.7	14.7
Ta	3.5	4.3	4.3	4.5	4.4	3.8	4.3
Pb^{206}	36.6	38.3	39.6	41.4	39.6	42.7	45.4
Pb^{207}	35.1	38.2	39.3	38.6	39.1	41.7	43.6
Pb^{208}	36.5	39.6	39.9	40.8	40.2	42.7	44.8
Th	34.8	44.3	43.5	45.2	42.1	35.6	38.4
U	8.4	11.3	10.7	11.1	11.4	11.4	12.1

Appendix G.
WBH glass
LA-ICP-MS
trace element
analyses
(ppm)

UNIT	WG	WG	LN	LN	LN	LN	LN
SAMPLE	06WS-069	06WS-069	06WS-035	06WS-035	06WS-035	06WS-035	06WS-035
ANALYSIS	Glass 9	Glass 10	Glass 1	Glass 2	Glass 3	Glass 4	Glass 5
Sc	5.3	5.5	6.2	7.8	6.6	6.8	6.2
Ti	1975.8	1931.2	1999.7	2104.6	2035.3	2077.0	2038.6
Rb	283.6	213.7	286.0	283.6	284.6	273.7	290.4
Sr	22.6	31.3	10.5	13.6	9.9	12.5	11.0
Y	60.2	58.9	48.6	64.9	59.0	62.8	54.9
Zr	404.0	401.8	317.0	403.7	372.2	386.1	347.2
Nb	65.7	62.4	58.6	60.9	59.4	61.0	59.9
Cs	4.9	3.5	3.8	3.6	3.7	3.6	3.9
Ba	693.3	953.7	476.0	633.1	535.0	535.3	421.3
La	78.2	78.7	60.1	78.5	70.9	73.0	65.9
Ce	176.6	178.9	144.3	165.4	151.2	153.8	149.4
Pr	16.9	17.3	12.6	16.1	14.6	14.7	13.6
Nd	60.7	62.2	43.3	57.1	52.0	51.5	47.3
Sm	11.5	11.5	8.0	11.1	9.9	9.6	8.6
Eu	0.8	1.0	0.4	0.7	0.6	0.6	0.4
Gd	10.6	10.9	7.2	10.2	9.1	9.1	7.8
Tb	1.8	1.8	1.2	1.7	1.5	1.5	1.4
Dy	10.8	11.6	7.2	10.1	9.1	9.3	8.2
Ho	2.2	2.3	1.5	2.1	1.8	1.9	1.7
Er	6.6	6.9	4.4	6.2	5.6	5.8	5.0
Tm	1.0	1.1	0.7	1.0	0.9	0.9	0.8
Yb	6.3	6.1	4.0	5.6	5.0	5.2	4.4
Lu	1.0	1.0	0.6	0.9	0.8	0.8	0.8
Hf	13.3	12.9	8.6	11.6	10.5	10.6	9.4
Ta	4.0	3.8	3.1	3.7	3.6	3.5	3.3
Pb^{206}	42.7	42.6	32.1	31.0	31.3	29.6	30.7
Pb^{207}	41.4	43.3	32.4	29.7	31.1	29.8	30.9
Pb^{208}	42.9	43.1	33.2	28.7	31.9	30.5	31.5
Th	35.1	34.4	29.0	34.1	34.7	34.9	31.3
U	11.8	10.7	9.3	7.6	8.7	8.7	8.9

Appendix G.
WBH glass
LA-ICP-MS
trace element
analyses
(ppm)

UNIT	LN	LN	LN	LN	LN	WC	WC
SAMPLE	06WS-035	06WS-035	06WS-035	06WS-035	06WS-035	06WS-037	06WS-037
ANALYSIS	Glass 6	Glass 7	Glass 8	Glass 9	Glass 10	Glass 1	Glass 2
Sc	6.6	5.9	6.4	7.8	7.1	8.2	9.0
Ti	1991.1	2043.7	2007.8	2089.3	2069.7	2403.8	2374.4
Rb	278.2	283.5	275.5	285.6	273.3	263.9	256.3
Sr	12.9	13.3	14.6	10.4	8.1	36.7	29.2
Y	53.4	57.2	54.9	62.7	64.3	71.4	68.6
Zr	345.3	372.2	349.2	400.7	405.4	515.4	480.8
Nb	58.0	60.8	58.6	61.6	61.0	64.1	65.2
Cs	3.7	3.9	3.7	3.7	3.7	3.9	3.9
Ba	468.5	422.3	620.2	431.2	253.1	742.5	674.8
La	65.4	69.4	65.5	72.8	75.8	78.9	77.4
Ce	147.5	151.9	147.2	152.8	153.4	153.2	166.2
Pr	13.6	14.1	13.6	14.6	15.0	15.5	15.8
Nd	46.5	48.7	46.7	51.7	53.3	56.0	55.8
Sm	8.5	9.2	8.9	9.8	9.9	10.8	10.8
Eu	0.5	0.5	0.5	0.4	0.4	0.9	0.9
Gd	8.0	8.3	8.0	9.2	9.5	10.9	10.9
Tb	1.3	1.4	1.4	1.5	1.6	1.8	1.8
Dy	8.0	8.5	8.3	9.2	9.5	10.6	10.2
Ho	1.7	1.7	1.7	1.9	1.9	2.2	2.1
Er	4.8	5.2	5.1	5.6	5.8	6.6	6.1
Tm	0.8	0.8	0.8	0.9	0.9	1.1	1.0
Yb	4.5	4.6	4.5	5.3	5.1	6.0	5.5
Lu	0.7	0.8	0.8	0.9	0.9	1.0	0.9
Hf	9.5	10.0	9.7	11.0	11.2	13.4	12.6
Ta	3.2	3.4	3.3	3.6	3.6	3.6	3.7
Pb^{206}	29.8	29.6	31.0	30.5	28.3	30.0	33.5
Pb^{207}	30.3	29.5	31.4	30.9	29.0	30.3	33.2
Pb^{208}	30.9	30.0	31.9	31.1	29.6	31.1	32.8
Th	31.3	32.0	31.9	36.2	37.0	36.3	34.0
U	8.8	8.4	8.9	8.7	8.5	8.3	9.0

Appendix G.
WBH glass
LA-ICP-MS
trace element
analyses
(ppm)

UNIT	WC	WC	WC	WC	WC	WC	WC
SAMPLE	06WS-037	06WS-037	06WS-037	06WS-037	06WS-037	06WS-037	06WS-037
ANALYSIS	Glass 3	Glass 4	Glass 5	Glass 6	Glass 7	Glass 8	Glass 9
Sc	8.4	11.3	9.7	9.6	10.8	10.1	8.6
Ti	2465.3	2675.1	2388.5	2319.4	2679.7	2377.3	2112.0
Rb	252.6	250.9	255.0	263.7	259.0	235.7	244.5
Sr	25.1	39.3	31.9	35.1	38.1	43.8	30.8
Y	73.8	84.9	67.3	57.2	65.9	60.6	53.2
Zr	527.2	596.1	486.8	423.9	447.5	425.5	414.4
Nb	67.2	72.9	65.3	62.3	67.1	59.6	59.3
Cs	3.9	4.0	4.0	4.0	4.0	3.5	3.7
Ba	667.3	950.5	667.5	715.2	891.0	905.9	706.5
La	86.3	96.8	76.3	66.4	72.1	65.9	64.2
Ce	173.3	177.1	157.8	147.5	160.8	144.9	143.4
Pr	17.6	18.9	15.5	13.8	15.4	13.9	13.2
Nd	64.5	70.2	55.1	48.6	56.3	49.4	47.2
Sm	12.5	13.3	10.4	9.2	10.6	9.4	8.8
Eu	0.8	1.1	0.7	0.8	1.0	1.1	0.8
Gd	12.2	13.4	10.4	9.0	10.2	8.7	8.6
Tb	2.1	2.1	1.7	1.5	1.7	1.4	1.4
Dy	12.1	12.7	10.0	8.8	10.4	8.6	8.4
Ho	2.5	2.7	2.0	1.8	2.1	1.8	1.7
Er	7.7	8.0	6.3	5.5	6.4	5.4	5.1
Tm	1.2	1.2	1.0	0.9	1.0	0.9	0.8
Yb	6.8	7.1	5.5	5.0	5.8	4.9	4.6
Lu	1.0	1.2	0.9	0.8	0.9	0.8	0.7
Hf	13.3	16.0	13.2	11.3	12.7	11.3	10.9
Ta	3.5	4.3	3.9	3.6	3.8	3.4	3.3
Pb^{206}	29.1	31.2	31.8	34.9	35.2	33.4	31.8
Pb^{207}	29.7	31.2	33.1	34.0	34.1	32.2	31.2
Pb^{208}	28.8	31.8	33.0	36.1	33.5	31.1	31.7
Th	35.2	41.1	35.5	31.1	29.2	29.5	27.7
U	8.1	8.4	9.0	9.1	7.9	8.0	7.7

Appendix G.
WBH glass
LA-ICP-MS
trace element
analyses
(ppm)

UNIT	WC
SAMPLE	06WS-037
ANALYSIS	Glass 10
Sc	10.1
Ti	2501.2
Rb	254.8
Sr	35.8
Y	66.7
Zr	461.1
Nb	64.2
Cs	3.9
Ba	761.9
La	71.9
Ce	157.3
Pr	15.3
Nd	54.5
Sm	10.4
Eu	0.9
Gd	9.8
Tb	1.6
Dy	9.5
Ho	2.0
Er	6.0
Tm	1.0
Yb	5.6
Lu	0.9
Hf	12.9
Ta	3.7
Pb^{206}	33.8
Pb^{207}	34.3
Pb^{208}	32.6
Th	33.5
U	9.2

APPENDIX H

LA-ICP-MS FELDSPAR DATA

Appendix G. WBH feldspar LA-ICP-MS trace element analyses (ppm)

UNIT	HS	HS	HS	HS	HS	HS	HS
SAMPLE	06WS-028	06WS-028	06WS-028	06WS-028	06WS-028	06WS-028	06WS-028
ANALYSIS	fspar 1	fspar 2	fspar 3	fspar 4	fspar 5	fspar 6	fspar 7
Sc	3.53	3.14	2.52	3.15	2.81	2.84	2.97
Ti	211.21	139.43	130.34	154.32	116.51	131.88	162.61
Rb	143.78	5.90	4.24	138.02	7.12	5.53	6.78
Sr	220.76	393.98	333.13	207.59	329.08	300.63	347.23
Y	4.79	1.32	0.74	2.67	0.73	0.81	1.59
Zr	10.28	1.88	0.27	0.31	1.47	2.29	3.46
Nb	1.79	0.19	0.06	0.05	0.16	0.42	0.67
Cs	0.30	0.05	0.01	0.10	0.04	0.04	0.09
Ba	9823.75	1218.42	1007.37	9449.93	1138.15	987.95	1059.61
La	6.72	17.82	18.33	4.70	16.56	15.46	20.12
Ce	9.55	31.94	33.30	5.95	28.96	31.20	34.75
Pr	0.60	2.03	2.08	0.22	1.59	1.88	2.30
Nd	1.85	5.61	5.37	0.43	3.84	4.86	6.40
Sm	0.32	0.64	0.56	0.04	0.32	0.48	0.79
Eu	3.41	4.21	4.22	3.21	3.18	3.80	4.56
Gd	1.44	0.68	0.57	1.04	0.38	0.53	0.74
Tb	0.04	0.05	0.03	0.00	0.02	0.03	0.05
Dy	0.26	0.19	0.10	0.01	0.07	0.12	0.29
Ho	0.05	0.03	0.01	0.00	0.01	0.02	0.05
Er	0.14	0.08	0.03	0.01	0.02	0.04	0.12
Tm	0.02	0.01	0.01	0.00	0.00	0.00	0.02
Yb	0.13	0.06	0.02	0.01	0.02	0.02	0.11
Lu	0.02	0.01	0.00	0.00	0.00	0.00	0.01
Hf	0.28	0.06	0.01	0.08	0.04	0.05	0.10
Ta	0.32	0.03	0.01	0.22	0.02	0.03	0.03
Pb^{206}	38.82	16.03	17.31	40.64	14.08	19.21	19.28
Pb^{207}	38.11	16.29	16.75	40.52	13.98	19.04	19.22
Pb^{208}	38.68	16.03	17.41	40.10	14.79	19.32	19.16
Th	0.79	0.08	0.03	0.01	0.03	0.12	0.20
U	0.28	0.06	0.02	0.04	0.03	0.04	0.15

Appendix G. WBH feldspar LA-ICP-MS trace element analyses (ppm)

UNIT	HS	HS	RS	RS	RS	RS	RS
SAMPLE	06WS-028	06WS-028	06WS-052	06WS-052	06WS-052	06WS-052	06WS-052
ANALYSIS	fspar 8	fspar 9	fspar 1	fspar 2	fspar 3	fspar 4	fspar 5
Sc	2.64	2.89	2.12	3.18	3.05	2.63	2.63
Ti	167.16	157.25	161.21	209.68	181.05	186.36	154.11
Rb	5.56	5.66	104.36	10.04	3.43	104.81	4.45
Sr	406.55	393.89	247.43	424.10	302.54	330.90	491.10
Y	1.37	1.05	4.16	4.42	1.56	4.66	1.16
Zr	4.15	2.82	2.28	10.77	8.40	0.26	1.01
Nb	0.65	0.32	0.19	1.71	0.77	0.05	0.12
Cs	0.06	0.04	0.10	0.11	0.02	0.08	0.01
Ba	1136.83	1187.02	9827.35	1157.44	813.84	13679.00	1429.78
La	19.08	18.57	7.13	24.83	16.95	8.55	21.84
Ce	34.42	32.98	6.48	42.78	34.77	7.54	32.64
Pr	2.25	2.12	0.39	3.13	2.26	0.41	2.17
Nd	6.21	5.60	0.98	9.31	6.24	1.03	5.90
Sm	0.63	0.58	0.14	1.17	0.75	0.15	0.52
Eu	4.33	4.85	3.70	5.03	3.83	5.30	4.78
Gd	0.69	0.69	1.24	1.04	0.67	1.80	0.58
Tb	0.04	0.04	0.02	0.10	0.06	0.02	0.03
Dy	0.23	0.17	0.15	0.48	0.27	0.08	0.13
Ho	0.04	0.03	0.03	0.08	0.05	0.04	0.03
Er	0.09	0.08	0.09	0.21	0.13	0.05	0.07
Tm	0.01	0.01	0.01	0.03	0.02	0.01	0.01
Yb	0.06	0.06	0.08	0.18	0.10	0.06	0.05
Lu	0.01	0.01	0.01	0.02	0.02	0.01	0.01
Hf	0.12	0.12	0.11	0.15	0.22	0.13	0.03
Ta	0.06	0.03	0.26	0.04	0.07	0.32	0.02
Pb^{206}	13.57	18.69	25.36	14.78	17.16	25.31	12.85
Pb^{207}	13.43	18.12	25.13	14.69	17.20	25.38	12.10
Pb^{208}	13.71	18.61	25.53	14.42	17.27	25.69	11.80
Th	0.33	0.13	-0.08	0.17	0.50	0.01	0.02
U	0.12	0.09	0.06	0.08	0.17	0.01	0.01

Appendix G. WBH feldspar LA-ICP-MS trace element analyses (ppm)

UNIT	RS	RS	RS	RS	RS	FS	FS
SAMPLE	06WS-052	06WS-052	06WS-052	06WS-052	06WS-052	06WS-059	06WS-059
ANALYSIS	fspar 6	fspar 7	fspar 8	fspar 9	fspar 10	fspar 1	fspar 2
Sc	2.59	2.53	2.63	2.38	3.21	3.74	3.08
Ti	154.99	136.60	151.84	136.83	166.40	89.74	144.62
Rb	6.70	3.51	4.11	3.63	142.26	5.15	105.88
Sr	400.50	385.85	407.26	360.27	216.19	292.16	260.39
Y	1.90	1.03	2.18	1.09	2.89	0.60	2.90
Zr	6.48	0.58	5.03	1.24	0.12	0.29	0.41
Nb	0.95	0.12	0.72	0.14	0.03	0.05	0.05
Cs	0.05	0.01	0.02	0.01	0.10	0.01	0.11
Ba	1168.43	1250.66	1133.28	1161.23	9893.75	1267.24	11794.37
La	20.56	21.51	19.43	20.22	5.00	13.02	6.04
Ce	35.11	35.10	31.92	33.03	6.11	18.28	6.31
Pr	2.33	2.29	2.12	2.16	0.22	1.25	0.28
Nd	6.43	6.13	5.64	5.69	0.44	3.34	0.60
Sm	0.69	0.61	0.56	0.51	0.04	0.34	0.05
Eu	4.31	4.82	4.31	4.53	3.22	6.82	6.98
Gd	0.69	0.63	0.64	0.59	0.89	0.52	1.05
Tb	0.05	0.04	0.05	0.03	0.00	0.02	0.00
Dy	0.29	0.15	0.22	0.13	0.01	0.08	0.01
Ho	0.06	0.03	0.05	0.03	0.00	0.01	0.00
Er	0.14	0.07	0.14	0.05	0.01	0.03	0.01
Tm	0.02	0.01	0.02	0.01	0.00	0.00	0.00
Yb	0.14	0.04	0.11	0.05	0.01	0.02	0.01
Lu	0.02	0.01	0.02	0.01	0.00	0.00	0.00
Hf	0.28	0.03	0.07	0.03	0.10	0.04	0.12
Ta	0.14	0.02	0.02	0.02	0.25	0.02	0.26
Pb^{206}	13.19	14.79	13.56	15.12	36.78	16.79	29.78
Pb^{207}	13.27	14.45	13.77	14.45	36.20	15.91	29.68
Pb^{208}	12.98	14.80	13.71	15.28	36.71	16.38	29.49
Th	0.84	0.02	0.06	0.01	0.00	0.03	0.00
U	0.57	0.05	0.16	0.08	0.00	0.01	0.01

Appendix G. WBH feldspar LA-ICP-MS trace element analyses (ppm)

UNIT	FS	FS	FS	FS	FS	FS	FS
SAMPLE	06WS-059	06WS-059	06WS-059	06WS-059	06WS-059	06WS-059	06WS-059
ANALYSIS	fspar 3	fspar 4	fspar 5	fspar 6	fspar 7	fspar 8	fspar 9
Sc	2.36	2.51	3.18	2.02	2.48	2.50	2.25
Ti	116.23	122.81	134.93	128.59	117.45	105.26	167.97
Rb	5.53	5.21	107.99	5.59	5.98	5.53	104.70
Sr	348.62	364.86	216.48	365.46	320.25	306.64	304.91
Y	1.16	0.67	2.06	0.86	0.58	0.60	3.95
Zr	0.92	0.50	0.38	0.77	0.06	0.22	11.34
Nb	0.11	0.06	0.05	0.13	0.02	0.03	1.00
Cs	0.01	0.01	0.07	0.02	0.00	0.00	0.15
Ba	1791.54	1717.96	8814.29	1616.01	1569.00	1614.46	10891.11
La	16.41	16.09	4.45	17.92	14.16	13.09	6.76
Ce	25.83	25.78	5.60	25.64	23.11	21.75	6.70
Pr	1.64	1.57	0.22	1.68	1.35	1.28	0.34
Nd	4.45	3.81	0.46	4.67	3.39	3.22	0.86
Sm	0.47	0.35	0.05	0.46	0.31	0.29	0.13
Eu	8.11	7.69	5.50	8.49	7.00	6.91	7.64
Gd	0.46	0.43	0.54	0.46	0.32	0.33	0.85
Tb	0.03	0.02	0.00	0.02	0.01	0.02	0.02
Dy	0.10	0.07	0.01	0.10	0.06	0.05	0.12
Ho	0.02	0.01	0.00	0.01	0.01	0.01	0.03
Er	0.05	0.03	0.01	0.04	0.02	0.02	0.07
Tm	0.00	0.00	0.00	0.00	0.00	0.00	0.01
Yb	0.04	0.01	0.01	0.04	0.01	0.01	0.08
Lu	0.00	0.00	0.00	0.00	0.00	0.00	0.02
Hf	0.04	0.03	0.11	0.04	0.02	0.01	0.49
Ta	0.04	0.03	0.27	0.03	0.03	0.02	0.33
Pb^{206}	15.25	15.59	33.33	15.40	15.05	15.87	33.25
Pb^{207}	15.03	15.53	33.26	15.21	14.96	15.85	31.36
Pb^{208}	15.50	16.08	34.02	15.26	14.95	16.05	31.60
Th	0.02	0.01	0.01	0.02	0.00	0.00	0.19
U	0.01	0.00	0.00	0.02	0.00	0.00	0.11

Appendix G. WBH feldspar LA-ICP-MS trace element analyses (ppm)

UNIT	BM	BM	BM	BM	BM	BM	BM
SAMPLE	06WS-062	06WS-062	06WS-062	06WS-062	06WS-062	06WS-062	06WS-062
ANALYSIS	fspar 1	fspar 2	fspar 3	fspar 4	fspar 5	fspar 6	fspar 7
Sc	3.17	2.49	3.08	2.88	2.64	2.95	2.50
Ti	156.75	155.76	163.99	165.97	145.39	157.51	146.07
Rb	7.18	4.86	7.45	3.67	3.88	7.72	5.33
Sr	337.49	361.79	318.04	309.66	297.74	325.56	351.13
Y	4.77	1.53	1.21	0.79	0.98	0.92	1.01
Zr	4.49	1.14	5.50	0.58	0.33	5.81	0.37
Nb	0.71	0.13	0.98	0.06	0.11	0.89	0.05
Cs	0.10	0.01	0.08	0.01	0.00	0.08	0.01
Ba	1363.10	1446.93	1397.30	1053.71	1124.97	1475.11	1510.93
La	21.10	21.52	19.79	14.03	14.71	18.74	19.86
Ce	33.51	33.74	34.85	27.83	28.40	32.27	34.66
Pr	2.35	2.31	2.12	1.70	1.77	1.94	2.09
Nd	6.78	6.83	5.77	4.53	4.67	5.02	5.93
Sm	0.79	0.73	0.56	0.46	0.48	0.49	0.56
Eu	3.99	4.45	3.88	3.58	3.51	3.86	4.18
Gd	0.77	0.66	0.53	0.42	0.42	0.46	0.49
Tb	0.08	0.05	0.04	0.03	0.04	0.03	0.03
Dy	0.28	0.19	0.17	0.11	0.14	0.12	0.11
Ho	0.05	0.03	0.03	0.01	0.03	0.02	0.02
Er	0.11	0.08	0.07	0.04	0.06	0.06	0.04
Tm	0.02	0.01	0.01	0.00	0.01	0.01	0.00
Yb	0.10	0.04	0.06	0.03	0.05	0.06	0.03
Lu	0.01	0.00	0.01	0.00	0.00	0.01	0.00
Hf	0.11	0.03	0.14	0.02	0.02	0.14	0.03
Ta	0.03	0.01	0.04	0.01	0.01	0.04	0.01
Pb^{206}	17.15	16.46	20.38	18.48	18.25	19.06	18.11
Pb^{207}	17.49	16.13	20.17	18.17	18.09	18.86	18.29
Pb^{208}	17.37	16.39	20.57	18.57	18.67	18.78	19.20
Th	0.62	0.04	0.36	0.07	0.05	0.24	0.01
U	0.14	0.02	0.11	0.03	0.02	0.12	0.01

Appendix G. WBH feldspar LA-ICP-MS trace element analyses (ppm)

UNIT	BM	BM	BM	BM	WG	WG	WG
SAMPLE	06WS-062	06WS-062	06WS-062	06WS-062	06WS-069	06WS-069	06WS-069
ANALYSIS	fspar 8	fspar 9	fspar 10	fspar 11	fspar 1	fspar 2	fspar 3
Sc	2.67	2.44	2.86	1.97	1.37	2.38	2.19
Ti	139.72	142.48	205.18	134.93	91.62	151.98	148.44
Rb	5.88	5.44	4.21	4.70	3.19	5.24	4.50
Sr	328.56	318.81	334.02	315.86	315.59	503.92	458.53
Y	0.85	0.71	1.07	0.64	1.56	2.33	0.88
Zr	0.73	1.46	0.66	0.21	1.85	3.26	0.22
Nb	0.10	0.20	0.13	0.04	0.23	0.40	0.04
Cs	0.01	0.01	0.01	0.00	0.05	0.08	0.01
Ba	1458.18	1395.05	1044.50	1599.69	1134.50	1676.43	1695.11
La	17.22	16.80	14.55	19.96	14.05	21.71	20.57
Ce	30.25	31.25	30.16	34.56	20.42	31.27	29.60
Pr	1.79	1.70	1.84	2.08	1.58	2.48	2.13
Nd	4.91	4.11	4.75	5.28	4.77	7.42	6.04
Sm	0.43	0.40	0.51	0.45	0.54	0.90	0.61
Eu	3.79	3.70	3.28	3.93	4.44	7.39	7.28
Gd	0.44	0.35	0.44	0.40	0.61	1.13	0.76
Tb	0.02	0.02	0.03	0.02	0.05	0.08	0.03
Dy	0.10	0.07	0.13	0.06	0.24	0.42	0.13
Ho	0.01	0.01	0.03	0.01	0.04	0.08	0.02
Er	0.05	0.03	0.06	0.03	0.14	0.24	0.05
Tm	0.00	0.00	0.01	0.00	0.02	0.03	0.01
Yb	0.02	0.02	0.04	0.01	0.11	0.21	0.03
Lu	0.00	0.00	0.00	0.00	0.02	0.03	0.00
Hf	0.02	0.05	0.02	0.01	0.05	0.09	0.02
Ta	0.02	0.03	0.01	0.01	0.02	0.03	0.01
Pb^{206}	17.98	16.62	16.43	14.89	8.82	16.59	18.26
Pb^{207}	17.80	16.78	16.48	15.64	8.62	16.81	18.20
Pb^{208}	18.33	16.57	17.02	16.13	8.79	17.23	19.15
Th	0.02	0.12	0.03	0.00	0.07	0.11	0.01
U	0.01	0.06	0.01	0.00	0.06	0.10	0.01

Appendix G. WBH feldspar LA-ICP-MS trace element analyses (ppm)

UNIT	WG	WG	WG	WG	WG	WG	WG
SAMPLE	06WS-069	06WS-069	06WS-069	06WS-069	06WS-069	06WS-069	06WS-069
ANALYSIS	fspar 4	fspar 5	fspar 6	fspar 7	fspar 8	fspar 9	fspar 10
Sc	1.73	2.80	2.83	2.23	2.34	2.75	2.31
Ti	149.47	184.65	187.81	146.68	177.44	237.01	145.44
Rb	5.12	119.56	131.10	4.53	107.65	8.00	5.84
Sr	528.57	296.07	318.97	445.61	286.21	356.82	410.39
Y	1.22	2.86	4.41	0.86	2.78	8.01	1.31
Zr	0.92	0.31	0.39	0.12	0.16	7.05	4.54
Nb	0.12	0.07	0.07	0.03	0.04	0.95	0.58
Cs	0.03	0.09	0.10	0.01	0.08	0.05	0.04
Ba	2114.89	12618.58	10894.57	1623.00	13149.73	1379.82	1738.34
La	25.61	6.22	8.33	18.82	7.15	19.44	22.44
Ce	36.99	6.61	10.76	29.03	7.06	30.92	32.70
Pr	2.81	0.32	1.03	2.00	0.32	2.34	2.25
Nd	8.24	0.70	2.25	5.53	0.65	6.88	6.25
Sm	0.93	0.07	0.30	0.54	0.05	0.92	0.63
Eu	10.03	5.14	3.84	6.65	5.33	5.73	6.56
Gd	1.30	1.31	1.23	0.64	1.43	0.84	0.83
Tb	0.08	0.00	0.04	0.03	0.00	0.09	0.04
Dy	0.42	0.03	0.18	0.12	0.01	0.47	0.18
Ho	0.08	0.01	0.03	0.02	0.00	0.09	0.03
Er	0.25	0.02	0.07	0.05	0.01	0.29	0.08
Tm	0.03	0.01	0.01	0.00	0.00	0.05	0.01
Yb	0.24	0.03	0.04	0.02	0.01	0.44	0.09
Lu	0.04	0.01	0.01	0.00	0.00	0.05	0.01
Hf	0.16	0.11	0.11	0.02	0.14	0.28	0.14
Ta	0.05	0.22	0.24	0.02	0.32	0.10	0.05
Pb^{206}	20.26	33.67	31.69	19.45	30.00	15.79	19.12
Pb^{207}	19.57	33.75	31.85	19.11	29.86	15.45	18.86
Pb^{208}	19.48	34.28	31.70	20.26	30.64	15.99	19.67
Th	0.10	0.01	0.02	0.00	0.00	0.73	0.11
U	0.23	0.01	0.02	0.00	0.01	0.29	0.07

Appendix G. WBH feldspar LA-ICP-MS trace element analyses (ppm)

UNIT	LN	LN	LN	LN	LN	LN	LN
SAMPLE	06WS-035	06WS-035	06WS-035	06WS-035	06WS-035	06WS-035	06WS-035
ANALYSIS	fspar 1	fspar 2	fspar 3	fspar 4	fspar 5	fspar 6	fspar 7
Sc	-7.34	3.45	3.47	4.27	4.08	4.20	4.17
Ti	224.76	165.78	211.49	418.05	152.53	161.55	181.57
Rb	7.93	4.11	4.64	7.97	3.82	6.54	5.09
Sr	640.67	467.37	401.34	330.51	410.39	427.03	426.60
Y	1.85	1.19	0.85	1.06	0.81	0.98	1.22
Zr	3.45	1.58	3.99	8.18	0.19	4.24	2.15
Nb	0.44	0.20	0.34	1.30	0.03	0.38	0.36
Cs	0.20	0.10	0.19	0.16	0.01	0.19	0.13
Ba	1892.68	1163.34	993.14	610.03	1068.15	1381.49	1293.18
La	36.72	32.64	14.15	7.44	20.36	25.88	19.14
Ce	53.85	49.60	25.97	14.13	34.15	40.67	32.42
Pr	4.25	3.46	1.73	1.00	2.25	2.64	2.23
Nd	12.50	9.35	4.79	2.92	5.99	6.91	6.27
Sm	1.26	0.90	0.52	0.37	0.57	0.63	0.75
Eu	7.81	4.80	3.96	2.77	4.09	4.41	4.47
Gd	3.69	0.98	0.48	0.34	0.62	0.69	0.83
Tb	0.10	0.05	0.03	0.03	0.03	0.04	0.06
Dy	0.34	0.21	0.11	0.14	0.12	0.14	0.28
Ho	0.05	0.03	0.02	0.02	0.02	0.02	0.05
Er	0.20	0.08	0.05	0.06	0.04	0.05	0.13
Tm	0.02	0.01	0.01	0.01	0.00	0.01	0.02
Yb	0.14	0.05	0.04	0.06	0.02	0.04	0.08
Lu	0.01	0.01	0.00	0.01	0.00	0.00	0.01
Hf	0.20	0.04	0.11	0.16	0.01	0.11	0.09
Ta	0.07	0.02	0.04	0.04	0.01	0.05	0.03
Pb^{206}	31.56	17.22	17.93	19.35	17.75	17.59	21.83
Pb^{207}	31.80	17.32	18.12	19.53	17.55	17.68	21.87
Pb^{208}	32.23	17.68	18.52	19.96	18.03	17.91	20.78
Th	0.07	0.01	0.02	0.19	0.01	0.05	0.05
U	0.04	0.01	0.05	0.08	0.00	0.02	0.05

Appendix G. WBH feldspar LA-ICP-MS trace element analyses (ppm)

UNIT	LN	LN	LN	WC	WC	WC	WC
SAMPLE	06WS-035	06WS-035	06WS-035	06WS-037	06WS-037	06WS-037	06WS-037
ANALYSIS	fspar 8	fspar 9	fspar 10	fspar 1	fspar 2	fspar 3	fspar 4
Sc	4.18	4.07	3.98	3.94	4.08	4.24	4.35
Ti	156.90	172.19	154.83	160.50	165.85	164.34	167.71
Rb	3.91	3.89	4.10	3.68	3.27	4.05	5.04
Sr	449.83	428.39	399.88	465.32	427.90	477.51	444.72
Y	1.37	0.96	0.79	3.52	0.75	0.89	1.08
Zr	0.59	1.55	0.78	0.70	0.17	0.85	2.00
Nb	0.09	0.16	0.13	0.06	0.04	0.07	0.23
Cs	0.03	0.07	0.04	0.01	0.00	0.01	0.05
Ba	1325.94	1145.27	1032.33	1067.78	932.45	1145.49	1057.77
La	27.94	21.87	20.84	31.95	14.53	22.72	22.54
Ce	45.21	37.22	34.59	53.21	25.85	36.69	38.73
Pr	2.97	2.50	2.27	3.98	1.76	2.51	2.57
Nd	8.07	6.77	6.10	11.33	4.82	6.76	6.78
Sm	0.78	0.67	0.58	1.20	0.54	0.67	0.68
Eu	4.53	4.29	3.93	4.40	3.98	4.47	4.07
Gd	0.76	0.66	0.61	1.25	0.50	0.69	0.70
Tb	0.05	0.04	0.03	0.11	0.03	0.04	0.04
Dy	0.17	0.14	0.12	0.39	0.12	0.14	0.17
Ho	0.03	0.02	0.02	0.07	0.02	0.02	0.03
Er	0.06	0.06	0.04	0.16	0.04	0.05	0.07
Tm	0.01	0.01	0.00	0.02	0.01	0.00	0.01
Yb	0.04	0.03	0.02	0.10	0.02	0.03	0.04
Lu	0.00	0.00	0.00	0.02	0.00	0.00	0.01
Hf	0.02	0.04	0.03	0.03	0.01	0.02	0.05
Ta	0.02	0.02	0.01	0.01	0.01	0.02	0.03
Pb^{206}	17.31	16.99	16.60	15.48	14.96	16.09	16.54
Pb^{207}	17.09	16.67	16.66	15.48	14.80	16.08	16.18
Pb^{208}	17.55	17.10	16.95	15.74	15.22	16.33	16.53
Th	0.02	0.01	0.00	0.14	0.01	0.02	0.13
U	0.01	0.01	0.00	0.04	0.00	0.00	0.06

Appendix G. WBH feldspar LA-ICP-MS trace element analyses (ppm)

UNIT	WC	WC	WC	WC	WC	WC
SAMPLE	06WS-037	06WS-037	06WS-037	06WS-037	06WS-037	06WS-037
ANALYSIS	fspar 5	fspar 6	fspar 7	fspar 8	fspar 9	fspar 10
Sc	4.08	4.10	4.20	3.97	4.04	3.96
Ti	167.89	246.69	154.32	194.92	161.58	174.08
Rb	4.54	5.67	4.07	3.39	3.87	4.07
Sr	454.86	431.05	435.49	465.49	489.83	509.17
Y	1.13	1.73	0.80	1.17	0.92	1.52
Zr	2.44	8.78	0.13	1.31	0.17	2.28
Nb	0.19	0.85	0.02	0.15	0.03	0.18
Cs	0.03	0.12	0.00	0.02	0.00	0.03
Ba	1092.39	874.68	1088.95	1022.27	1200.99	1124.68
La	22.24	16.98	20.82	19.45	24.37	22.10
Ce	35.60	30.29	35.74	33.58	38.36	34.88
Pr	2.46	2.27	2.31	2.39	2.61	2.50
Nd	6.71	6.60	6.14	6.77	7.01	7.04
Sm	0.69	0.81	0.60	0.75	0.69	0.79
Eu	4.15	4.11	4.18	4.36	4.71	4.79
Gd	0.68	0.73	0.59	0.68	0.69	0.73
Tb	0.04	0.05	0.03	0.05	0.04	0.06
Dy	0.17	0.25	0.12	0.19	0.14	0.24
Ho	0.03	0.04	0.02	0.03	0.02	0.04
Er	0.06	0.10	0.04	0.08	0.05	0.10
Tm	0.01	0.02	0.00	0.01	0.01	0.01
Yb	0.04	0.10	0.02	0.04	0.02	0.06
Lu	0.01	0.02	0.00	0.01	0.00	0.00
Hf	0.07	0.23	0.01	0.05	0.01	0.08
Ta	0.02	0.07	0.01	0.02	0.02	0.04
Pb^{206}	14.33	14.35	15.33	14.87	15.00	15.93
Pb^{207}	14.30	14.84	15.22	14.82	14.67	15.68
Pb^{208}	14.01	14.96	15.60	15.11	15.33	15.97
Th	0.10	0.81	0.01	0.11	0.00	0.17
U	0.02	0.24	0.01	0.03	0.00	0.05

APPENDIX I

OXYGEN ISOTOPE ANALYSES

Appendix I.
Order of oxygen isotope analyses with standard values

sample	unit	type	wt (mg)	δ18O	Corrected Values
UWG2		garnet std	2.5	5.71	5.80
06WS 059 - 1	Frechman	fspar	2.7	1.12	1.23
06WS 059 - 2	Springs	fspar	2.5	2.22	2.35
UWG2		garnet std	2.5	5.65	5.80
06WS 053 - 1	Rattlesnake	fspar	2.6	1.63	1.76
06WS 053 - 2	Springs	fspar	2.5	1.97	2.08
UWG2		garnet std	2.7	5.71	5.80
06WS 021 - 1	High	fspar	2.8	1.85	1.93
06WS 021 - 2	Springs	fspar	2.5	1.70	1.77
UWG2		garnet std	*standard lost during analysis*		
06WS 037- 1	Willow	fspar	2.6	0.74	0.82
06WS 037 - 2	Creek	fspar	2.7	0.70	0.77
UWG2		garnet std	2.8	5.76	5.80
UWG2		garnet std	2.5	4.49	5.80
O6WS 035 - 1	Lower Normal	fspar	2.6	-0.11	0.71
UWG2		garnet std	2.7	5.47	5.80
O6WS 035 - 2	Lower Normal	fspar	2.8	-0.74	-0.42
O6WS 041 - 1	Dive Creek	fspar	2.5	1.48	1.78
O6WS 041 - 2	Dive Creek	fspar	2.5	2.26	2.56
UWG2		garnet std	2.7	5.52	5.80
06WS 067 - 1	Windy Gap IV a	fspar	2.5	0.48	0.83
06WS 067 - 2	Windy Gap IV a	fspar	2.6	1.09	1.52
06WS 069 - 1	Windy Gap IV b	fspar	2.5	1.83	2.34
UWG2		garnet std	2.5	5.22	5.80
06WS 069 - 2	Windy Gap IV b	fspar	2.5	1.10	1.79
UWG2 - 6		garnet std	2.6	4.99	5.80

APPENDIX J

SAMPLE LOCATIONS

APPENDIX J.
Location of samples

SAMPLE NAME	UNIT	North	West
06WS-003	High Springs	43.16170	115.50307
06WS 004	High Springs	43.16760	115.51453
06WS 005	High Springs	43.17049	115.51522
06WS-017	High Springs	43.20475	115.55016
06WS 020	High Springs	43.16879	115.51749
06WS 021	High Springs	43.16840	115.51702
06WS-027	High Springs	43.20333	115.54602
06WS-028	High Springs	43.20333	115.54602
06WS-029	High Springs	43.20041	115.54828
06WS-030	High Springs	43.20041	115.54828
06WS-048	High Springs	43.22720	115.52393
06WS 053	Rattlesnake Springs	43.22969	115.58902
06WS 054	Rattlesnake Springs	43.22969	115.58902
06WS 051	Rattlesnake Springs	43.22969	115.58902
06WS 050	Rattlesnake Springs	43.22969	115.58902
06WS-052	Rattlesnake Springs	43.22969	115.58902
06WS-061	Rattlesnake Springs	43.20343	115.56940
06WS 001	Dive Creek	43.17583	115.52591
06WS-007	Dive Creek	43.17489	115.52432
06WS-023	Dive Creek	43.18492	115.52899
06WS 041	Dive Creek	43.18500	115.53000
06WS 045	Dive Creek	43.23555	115.53353
06WS-049	Frenchman Springs	43.20539	115.56747
06WS 058	Frenchman Springs	43.22922	115.58855
06WS 056	Frenchman Springs	43.22922	115.58855
06WS-057	Frenchman Springs	43.22922	115.58855
06WS 059	Frenchman Springs	43.22841	115.58989
06WS-060	Frenchman Springs	43.20343	115.56940
06WS 064	Henley	43.21244	115.43784
07WS-076	Henley	43.15487	115.41859
07WS-077	Henley	43.15658	115.41953
06WS 065	Bennett Mountain	43.21188	115.43655
06WS 063	Bennett Mountain	43.21209	115.43508
06WS 066	Windy Gap	43.21077	115.44046
06WS 067	Windy Gap	43.21034	115.44111
06WS 068	Windy Gap	43.20981	115.44223
06WS 069	Windy Gap	43.20920	115.44267
06WS 070	Windy Gap	43.20844	115.44332
06WS 071	Windy Gap	43.20727	115.44417
06WS 072	Lower Reverse	43.32876	115.56045
06WS 035	Lower Normal	43.20477	115.44498
06WS 034	Lower Normal	43.20477	115.44498
06WS 036	Lower Normal	43.20496	115.44503
06WS 039	Willow Creek	43.20400	115.44533
06WS 037	Willow Creek	43.20400	115.44533
06WS-038	Willow Creek	43.20400	115.44533
06WS 040	Willow Creek	43.20382	115.44507